



UNIVERSITAT POLITÈCNICA  
DE CATALUNYA  
BARCELONATECH

## *Structural barrier effect on cotton fabrics*

Qiuyue Wu

**ADVERTIMENT** La consulta d'aquesta tesi queda condicionada a l'acceptació de les següents condicions d'ús: La difusió d'aquesta tesi per mitjà del repositori institucional UPCommons (<http://upcommons.upc.edu/tesis>) i el repositori cooperatiu TDX (<http://www.tdx.cat/>) ha estat autoritzada pels titulars dels drets de propietat intel·lectual **únicament per a usos privats** emmarcats en activitats d'investigació i docència. No s'autoritza la seva reproducció amb finalitats de lucre ni la seva difusió i posada a disposició des d'un lloc aliè al servei UPCommons o TDX. No s'autoritza la presentació del seu contingut en una finestra o marc aliè a UPCommons (*framing*). Aquesta reserva de drets afecta tant al resum de presentació de la tesi com als seus continguts. En la utilització o cita de parts de la tesi és obligat indicar el nom de la persona autora.

**ADVERTENCIA** La consulta de esta tesis queda condicionada a la aceptación de las siguientes condiciones de uso: La difusión de esta tesis por medio del repositorio institucional UPCommons (<http://upcommons.upc.edu/tesis>) y el repositorio cooperativo TDR (<http://www.tdx.cat/?locale-attribute=es>) ha sido autorizada por los titulares de los derechos de propiedad intelectual **únicamente para usos privados enmarcados** en actividades de investigación y docencia. No se autoriza su reproducción con finalidades de lucro ni su difusión y puesta a disposición desde un sitio ajeno al servicio UPCommons No se autoriza la presentación de su contenido en una ventana o marco ajeno a UPCommons (*framing*). Esta reserva de derechos afecta tanto al resumen de presentación de la tesis como a sus contenidos. En la utilización o cita de partes de la tesis es obligado indicar el nombre de la persona autora.

**WARNING** On having consulted this thesis you're accepting the following use conditions: Spreading this thesis by the institutional repository UPCommons (<http://upcommons.upc.edu/tesis>) and the cooperative repository TDX (<http://www.tdx.cat/?locale-attribute=en>) has been authorized by the titular of the intellectual property rights **only for private uses** placed in investigation and teaching activities. Reproduction with lucrative aims is not authorized neither its spreading nor availability from a site foreign to the UPCommons service. Introducing its content in a window or frame foreign to the UPCommons service is not authorized (*framing*). These rights affect to the presentation summary of the thesis as well as to its contents. In the using or citation of parts of the thesis it's obliged to indicate the name of the author.





UNIVERSITAT POLITÈCNICA  
DE CATALUNYA  
BARCELONATECH

PhD program in Textile and Paper Engineering

# **Structural Barrier Effect on Cotton Fabrics**

Ph.D. Thesis

**Doctoral thesis by:**

Qiuyue Wu

**Thesis advisor:**

Manuel Jose Lis Arias

Institute of Textile Research and Industrial Cooperation of Terrassa. INTEXTER

Terrassa, 2022

“Be patient.

You will cross the bridge when you get to it”

## ACKNOWLEDGMENTS

Throughout the writing of this dissertation, I have received a great deal of support and assistance.

I would first like to thank my supervisor, Professor Manuel Jose Lis Arias, whose expertise was invaluable in formulating the research questions and methodology. Your insightful feedback pushed me to sharpen my thinking and brought my work to a higher level. In addition, you have given me many positive influences in my life. You are always full of energy, humble, polite and enthusiastic in dealing with people, and you are good at finding the best part in everyone and giving them the maximum praise. It is really admirable to see you working hard and learning new things while taking charging of multiple research projects at the same time. Most importantly, what I have learnt from you is that always keep patience and optimism even though things didn't go your way.

In addition, my sincere acknowledgement to Marina Textil Inc. (Spain) for research grant support and supply of survey materials is much needed. In particular, my project collaborators, Helena Esteve and Marta Sobocinska are highly appreciated.

I would particularly like to express my thanks to Francesc Casanovas Diaz, Remedios Prieto Fuentes, Mercedes Escusa Julian and Vanesa Martínez for their wonderful collaboration and patient support with the tools that I needed to choose the right direction and successfully complete my dissertation. For my coordinators, Diana Cayuela Maria and Sara González Villafranca, they deserve to be thanked due to their valuable guidance and kind assistance throughout my studies.

Finally, I could not have completed this dissertation without the support of my parents, who provided empathetic ears as well as happy distractions to rest my mind outside of my research. I'm so blessed that they are always there for me.

## ABSTRACT

Cotton, being a natural hollow fiber with remarkable economic values including moisture absorption, air permeability, softness, comfort, and warmth retention, has become one of the most essential raw materials for the textile industry. However, cotton fibers are inherently with high inflammability and low thermal stability. It's promising to endow cotton with fire protection in order to broaden its application fields and reduce fire risks.

The novel halogen-free flame retardants (FRs) such as phosphorus-containing chemicals, metal hydroxides & metal oxides, and silicon-containing chemicals have been drawing a lot of research interest. 10-(2,5-dihydroxyphenyl)-9,10-dihydro-9-oxa-10-phosphaphenanthrene-10-oxide (DOPO-HQ), made from the reaction of 9,10-dihydro-9-oxa-10-phosphaphenanthrene-10-oxide (DOPO) and p-benzoquinone, is inherently with excellent chemical stability and heat resistance due to its own rigid aromatic structure and stable P-O-C bond. Metal-organic frameworks (MOFs) with high crystallinity and specific surface area are stable at high temperatures. During the thermal decomposition process, the metal oxides that are generated from MOF particles on the surface of cotton will act as a physical barrier to protect the substrate from further burning while also efficiently adsorbing gases and smoke. Tetraethyl orthosilicate (TEOS) can be utilized in combination with DOPO-HQ for P/Si synergistic effects and cross-link cotton fabrics through Si-O-Si network. It works as heat insulation and oxygen barrier by forming siliceous carbon layer and simultaneously helps reducing the overflow of flammable gases in combustion. Driven by current demand for fire safety and environmental protection, the structural barriers consisting of DOPO-HQ@UIO-66-COOH and TEOS were successfully assembled onto cotton fabrics through a facile approach in this thesis.

In chapter I, the general introduction, research objectives and experimental methodology of this thesis were described.

In chapter II, DOPO-HQ was investigated the impacts on the improvement of fire performances for cotton fabrics. It was desirable to discover the appropriate incorporation of DOPO-HQ for applying to cotton substrates. Two types of MOFs,

Zr-based MOFs (UIO-66-COOH) and Zn-based MOFs (ZIF-8), were investigated and analyzed through a variety of testing results, which indicated that the use of UIO-66-COOH was more advantageous for developing barrier effects of cotton fabrics. The comparison of two synthetic approaches (layer-by-layer and hydrothermal synthesis) showed that the latter could provide more efficient introduction and production of UIO-66-COOH for the assembly of fire barriers onto cotton fabrics. DOPO-HQ was adequately incorporated into porous UIO-66-COOH support. DOPO-HQ@UIO-66-COOH composites dispersion were investigated and applied onto cotton fabrics, which exhibited positive effects on promoting the formation of protective carbonaceous layer and thus maintaining the original morphology of cotton fabrics in the burning process. Compared to pristine cotton, the treated cotton sample performed superior thermal stability and smoke suppression properties in terms of vertical burning test and thermal analysis. Furthermore, the structural barriers composed of DOPO-HQ@UIO-66-COOH and TEOS presented broad prospects for fire protection. It could substantially reduce the redundancy of application process and achieve excellent synergistic barrier effects when DOPO-HQ@UIO-66-COOH was utilized in combination with TEOS for cotton fabrics.

In chapter III, it was found by means of UV-vis spectroscopy that the absorption behavior of cotton tissue to DOPO-HQ@UIO-66-COOH at different temperatures was more in line with that to UIO-66-COOH, suggesting that the formation of DOPO-HQ@UIO-66-COOH composites with ultrasonic assistance was driven predominantly by UIO-66-COOH.

In chapter IV, the main conclusions and future perspectives were summarized.

## RESUMEN

El algodón, al ser una fibra hueca natural con notables valores económicos que incluyen absorción de humedad, permeabilidad al aire, suavidad, comodidad y retención del calor, se ha convertido en una de las materias primas más esenciales para la industria textil. Sin embargo, las fibras de algodón tienen, inherentemente, una alta inflamabilidad y una baja estabilidad térmica. resulta prometedor dotar al algodón de protección contra incendios para ampliar sus campos de aplicación y reducir los riesgos de incendio.

Los nuevos FR libres de halógenos, como los productos químicos que contienen fósforo, los hidróxidos metálicos, los óxidos metálicos, y los que contienen silicio, han despertado mucho interés en la industria. 10-(2,5-dihidroxifenil)-9,10-dihidro-9-oxa-10-fosfafenantreno-10-óxido(DOPO-HQ), elaborado a partir de la reacción de 9,10-dihidro-9-oxa-10- fosfafenantreno-10-óxido (DOPO) y p-benzoquinona, es inherentemente con estabilidad química y resistencia al calor por su propia estructura aromática rígida y enlace P-O-C estable. Las bases metalorgánicas (MOF) con alta cristalinidad y superficie específica son estables a altas temperaturas. Durante el proceso de descomposición térmica, los óxidos metálicos que se generan a partir de las partículas de MOF en algodón, actuarán como una barrera física para proteger el sustrato de mayor combustión y, al mismo tiempo, absorber de manera eficiente los gases y el humo. El ortosilicato de tetraetilo (TEOS) se puede utilizar en combinación con DOPO-HQ para efectos sinérgicos de P/Si y telas de algodón a través de la red Si-O-Si. Funciona como aislamiento térmico y barrera al oxígeno al formar una capa de carbón silíceo y, al mismo tiempo, ayuda a reducir los gases inflamables en la combustión. Impulsado por la demanda actual de seguridad contra incendios y protección ambiental, las barreras estructurales que consisten en DOPO-HQ@UIO-66-COOH y TEOS se ensamblaron con éxito en tejidos de algodón a través de un enfoque sencillo en esta tesis.

En el capítulo I, la introducción general, los objetivos de investigación y la metodología experimental de esta tesis.



En el capítulo II, DOPO-HQ se estudia la mejora del comportamiento frente al fuego de los tejidos de algodón. Estudiar la incorporación adecuada de DOPO-HQ para aplicar sobre sustratos de algodón e investigar y analizar dos tipos de MOF: basados en Zr (UIO-66-COOH) y en Zn (ZIF-8), a través de una variedad de pruebas, cuyos resultados indican que, el uso de UIO-66-COOH es más ventajoso para los efectos de barrera en tejidos de algodón. La comparación de dos enfoques sintéticos (capa por capa y síntesis hidrotérmal) mostró que este último podría dar una introducción y producción más eficiente de UIO-66-COOH para mejorar barreras contra incendios en algodón. Se incorporó adecuadamente DOPO-HQ al soporte poroso UIO-66-COOH. La dispersión de compuestos DOPO-HQ@UIO-66-COOH se aplicó sobre tejidos de algodón, lo que mostró efectos positivos en la mejora de la formación de una capa protectora de carbono y, por lo tanto, en el mantenimiento de la morfología original de los tejidos de algodón en el proceso de combustión. En comparación con el algodón prístino, el algodón tratado, tuvo una estabilidad térmica superior y de supresión de humo en prueba de combustión vertical y análisis térmico. Además, las barreras estructurales compuestas por DOPO-HQ@UIO-66-COOH y TEOS presentaban amplias perspectivas para la protección contra incendios. Cuando se utilizó DOPO-HQ@UIO-66-COOH en combinación con TEOS para tejidos de algodón.

En el capítulo III se encontró, mediante espectroscopía UV-vis, que el comportamiento de absorción del tejido de algodón a DOPO-HQ@UIO-66-COOH a diferentes temperaturas estaba más acorde con el de UIO-66-COOH, sugiriendo que la formación de compuestos DOPO-HQ@UIO-66-COOH con asistencia ultrasónica, mejora la formación de UIO-66-COOH. En el capítulo IV se resumieron las principales conclusiones y perspectivas futuras.

## CONTENTS

<b>ACKNOWLEDGMENTS</b> .....	<b>I</b>
<b>ABSTRACT</b> .....	<b>II</b>
<b>RESUMEN</b> .....	<b>IV</b>
<b>LIST OF TABLES</b> .....	<b>I</b>
<b>LIST OF FIGURES</b> .....	<b>I</b>
<b>ABBREVIATIONS</b> .....	<b>IV</b>
<b>Chapter I. State of the art, objectives and experimental methodology</b> .....	<b>1</b>
1.1 State of the art .....	2
1.1.1 The properties of cotton fiber .....	4
1.1.2 The burning behavior of cotton fiber .....	4
1.1.3 Significance of fire barrier effects for cotton fabrics .....	6
1.1.4 Flame retardants for cotton fabrics .....	6
1.1.4.1 Halogenated flame retardants .....	7
1.1.4.2 Metal hydroxides and metal oxides flame retardants .....	7
1.1.4.3 Phosphorus-containing flame retardants .....	8
1.1.4.4 Nitrogen-containing flame retardants .....	9
1.1.4.5 Silicon-containing flame retardants .....	9
1.1.4.6 Synergistic flame retardant system .....	10
1.1.5 Finishing approaches for barrier effects .....	11
1.1.5.1 Dip-Pad-Dry .....	11
1.1.5.2 LBL Assembly .....	12
1.1.5.3 Sol-Gel .....	12
1.1.5.4 Microcapsule .....	13
1.1.5.5 Plasma technology .....	13
1.2 Objectives of the thesis .....	14
1.3 Experimental methodology .....	15
1.3.1 Materials and Reagents .....	15
1.3.2 Characterization techniques .....	15
1.3.2.1 Particle size and stability evaluation .....	15
1.3.2.2 Fourier transform infrared (FTIR) spectroscopy .....	16
1.3.2.3 Scanning electron microscope (SEM) .....	17
1.3.2.4 Thermal analysis (TGA, DTG) .....	17
1.3.2.5 Ultra violet-visible (UV-vis) spectroscopy .....	18
1.3.2.5 Vertical burning test .....	19
1.3.2.6 Heat transfer test .....	19
1.3.2.7 Tensile strength test .....	20
1.3.2.8 X-ray diffraction analysis (XRD) .....	21
1.4 References .....	22

<b>Chapter II. Fire barrier investigation</b> .....	<b>28</b>
2.1 Introduction .....	29
2.1.1 DOPO-containing compounds.....	29
2.1.2 Metal–organic frameworks (MOFs) .....	31
2.1.2.1 The structure and types of MOFs .....	31
2.1.2.2 The development of MOFs.....	33
2.1.2.3 Applications of MOFs .....	33
2.1.2.4 The flame-retardant mechanism of MOFs .....	35
2.1.2.5 Synthesis methods of MOFs.....	36
2.1.2.6 Approaches for incorporating MOFs with textiles .....	37
2.2 Experimental .....	39
2.2.1 Fire barrier investigation of DOPO-HQ.....	39
2.2.1.1 Preparation of DOPO-HQ finishing solution .....	39
2.2.1.2 The application of DOPO-HQ solution .....	39
2.2.1.3 Conclusions .....	42
2.2.2 Fire barrier investigation of ZIF-8 .....	43
2.2.2.1 Hydrothermal synthesis of ZIF-8 dispersion .....	43
2.2.2.2 The application of ZIF-8 dispersion in combination with BPEI and VTES .....	44
2.2.2.3 The application of ZIF-8 dispersion in combination with DOPO-HQ@CS .....	49
2.2.2.4 The application of ZIF-8 dispersion in combination with DOPO-HQ@PVA .....	54
2.2.2.5 Conclusions .....	57
2.2.3 Fire barrier investigation of UIO-66-COOH .....	59
2.2.3.1 UIO-66-COOH synthesis by LBL assembly .....	60
2.2.3.2 The application of UIO-66-COOH (LBL) in combination with BPEI.....	63
2.2.3.3 Hydrothermal synthesis of UIO-66-COOH homogeneous dispersion .....	66
2.2.3.4 The application of UIO-66-COOH homogeneous dispersion .....	68
2.2.3.5 The application of UIO-66-COOH homogeneous dispersion in combination with BPEI.....	72
2.2.3.6 The application of UIO-66-COOH homogeneous dispersion in combination with BPEI and VTES .....	75
2.2.3.7 Conclusions .....	78
2.2.4 Fire barrier investigation of DOPO-HQ@UIO-66-COOH composites.....	85
2.2.4.1 Sample preparation of DOPO-HQ@UIO-66-COOH dispersion .....	85
2.2.4.2 The visible stability of DOPO-HQ@UIO-66-COOH dispersion .....	86
2.2.4.3 Analysis of DOPO-HQ@UIO-66-COOH composites.....	86

2.2.4.4 The application of DOPO-HQ@UIO-66-COOH composites dispersion .....	88
2.2.4.5 The application of DOPO-HQ@UIO-66-COOH composites dispersion in combination with CS .....	95
2.2.4.6 The application of DOPO-HQ@UIO-66-COOH composites dispersion in combination with TEOS .....	99
2.2.4.7 Conclusions .....	105
2.3 Summary .....	106
2.4 References .....	107
<b>Chapter III. Absorption behavior analysis of cotton fabrics to DOPO- HQ@UIO-66-COOH composites .....</b>	<b>119</b>
3.1 Introduction .....	120
3.2 Absorption behavior analysis of cotton fabrics .....	122
3.2.1 Absorption of DOPO-HQ .....	122
3.2.2 Absorption of UIO-66-COOH .....	132
3.2.3 Absorption of DOPO-HQ@UIO-66-COOH .....	142
3.3 Summary .....	152
3.4 References .....	155
<b>Chapter IV. Final conclusions and future perspectives .....</b>	<b>156</b>
4.1 Final conclusions .....	157
4.2 Future perspectives .....	159
<b>Appendix. List of publications .....</b>	<b>160</b>
<b>Appendix. General bibliography .....</b>	<b>162</b>

## LIST OF TABLES

### Chapter II. Fire barrier investigation

<b>Table 2.1</b>	The treatment data of cotton sample .....	40
<b>Table 2.2</b>	The treatment data of cotton sample .....	45
<b>Table 2.3</b>	TGA data of cotton samples under air atmosphere .....	48
<b>Table 2.4</b>	The treatment data of cotton sample .....	50
<b>Table 2.5</b>	TGA data of cotton samples under air atmosphere .....	53
<b>Table 2.6</b>	The results of tensile breaking strength of cotton fabric before and after treatment .....	56
<b>Table 2.7</b>	Heat transfer index results of cotton fabrics before and after treatment.....	57
<b>Table 2.8</b>	TGA data of cotton samples under air atmosphere .....	62
<b>Table 2.9</b>	TGA data of cotton samples under air atmosphere .....	66
<b>Table 2.10</b>	The properties of UIO-66-COOH homogeneous dispersion ....	67
<b>Table 2.11</b>	The treatment data of cotton sample .....	69
<b>Table 2.12</b>	TGA data of cotton samples under air atmosphere .....	71
<b>Table 2.13</b>	TGA data of cotton samples under air atmosphere .....	75
<b>Table 2.14</b>	TGA data of cotton samples under air atmosphere .....	77
<b>Table 2.15</b>	TGA data of cotton samples under air atmosphere .....	84
<b>Table 2.16</b>	The treatment data of cotton sample .....	89
<b>Table 2.17</b>	TGA data of cotton samples under air atmosphere .....	93
<b>Table 2.18</b>	The treatment data of cotton sample .....	95
<b>Table 2.19</b>	TGA data of cotton samples under air atmosphere .....	98
<b>Table 2.20</b>	The particle size of TEOS finishing solution .....	100
<b>Table 2.21</b>	TGA data of cotton samples under air atmosphere .....	103

### Chapter III. Absorption behavior analysis of cotton fabrics to DOPO-HQ@UIO-66-COOH composites

<b>Table 3.1</b>	The relevant data of 0.5 wt% DOPO-HQ (30 °C) .....	123
<b>Table 3.2</b>	The relevant data of 1 wt% DOPO-HQ (30 °C) .....	124
<b>Table 3.3</b>	The relevant data of 1.5 wt% DOPO-HQ (30 °C) .....	124
<b>Table 3.4</b>	The relevant data of 0.5 wt% DOPO-HQ (60 °C) .....	126
<b>Table 3.5</b>	The relevant data of 1 wt% DOPO-HQ (60 °C) .....	127
<b>Table 3.6</b>	The relevant data of 1.5 wt% DOPO-HQ (60 °C) .....	127
<b>Table 3.7</b>	The relevant data of 0.5 wt% DOPO-HQ (90 °C) .....	129
<b>Table 3.8</b>	The relevant data of 1 wt% DOPO-HQ (90 °C) .....	130
<b>Table 3.9</b>	The relevant data of 1.5 wt% DOPO-HQ (90 °C) .....	131
<b>Table 3.10</b>	The relevant data of 0.5 wt% UIO-66-COOH (30 °C) .....	133
<b>Table 3.11</b>	The relevant data of 1 wt% UIO-66-COOH (30 °C) .....	134
<b>Table 3.12</b>	The relevant data of 1.5 wt% UIO-66-COOH (30 °C) .....	135
<b>Table 3.13</b>	The relevant data of 0.5 wt% UIO-66-COOH (60 °C) .....	136
<b>Table 3.14</b>	The relevant data of 1 wt% UIO-66-COOH (60 °C) .....	137
<b>Table 3.15</b>	The relevant data of 1.5 wt% UIO-66-COOH (60 °C) .....	138
<b>Table 3.16</b>	The relevant data of 0.5 wt% UIO-66-COOH (90 °C) .....	139

<b>Table 3.17</b> The relevant data of 1 wt% UIO-66-COOH (90 °C) .....	140
<b>Table 3.18</b> The relevant data of 1.5 wt% UIO-66-COOH (90 °C) .....	141
<b>Table 3.19</b> The relevant data of 0.5 wt% DOPO-HQ@UIO-66-COOH (30 °C) .....	143
<b>Table 3.20</b> The relevant data of 1 wt% DOPO-HQ@UIO-66-COOH (30 °C) .....	144
<b>Table 3.21</b> The relevant data of 1.5 wt% DOPO-HQ@UIO-66-COOH (30 °C) .....	145
<b>Table 3.22</b> The relevant data of 0.5 wt% DOPO-HQ@UIO-66-COOH (60 °C) .....	146
<b>Table 3.23</b> The relevant data of 1 wt% DOPO-HQ@UIO-66-COOH (60 °C) .....	147
<b>Table 3.24</b> The relevant data of 1.5 wt% DOPO-HQ@UIO-66-COOH (60 °C) .....	148
<b>Table 3.25</b> The relevant data of 0.5 wt% DOPO-HQ@UIO-66-COOH (90 °C) .....	149
<b>Table 3.26</b> The relevant data of 1 wt% DOPO-HQ@UIO-66-COOH (90 °C) .....	150
<b>Table 3.27</b> The relevant data of 1.5 wt% DOPO-HQ@UIO-66-COOH (90 °C) .....	151
<b>Table 3.28</b> The relevant data of DOPO-HQ by KILBY mathematical model.....	152
<b>Table 3.29</b> The relevant data of UIO-66-COOH by KILBY mathematical model .....	153
<b>Table 3.30</b> The relevant data of DOPO-HQ@UIO-66-COOH by KILBY mathematical model .....	153

## LIST OF FIGURES

### Chapter I. State of the art, objectives and experimental methodology

<b>Figure 1.1</b> Chemical structure of cotton .....	4
<b>Figure 1.2</b> Pyrolysis process of cotton fiber [from Ref. (Horrocks, 1983)] ...	5
<b>Figure 1.3</b> Zetasizer nano ZS90 (Malvern).....	16
<b>Figure 1.4</b> Nicolet iS10 FTIR spectrometer (Thermo Fisher) .....	16
<b>Figure 1.5</b> JSM-5610 Scanning electron microscope (JEOL) .....	17
<b>Figure 1.6</b> Thermal analysis system TGA 2 STARe (Mettler-Toledo) .....	18
<b>Figure 1.7</b> UV-2401 PC spectrophotometer (Shimadzu).....	18
<b>Figure 1.8</b> Fire testing setup .....	19
<b>Figure 1.9</b> Convective heat apparatus .....	19
<b>Figure 1.10</b> Universal testing machine (Zwick/Roell) .....	20
<b>Figure 1.11</b> D8 X-ray diffractometer (Bruker) .....	21

### Chapter II. Fire barrier investigation

<b>Figure 2.1</b> Chemical structure of DOPO-HQ .....	31
<b>Figure 2.2</b> Schematic diagram of the MOFs structure.....	32
<b>Figure 2.3</b> Digital photos of cotton samples in the vertical burning test after ignition .....	40
<b>Figure 2.4</b> The SEM images of cotton fabrics before and after combustion .....	41
<b>Figure 2.5</b> Chemical structure of ZIF-8.....	43
<b>Figure 2.6</b> Digital photos of ZIF-8 homogeneous dispersion at different time.....	45
<b>Figure 2.7</b> Digital photos of cotton samples in the vertical burning test after ignition.....	46
<b>Figure 2.8</b> The SEM images of cotton samples before and after combustion .....	47
<b>Figure 2.9</b> TGA and DTG curves of (a) pristine cotton sample, (b) ZIF-8 sample (c) ZIF-8/BPEI sample and (d) ZIF-8/BPEI/VTES sample .....	48
<b>Figure 2.10</b> Digital photos of cotton samples in the vertical burning test after ignition.....	51
<b>Figure 2.11</b> The SEM images of cotton samples before and after combustion .....	52
<b>Figure 2.12</b> TGA and DTG curves of (a) pristine cotton sample (b) DOPO-HQ@CS/ZIF-8 (1BL) sample and (c) DOPO-HQ@CS/ZIF-8 (3BL) sample.....	53
<b>Figure 2.13</b> SEM images of (a) ZIF-8/PVA sample and (b) ZIF-8/DOPO-HQ@PVA sample.....	55
<b>Figure 2.14</b> Chemical structure of UIO-66-COOH.....	59
<b>Figure 2.15</b> Schematic of layer-by-layer synthesis of UIO-66-COOH on cotton substrates .....	60

<b>Figure 2.16</b> The SEM image analysis of pristine cotton and treated samples .....	61
<b>Figure 2.17</b> TGA and DTG curves of (a) pristine cotton sample, (b) UIO-66-COOH (1BL) sample and (c) UIO-66-COOH (2BL) sample .....	62
<b>Figure 2.18</b> The SEM image analysis of treated samples .....	64
<b>Figure 2.19</b> TGA and DTG curves of (a) pristine cotton sample, (b) U2BL-P1 sample, (c) U2BL-P2 sample and (d) U2BL-P3 sample .....	65
<b>Figure 2.20</b> Hydrothermal synthesis of UIO-66-COOH .....	68
<b>Figure 2.21</b> Digital photos of UIO-66-COOH homogeneous dispersion at different time .....	68
<b>Figure 2.22</b> The SEM image analysis of pristine cotton and treated samples .....	70
<b>Figure 2.23</b> TGA and DTG curves of (a) pristine cotton sample, (b) UIO-66-COOH (1L) sample and (c) UIO-66-COOH (2L) sample .....	71
<b>Figure 2.24</b> The SEM image analysis of treated samples .....	73
<b>Figure 2.25</b> TGA and DTG curves of (a) pristine cotton sample, (b) U2P1 sample, (c) U2P2 sample, (d) U2AP1 sample and (e) U2AP2 sample .....	74
<b>Figure 2.26</b> The SEM image analysis of cotton samples .....	76
<b>Figure 2.27</b> TGA and DTG curves of (a) pristine cotton sample, (b) U1AP1V1 sample, (c) U2AP1V1 sample and (d) U1AP1V2 sample .....	77
<b>Figure 2.28</b> Graphical representation of hybrid coating assembled onto cotton fabrics .....	78
<b>Figure 2.29</b> Digital photos of cotton samples in the vertical burning test after ignition .....	79
<b>Figure 2.30</b> The SEM images of (a) pristine cotton, (b) UIO-66-COOH sample, (c) UIO-66-COOH/BPEI sample (d) UIO-66-COOH/BPEI/VTES sample, (e) UIO-66-COOH residual chars, (f) UIO-66-COOH/BPEI residual chars and (g) UIO-66-COOH/BPEI/VTES residual chars .....	81
<b>Figure 2.31</b> The FTIR spectra of pristine cotton and sample UIO-66-COOH/BPEI/VTES .....	82
<b>Figure 2.32</b> TGA and DTG curves of (a) pristine cotton sample (b) UIO-66-COOH sample, (c) UIO-66-COOH/BPEI sample and (d) UIO-66-COOH/BPEI/VTES sample .....	84
<b>Figure 2.33</b> DOPO-HQ@UIO-66-COOH composites dispersion .....	86
<b>Figure 2.34</b> Digital photos of DOPO-HQ@UIO-66-COOH dispersion at different time .....	86
<b>Figure 2.35</b> The comparison results of (a) SEM images and (b) XRD patterns .....	87
<b>Figure 2.36</b> Graphical representation of functionalization treatment process for cotton fabric .....	88
<b>Figure 2.37</b> The SEM images of cotton samples before and after combustion .....	90
<b>Figure 2.38</b> Digital photos of cotton samples in the vertical burning test after ignition .....	91



<b>Figure 2.39</b> TGA and DTG curves of (a) pristine cotton sample, (b) DOPO-HQ@UIO-66-COOH (1L) sample and (c) DOPO-HQ@UIO-66-COOH (10L) sample .....	92
<b>Figure 2.40</b> The FTIR spectra of pristine cotton and DOPO-HQ@UIO-66-COOH (10L) .....	94
<b>Figure 2.41</b> Digital photos of cotton samples in the vertical burning test after ignition .....	96
<b>Figure 2.42</b> TGA and DTG curves of (a) pristine cotton sample, (b) CS/DOPO-HQ@UIO-66-COOH (1BL) sample and (c) CS/DOPO-HQ@UIO-66-COOH (3BL) sample .....	97
<b>Figure 2.43</b> Chemical structure of TEOS .....	99
<b>Figure 2.44</b> Finishing procedure for applying DOPO-HQ@UIO-66-COOH and TEOS onto cotton substrates .....	100
<b>Figure 2.45</b> The SEM images of cotton samples before and after combustion .....	101
<b>Figure 2.46</b> TGA and DTG curves of (a) pristine cotton sample, (b) DOPO-HQ@UIO-66-COOH sample, (c) TEOS sample and (d) DOPO-HQ@UIO-66-COOH/TEOS sample .....	103
<b>Figure 2.47</b> The FTIR spectra of pristine cotton and sample DOPO-HQ@UIO-66-COOH/TEOS .....	104

### Chapter III. Absorption behavior analysis of cotton fabrics to DOPO-HQ@UIO-66-COOH composites

<b>Figure 3.1</b> Calibration curve for UV-vis spectrophotometric determination of DOPO-HQ in aqueous solution ( $\lambda_{\max} = 206.5$ nm) .....	122
<b>Figure 3.2</b> Evolution of DOPO-HQ in different concentration with $t^{1/2}$ at 30 °C .....	125
<b>Figure 3.3</b> Evolution of DOPO-HQ in different concentration with $t^{1/2}$ at 60 °C .....	128
<b>Figure 3.4</b> Evolution of DOPO-HQ in different concentration with $t^{1/2}$ at 90 °C .....	131
<b>Figure 3.5</b> Calibration curve for UV-vis spectrophotometric determination of UIO-66-COOH in aqueous solution ( $\lambda_{\max} = 212.5$ nm) .....	132
<b>Figure 3.6</b> Evolution of UIO-66-COOH in different concentration with $t^{1/2}$ at 30 °C .....	135
<b>Figure 3.7</b> Evolution of UIO-66-COOH in different concentration with $t^{1/2}$ at 60 °C .....	138
<b>Figure 3.8</b> Evolution of UIO-66-COOH in different concentration with $t^{1/2}$ at 90 °C .....	141
<b>Figure 3.9</b> Calibration curve for UV-vis spectrophotometric determination of DOPO-HQ@UIO-66-COOH in aqueous solution ( $\lambda_{\max} = 209.5$ nm) .....	142
<b>Figure 3.10</b> Evolution of DOPO-HQ@UIO-66-COOH in different concentration with $t^{1/2}$ at 30 °C .....	145
<b>Figure 3.11</b> Evolution of DOPO-HQ@UIO-66-COOH in different concentration with $t^{1/2}$ at 60 °C .....	148
<b>Figure 3.12</b> Evolution of DOPO-HQ@UIO-66-COOH in different concentration with $t^{1/2}$ at 90 °C .....	151

**ABBREVIATIONS**

AMEO	Aminopropyltriethoxysilane.
AP	Ammonium phytate
APP	Ammonium polyphosphate
APTES	(3-Aminopropyl)triethoxysilane
BD	Schiff base
BPEI	Branched polyethyleneimine
BTC	1,3,5-benzenetricarboxylate
BDC	1,4-benzenedicarboxylate
BTCA	1,2,3,4-butanetetracarboxylic acid
BL	Bilayer
CTIF	World Fire Statistics by International Association of Fire and Rescue Services
CS	Chitosan
C <sub>4</sub> H <sub>6</sub> N <sub>2</sub>	2-Methylimidazole
DIA	Phosphorus-modified siloxanes
DMF	Dimethylformamide
DOPO	9,10-dihydro-9-oxa-10-phosphaphenanthrene-10-oxide
DOPO-HQ	10-(2,5-dihydroxyphenyl)-9,10-dihydro-9-oxa-10-phosphaphenanthrene-10-oxide
DOPO-VTS	10-(2-trimethoxysilyl-ethyl)-9-hydro-9-oxa-10-phosphaphenanthrene-10-oxide
DOPO-PIP-Si	1-(9,10-dihydro-9-oxa-10-phosphaphenanthrene-10-oxide)-4-(trimethoxysilyl-methyl) piperazine

---

DI	Deionized water
DLS	Dynamic light scattering
DTG	Derivative thermogravimetry
FRs	Flame retardants
FTIR	Fourier transform infrared
H <sub>3</sub> BTC	Trimesic acid
HPCs	Hierarchical porous carbons
IFRs	Intumescent flame retardants
IPDI	Isophorone diisocyanate
IRMOF	Isorecticular Metal Framework
LOI	Limiting oxygen index
LBL	Layer-by-layer
MOFs	Metal–organic frameworks
MMT	Montmorillonite
MAC	Melamine cyanurate
MIL	Materials Institute Lavoisier
PA	Phytic Acid
PKHRR	Peak Heat Release Rate
PVA	Poly(vinyl alcohol)
PEI	Polyethyleneimine
PBB	Polybrominated biphenyls
PBDE	Polybrominated biphenyl ether
RoHS	Restriction of Hazardous Substances
SHP	Sodium hypophosphite

SEM	Scanning electron microscope
TEOS	Tetraethyl orthosilicate
TGA	Thermogravimetric analysis
THF	Tetrahydrofuran
UV-vis	Ultra violet-visible
UiO	University of Oslo
VTES	Vinyltriethoxysilane
ZIF	Zeolitic Imidazolate Framework
$\text{Zn}(\text{CH}_3\text{CO}_2)_2 \cdot 2\text{H}_2\text{O}$	Zinc acetate
$\text{ZrCl}_4$	Zirconium chloride
$T_{10\%}$	Initial decomposition temperature at which 10% sample weight is lost
$T_{\text{max}}$	Temperature of maximum rate of weight loss
$R_{\text{max}}$	Weight loss rate at the maximal peak ( $T_{\text{max}}$ )
$\lambda_{\text{max}}$	Maximum absorption wavelength

## **Chapter I. State of the art, objectives and experimental methodology**

## 1.1 State of the art

With the development of society and science technology, the application of various textile substrates has become increasingly widespread. Yet the loss of people's lives and property caused by frequent textile fires have attracted the attention of government, consumers and manufacturers. The presence and use of textile materials with fire-protection function are able to weaken the burning conditions, delay the spread of fire, and allow people to evacuate or take measures for extinguishing the fire. Therefore, textile flammability regulations have gradually become a significant part of trade barriers in a number of countries.

Cotton fabrics are popular in the textile industry with a long history for their superior characteristics of moisture permeability and comfort-dressing (Zhao et al., 2017). However, compared with wool, silk and some synthetic fibers, the flash point and ignition point of cotton fibers are lower as well with limiting oxygen index (LOI) of 18.4% (Basak et al., 2015; Cheema et al., 2013; Mark et al., 2002), which are considered as flammable or combustible materials, easily causing fire accidents, environmental hazards, personal injury and property losses (Duan et al., 2019). Based on the newest report of World Fire Statistics by International Association of Fire and Rescue Services (CTIF), average of 3.7 million fires and 40.8 thousand fire deaths per year in participating countries were recorded to fire services from 1993-2019. For public safety, it's necessary to endow cotton fabrics with fire barrier effects by using facile and green approach.

As early as 400 B.C., flame retardant materials have been invented for first time, but the demands didn't increase dramatically until the 17<sup>th</sup> century ("A Brief History of FR," 2015). In 1820, it was found that the jute and linen fabrics after incorporating some inorganic substances such as borax, ammonium phosphate and ammonium chloride could obtain flame retardant effects. After testing dozens of compounds, Oppenheim and Versmann discovered that the chemical mixtures containing phosphorus and nitrogen would provide fire protection for fibers in 1859 (Giraud et al., 2016). Over the past several decades, for the goal of inhibiting the combustion of cotton fabrics, halogenated and formaldehyde-based flame retardants (FRs) accounting for a large share of the market have been widely used in textile industry (Wang et al., 2016). They could quench high-

energy radicals through the formation of free radicals, which acted in the gas phase through a low-cost and efficient way (Chen and Wang, 2009). However, most halogen FRs are accompanied by corrosive or toxic gases and fumes, which are generated during the combustion process, becoming environmental hazards by persistence and bio-accumulation, leading to the increasing concerns and threats over human health. Back in 2006, brominated FRs, such as Polybrominated biphenyls (PBB) and Polybrominated biphenyl ether (PBDE) were restricted in Europe as stated in Restriction of Hazardous Substances (RoHS) Directive. Since then, more halogenated FRs were controlled or banned worldwide for promoting halogen-free manufacturing (Lazar et al., 2020). Hence, the development and application of innovative halogen-free chemicals have recently drawn a lot of interest (Costes et al., 2017). By introducing phosphorus-based compounds, nitrogen-based compounds, silicon-based compounds, metal hydroxides and metal oxides, as well as some other types of FRs, the fire-resistance performance of cotton matrix are expected to be enhanced to varying degrees. So far, many previous studies (Chen et al., 2019; Hu et al., 2011) have concentrated on this field but developing fire barrier properties for cotton fibers remains a challenging work. To create an efficient, reliable and structural fire barrier onto cotton matrix, the explanatory studies for the synergistic effects of FRs still need to be explored in depth. Colleoni et al. demonstrated that when cotton fabric was introduced with high concentrations of inorganic reagents by using six layers deposition of silica sol, the heat protection of samples was provided but the wear resistance of the cotton was considerably compromised attributed to the rigid and thick coating (Colleoni et al., 2013). Furthermore, multilayer of sodium phytate and APTES were dispersed uniformly on the surface of cotton with add-on of 33.4 wt% for fire retardant performance (Li et al., 2017). 20 BLs CS/MMT composites were assembled onto cotton fabric by layer-by-layer, which had enhanced the char forming ability of cotton from 2.4 wt% to 8.5 wt% residues as revealed by TGA under nitrogen atmosphere (Choi et al., 2018). However, it's also worth noting to reduce significant impacts on the physical properties of pristine cotton substrate due to excessive weight gain after treatment and avoid the redundancy of application procedure.

### 1.1.1 The properties of cotton fiber

The cotton fiber is mainly composed of cellulose with the chemical formula  $(C_6H_{10}O_5)_n$  as the Figure 1.1 shown, which is the most abundant organic polymer on earth (Gordon and Hsieh, 2007; Varghese and Mittal, 2018). As natural hollow fiber, cotton is inherently with many excellent economic properties such as moisture absorption, air permeability, softness, comfort and warmth retention, making it the most important raw material for textile industry and becoming an indispensable part of people's daily life (Hosseini Ravandi and Valizadeh, 2011; Liu et al., 2014; Yu, 2015). However, cotton fibers are particularly flammable because of the degradation of large molecular chains in the fibers caused by bond cracking when exposed to heat. Heating usually leads to cellulose dehydration and decomposition, which is affected by the temperature, heating rate and the presence of other compounds. At lower temperatures, heating facilitates dehydration and increases subsequent char formation. At higher temperatures, heating causes rapid volatilization through the formation of L-glucose, resulting in the formation of more gaseous combustible products (Hsieh, 2007). To address the flammable nature of cotton fibers, it is essential to understand the combustion characteristics of cotton fibers.

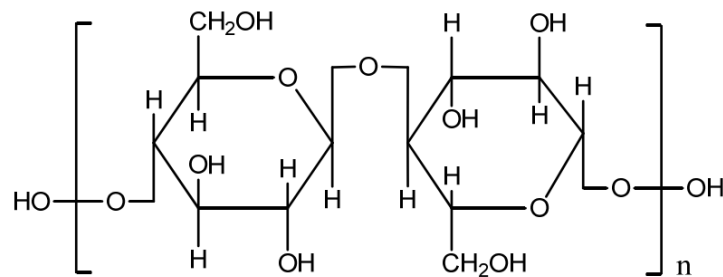


**Figure 1.1** Chemical structure of cotton

### 1.1.2 The burning behavior of cotton fiber

In general, the necessary conditions for combustion are flammability, oxygen and heat source, one of which is indispensable. In addition, when the combustible material is with heat-generating properties, it could burn even without heating; when the combustible material is with polyoxygen structure, it could burn or explode despite the absence of oxygen.



Combustion and pyrolysis are two thermal degradation processes, which can represent the burning behavior of cotton fiber. Under the effect of heat, cellulose combustion is the process of oxidation by consuming the pyrolysis products and generating excess heat. The most crucial point of the burning process of cotton fibers is the pyrolysis. The pyrolysis process of cellulose is relatively complicated, and it is believed that when the temperature is over 350 °C, the pyrolysis reaction is mainly in two directions based on many scholarly studies (Zhu et al., 2004). (1) Cellulose is dehydrated and carbonized to generate water, carbon dioxide and solid residue. (2) The non-volatile liquid L-glucose is caused by cellulose depolymerization. As the L-glucose is further cracked, accompanied by the formation of low molecular weight lysates and secondary char. With the presence of oxygen, the flammable pyrolysis products of L-glucose are further oxidized and make a lot of heat, which will promote more cellulose cleavage. Furthermore, these two reactions are competing reactions and simultaneously present in the entire pyrolysis process of cellulose as Figure 1.2 shown (Horrocks, 1983).

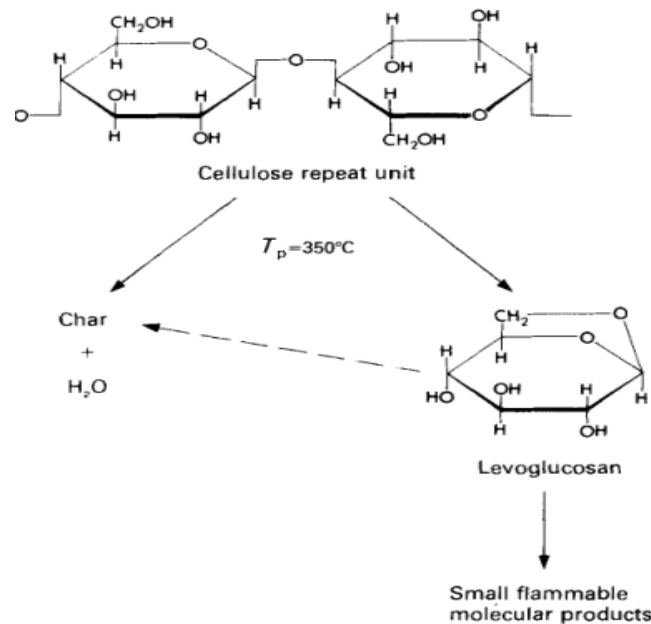


**Figure 1.2** Pyrolysis process of cotton fiber [from Ref. (Horrocks, 1983)]

The pyrolysis of cellulose is generally viewed as a relatively complex process. One of the most widely used analytical tools for studying the pyrolysis of cellulose is thermogravimetric analysis (TGA). It can be utilized for the thermal characterization of both inorganic and organic materials, including cellulose and other polymers. From the TGA results, not only quantitative data on the loss of

sample mass as a function of increasing temperature or time but also essential information about the thermal properties of the material and its composition can be obtained. Additionally, derivative thermogravimetry (DTG) is useful to investigate the differences between TGA curves (Cabralés and Abidi 2010).

### **1.1.3 Significance of fire barrier effects for cotton fabrics**

The consumption of textile products and varieties shows an increasing trend year by year, and their applications cover all aspects of real life such as transportation, medical, military, and industrial (Schwarz and Kovacevic, 2017). However, due to their flammability, textile items have become a potential source of fire incidents over time. As abundant cotton is with many performance advantages, the production of cotton fabrics accounts for a large proportion of textiles produced around the world, which is of great significance to make fire barrier effects for cotton fabrics. In addition to the fact that natural cotton fibers are easier to catch fire than wool, silk and other synthetic fibers, the potential generated gas toxicities of cotton combustion are relatively stronger than other fibers (Materials, 1979). As a result, to strengthen the fire performances of cotton fabrics is a critical topic to be studied in depth.

### **1.1.4 Flame retardants for cotton fabrics**

Researchers in both industrial and academic fields have been working on the development of various flame retardants (Alongi et al., 2013a). Typically, flame retardants (FRs) work in one or more of the following ways. (1) Eliminate heat; (2) Increase the decomposition temperature, at which a large amount of volatile substances will be produced; (3) Reduce the formation and carbonization of volatile gases and combustible gases (4) Prevent oxygen from entering the flame or dilute the flame; (5) Increase the ignition temperature of gaseous fuel and interfere with the chemical reaction of the flame (Horrocks, 2008). In the past, halogen FRs were popular for their low dosage and good retardancy effects on cotton fabrics. But in order to meet environmental regulatory requirements, the halogen containing FRs are gradually phased out and banned. At present, the development of halogen-free, non-toxic, low-smoke FRs for cotton textiles has become one of the hot spots (Alongi et al., 2013b).

#### **1.1.4.1 Halogenated flame retardants**

Due to the halogenated flame retardant has the advantages of low price, good stability, low dosage, etc., it has become the most extensively used class of organic FRs (Marturano et al., 2017). Among them, bromine, chlorine, fluorine and iodine are the elements in the chemical group known as halogens, but the most common ones are chlorine compounds and bromine compounds because of their good flame-retardant effects and the availability of raw materials. Specifically, polybrominated diphenyl ether (PBDE) is frequently used for cotton, polyester and its blended fabrics (Saini et al., 2016). Halogenated FRs are highly efficient that work in both gas and condensed phases, primarily achieving the effects by inhibiting the chain-branching reaction in the gas phase (Chen and Wang, 2009).

However, in the case of high temperature or flame, the products of halogenated flame retardant are corrosive and toxic, as well as producing thick smoke in the combustion process, which in turn cause certain influence on the environment (Venier et al., 2015). As people pay more and more attention to environmental protection and ecological problems, halogen-based FRs gradually recede from the stage of history, and halogen-free FRs have become popular research topic because of their advantages such as less smoke and non-toxic safety (Levința et al., 2019; Shaw, 2010).

#### **1.1.4.2 Metal hydroxides and metal oxides flame retardants**

Metal hydroxides and metal oxides flame retardants are the most representative type of inorganic FRs that they can prevent the matrix materials from fumes and dripping, when they are heated and decomposed without generating smokes. Aluminum hydroxide, magnesium hydroxide, water talc are the main inorganic hydrated metal compounds, of which aluminum hydroxide is the most prevalent inorganic flame-retardant products because of its non-toxic and superior stability (Liu et al., 2020). Adding aluminum hydroxide into the polymeric materials can reduce the concentration of combustible polymers on one hand, and on the other hand, aluminum hydroxide will start dehydration and endothermic decomposition to generate water vapor around 250 °C, which reduces the surface temperature

of polymers and the concentration of combustible substances and oxygen to avoid the further temperature rise and inhibit the combustion of polymers (Ratna, 2012; Wang et al., 2010). Besides, aluminum hydroxide will generate  $\text{Al}_2\text{O}_3$  on the surface of the polymers. It has a significant flame-retardant effect in the early stage of combustion as a result of the low dehydration temperature of aluminum hydroxide. Nevertheless, metal hydroxides and metal oxides are mainly filler-type FRs, the addition of which will affect the processing properties and mechanical properties of materials to a different extent (Chen and Wang, 2009; Höfer, 2012).

#### **1.1.4.3 Phosphorus-containing flame retardants**

Phosphorus-containing flame retardants is one of the most important FRs for the modification of textile fabrics. According to the differences in chemical composition and molecular structure of phosphorus-containing FRs, they can be divided into three types, organic phosphorus, inorganic phosphorus and phosphorus-based intumescent flame retardants (IFRs) (Levchik, 2014; Velencoso et al., 2018). Organic phosphorus FRs are mainly additive FRs with dual functions of flame retardancy and plasticization, including phosphoric acid esters, organic phosphates, etc.. Inorganic phosphorus FRs are mainly red phosphorus, ammonium polyphosphate (APP). Phosphorus-based IFRs are composed of acid source, carbon source and air source (Bourbigot et al., 2004; Ma et al., 2007). In the combustion process, phosphorus-containing FRs generate phosphoric acid, metaphosphoric acid and other derivatives that could catalyze the dehydration and carbonization of fabrics, forming a dense carbon layer to inhibit the production of L-glucose, while the surface of unburned substrates is covered with phosphoric acid derivatives in solid or liquid film that prevents oxygen from entering and free radicals from escaping (P.M and Arao, 2015). At the same time, phosphoric acid derivatives can react with the hydroxymethyl groups of substrates to form P-O-C bond, which causes the formation of a polyaromatic network structure with high thermal stability on the surface of substrates, thus inhibiting the continued burning of materials. Furthermore, the presence of  $\text{PO}\cdot$  and  $\text{HPO}\cdot$  free radicals during combustion can capture the  $\text{H}\cdot$  or  $\text{OH}\cdot$  free radicals in the gas phase and promote the formation

of intumescent carbon layer on the surface of the fabrics to isolate oxygen and heat (Siriviriyannun et al., 2008; Xing et al., 2011).

#### **1.1.4.4 Nitrogen-containing flame retardants**

Nitrogen-containing flame retardants decompose and absorb heat in the combustion process, which can reduce the surface temperature of substrates, and produce incombustible gases such as  $N_2$ ,  $H_2O$ ,  $CO_2$ . On the one hand, these gases will reduce the concentration of combustible substances and oxygen. On the other hand, nitrogen-containing compounds decompose into nitrogen oxides that can react with the free radicals in the combustion system, reducing the concentration of free radicals and suppressing the further burning (Gaan et al., 2008; Levchik, 2007). Nitrogen-containing FRs have the characteristics of low toxicity and high efficiency of flame retardancy. Melamine, melamine cyanurate (MAC) FRs are the most typical representatives of nitrogen-based FRs (Luo et al., 2019). Nitrogen-containing FRs are generally not used alone in the flame-retardant finishing of cotton fabrics. They are usually used associated with phosphorus, silicon and other types of flame retardants to achieve a synergistic effect (Xie et al., 2013).

#### **1.1.4.5 Silicon-containing flame retardants**

In addition to excellent flame-retardant properties, silicon-containing flame retardants also have high thermal stability and environment-friendliness (Kilinc, 2014). Silicon-containing FRs mainly exist in the form of silica, organosilanes, silicones (polysiloxanes) and silicates (Rezvani Ghomi et al., 2020). In terms of mechanism, the silicon-containing compounds can form a siliceous carbon layer when the material is thermally decomposed, which can prevent the burning of materials by heat insulation and oxygen barrier (Kashiwagi et al., 2000). Meanwhile, it also reduces the overflow of flammable gas and achieves the desired flame-retardant results (Carosio et al., 2011).

#### **1.1.4.6 Synergistic flame retardant system**

With the widespread use of single-series FRs, people start to prepare novel flame retardants containing two or more retardancy elements through chemical synthesis or compounding methods (Wang, 2016). The synergistic effect is greater than the sum of the flame-retardant effect of each component applied separately. Synergistic flame retardants can significantly improve the fire retardancy properties of cotton fabrics with the advantages of flexible use and lower cost (Lewin, 2001).

The following are some of the common combinations of flame retardants.

##### **Phosphorus-Nitrogen containing FRs**

Phosphorus-nitrogen containing FRs can promote char formation in the presence of polyhydroxy compounds, and reduce the production of combustibles during the pyrolysis process (Toldy et al., 2006). The principle is that the phosphorus-containing components are heated to release polyphosphoric acid, which can not only inhibit the production of L-glucose, but also can help the carbonization of cellulose. In the meantime, nitrogen-containing components decompose at high temperatures to generate non-combustible gases. The protective layers will be formed by the non-combustible gases and decomposition products of phosphorus-containing components. The insulating layers are composed of phosphorus-carbon, which is able to make the polymer material expand and greatly reduce the thermal conductivity (Chang et al., 2007; Jiang et al., 2015).

##### **Phosphorus-Silicon containing FRs**

Phosphorus-silicon containing FRs are pyrolyzed to produce polyphosphoric acid, which promotes the dehydration of cotton fibers into char. At the same time, the compounds are helpful to generate silicon-carbon layers during the combustion process, which has the functions of isolating internal and external heat transfer, as well as oxygen exchange. Based on the above, the main fire retardancy behaviors of phosphorus-silicon synergistic effects have been reflected. (Cireli et al., 2007; Hamdani - Devarenes et al., 2009).

## **Nitrogen-Silicon containing FRs**

In the synergistic system of nitrogen-silicon containing FRs, silicon-containing part have the actions of promoting carbon formation, and the nitrogen components play an important role in the gas phase. In the combustion process of substrates, they always work together in both gas phase and condensed phase (Agrawal and Narula, 2014).

## **Phosphorus-Nitrogen-Silicon containing FRs**

In the phosphorus-nitrogen-silicon synergistic system, phosphorus-containing compounds are decomposed by heat to form chemical substances such as phosphoric acid, which further promote the dehydration and carbonization of textile substrates. The formation of carbon layers can contribute to hindering the transfer of heat, while the thermal decomposition of nitrogen-containing compounds will produce ammonia and other non-combustible gases, which could affect and dilute the combustible gases that generated in the burning process. The silicon dioxide formed by silicon-containing compounds after heating help to make further efforts for thickening the carbon layer and attaining the retarding effect. The flame retardant containing silicon, nitrogen and phosphorus can effectively shorten the finishing time in the treatment process, and improve the firmness of FRs applied on the surface of substrates (Kappes et al., 2016; Wang et al., 2016).

### **1.1.5 Finishing approaches for barrier effects**

For imparting barrier effects to cotton fabrics, there are a variety of application methods, the most widely used and classic of which are process of dip-pad-dry. In addition, graft polymerization, LBL assembly, sol-gel, etc. are also the common and available techniques.

#### **1.1.5.1 Dip-Pad-Dry**

The " dip-pad-dry " process is a certain amount of flame retardants or some other auxiliary solution for as padding finishing liquid. This method for treatment of cellulosic fabrics is quite common and appropriate (Cassidy and Goswami, 2017).

"Dip" is to immerse textile fabric onto finishing liquid for a certain time. "Pad" is to utilize padding mangle with stable pressure and speed for helping the textile fabric to acquire uniform rolling liquid effect and maintain a certain amount of liquid; "Dry" is to dry the moisture contained in the fabric, and make the fabric retain the amount of finishing liquid required by the process.

#### **1.1.5.2 LBL Assembly**

Layer-by-layer (LBL) assembly technology is a kind of new process for surface modification that was rapidly developed in the 1990s. The polyelectrolyte self-assembled multilayers are produced by alternating deposition of oppositely charged polyelectrolyte solutions. In addition to electrostatic interactions, hydrogen bonding, covalent bonding and donor-acceptor interactions are also contributed to the intermolecular binding forces of multilayers (Carosio et al., 2015; Li et al., 2010). Compared with other traditional coating methods for cotton fabric, the superiority of LBL assembly technology is general convenience and nanometer-level thickness (Huang et al., 2012). It could impart flame retardancy and thermal stability to cotton textiles with minimal impact on the environment (Guin et al., 2014).

#### **1.1.5.3 Sol–Gel**

The sol-gel technique is a wet chemical nanotechnology of preparing materials under mild conditions. More than a century ago, Ebelment successfully synthesized silica by the sol-gel method for the first time (Livage, 2004). Sol-Gel technique is used for inorganic substances such as metal alkoxide that act as precursors. The raw materials are uniformly mixed in the liquid phase. The stable transparent sol system is formed via two steps known as hydrolysis and polycondensation reactions. After the sol is aged, the colloidal particles slowly polymerize to form a gel with a three-dimensional network structure. Gels are dried, sintered and cured to prepare molecular and even nano sub-structured materials (Alongi et al., 2011a, 2011b).



#### **1.1.5.4 Microcapsule**

Firstly, the flame retardants will be wrapped into the microcapsules, then the substrates will be immersed into the solution of FR microcapsules and reactive resin (Bojana and Marica, 2016). Finally, the FR microcapsules could be firmly deposited onto textile substrates after the process of curing. Microcapsules are useful for some flame-retardants with smaller molecules that can't react with polymer materials, allowing the textile fabric to achieve a particular level of fire retardancy function.

#### **1.1.5.5 Plasma technology**

Plasma technology is an effective surface treatment solution for a variety of materials that is gaining popularity (Chu et al., 2002). Studies (Huong et al., 2020) have found that grafting flame-retardants onto the surface of textile substrates through plasma technology could acquire better treatment results and higher mechanical strength. But compared with other finishing approaches, the cost of plasma technology is relatively significant.

## 1.2 Objectives of the thesis

The general goal of this thesis is to construct structural protective barriers onto cotton fabrics by using a facile and green approach and investigate the effects of fire performances. Metal–organic frameworks (MOFs) and DOPO-containing compounds will be used in combination with other polymeric materials for cotton fabrics to produce organic-inorganic composites that function efficiently and synergistically for fire protection.

In order to achieve this aim, it's desirable to divide it into the following specific objectives.

- (1) To incorporate MOFs at the micro/nano-scale into cotton substrates either individually or in combination with other polymeric materials for comparing the differences in fire performance.
- (2) To explore the appropriate ways to introduce DOPO-containing chemicals on cotton substrates and thus develop the structural barriers.
- (3) To avoid the use of toxic and ecologically damaging reagents and simultaneously reduce the redundancy of application procedure.

## 1.3 Experimental methodology

### 1.3.1 Materials and Reagents

Commercial bleached cotton twill fabric with 250 g/m<sup>2</sup> were used for functionalization treatments.

10-(2,5-dihydroxyphenyl)-9,10-dihydro-9-oxa-10-phosphaphenanthrene-10-oxide (DOPO-HQ) was offered by Alfa Chemistry Co., Ltd (Zhengzhou City, China). Vinyltriethoxysilane (VTES) was provided by Qingdao Hengda Zhongcheng Technology Co., Ltd (Qingdao City, China). Zinc acetate (Zn(CH<sub>3</sub>CO<sub>2</sub>)<sub>2</sub>·2H<sub>2</sub>O) was sourced from Panerac Quimica SA company (Barcelona, Spain). Low molecular weight chitosan (CS), Zirconium chloride (ZrCl<sub>4</sub>), Trimesic acid (H<sub>3</sub>BTC), Branched polyethyleneimine (BPEI) (Mw 25,000), 2-Methylimidazole (C<sub>4</sub>H<sub>6</sub>N<sub>2</sub>), and Tetraethyl orthosilicate (TEOS) were all purchased from Aldrich Chemicals company (St. Louis, MI, USA).

All chemicals were employed as received without additional purification. Deionized water (DI) was used in all experiments.

### 1.3.2 Characterization techniques

#### 1.3.2.1 Particle size and stability evaluation

The particle size of all prepared samples was analyzed by Malvern Zetasizer nano ZS90 (UK) by Dynamic light scattering (DLS) technique. DLS is a non-invasive approach for measuring the size of particles that has been extensively utilized in physics, chemistry, material science and other fields (Sakho et al., 2017). The visible stability of MOFs homogeneous dispersion was observed by digital photos of samples at different time.



**Figure 1.3** Zetasizer nano ZS90 (Malvern)

### 1.3.2.2 Fourier transform infrared (FTIR) spectroscopy

Fourier-transform infrared spectroscopy (FTIR) is one of valuable and user-friendly research tools for the surface chemistry of different membranes with specific application (Mohamed et al., 2017). It's a technique to acquire the infrared spectrum of solid, liquid and gas by absorption or emission. FTIR can simultaneously collect data with high spectral resolution over a wide spectral range. It has significant advantages over dispersive spectrometers, which is able to measure intensities in a narrow wavelength range at once (Griffiths and Haseth, 2007). FTIR spectra of all the samples were measured by Nicolet iS10 FTIR spectrometer (Thermo Fisher, USA). The scanning wavelength range was 4000–500  $\text{cm}^{-1}$  and the spectral resolution was 4  $\text{cm}^{-1}$ .



**Figure 1.4** Nicolet iS10 FTIR spectrometer (Thermo Fisher)

### 1.3.2.3 Scanning electron microscope (SEM)

A scanning electron microscope (SEM) is a type of electron microscope that produces an image of a sample by scanning the surface with a focused beam of electrons. Electrons interact with atoms in the sample to produce a variety of signals that contain information about the surface topography and composition of the sample. The electron beam is scanned in a raster scan pattern and the position of the electron beam is combined with the intensity of the detected signal to produce an image. In the most common SEM mode, a secondary electron detector is used to detect the secondary electrons emitted by the atoms excited by the electron beam. The number of secondary electrons that can be detected and the signal strength depend in particular on the topography of the sample. SEM can achieve a resolution of better than 1 nm (Parvez, 2019). The morphology of the cotton fiber and the residual carbon were observed by using SEM (JSM-5610, JEOL, Japan) installed at imaging platform center of Polytechnic University of Catalonia (UPC) at an acceleration voltage of 10 kV.



**Figure 1.5** JSM-5610 Scanning electron microscope (JEOL)

### 1.3.2.4 Thermal analysis (TGA, DTG)

Thermogravimetric analysis (TGA) is an analytical technique in which the mass of the sample is monitored as a function of temperature or time for evaluating the thermal stability of materials (Mudalige et al., 2019). The device consists of a highly sensitive scale for measuring weight changes and a programmable furnace for controlling the heat of the sample. The balance is located above the furnace and is isolated from the heat. A commercial TGA equipment is able to

have an equilibrium sensitivity of  $0.1\mu\text{g}$  at  $> 1000\text{ }^{\circ}\text{C}$  in air or another gaseous atmosphere, as well as a variable controlled ramp-up rate. The rate capability of the TGA can be varied between  $0.1\text{ }^{\circ}\text{C}/\text{min}$  and  $200\text{ }^{\circ}\text{C}/\text{min}$  (Ebnesajjad, 2014). Derivative thermogravimetry (DTG) is a thermal analysis in which the rate of change of material weight during heating is plotted against temperature (Cazes, 2004). The thermal properties of cotton fabrics were evaluated by using Thermal analysis system TGA 2 STARe (Mettler-Toledo, Switzerland). All the samples were loaded into alumina holder and heated from  $30\text{ }^{\circ}\text{C}$  to  $800\text{ }^{\circ}\text{C}$  with heating rate of  $10\text{ }^{\circ}\text{C}\cdot\text{min}^{-1}$  and gas flow of  $50\text{ ml}\cdot\text{min}^{-1}$ . The tests were measured under air atmosphere in this thesis.



**Figure 1.6** Thermal analysis system TGA 2 STARe (Mettler-Toledo)

### 1.3.2.5 Ultra violet-visible (UV-vis) spectroscopy

Ultra violet-visible (UV-vis) spectroscopy is one of the significant characterization techniques to identify UV-visible light that is absorbed by molecules (Pentassuglia et al., 2018). UV-2401 PC spectrophotometer (Shimadzu, Japan) was used to make quantitative measurements for prepared DOPO-HQ, UIO-66-COOH, and DOPO-HQ@UIO-66-COOH samples, specifically for concentration analysis.



**Figure 1.7** UV-2401 PC spectrophotometer (Shimadzu)

### 1.3.2.5 Vertical burning test

Drawing on the ASTM D6413 testing method, the control and treated fabric strips were conducted on a self-made flame testing setup. Samples measuring 280 mm × 75 mm were fixed at the same position and then exposed to a vertical flame. Subsequently the burning behavior of all the samples were observed and recorded by digital camera.



**Figure 1.8** Fire testing setup

### 1.3.2.6 Heat transfer test

According to EN ISO 9151 standard, the sample is held and exposed to an incident heat flux of  $80 \text{ kW/m}^2 \pm 5\%$ . The heat transmission is measured by a calorimeter located above the fabric and in contact with it. Time is recorded that the sample can remain exposed before its calorimeter's temperature rise of  $24 \text{ }^\circ\text{C} \pm 0.2 \text{ }^\circ\text{C}$ .



**Figure 1.9** Convective heat apparatus

### 1.3.2.7 Tensile strength test

The tensile test is the most fundamental mechanical technique for identifying how materials will respond to tension load (Smith and Mishra, 2014). The mechanical properties of cotton fabric samples were calculated on Universal tensile testing machine (Zwick/Roell, ProLine). The samples ( $300 \times 30 \text{ mm}^2$ ) were tested according with a tensile speed of 100 mm/min. The critical indicators of Young's modulus, breaking strength and elongation at break were recorded for comparison.



**Figure 1.10** Universal testing machine (Zwick/Roell)



### 1.3.2.8 X-ray diffraction analysis (XRD)

In 1912, Max von Laue discovered that for X-ray wavelengths, crystalline matter could act as a three-dimensional diffraction grating, similar to the spacing of planes in a crystal lattice (Inan, 2017). Nowadays, X-ray diffraction analysis (XRD) is a microstructural analysis method used to study crystal structures and atomic spacings. It can be used to evaluate minerals, polymers, corrosion products and unknown materials. For the powder samples obtained in our study, the XRD experiments were performed on Bruker D8 diffractometer (Madison, WI, USA) with a step size of  $0.02^\circ$  at room temperature.

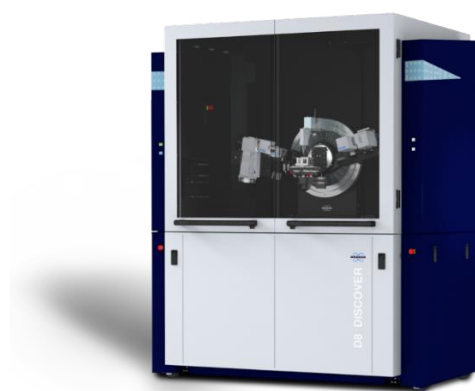


**Figure 1.11** D8 X-ray diffractometer (Bruker)

## 1.4 References

- A Brief History of FR, 2015. WorkingPerson.me. URL <https://workingperson.me/a-brief-history-of-fr/> (accessed 1.7.21).
- Agrawal, S., Narula, A.K., 2014. Synthesis and characterization of phosphorus- and silicon-containing flame-retardant curing agents and a study of their effect on thermal properties of epoxy resins. *J Coat Technol Res* 11, 631–637. <https://doi.org/10.1007/s11998-014-9579-6>
- Alongi, J., Carletto, R., Bosco, F., Carosio, F., Di Blasio, A., Cuttica, F., Antonucci, V., Giordano, M., Malucelli, G., 2013a. Caseins and hydrophobins as novel green flame retardants for cotton fabrics. *Polymer Degradation and Stability* 99. <https://doi.org/10.1016/j.polymdegradstab.2013.11.016>
- Alongi, J., Carletto, R.A., Di Blasio, A., Cuttica, F., Carosio, F., Bosco, F., Malucelli, G., 2013b. Intrinsic intumescent-like flame retardant properties of DNA-treated cotton fabrics. *Carbohydrate Polymers* 96, 296–304. <https://doi.org/10.1016/j.carbpol.2013.03.066>
- Alongi, J., Ciobanu, M., Malucelli, G., 2011a. Novel flame retardant finishing systems for cotton fabrics based on phosphorus-containing compounds and silica derived from sol–gel processes. *Carbohydrate Polymers* 85, 599–608. <https://doi.org/10.1016/j.carbpol.2011.03.024>
- Alongi, J., Ciobanu, M., Malucelli, G., 2011b. Sol–gel treatments for enhancing flame retardancy and thermal stability of cotton fabrics: optimisation of the process and evaluation of the durability. *Cellulose* 18, 167–177. <https://doi.org/10.1007/s10570-010-9470-2>
- Basak, S., Samanta, K.K., Chattopadhyay, S.K., 2015. Fire retardant property of cotton fabric treated with herbal extract. *The Journal of The Textile Institute* 106, 1338–1347. <https://doi.org/10.1080/00405000.2014.995456>
- Bojana, B.P., Marica, S., 2016. Microencapsulation technology and applications in added-value functional textiles. *Physical Sciences Reviews* 1. <https://doi.org/10.1515/psr-2015-0003>
- Bourbigot, S., Bras, M.L., Duquesne, S., Rochery, M., 2004. Recent Advances for Intumescent Polymers. *Macromolecular Materials and Engineering* 289, 499–511. <https://doi.org/10.1002/mame.200400007>
- Cabrales, Luis, and Nouredine Abidi. 2010. 'On the Thermal Degradation of Cellulose in Cotton Fibers'. *Journal of Thermal Analysis and Calorimetry* 102 (November): 485–91. <https://doi.org/10.1007/s10973-010-0911-9>.
- Carosio, F., Fontaine, G., Alongi, J., Bourbigot, S., 2015. Starch-Based Layer by Layer Assembly: Efficient and Sustainable Approach to Cotton Fire Protection. *ACS Appl. Mater. Interfaces* 7, 12158–12167. <https://doi.org/10.1021/acsami.5b02507>
- Carosio, F., Laufer, G., Alongi, J., Camino, G., Grunlan, J.C., 2011. Layer-by-layer assembly of silica-based flame retardant thin film on PET fabric. *Polymer Degradation and Stability* 96, 745–750. <https://doi.org/10.1016/j.polymdegradstab.2011.02.019>
- Cassidy, T., Goswami, P., 2017. *Textile and Clothing Design Technology*. CRC Press.
- Cazes, J., 2004. *Analytical Instrumentation Handbook*. CRC Press.
- Chang, S., Sachinvala, N., Sawhney, P., Parikh, D., Jarrett, W., Grimm, C., 2007. Epoxy phosphonate crosslinkers for providing flame resistance to cotton

- textiles. *Polymers for Advanced Technologies* 18, 611–619. <https://doi.org/10.1002/pat.867>
- Cheema, H.A., El-Shafei, A., Hauser, P.J., 2013. Conferring flame retardancy on cotton using novel halogen-free flame retardant bifunctional monomers: synthesis, characterizations and applications. *Carbohydrate Polymers* 92, 885–893. <https://doi.org/10.1016/j.carbpol.2012.09.081>
- Chen, L., Wang, Y.-Z., 2009. A review on flame retardant technology in China. Part I: development of flame retardants. <https://doi.org/10.1002/PAT.1550>
- Chen, T., Hong, J., Peng, C., Chen, G., Yuan, C., Xu, Y., Zeng, B., Dai, L., 2019. Superhydrophobic and flame retardant cotton modified with DOPO and fluorine-silicon-containing crosslinked polymer. *Carbohydrate Polymers* 208, 14–21. <https://doi.org/10.1016/j.carbpol.2018.12.023>
- Choi, K., Seo, S., Kwon, H., Kim, D., Park, Y.T., 2018. Fire protection behavior of layer-by-layer assembled starch–clay multilayers on cotton fabric. *J Mater Sci* 53, 11433–11443. <https://doi.org/10.1007/s10853-018-2434-x>
- Chu, P.K., Chen, J.Y., Wang, L.P., Huang, N., 2002. Plasma-surface modification of biomaterials. *Materials Science and Engineering: R: Reports* 36, 143–206. [https://doi.org/10.1016/S0927-796X\(02\)00004-9](https://doi.org/10.1016/S0927-796X(02)00004-9)
- Cireli, A., Onar, N., Ebeoglugil, M.F., Kayatekin, I., Kutlu, B., Culha, O., Celik, E., 2007. Development of flame retardancy properties of new halogen-free phosphorous doped SiO<sub>2</sub> thin films on fabrics. *J. Appl. Polym. Sci.* 105, 3748–3756. <https://doi.org/10.1002/app.26442>
- Colleoni, C., Donelli, I., Freddi, G., Guido, E., Migani, V., Rosace, G., 2013. A novel sol-gel multi-layer approach for cotton fabric finishing by tetraethoxysilane precursor. *Surface and Coatings Technology* 235, 192–203. <https://doi.org/10.1016/j.surfcoat.2013.07.033>
- Costes, L., Laoutid, F., Brohez, S., Dubois, P., 2017. Bio-based flame retardants: When nature meets fire protection. *Materials Science and Engineering: R: Reports* 117, 1–25. <https://doi.org/10.1016/j.mser.2017.04.001>
- Duan, H., Ji, S., Yin, T., Tao, X., Chen, Y., Ma, H., 2019. Phosphorus–nitrogen - type fire - retardant vinyl ester resin with good comprehensive properties. *J Appl Polym Sci* 136, 47997. <https://doi.org/10.1002/app.47997>
- Ebnesajjad, S., 2014. Chapter 4 – Surface and Material Characterization Techniques. undefined.
- Gaan, S., Sun, G., Hutches, K., Engelhard, M.H., 2008. Effect of nitrogen additives on flame retardant action of tributyl phosphate: Phosphorus–nitrogen synergism. *Polymer Degradation and Stability* 93, 99–108. <https://doi.org/10.1016/j.polymdegradstab.2007.10.013>
- Giraud, S., Rault, F., Cayla, A., Salaün, F., 2016. HISTORY AND EVOLUTION OF FIRE RETARDANTS FOR TEXTILES.
- Gordon, S., Hsieh, Y.-L. (Eds.), 2007. Introduction, in: *Cotton, Woodhead Publishing Series in Textiles*. Woodhead Publishing, pp. xv–xx. <https://doi.org/10.1016/B978-1-84569-026-7.50020-2>
- Griffiths, P.R., Haseth, J.A.D., 2007. *Fourier Transform Infrared Spectrometry*. John Wiley & Sons.
- Guin, T., Kreckler, M., Milhorn, A., Grunlan, J.C., 2014. Maintaining hand and improving fire resistance of cotton fabric through ultrasonication rinsing of multilayer nanocoating. *Cellulose* 21, 3023–3030. <https://doi.org/10.1007/s10570-014-0286-3>

- Hamdani - Devarenes, S., Longuet, C., Perrin, D., Lopez-cuesta, J.-M., Ganachaud, F., 2009. Flame retardancy of silicone-based materials. *Polymer Degradation and Stability* 94, 465–495. <https://doi.org/10.1016/j.polymdegradstab.2008.11.019>
- Höfer, R., 2012. 10.21 - Processing and Performance Additives for Plastics, in: Matyjaszewski, K., Möller, M. (Eds.), *Polymer Science: A Comprehensive Reference*. Elsevier, Amsterdam, pp. 369–381. <https://doi.org/10.1016/B978-0-444-53349-4.00272-7>
- Horrocks, A.R., 2008. Flame-retardant Finishing of Textiles. *Review of Progress in Coloration and Related Topics* 16, 62–101. <https://doi.org/10.1111/j.1478-4408.1986.tb03745.x>
- Horrocks, A.R., 1983. An Introduction to the Burning Behaviour of Cellulosic Fibres. *Journal of the Society of Dyers and Colourists* 99, 191–197. <https://doi.org/10.1111/j.1478-4408.1983.tb03686.x>
- Hosseini Ravandi, S.A., Valizadeh, M., 2011. 2 - Properties of fibers and fabrics that contribute to human comfort, in: Song, G. (Ed.), *Improving Comfort in Clothing*, Woodhead Publishing Series in Textiles. Woodhead Publishing, pp. 61–78. <https://doi.org/10.1533/9780857090645.1.61>
- Hsieh, Y.L., 2007. Chemical structure and properties of cotton, in: *Cotton*. Elsevier, pp. 3–34. <https://doi.org/10.1533/9781845692483.1.3>
- Hu, S., Hu, Y., Song, L., Lu, H., 2011. Effect of modified organic–inorganic hybrid materials on thermal properties of cotton fabrics. *J Therm Anal Calorim* 103, 423–427. <https://doi.org/10.1007/s10973-010-1093-1>
- Huang, G., Liang, H., Wang, X., Gao, J., 2012. Poly(acrylic acid)/Clay Thin Films Assembled by Layer-by-Layer Deposition for Improving the Flame Retardancy Properties of Cotton. *Ind. Eng. Chem. Res.* 51, 12299–12309. <https://doi.org/10.1021/ie300820k>
- Huong, N., Vu, K., Ngô, T., Phan, D.-N., 2020. Application of Plasma Activation in Flame-Retardant Treatment for Cotton Fabric. *Polymers* 12. <https://doi.org/10.3390/polym12071575>
- Inan, T.Y., 2017. 2 - Thermoplastic-based nanoblends: Preparation and characterizations, in: Visakh, P.M., Markovic, G., Pasquini, D. (Eds.), *Recent Developments in Polymer Macro, Micro and Nano Blends*. Woodhead Publishing, pp. 17–56. <https://doi.org/10.1016/B978-0-08-100408-1.00002-9>
- Jiang, W., Jin, F.-L., Park, S.-J., 2015. Synthesis of a novel phosphorus-nitrogen-containing intumescent flame retardant and its application to fabrics. *Journal of Industrial and Engineering Chemistry* 27, 40–43. <https://doi.org/10.1016/j.jiec.2015.01.010>
- Kappes, R.S., Urbainczyk, T., Artz, U., Textor, T., Gutmann, J.S., 2016. Flame retardants based on amino silanes and phenylphosphonic acid. *Polymer Degradation and Stability* 129, 168–179. <https://doi.org/10.1016/j.polymdegradstab.2016.04.012>
- Kashiwagi, T., Gilman, J., Butler, K., Harris, R., Shields, J., Asano, A., 2000. Flame retardant mechanism of silica gel/silica. *Fire and Materials* 24, 277–289. [https://doi.org/10.1002/1099-1018\(200011/12\)24:6<277::AID-FAM746>3.0.CO;2-A](https://doi.org/10.1002/1099-1018(200011/12)24:6<277::AID-FAM746>3.0.CO;2-A)
- Kilinc, M., 2014. Silicon Based Flame Retardants. *Non-Halogenated Flame Retardant Handbook* 169–199. <https://doi.org/10.1002/9781118939239.ch5>

- Lazar, S.T., Kolibaba, T.J., Grunlan, J.C., 2020. Flame-retardant surface treatments. *Nat Rev Mater* 5, 259–275. <https://doi.org/10.1038/s41578-019-0164-6>
- Levchik, S., 2014. Phosphorus-Based FRs, in: *Non-Halogenated Flame Retardant Handbook*. John Wiley & Sons, Ltd, pp. 17–74. <https://doi.org/10.1002/9781118939239.ch2>
- Levchik, S., 2007. Introduction to Flame Retardancy and Polymer Flammability. *Flame Retardant Polymer Nanocomposites* 1–29.
- Levința, N., Vuluga, Z., Teodorescu, M., Corobea, M.C., 2019. Halogen-free flame retardants for application in thermoplastics based on condensation polymers. *SN Appl. Sci.* 1, 422. <https://doi.org/10.1007/s42452-019-0431-6>
- Lewin, M., 2001. Synergism and catalysis in flame retardancy of polymers. *Polymers for Advanced Technologies* 12, 215–222. <https://doi.org/10.1002/pat.132>
- Li, Y.-C., Schulz, J., Mannen, S., Delhom, C., Condon, B., Chang, S., Zammarano, M., Grunlan, J.C., 2010. Flame Retardant Behavior of Polyelectrolyte–Clay Thin Film Assemblies on Cotton Fabric. *ACS Nano* 4, 3325–3337. <https://doi.org/10.1021/nn100467e>
- Li, Z.-F., Zhang, C.-J., Cui, L., Zhu, P., Yan, C., Liu, Y., 2017. Fire retardant and thermal degradation properties of cotton fabrics based on APTES and sodium phytate through layer-by-layer assembly. *Journal of Analytical and Applied Pyrolysis* 123, 216–223. <https://doi.org/10.1016/j.jaap.2016.11.026>
- Liu, Q., Wang, D., Li, Zekun, Li, Zhifa, Peng, X., Liu, C., Zhang, Y., Zheng, P., 2020. Recent Developments in the Flame-Retardant System of Epoxy Resin. *Materials* 13, 2145. <https://doi.org/10.3390/ma13092145>
- Liu, X., Li, Y., Hu, J., Jiao, J., Li, J., 2014. Smart moisture management and thermoregulation properties of stimuli-responsive cotton modified with polymer brushes. *RSC Adv.* 4, 63691–63695. <https://doi.org/10.1039/C4RA11080C>
- Livage, J., 2004. Basic Principles of Sol-Gel Chemistry, in: Aegerter, M.A., Mennig, M. (Eds.), *Sol-Gel Technologies for Glass Producers and Users*. Springer US, Boston, MA, pp. 3–14. [https://doi.org/10.1007/978-0-387-88953-5\\_1](https://doi.org/10.1007/978-0-387-88953-5_1)
- Luo, D., Duan, W., Liu, Y., Chen, N., Wang, Q., 2019. Melamine cyanurate surface treated by nylon of low molecular weight to prepare flame-retardant polyamide 66 with high flowability. *Fire and Materials* 43, 323–331. <https://doi.org/10.1002/fam.2703>
- Ma, H., Tong, L., Xu, Z., Fang, Z., Jin, Y., Lu, F., 2007. A novel intumescent flame retardant: Synthesis and application in ABS copolymer. *Polymer Degradation and Stability* 92, 720–726. <https://doi.org/10.1016/j.polymdegradstab.2006.12.009>
- Mark, R.E., Borch, J., Habeger, C., 2002. *Handbook of Physical Testing of Paper*. CRC Press.
- Marturano, V., Cerruti, P., Ambrogi, V., 2017. Polymer additives. *Physical Sciences Reviews* 2. <https://doi.org/10.1515/psr-2016-0130>
- Materials, N.R.C. (U.S.) C. on F.S.A. of P., 1979. *Fire Safety Aspects of Polymeric Materials: Report of the Committee on Fire Safety Aspects of Polymeric Materials*, National Materials Advisory Board, Commission on

- Sociotechnical Systems, National Research Council. National Academy of Sciences.
- Mohamed, M.A., Jaafar, J., Ismail, A. F., Othman, M.H.D., Rahman, M.A., 2017. Chapter 1 - Fourier Transform Infrared (FTIR) Spectroscopy, in: Hilal, N., Ismail, Ahmad Fauzi, Matsuura, T., Oatley-Radcliffe, D. (Eds.), *Membrane Characterization*. Elsevier, pp. 3–29. <https://doi.org/10.1016/B978-0-444-63776-5.00001-2>
- Mudalige, T., Qu, H., Van Haute, D., Ansar, S.M., Paredes, A., Ingle, T., 2019. Chapter 11 - Characterization of Nanomaterials: Tools and Challenges, in: López Rubio, A., Fabra Rovira, M.J., Martínez Sanz, M., Gómez-Mascaraque, L.G. (Eds.), *Nanomaterials for Food Applications, Micro and Nano Technologies*. Elsevier, pp. 313–353. <https://doi.org/10.1016/B978-0-12-814130-4.00011-7>
- Parvez, K., 2019. Chapter 2 - Characterization Techniques of Two-Dimensional Nanomaterials, in: Nurunnabi, M., McCarthy, J.R. (Eds.), *Biomedical Applications of Graphene and 2D Nanomaterials, Micro and Nano Technologies*. Elsevier, pp. 27–41. <https://doi.org/10.1016/B978-0-12-815889-0.00002-7>
- Pentassuglia, S., Agostino, V., Tommasi, T., 2018. EAB—Electroactive Biofilm: A Biotechnological Resource, in: Wandelt, K. (Ed.), *Encyclopedia of Interfacial Chemistry*. Elsevier, Oxford, pp. 110–123. <https://doi.org/10.1016/B978-0-12-409547-2.13461-4>
- P.M, V., Arao, Y., 2015. Flame Retardants: Polymer Blends, Composites and Nanocomposites. <https://doi.org/10.1007/978-3-319-03467-6>
- Ratna, D., 2012. 3 - Thermal properties of thermosets, in: Guo, Q. (Ed.), *Thermosets*. Woodhead Publishing, pp. 62–91. <https://doi.org/10.1533/9780857097637.1.62>
- Rezvani Ghomi, E., Khosravi, F., Mossayebi, Z., Saedi Ardahaei, A., Morshedi Dehaghi, F., Khorasani, M., Neisiany, R.E., Das, O., Marani, A., Mensah, R.A., Jiang, L., Xu, Q., Förstth, M., Berto, F., Ramakrishna, S., 2020. The Flame Retardancy of Polyethylene Composites: From Fundamental Concepts to Nanocomposites. *Molecules* 25, 5157. <https://doi.org/10.3390/molecules25215157>
- Saini, A., Rauert, C., Simpson, M.J., Harrad, S., Diamond, M.L., 2016. Characterizing the sorption of polybrominated diphenyl ethers (PBDEs) to cotton and polyester fabrics under controlled conditions. *Science of The Total Environment* 563–564, 99–107. <https://doi.org/10.1016/j.scitotenv.2016.04.099>
- Sakho, E.H.M., Allahyari, E., Oluwafemi, O., Thomas, S., Kalarikkal, N., 2017. Dynamic Light Scattering (DLS), in: *Thermal and Rheological Measurement Techniques for Nanomaterials Characterization*. pp. 37–49. <https://doi.org/10.1016/B978-0-323-46139-9.00002-5>
- Schwarz, I., Kovacevic, S., 2017. *Textile Application: From Need to Imagination*. <https://doi.org/10.5772/intechopen.68376>
- Shaw, S., 2010. Halogenated Flame Retardants: Do the Fire Safety Benefits Justify the Risks? *Reviews on Environmental Health* 25. <https://doi.org/10.1515/REVEH.2010.25.4.261>
- Siriviriyannun, A., O’Rear, E., Yanumet, N., 2008. Self-extinguishing cotton fabric with minimal phosphorus deposition. *Cellulose* 15, 731–737. <https://doi.org/10.1007/s10570-008-9223-7>

- Smith, C.B., Mishra, R.S., 2014. Chapter 2 - Fundamentals of Formability, in: Smith, C.B., Mishra, R.S. (Eds.), *Friction Stir Processing for Enhanced Low Temperature Formability*. Butterworth-Heinemann, Boston, pp. 7–9. <https://doi.org/10.1016/B978-0-12-420113-2.00002-7>
- Toldy, A., Tóth, N., Anna, P., Marosi, G., 2006. Synthesis of phosphorus-based flame retardant systems and their use in an epoxy resin. *Polymer Degradation and Stability* 91, 585–592. <https://doi.org/10.1016/j.polymdegradstab.2005.02.025>
- Varghese, A.M., Mittal, V., 2018. 5 - Surface modification of natural fibers, in: Shimpi, N.G. (Ed.), *Biodegradable and Biocompatible Polymer Composites*, Woodhead Publishing Series in Composites Science and Engineering. Woodhead Publishing, pp. 115–155. <https://doi.org/10.1016/B978-0-08-100970-3.00005-5>
- Velencoso, M.M., Battig, A., Markwart, J.C., Scharrel, B., Wurm, F.R., 2018. Molecular Firefighting—How Modern Phosphorus Chemistry Can Help Solve the Challenge of Flame Retardancy. *Angew Chem Int Ed Engl* 57, 10450–10467. <https://doi.org/10.1002/anie.201711735>
- Venier, M., Salamova, A., Hites, R.A., 2015. Halogenated Flame Retardants in the Great Lakes Environment. *Acc. Chem. Res.* 48, 1853–1861. <https://doi.org/10.1021/acs.accounts.5b00180>
- Wang, D.-Y., 2016. *Novel Fire Retardant Polymers and Composite Materials*. Woodhead Publishing.
- Wang, S., Sui, X., Li, Y., Li, J., Xu, H., Zhong, Y., Zhang, L., Mao, Z., 2016. Durable flame retardant finishing of cotton fabrics with organosilicon functionalized cyclotriphosphazene. *Polymer Degradation and Stability* 128, 22–28. <https://doi.org/10.1016/j.polymdegradstab.2016.02.009>
- Wang, Z.-Y., Liu, Y., Wang, Q., 2010. Flame retardant polyoxymethylene with aluminium hydroxide/melamine/novolac resin synergistic system. *Polymer Degradation and Stability - POLYM DEGRAD STABIL* 95, 945–954. <https://doi.org/10.1016/j.polymdegradstab.2010.03.028>
- Xie, K., Gao, A., Zhang, Y., 2013. Flame retardant finishing of cotton fabric based on synergistic compounds containing boron and nitrogen. *Carbohydrate polymers* 98, 706–10. <https://doi.org/10.1016/j.carbpol.2013.06.014>
- Xing, W., Jie, G., Song, L., Hu, S., Lv, X., Wang, X., Hu, Y., 2011. Flame retardancy and thermal degradation of cotton textiles based on UV-curable flame retardant coatings. *Thermochimica Acta* 513, 75–82. <https://doi.org/10.1016/j.tca.2010.11.014>
- Yu, C., 2015. Chapter 2 - Natural Textile Fibres: Vegetable Fibres, in: Sinclair, R. (Ed.), *Textiles and Fashion*, Woodhead Publishing Series in Textiles. Woodhead Publishing, pp. 29–56. <https://doi.org/10.1016/B978-1-84569-931-4.00002-7>
- Zhao, B., Liu, Y.-T., Zhang, C.-Y., Liu, D.-Y., Li, F., Liu, Y.-Q., 2017. A novel phosphoramidate and its application on cotton fabrics: Synthesis, flammability and thermal degradation. *Journal of Analytical and Applied Pyrolysis* 125, 109–116. <https://doi.org/10.1016/j.jaap.2017.04.011>
- Zhu, P., Sui, S., Wang, B., Sun, K., Sun, G., 2004. A study of pyrolysis and pyrolysis products of flame-retardant cotton fabrics by DSC, TGA, and PY–GC–MS. *Journal of Analytical and Applied Pyrolysis* 71, 645–655. <https://doi.org/10.1016/j.jaap.2003.09.005>

## **Chapter II. Fire barrier investigation**



## 2.1 Introduction

### 2.1.1 DOPO-containing compounds

The 9,10-dihydro-9-oxa-10-phosphaphenanthrene-10-oxide (DOPO) as a novel flame retardant intermediate, synthesized from 2-phenylphenol and phosphorus trichloride, was synthesized and reported by Sanko Chemical Co., Ltd. for the first time in 1972 (Wei et al., 2019). Owing to the high reactivity of O=P-H bond, DOPO could react with chemicals containing alkenes, schiff bases, ketone, carbonyls, etc., providing simple approaches to prepare multiple DOPO-derivatives (Tang et al., 2019). Additionally, it enables DOPO-containing compounds to chemically modify the polymer matrix in a variety of ways by covalent binding for the purpose of enhancing fire performances. At present, because of the superior reactivity, thermal stability and oxidation resistance, DOPO and its derivatives have been the research focuses among the various phosphorus-containing compounds (Duan et al., 2019; S. Liu et al., 2016; Wang and Cai, 2017). Hu et al. designed a route to synthesize the phosphorus-modified siloxanes (DIA) by DOPO, Isophorone diisocyanate (IPDI) and Aminopropyltriethoxysilane (AMEO). The organic-inorganic hybrid coating was formed on the surface of cotton fabric after DIA treatment via sol-gel process, which increased the char layers and in turn led to improved thermal stability of cotton (Hu et al., 2011). Coincidentally, both Vasiljevic and Chernyy presented a method to synthesize the 10-(2-trimethoxysilyl-ethyl)-9-hydro-9-oxa-10-phosphaphenanthrene-10-oxide (DOPO-VTS) nanosol coating solution for applying onto cotton textiles (Chernyy et al., 2015; Peng et al., 2016; Vasiljević et al., 2015). Compared with pure DOPO finishing, it could be viewed the synergetic effects of P and Si elements in condensed phase endow the cotton fiber with better thermal and oxidative stability. Based on these researches, Zhou et al. further studied the flame-retardant mechanisms of DOPO containing SiO<sub>2</sub> hybrid sol on cotton fabrics by the preparation of SiO<sub>2</sub> sol, SiO<sub>2</sub>-KH570 sol, DOPO, SiO<sub>2</sub>-DOPO sol and SiO<sub>2</sub>-KH570-DOPO sol respectively (Zhou et al., 2019). It was found that besides the synergistic effects, DOPO consistently played an active role in dehydration and carbonation in the condensed phase during the combustion process. DOPO hybrid sol was beneficial in promoting the formation

of three-dimensional microscopic gel coating to enhance the anti-flammable properties of cotton fabric. Chen et al. suggested a method to introduce DOPO and fluorine-silicon-containing polymer network on the surface of cotton fabric. The modified cotton manifested both superhydrophobic and good heat resistance properties (Chen et al., 2019). A method was proposed to prepare phosphorus-nitrogen-silicone FRs (BDD) based on DOPO and Schiff Base (BD). Since BDD could act as the intumescent FRs for cotton fibers, working synergistically between gas phase and condensed phase, the modified cellulose membrane was attained the desired results of increased limiting oxygen index (LOI) and decreased peak heat release rate (PHRR) (Li et al., 2020). Comparably, another Si/P/N flame retardant 1-(9,10-dihydro-9-oxa-10-phosphaphenanthrene-10-oxide)-4-(trimethoxysilyl-methyl) piperazine (DOPO-PiP-Si) was investigated and successfully applied to cotton fabric by Zhang et al., achieving increased LOI value to 27.6% and lowered char length to 12.2 cm, simultaneously possessing high tensile strength of cotton (Zhang et al., 2020). In order to reduce the water pollution, Liu and co-workers innovatively conducted the finishing process with DOPO using supercritical CO<sub>2</sub> in a self-built apparatus for cotton fabric. Also, decreased combustibility was revealed, as well as enhanced fire performances for the samples after treatment (Liu et al., 2020).

The 10-(2,5-dihydroxyphenyl)-9,10-dihydro-9-oxa-10-phosphaphenanthrene-10-oxide (DOPO-HQ) (Figure 2.1), made from the reaction of DOPO and p-benzoquinone, has been regarded as highly efficient reactive flame retardants due to its own excellent properties (Liu et al., 2018). As a result of its rigid aromatic structure and stable P-O-C bond, DOPO-HQ is inherently with good chemical stability and heat resistance (He et al., 2019; Shi et al., 2018). Under high temperature conditions, DOPO-HQ is able to decompose and release PO• radicals, which are provided with quenching effects on the highly active H• and OH• radicals generated by the pyrolysis of cotton materials, thereby inhibiting the chain reaction and decreasing heat release in gas phase (Y. Liu et al., 2016; Rakotomalala et al., 2010). Simultaneously, with the presence of decomposition products of DOPO-HQ in combustion, such as phosphoric acid that could dehydrate and carbonize the cotton fabrics to form protective char layer as a barrier on the surface, oxygen and heat are insulated from transferring inside to

obtain the fire barrier effects in condensed-phase (Hergenrother et al., 2005). And when DOPO-HQ is utilized in combination with other flame-retardant elements, the synergistic actions are supposed to be produced, further developing the thermal properties of cotton substrates.

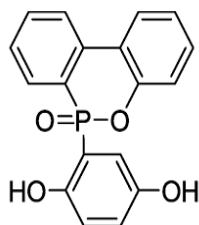


**Figure 2.1** Chemical structure of DOPO-HQ

### 2.1.2 Metal–organic frameworks (MOFs)

Metal–organic frameworks (MOFs) (Lu et al., 2017) are hybrid compounds consisting of inorganic metal nodes with high-density connected by organic ligands by the self-assembly to form a crystalline structure that are inherently with tunable morphology, ultra-high porosity, large specific surface area and various characteristics (Chen et al., 2021; Liang et al., 2019). In contrast to classical porous materials such as zeolite and activated carbon, MOFs with multiple cations and organic linkers are available for fine chemical and structural control as designed (Cortés and Macías, 2021). They are promising and advanced materials for environmental (Mukherjee et al., 2019), gas storage/separation (H. Li et al., 2018), drug delivery (Sun et al., 2020), electrochemical sensing (Jiang et al., 2017), flame retardant additives (Qi et al., 2019), catalysis (Pascanu et al., 2019) and among others (Cheng et al., 2019). MOFs constructed using biocompatible metals such as Zr, Fe, etc., are not only highly stable but also meet the major concerns for environmental and human safety (Barton et al., 2021).

#### 2.1.2.1 The structure and types of MOFs

The structure of Metal–organic frameworks (MOFs) was represented in Figure 2.2 below. The combination between inorganic metal nodes and organic linkers contribute to various one-dimension, two-dimension, or three-dimensional networks. The typical MOFs (G. Li et al., 2020) includes IRMOFs (IRMOF for

Isorecticular Metal Framework), MILs (MIL for Materials Institute Lavoisier), ZIFs (ZIF for Zeolitic Imidazolate Framework), UiOs (UiO for University of Oslo), etc.,

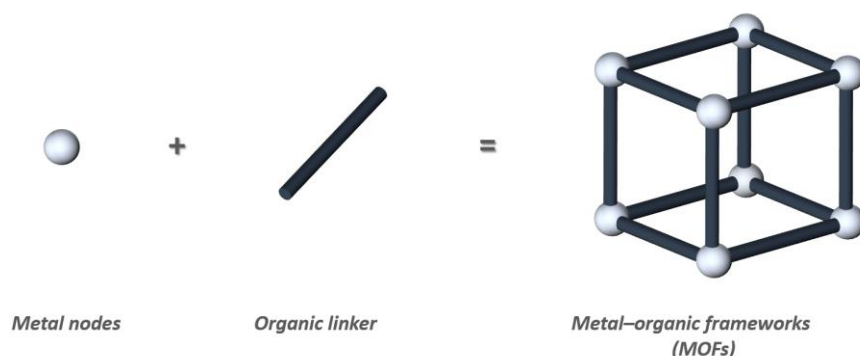


**Figure 2.2** Schematic diagram of the MOFs structure

The UiO series are zirconium-based MOF materials, such as UiO-66 (J. Katz et al., 2013), NU-1000 (Yang et al., 2015) and MOF-808 (Ardila-Suárez et al., 2019). Their structures are built via different combination of hexanuclear clusters of  $Zr_6O_4(OH)_4^{12+}$  and multiple carboxylic acid linkers (D'Amato et al., 2021). They are highly thermally stable and able to retain the skeletal structures in a variety of solvents.

The ZIF series are also known as zeolite-like imidazolium ester skeleton materials, in which the central metal is mostly Zn or Co and the organic ligand is imidazole. The structures of ZIFs are very similar to that of traditional zeolite molecular sieve, but also with the advantages of MOFs, thus allowing for a wide range of applications. ZIF-8, a broadly studied class of ZIFs, exhibits good chemical and thermal stability with structure of cubic lattice and sodalite topology (Gao et al., 2016).

The MIL series are mainly synthesized by different divalent transition-metal ions and dicarboxylic acid. There are also new MIL materials synthesized by self-assembly of trivalent metal ions such as  $Fe^{3+}$ ,  $Cr^{3+}$ ,  $Al^{3+}$ , etc. with carboxylic acid ligands. Due to huge specific surface area and stable structural characteristics, they have attracted a lot of attention, especially for MIL-100 (Mahmoodi et al., 2018) and MIL-101 (Kayal et al., 2015).

### 2.1.2.2 The development of MOFs

In 1995, a coordination compound, named as MOF, with two-dimensional structure synthesized from the rigid organic ligands (tricarboxylic acid) and the transition metal (Co) via solvothermal synthesis was claimed by Professor Omar Yaghi in *Nature* (Rubio-Martinez et al., 2017). After that, MOF-1, MOF-2, MOF-5, MOF-177 and MOF-74 were successively reported by Yaghi's group. In 2004 and 2005, Gérard Férey's group at the University of Versailles reported two kinds of MOFs, MIL-100 (Cr) (BTC as the ligand) and MIL-101 (Cr) (BDC as the ligand) that could act as molecular sieve with extra-large pores in *Angew. Chem. Int. Ed.* (Férey et al., 2004) and *Science* (Férey et al., 2005) respectively. In 2006, Yaghi's group turned their attention to molecular sieve materials with superior stability properties and reported the synthesis of 12 molecular sieve-like imidazole backbone materials called as ZIF-1 to ZIF-12, which exhibited superior thermal and chemical stability (Park et al., 2006). Among them, ZIF-8 and ZIF-11 were not only stable up to 550 °C, but also in a variety of solvents that conducive to more applications. Subsequently, more ZIFs such as ZIF-20, ZIF-68, ZIF-95, ZIF-100 were found by Yaghi's group, which led to a great expansion of the ZIF family. To date, the development of MOFs has been flourishing, with an increasing number of researchers dedicated to discovering varieties of novel MOFs.

### 2.1.2.3 Applications of MOFs

The controlled structure, pores, functional groups, and specific surface area of MOFs have offered unlimited possibilities for their application.

#### **Gas storage/separation**

With the shortage of fossil fuels and the growing problem of environmental pollution, it is urgent to find new and clean alternative energy sources. Hydrogen is a new energy source of great interest, and the use of MOFs as adsorbents for hydrogen storage has received much attention. In addition to gas storage, MOFs are also able to be used for gas separation due to their unique pore chemistry (Li et al., 2019).

## **Catalysis**

MOFs contain some unsaturated metal sites and functional groups, which have a high catalytic activity and a positive effect on the reaction. The introduction of functional materials such as inorganic nanoparticles in MOFs can work synergistically with MOFs to exhibit enhanced catalytic activity and selectivity (Chen and Xu, 2019).

## **Drug delivery**

MOFs are regarded as promising materials for biomedical applications due to their excellent properties that quite useful in the field of drug delivery and disease treatment. In particular, it can be effectually for MOFs to increase the loading capacity for drugs with good biocompatibility (Wu and Yang, 2017).

## **Electrochemical sensing**

MOFs have been widely used in electrochemical sensors. The response selectivity and sensitivity could be improved through MOF-based materials with good selectivity of guest molecules, concentrated analytes and fast mass transfer (T. Ma et al., 2020).

## **Flame retardants**

In recent years, MOFs have also been researched for uses in the field of flame retardants. Some MOFs has shown great potential for improving the fire retardancy and smoke suppression properties of polymeric materials (Zhang et al., 2020). As a novel type of porous materials, their adsorption performances are outstanding because of the large pore volume and specific surface area, allowing them to absorb toxic fumes generated from the combustion of polymer materials and thus improve the smoke suppression of substrates. Additionally, the organic ligands used for synthesizing MOFs could not only enhance the compatibility between MOFs and polymers, but also enable the introduction of some other flame-retardant elements, such as phosphorus and nitrogen.

#### 2.1.2.4 The flame-retardant mechanism of MOFs

Metal-organic frameworks (MOFs) are a new type of porous materials with organic/inorganic coordination networks (Rowsell and Yaghi, 2004). They are stable at high temperatures typically above 200 °C, exhibiting a high degree of crystallinity and are characterized by a very high surface area (Shekhah et al., 2011). MOFs are considered inherently possessed with superior thermal stability, which are comparable with inorganic FRs. Organic ligands can not only contribute to excellent compatibility, but also flame-retardant elements or functional groups, such as nitrogen, phosphorus groups and aromatic derivatives (Hou et al., 2017). Meanwhile, some scientific literature describing innovative uses of MOFs for cotton fabric substrates are emerging. UiO-66 (Zr-based metal-organic framework) has been extensively studied because of its broad applications and remarkable stability, it was reported seeding the growth on the surface of cotton fibers by facile two-step synthesis (Schelling et al., 2018). Coordinated zinc metal centers and 2-methylimidazole were combined to generate ZIF-8 (Zn-based metal-organic framework). An approach was put forth that made use of ZnO rods as the source of Zn<sup>2+</sup> ions and nucleation site for ZIF-8 to be incorporated with cotton (Schelling et al., 2020).

During the thermal decomposition process, the metal oxides generated by MOFs on the surface of polymer substrates will work as a physical barrier to protect the polymer from further burning while also efficiently adsorbing gases and smoke. In the same way, some non-flammable gases produced from MOF particles can also dilute the concentration of combustible gases. Since the amount of combustibles present is decreased, the amount of heat released is accordingly declined. As a result of these actions, less fuel will be available for combustion, leading to lower heat release. Generally speaking, absorption of gases and smoke, formation of heat-insulating layer, and gas dilution are mainly contributed to the flame-retardant mechanism of MOFs (Nabipour et al., 2020b).

### **2.1.2.5 Synthesis methods of MOFs**

Various synthetic methods have been developed to design MOFs with different surface properties such as crystal structure, particle size, pore size distribution and morphology (Ozer, 2020).

#### **Hydrothermal/Solvothermal synthesis**

Hydrothermal synthesis is a method that prepare all the reactants in the form of solution with distilled water as the solvent in a sealed vessel to complete the growth of crystal at a certain temperature and pressure. The high temperature and pressure of the reaction environment could accelerate the dissolution of the reactants and raise the reaction efficiency (Lee et al., 2013). The principle of solvothermal synthesis is the same as that of hydrothermal method, except that the solvent used is replaced with other organic solvents, such as methanol, ethanol and dimethylformamide (DMF).

#### **Microwave synthesis**

The microwave synthesis method discards the traditional method of heating with electricity. It involves mixing metal salts with organic ligands in organic solvents and then synthesizing MOFs under microwave irradiation, which allows reaching the required temperature in the reaction system in a very short time, thus greatly reducing the reaction time and saving energy (Klinowski et al., 2010).

#### **Sonochemical (ultrasonic-assisted) synthesis**

Sonochemistry is the preparation of MOFs by mixing metal salts and organic ligands in organic solvents and then placing them in an ultrasonic device to adjust the temperature and power. By sonochemical synthesis, it can be used to enhance the chemical activity of the reaction materials, reduce the crystallization time and facilitate the synthesis of MOFs with smaller crystal sizes (Samuel et al., 2018).



## **Electrochemical synthesis**

Electrochemical synthesis is a kind of energy-efficient reaction that can be completed without heating, generally at room temperature. In 2005, researchers of BASF firstly published the electrochemical synthesis of MOFs (Al-Kutubi et al., 2015). It is based on the principle of dissolving organic ligands in a solvent to act as electrolytes, providing the metal ions needed for synthesis by electrodes instead of metal salts (Pirzadeh et al., 2018).

## **Mechanochemical synthesis**

The mechanochemical synthesis is to make the desired MOFs by mixing metal salts and organic ligands in high energy ball-milling machine. It's an easy-to-operate method that could accelerate the synthesis reaction process by increasing the contact area between reactant particles (Tanaka, 2020).

In addition, there are more synthesis methods of MOFs such as diffusion and ionothermal (Mehra et al., 2021).

### **2.1.2.6 Approaches for incorporating MOFs with textiles**

Textiles could be used as MOFs substrates to realize a variety of promising applications including antistatic, self-cleaning, electromagnetic-shielding, antimicrobial, waterproof and flame-retardant (Yu et al., 2016). And there are some approaches have been developed for coating MOFs on fibers (Ma et al., 2019). Beyond direct blending of MOFs particles with textile fibers, dipping, padding, spraying, in situ growth and other procedures have been explored by researchers to immobilize reagents on textile substrates. Li et al. first incorporated MOF coating onto cotton textile by alternatively dipped in metal ions and ligand solution for several times and then calcined the sample to form hierarchical porous carbons (HPCs) doped with metal nanoparticles (D.-J. Li et al., 2018). Chen et al. obtained MOF/PEI composites by a facile synthetic method and applied them to cotton fabrics to construct dense and continuous protective layers for destruction of nerve agents (Chen et al., 2019). In order to coat fibers more efficiently with MOFs, the textile fabrics could be chemically modified to

obtain more reactive groups such as carboxylates and hydroxyl groups to promote MOFs nucleation on the fibers (K. Ma et al., 2020).

## 2.2 Experimental

Two types of MOFs, Zr-based MOFs (UIO-66-COOH) and Zn-based MOFs (ZIF-8), were selected and investigated to be incorporated into cotton fabrics either individually or in combination with other polymeric materials for comparing the impacts on fire performances of cotton samples by characterization techniques such as SEM, TGA and vertical burning test. Meanwhile, the appropriate ways to introduce DOPO-HQ on cotton fabrics were explored, leading to the development of more effective and facile approach for constructing structural protective barriers.

### 2.2.1 Fire barrier investigation of DOPO-HQ

#### 2.2.1.1 Preparation of DOPO-HQ finishing solution

Based on the chemical properties of DOPO-HQ, it's more soluble in the organic solvent, such as dimethylformamide (DMF) and tetrahydrofuran (THF). For environment-friendly conscious, the low concentration of DOPO-HQ finishing solution (1.5 wt%) was prepared by dissolving it into ethanol with heating up to 60 °C to investigate the performances of cotton fabrics after incorporating DOPO-HQ.

#### 2.2.1.2 The application of DOPO-HQ solution

Cotton fabric was treated with 1.5 wt% DOPO-HQ finishing solution via multiple dip-pad-dry cycles at ambient conditions, and the corresponding add-ons were calculated from the following equation.

$$\text{Add-on (wt\%)} = \frac{\text{Last weight of specimen(g)} - \text{Initial weight of specimen(g)}}{\text{Initial weight of specimen(g)}} * 100$$

In detail, the treatment data of each sample was shown in Table 2.1 below. There was no doubt that additional DOPO-HQ could be introduced to cotton substrates through repeated finishing processes. The fire barrier effects of cotton fabrics treated with different amounts of DOPO-HQ could be evaluated by comparing them with pristine cotton.

**Table 2.1** The treatment data of cotton sample

Sample	Dip-pad-dry cycles	$W_0/g$	$W_1/g$	Add-on/wt%
D2	2	6.07	6.30	3.79
D4	4	6.13	6.42	4.73
D6	6	6.03	6.51	7.96
D8	8	6.04	6.53	8.11
D10	10	6.02	6.53	8.47

\*  $W_0$  and  $W_1$  refer to initial and final weight of specimen, respectively.

### Vertical burning test

To access the flammability and fire resistance of cotton samples, vertical burning tests were carried out. Given cotton fibers were highly flammable, these samples were exposed to a naked flame for 10 seconds before the ignition source was removed in order to record the combustion process (Figure 2.3).

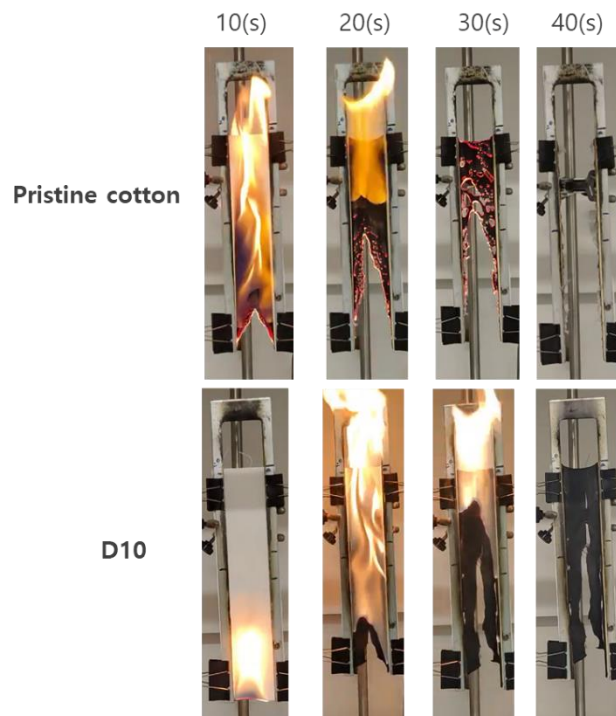


**Figure 2.3** Digital photos of cotton samples in the vertical burning test after ignition

As shown in the above picture, the pristine cotton was vigorously burning and flame spread extremely rapid after ignition. During combustion, the fabric was

entirely consumed, leaving no residual chars. Differently, sample D10 performed fire barrier effects with producing more insulating char layers. It helped to slow down the tendency of burning and suppress the fire to protect the cotton substrates.

## SEM

To study the surface morphology of cotton fabrics before and after burning, all samples were observed by using Scanning electron microscope (SEM). The morphology of pristine cotton, sample D10 and residual chars were exhibited in Figure 2.4 below.

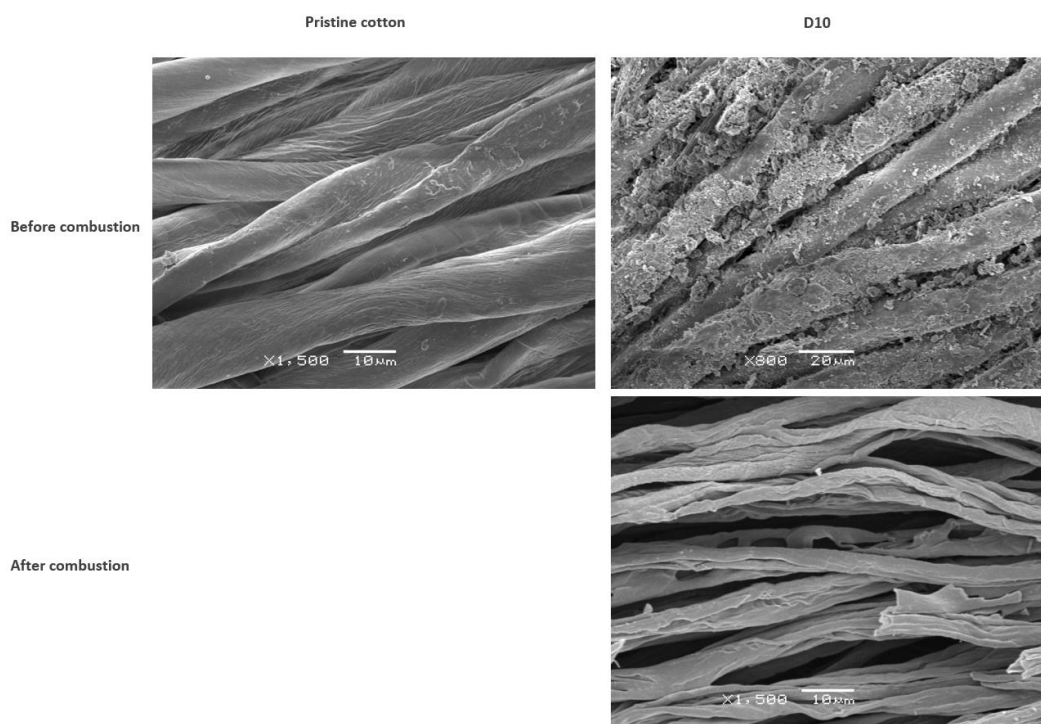


**Figure 2.4** The SEM images of cotton fabrics before and after combustion

It could be noticed that the surface of pristine cotton was relatively smooth, flat and clean. Seemingly, when substantial amounts of DOPO-HQ dissolved in ethanol were applied to cotton fabrics, it generated some agglomeration and the distribution of DOPO-HQ was not quite uniform, either. For this reason, a reliable carrier was required to incorporate DOPO-HQ onto cotton substrates. And considering the surface morphology of sample D10 after combustion, there was slight swelling of the cotton fabric, which was due to the phosphoric acid

derivatives produced during the burning process that promoted the dehydration of the cellulose into char and protected the internal fibers from further degradation. Thereby DOPO-HQ had a positive effect on the formation of intumescent char layers which blocked the transfer of heat and oxygen, effectively delaying the burning of cotton substrates.

### **2.2.1.3 Conclusions**

Among all phosphorus-containing compounds, DOPO-HQ made from the reaction of DOPO and p-benzoquinone, was inherently with excellent chemical stability and heat resistance due to its own rigid aromatic structure and stable P-O-C bond. When DOPO-HQ was decomposed at high temperatures, its derivatives, such as phosphoric acid, could function properly in the condensed phase. And the presence of phosphorus-containing radicals would further contribute to suppressing the burning of cotton textiles by capturing the H• or OH• free radicals in the gas phase. It was evident that the treated fabric would perform better in fires when higher amounts of DOPO-HQ were introduced into cotton substrates. Consequently, it was desirable to investigate the appropriate approaches for incorporating halogen-free DOPO-HQ into cotton fabrics in the following sections.

## 2.2.2 Fire barrier investigation of ZIF-8

Zeolitic imidazolate frameworks (ZIFs) is a typical subclass of MOFs with a topology similar to that of silica and zeolite networks, with tetrahedra consisting of metal ions and imidazole-based ligands connected by coordination bonds (Li et al., 2022). Through the strong interaction between nitrogen atoms of imidazolate ligands and metal cations, ZIFs owns greater chemical stability and thermal properties compared to some other types of MOFs. Among a wide range of ZIFs, ZIF-8 (Kwon and Jeong, 2013) and ZIF-67 are the two types most often applied in the flame retardancy field (Pan et al., 2020).

Due to its extensive use, ZIF-8 (Figure 2.5) is getting a lot of interest. There was a study revealed that ZIF-8@cellulose composite aerogels was synthesized by layer-by-layer assembly (Nabipour et al., 2020a). Fundamentally, element N and Zn are the significant presence to endow ZIF-8 with fire retardancy properties. The generated  $\text{NH}_3$  could dilute combustible gases and zinc oxide as the degradation product could act as charring agent during combustion. The carbonized layers would protect the underlying substrate from further burning (Nabipour et al., 2020c).

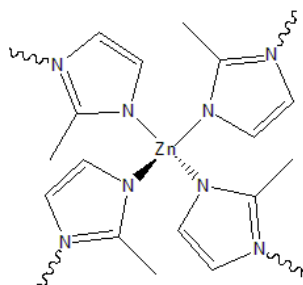


**Figure 2.5** Chemical structure of ZIF-8

### 2.2.2.1 Hydrothermal synthesis of ZIF-8 dispersion

The preparation process of ZIF-8 dispersion was inspired from some previous study (Shang et al., 2021; Su et al., 2018), which tended to be environmentally friendly by purely aqueous solution without organic solvents. The detailed protocol was as follows: 1.5 g zinc acetate (6.85 mmol of  $\text{Zn}^{2+}$ ) and 39.3 g 2-methylimidazole (0.48 mol of  $\text{C}_4\text{H}_6\text{N}_2$ ) were completely dissolved in 30 ml and 170 ml of deionized water, respectively. Then the two were mixed with magnetic

stirring for 5h at 60 °C and followed 15h at room temperature in order to obtain the homogeneous ZIF-8 dispersion.

### 2.2.2.2 The application of ZIF-8 dispersion in combination with BPEI and VTES

Branched polyethyleneimine (BPEI) is a polymer with repeating units consisting of ethylene diamine groups that has high cationic charge density and water solubility. Strong hydrogen bond interactions could be generated between abundant amines of BPEI and the carboxyl groups of cellulose (Guo et al., 2017), which has the potential to combine with other flame retardant elements for synergistic and intumescent effects. Silicon-based FRs are also widely known with their high thermal stability and environment-friendliness (Mercado et al., 2006). In terms of mechanism, they can form a siliceous carbon layer when the polymeric material is thermally decomposed, which can prevent the substrate from burning by heat insulation and oxygen barrier. Meanwhile, they reduce the overflow of flammable gases to suppress the fire (Carosio et al., 2011). Among a variety of silicon-containing compounds, vinyltriethoxysilane (VTES), a common silane coupling agent (Yi et al., 2010), with both vinyl groups and hydrolytically sensitive ethoxysilyl groups (Wolff, 1996), it could cross-link cellulosic fibers through Si–O–Si network (Vasiljević et al., 2015) and promote silicon-nitrogen synergy system as well.

VTES finishing solution was prepared by dissolving VTES (8 g) into DI (92 ml) by ultrasonication for 10 min and magnetic stirring for 8h at room temperature. The cotton fabrics were treated by resultant ZIF-8 homogeneous dispersion at first, followed by BPEI (3 wt%) and VTES (8 wt%) solution via dip-pad-dry process. The cotton samples after finishing treatment were denoted as ZIF-8, ZIF-8/PEI and ZIF-8/PEI/VTES. The add-on (wt%) of each formulation was calculated from the following equation:

$$\text{Add-on (wt\%)} = \frac{\text{Last weight of specimen(g)} - \text{Initial weight of specimen(g)}}{\text{Initial weight of specimen(g)}} * 100$$

In detail, the treatment data of each sample was shown in Table 2.2 below.



**Table 2.2** The treatment data of cotton sample

Sample	$W_0/g$	$W_1/g$	Add-on/wt%
ZIF-8	10.23	10.5	2.64
ZIF-8/BPEI	10.23	10.82	5.77
ZIF-8/BPEI/VTES	10.23	11.3	10.46

\*  $W_0$  and  $W_1$  refer to initial and final weight of specimen, respectively.

### Particle size and stability of ZIF-8 dispersion

The particle size was instantly verified to be 324 nm by Malvern Zetasizer Nano ZS90 after successfully producing the synthesized ZIF-8 dispersion. With nanoscale particle size, it was beneficial to distribute ZIF-8 more uniformly on cotton fibers and improving the add-on. The evolution of ZIF-8 dispersion stability with time could be intuitively seen from the digital photos (Figure 2.6). Without apparent gravitational phase separation, it was quite advantageous that ZIF-8 had remained stable under ambient circumstances for a considerable period of time.

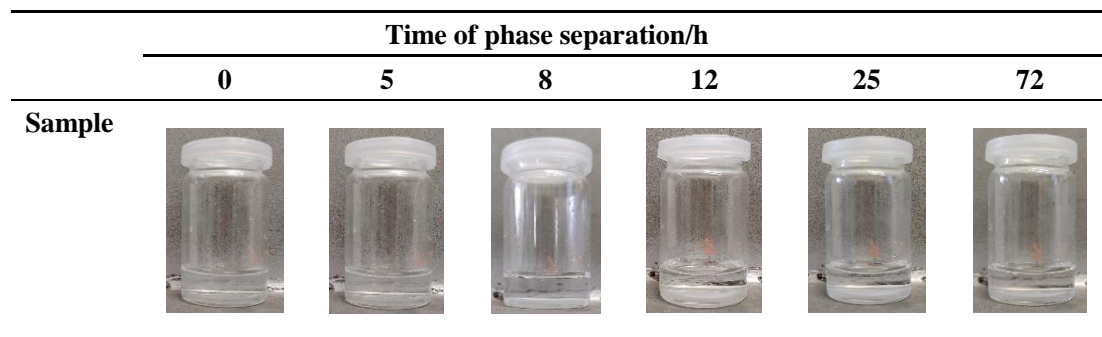


**Figure 2.6** Digital photos of ZIF-8 homogeneous dispersion at different time

### Vertical burning test

Pristine cotton and treated samples were exposed to a naked flame for 10 seconds before the ignition source was removed in order to record the combustion process (Figure 2.7).

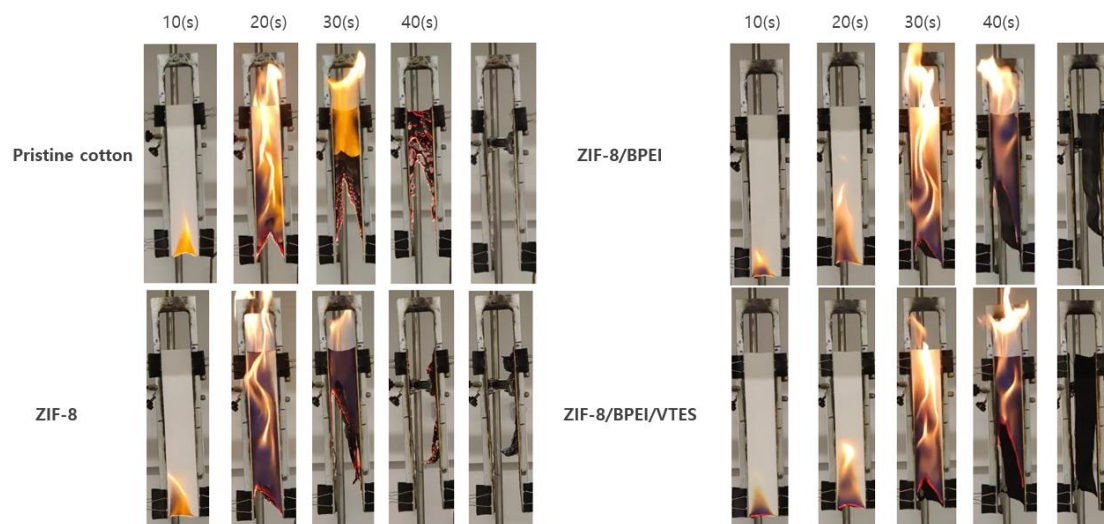


**Figure 2.7** Digital photos of cotton samples in the vertical burning test after ignition

The pure cotton was aggressively burning, and the flame spread exceptionally quickly after ignition, as seen in Figure 2.7. The pristine cotton fabric was completely consumed during combustion, with no residual chars. By contrast, when pure cotton was finished by ZIF-8 dispersion only, the flame spread of treated sample was not delayed, accompanied by yielding a small amount of protective carbon layer. The use of BPEI as an effective carbon source in combination with ZIF-8 resulted in a lower flame spread rate and a denser heat-insulating layer as sample ZIF-8/BPEI. Compared to the pristine cotton fabric, sample ZIF-8/BPEI/VTES produced a large amount of residual chars in the burning process, providing better fire barriers while delaying the propagation of the flame.

## SEM

To study the surface morphology of cotton fabrics before and after combustion, all cotton samples were observed by using SEM. The morphology of sample ZIF-8, sample ZIF-8/BPEI, sample ZIF-8/BPEI/VTES and their residual chars were exhibited in Figure 2.8 below.

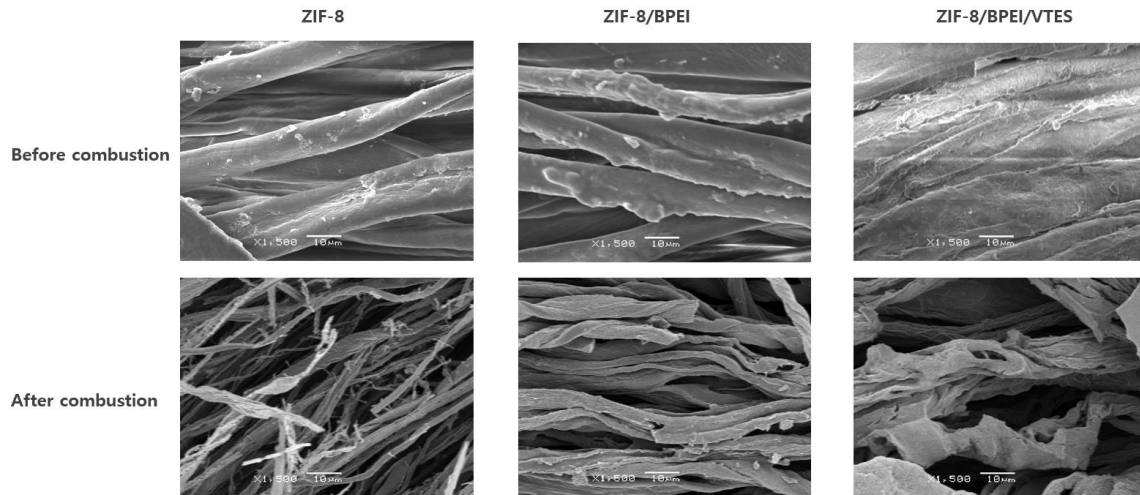


**Figure 2.8** The SEM images of cotton samples before and after combustion

As previously envisaged, it could be seen that the nano-sized particles of ZIF-8 were produced and uniformly adsorbed on the surface of cotton fibers. But it was possible that the affinity between ZIF-8 and cellulose was not sufficient, as a result very few ZIF-8 particles were successfully grown on cotton fibers. BPEI was a blowing source, it assisted ZIF-8 in penetrating into the spaces between cellulose fibers, distributing them evenly, and building more continuous and film-like structure via bonding actions for fire suppression. With VTES, the strong Si–O–Si cross-linking enabled ZIF-8 and BPEI to adhere tightly to cotton fibers. In the burning process, the siloxane compound was able to generate silica layers to avoid further combustion and degradation of residual chars (Jiang et al. 2019). The structure of cotton fiber was still not ideally preserved after combustion, despite the fact that sample ZIF-8/BPEI/VTES facilitated the expanded carbonized layers covering the surface of cotton fabrics to protect it from fire.

### Thermal analysis

To further distinguished the variations in thermal properties between treated samples and pristine cotton, thermogravimetric analysis (TGA) was necessary to be conducted.

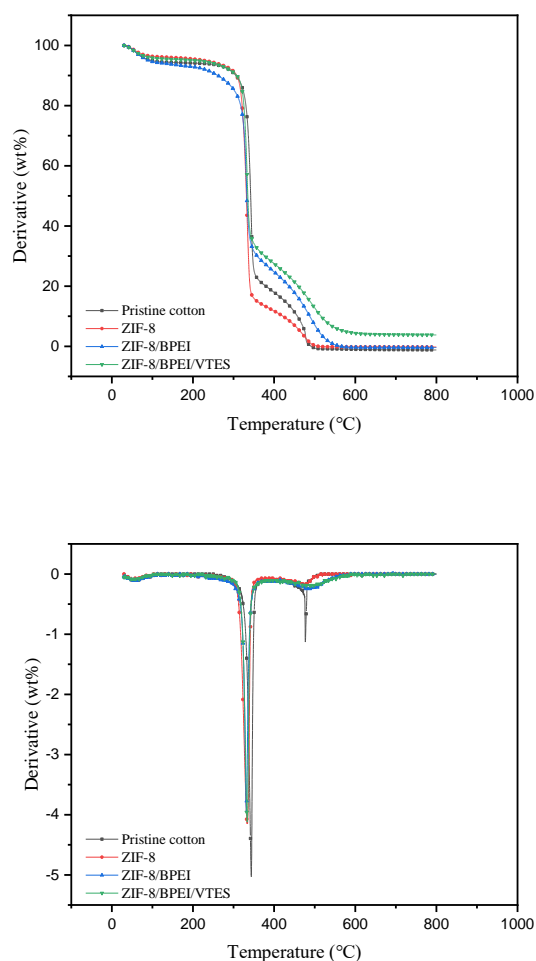


**Figure 2.9** TGA and DTG curves of (a) pristine cotton sample, (b) ZIF-8 sample, (c) ZIF-8/BPEI sample and (d) ZIF-8/BPEI/VTES sample

**Table 2.3** TGA data of cotton samples under air atmosphere

Sample	$T_{10\%}$ (°C)	Stage1		Stage2		Residue at 800 °C (wt%)
		$T_{max}$ (°C)	$R_{max}$ (wt%/min)	$T_{max}$ (°C)	$R_{max}$ (wt%/min)	
Pristine cotton	318.5	341.6	37.6	479	93.4	-1.21
ZIF-8	318.9	334	37.2	481.2	91.8	-0.3225
ZIF-8/BPEI	283.6	330.8	38.2	482	90.2	-0.3836
ZIF-8/BPEI/VTES	319.4	331.9	37.8	496.2	86.4	3.8011

\* The heating rate is fixed by 10 °C/min.  $T_{10\%}$  is the initial decomposition temperature at which 10% sample weight is lost.  $T_{max}$  is the temperature of maximum rate of weight loss.  $R_{max}$  is weight loss rate at the maximal peak ( $T_{max}$ ).

Figure 2.9 showed that the thermal degradation curves of pristine cotton, sample ZIF-8, sample ZIF-8/BPEI and ZIF-8/BPEI/VTES under air gas atmosphere, along with the key data were listed in the Table 2.3. The initial decomposition temperature ( $T_{10\%}$ ) of pristine cotton, sample ZIF-8, sample ZIF-8/BPEI and ZIF-8/BPEI/VTES were 318.5 °C, 318.9 °C, 283.6 °C and 319.4 °C respectively. This indicated that when the outermost layer of the cotton was BPEI, it decomposed at relatively low temperatures, working as blowing agent to generate ammonia and carbon layers. However, the carbon residues of sample ZIF-8/BPEI at 500 - 800 °C was not much higher than that of pristine cotton. Besides, when VTES was associated with ZIF-8 and BPEI, it didn't perform positive impacts at stage 1, either. While it helped to raise  $T_{max}$  from 479 °C to 496.2 °C and lower  $R_{max}$  from 93.4 wt%/min to 86.4 wt%/min at stage 2, and greatly increased the final amount of residue yield by forming siliceous insulation layer at high temperatures.

### **2.2.2.3 The application of ZIF-8 dispersion in combination with DOPO-HQ@CS**

Chitosan (CS) is a linear polysaccharide obtained by deacetylation of chitin, consisting of glucosamine and N-acetyl glucosamine monomers linked by  $\beta$ -4 glycosidic bonds (Gaspar et al., 2016). It's a natural semi-synthetic biopolymer with a diverse range of applications due to the advantages of low price, wide source and environmentally friendly (Bakshia et al., 2019). CS cannot be directly dissolved in water, but it owns good solubility in various acid aqueous solution (Cheng et al., 2017). CS is positively charged with abundant reactive amino and hydroxyl groups, which can be used as a char-forming agent in the flame retardant system (Beulah et al., 2019; Malucelli, 2020). CS decomposes at high temperatures to form carbon layers in the condensed phase, which on the one hand inhibits heat exchange, and on the other hand, the generated ammonia further dilutes the concentration of combustibles in the gas phase. The products from the thermal decomposition of acid sources can facilitate the dehydration and carbonization of chitosan when it is combined with some acid sources to create an intumescent flame retardant system (Chen et al., 2016). Some researchers deposited cationic CS and ionic ammonium phytate (AP) onto cotton matrix through layer-by-layer method for investigating its fire-safety. As a result of the

treated cotton producing more char residues at 700 °C than the control fabric, they concluded that CS and AP were beneficial for catalytic carbonization (P. Li et al., 2020). Moreover, Galina Laufer et al. made use of cationic chitosan and anionic phytic acid (PA) to build intumescent multilayer nanocoating on cotton fabrics via LBL assembly. The highest reduction in peak heat release rate (PKHRR) and total heat release were up to 60% and 76% respectively for the cotton sample coated with 32BL CS–PA films (Laufer et al., 2012).

DOPO-HQ@CS finishing solution was prepared as the procedure: 4 wt% DOPO-HQ was dispersed in 1 wt% chitosan solution with solvent of 1% acetic acid by magnetic stirring at room temperature for 24h. Alternate deposition of DOPO-HQ@CS and ZIF-8 finishing solutions were used onto cotton fabrics to assemble the fire barriers. The detailed treatment data were shown in Table 2.4. Accordingly, the treated cotton samples were identified as DOPO-HQ@CS/ZIF-8 (1BL) and DOPO-HQ@CS/ZIF-8 (3BL), depending on the number of deposition layers.

**Table 2.4** The treatment data of cotton sample

Sample	W <sub>0</sub> /g	W <sub>1</sub> /g	Add-on/wt%
DOPO-HQ@CS/ZIF-8 (1BL)	5.86	6.8	16
DOPO-HQ@CS/ZIF-8 (3BL)	5.9	7.05	19.49

\* W<sub>0</sub> and W<sub>1</sub> refer to initial and final weight of specimen, respectively.

### Vertical burning test

Vertical burning tests were carried out on cotton sample pieces to assess their flammability and fire resistance. These samples were exposed to a naked flame for 10 seconds before the ignition source was removed in order to observe the combustion process.

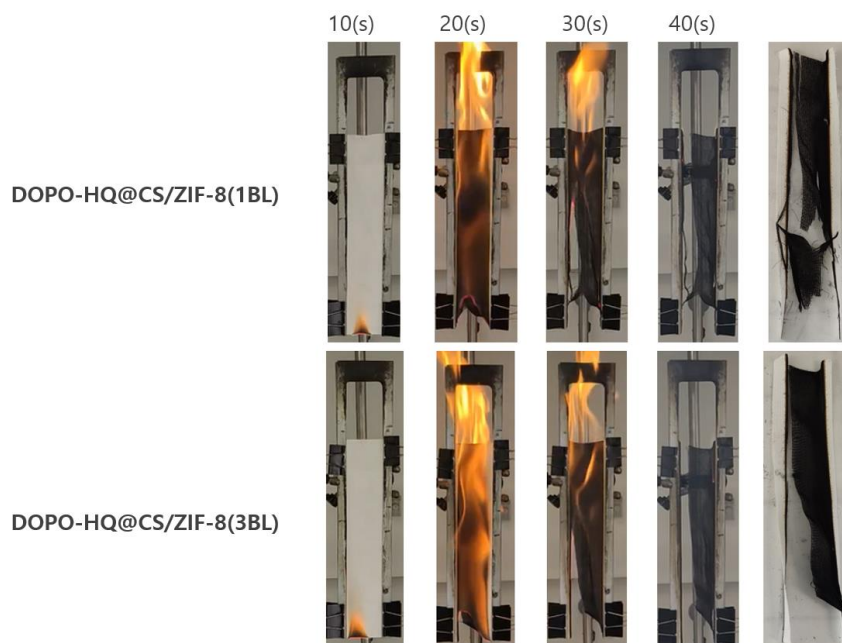


**Figure 2.10** Digital photos of cotton samples in the vertical burning test after ignition

Due to the strong affinity between chitosan and cotton fibers, sample DOPO-HQ@CS/ZIF-8 (1BL) and DOPO-HQ@CS/ZIF-8 (3BL) were gained add-on of 16 wt% and 19.49 wt% respectively. With such high add-on, it was clear that the treated cotton samples were both able to generate massive carbon residues for inhibiting the fire during the burning process as seen in Figure 2.10. However, the overall rate of flame spread didn't seem to be improved.

## SEM

Cotton fabrics were observed with SEM to make the morphology investigation. Figure 2.11 below showed the surface morphology images of sample DOPO-HQ@CS/ZIF-8 (3BL) before and after combustion.

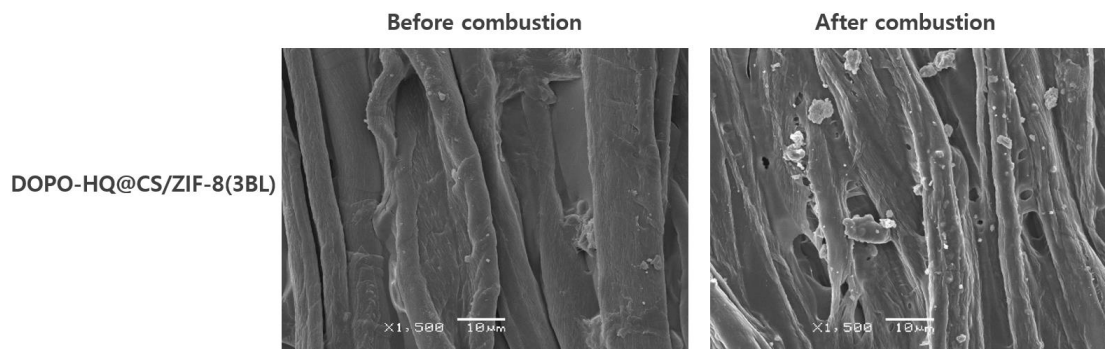


**Figure 2.11** The SEM images of cotton samples before and after combustion

As shown in the picture, each cotton fiber was fully coated because of the use of multilayer DOPO-HQ@CS and ZIF-8. DOPO-HQ and ZIF-8 particles were well introduced and distributed on cotton fibers through the chitosan network, which was more visible after combustion due to the thermal degradation of chitosan. After the burning process, it appeared as if the treated cotton sample still retained its shape and integrity. The presence of air bubbles between cotton fibers was proof that the generated gases were released during combustion as a means of diluting combustible volatiles concentration in the gas phase. Then, it was intended to quantify the thermal properties of cotton samples at high temperatures by TGA to investigate the practical barrier effects. Also, it was still necessary to consider that the 19.49 wt% weight gain of sample DOPO-HQ@CS/ZIF-8 (3BL) might inevitably bring negative influences on the physical properties of pristine cotton fabric.

### Thermal analysis

The thermogravimetric analysis (TGA) was proposed in order to clearly discern the differences in thermal characteristics between treated and untreated cotton samples.



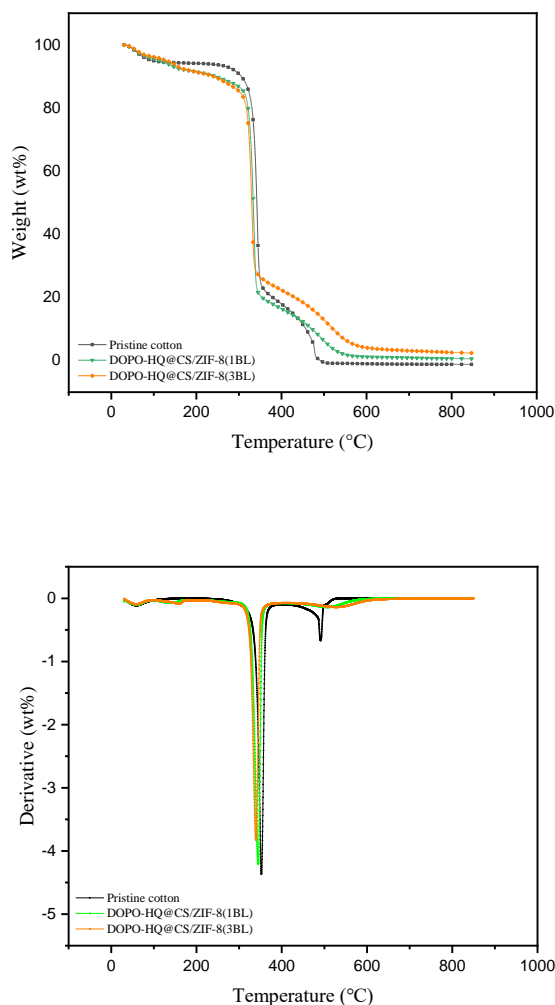


**Figure 2.12** TGA and DTG curves of (a) pristine cotton sample (b) DOPO-HQ@CS/ZIF-8 (1BL) sample and (c) DOPO-HQ@CS/ZIF-8 (3BL) sample

**Table 2.5** TGA data of cotton samples under air atmosphere

Sample	$T_{10\%}$ (°C)	Stage1		Stage2		Residue at 800°C (wt%)
		$T_{max}$ (°C)	$R_{max}$ (wt%/min)	$T_{max}$ (°C)	$R_{max}$ (wt%/min)	
Pristine cotton	318.5	341.6	37.6	479	93.4	-1.21
DOPO-HQ@CS/ZIF-8 (1BL)	254.8	334.6	36.5	483.5	90.8	0.5768
DOPO-HQ@CS/ZIF-8 (3BL)	254.3	333.2	36.3	484.8	83.6	2.3806

\* The heating rate is fixed by 10 °C/min.  $T_{10\%}$  is the initial decomposition temperature at which 10% sample weight is lost.  $T_{max}$  is the temperature of maximum rate of weight loss.  $R_{max}$  is weight loss rate at the maximal peak ( $T_{max}$ ).

At 500 °C - 800 °C, the residual char content of treated samples was higher than that of pure cotton fabric, as shown in Figure 2.12 and Table 2.5. As more layers of DOPO-HQ@CS and ZIF-8 were deposited onto cotton substrates, the char formation capacity of treated fabric was also increased. The initial decomposition temperature ( $T_{10\%}$ ) of cotton samples after treatment were around 254 °C, which were substantially lower than that of pristine cotton fabric. Given that the chemical composition of chitosan was linear polysaccharide, the chitosan covering the surface of cotton fabrics was easier to reach the temperature of decomposition. The whole thermal degradation of the cotton fabric could be divided into two stages: the first was the principal thermal breakdown stage, which accounted for the majority of the overall weight loss. Evidently, the treated samples didn't exhibit any barrier effect at stage 1 since neither  $T_{max}$  was raised nor  $R_{max}$  was decreased. At stage 2, compared to pristine cotton, the  $T_{max}$  of sample DOPO-HQ@CS/ZIF-8 (3BL) was slightly increased from 479 °C to 484 °C, and the corresponding  $R_{max}$  was declined from 93.4 wt%/min to 83.6 wt%/min.

#### **2.2.2.4 The application of ZIF-8 dispersion in combination with DOPO-HQ@PVA**

Poly(vinyl alcohol) (PVA) is a water-soluble and biodegradable polymer that are extensively applied in textile industry, packaging materials and adhesives fields because of its low-cost, non-toxicity, good mechanical qualities and high transparency properties (Halima, 2016). It has a large amount of hydroxyl groups (-OH), which allows for reactions like grafting or cross-linking with cotton fibers (Zia et al., 2012), meanwhile retaining the hydrophilic surface of textile substrates (Singh et al., 2021). PVA can be considered as a carbonization agent in the intumescent flame retardant system, working together with acid sources such as phosphorus-containing compounds to suppress fire (Wilkie and Morgan, 2009). Brandon and coworkers developed a nanocoating consisting of polyvinyl alcohol (PVA) and montmorillonite (MMT) via spraying method to improve the flame retardancy performances of double-walled corrugated cardboard (Williams et al., 2021). Besides, 1,2,3,4-butanetetracarboxylic acid (BTCA) as an efficient crosslinking agent with the catalyst of sodium hypophosphite (SHP) could improve the abrasion resistance of cotton fabrics when used in combination with

PVA (Zhou et al., 2004). In order to enhance the physical strength of treated cotton samples, PVA was utilized to modify cotton fabrics and incorporate with DOPO-HQ for investigating the barrier effects. The preparation process of PVA and DOPO-HQ@PVA finishing solution was displayed as follows:

7 wt% PVA, 1 wt% BTCA and 0.25 wt% SHP were mixed and dissolved into distilled water under magnetically stirring for 10 hours at room temperature to make the required PVA finishing solution, which was measured with pH value of 3.01. DOPO-HQ@PVA was obtained by adding 2 wt% DOPO-HQ into the previously resultant PVA finishing solution with the aid of vigorous magnetic stirring. The pH value of DOPO-HQ@PVA finishing solution was detected as 3.12.

After successfully preparing the uniform finishing solution of PVA and DOPO-HQ@PVA, cotton fabrics were first treated with ZIF-8 dispersion and then with PVA (DOPO-HQ@PVA) by using dip-pad-dry procedure. The cotton samples after treatment were labeled as ZIF-8/PVA and ZIF-8/DOPO-HQ@PVA, respectively.

## SEM

SEM was applied to compare the differences in surface morphology of cotton samples as seen in Figure 2.13.

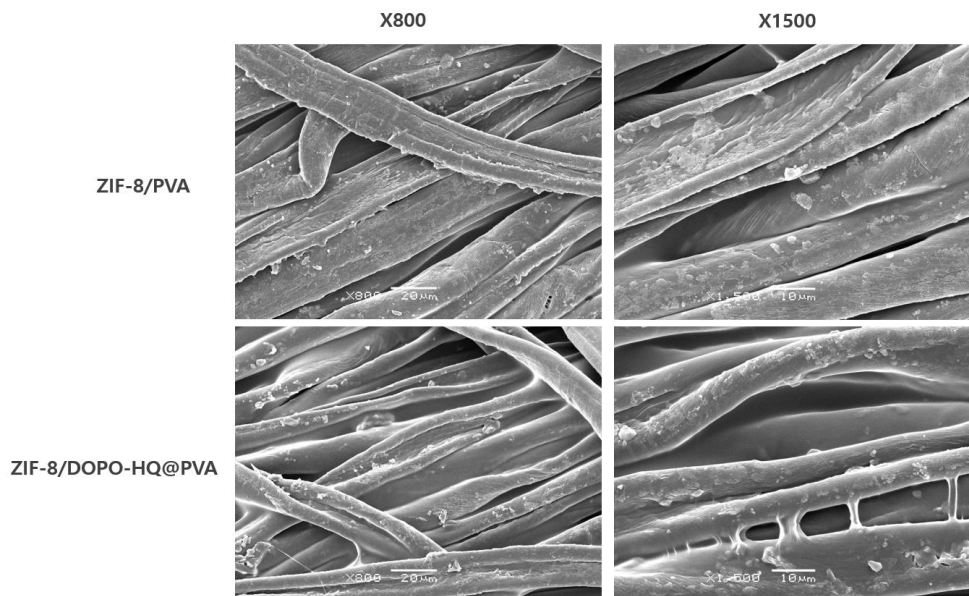


**Figure 2.13** SEM images of (a) ZIF-8/PVA sample and (b) ZIF-8/DOPO-HQ@PVA sample

With BTCA as the cross-linking agent and SHP as the catalyst, multiple hydrogen bonds were constructed between PVA and cotton fibers, forming uniform and continuous film and making the physical properties of pristine cotton fabric improved. For both sample ZIF-8/DOPO-HQ@PVA and ZIF-8/PVA, it was clearly observed that DOPO-HQ and ZIF-8 particles were distributed inside through the network of PVA covering on each cotton fiber. While it seemed that PVA could productively incorporate and transport DOPO-HQ into cotton fabrics, the fire barrier performances of treated cotton samples had to be verified by other testing methods such as heat transfer.

### Tensile breaking strength

The pristine cotton and treated cotton samples were tested for their physical strength through a universal tensile testing machine (Zwick/Roell, ProLine), and the critical indicators of Young's modulus, breaking strength and elongation at break were recorded in Table 2.6 below.

**Table 2.6** The results of tensile breaking strength of cotton fabric before and after treatment

Sample	Young's modulus (N)	Breaking strength (N)	Elongation at break (%)
Pristine cotton	12.35	1193	13.19
ZIF-8/PVA	28.2	1511.53	20.00
ZIF-8/DOPO-HQ@PVA	52	1517.87	19.54

Strength testing for textile fabrics is the process of each fiber from stretching to breaking under constant external force. The Young's modulus (initial modulus) represents the resistance of the fiber to small deformations, reflecting the stiffness of the fiber deformed by small stretching or bending effects that depends on the chemical structure of the polymer and the intermolecular interaction force. In contrast to pure cotton fabric, it was found that when ZIF-8 was used in combination with PVA, there was no strength loss caused, even improved the tensile breaking ability from 1193 N to 1511.53 N and elongation at break from 13.19% to 20%, which reflected the increased flexibility of cotton fibers. Additionally, the Young's modulus of sample ZIF-8/DOPO-HQ@PVA was up to

52 N, demonstrating the positive response of DOPO-HQ to tearing resistance at the initial stage when applied in combination with ZIF-8 and PVA.

### Heat transfer

The cotton samples were fixed and exposed to an incident heat flux of  $(80 \pm 2)$  kW/m<sup>2</sup> in accordance with EN ISO 9151, heat transfer index was calculated based on the length of time that cotton fabrics could remain exposed before calorimeter's temperature rise of  $(24 \pm 0,2)$  °C as stated in Table 2.7 below.

**Table 2.7** Heat transfer index results of cotton fabrics before and after treatment

Sample	Heat transfer index/s
Pristine cotton	14.6
ZIF-8/PVA	12
ZIF-8/DOPO-HQ@PVA	12.4

As seen from the data, it took 14.6 seconds for pristine cotton to rise 24 °C, whereas the heat transfer time were shorted to 12 seconds and 12.4 seconds for sample ZIF-8/PVA and ZIF-8/DOPO-HQ@PVA. This indicated an increase in the thermal conductivity of the treated fabric surface, making it less conducive to flame retardancy. Though the incorporation of PVA resulted in a significant increase in the strength of cotton samples, PVA as hydrophilic and flammable polymer was easily and quickly heated up when it was applied as the outermost layer on substrates, which was contrary to the purpose of developing barrier properties for cotton fabrics.

#### 2.2.2.5 Conclusions

ZIF-8 containing nitrogen flame-retardant element is free of halogens and formaldehyde, and the zinc oxide produced at high temperatures that can efficiently acts as a fire barrier, making it prospective for applying to cotton substrates. However, taking into account all the results in actual fire performances of the finished fabrics, there was still much room for improvement with regard to vertical burning and thermogravimetric behaviors for the use of ZIF-8 in combination with the other polymeric materials (BPEI, VTES). When the

incorporation of ZIF-8 and DOPO-HQ@CS were introduced into cotton fabrics, it helped to develop the fire performances of substrates but inevitably affected the physical properties owing to the excessive weight gain. Correspondingly, the incorporation of ZIF-8 and DOPO-HQ@PVA didn't cause any loss of physical strength in the pure cotton and even supported the enhancement of tensile breaking ability. Yet as hydrophilic and flammable polymer, PVA was found to facilitate the thermal conductivity of substrates, which made it less suitable for building fire barriers on cotton fabrics.

### 2.2.3 Fire barrier investigation of UiO-66-COOH

Zirconium is a biologically abundant element in nature, and Zr-based metal-organic frameworks (Zr-MOFs) were first discovered and reported by Lillerud et al. in 2008. Zr-MOFs are considered with higher thermal and chemical stability than other types of MOFs, which makes them suitable for industrial processes (Rodríguez et al., 2014). UiO-66 (UiO: University of Oslo) as one kind of Zr-based MOFs has been extensively studied because of its broad applications and outstanding stability, and it was reported to grow on the surface of cotton fibers by facile two-step synthesis for enhancing adsorption of water micropollutants (Schelling et al., 2018). Some researchers prepared chlorine loaded UiO-66-NH<sub>2</sub>, which was used to coat polyester fabrics for eliminating biological and chemical threats (Cheung et al., 2021).

Submicrometer particles of UiO-66-COOH with free pendant –COOH groups (Figure 2.14) could be synthesized by eco-friendly hydrothermal procedure (Andrés et al., 2019). Water-based synthesis will greatly lower manufacturing costs in addition to the advantages of employing non-toxic solvents. It has good compatibility with cotton substrates owing to organic linkers' presence. (Khabzina et al., 2018). Because of the large pore volume and specific surface area, allowing it to absorb toxic fumes generated from the combustion of polymer materials. And some non-flammable gases generated by UiO-66-COOH particles also help to dilute the concentration of combustible gases, thus improving the smoke suppression (Martínez-Ahumada et al., 2021; Nabipour et al., 2020b). At high temperatures, UiO-66-COOH is able to decompose to produce zirconia on the surface of cotton substrates that works as a physical barrier to protect the fabric from further burning (Wang et al., 2019).

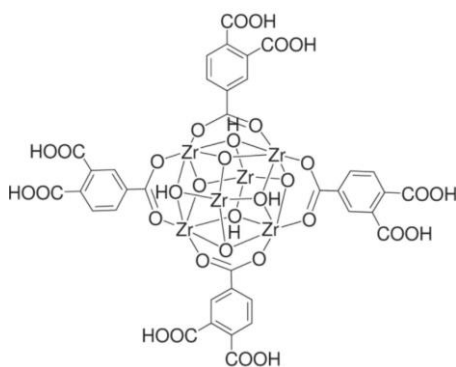


**Figure 2.14** Chemical structure of UiO-66-COOH

### 2.2.3.1 UIO-66-COOH synthesis by LBL assembly

The layer-by-layer (LBL) approach for synthesizing MOFs is also known as liquid-phase epitaxy by introducing reaction partners successively and repetitively on the substrate (So et al., 2014). In recent years, the LBL technique has shown promise for the synthesis of homogenous MOF films with controlled thickness (Shekhah et al., 2012). MOF-5 was successfully obtained by repeated and alternating immersion of silk fabric in a solution of metal ions and organic ligands via electrostatic layer-by-layer deposition (Khanjani and Morsali, 2014).

Based on alternate deposition of a positively charged layer and a negatively charged layer onto cotton fabrics, the UIO-66-COOH was synthesized by the following process. 2.4 g (10 mmol)  $ZrCl_4$  was completely dissolved in 50 ml deionized water as Solution A (positive charge), while 2.2 g (10 mmol)  $H_3BTC$  was dissolved in 50ml deionized water with the help of Turrax digital homogenizer (16000 rpm \* 1 min) as Solution B (negative charge). The cotton fabric was alternatively dipped in Solution A and Solution B for each 5 min, subsequently dried at 75 °C for 4 min, which was considered to form one bilayer (BL) of UIO-66-COOH as illustrated in Figure 2.15.

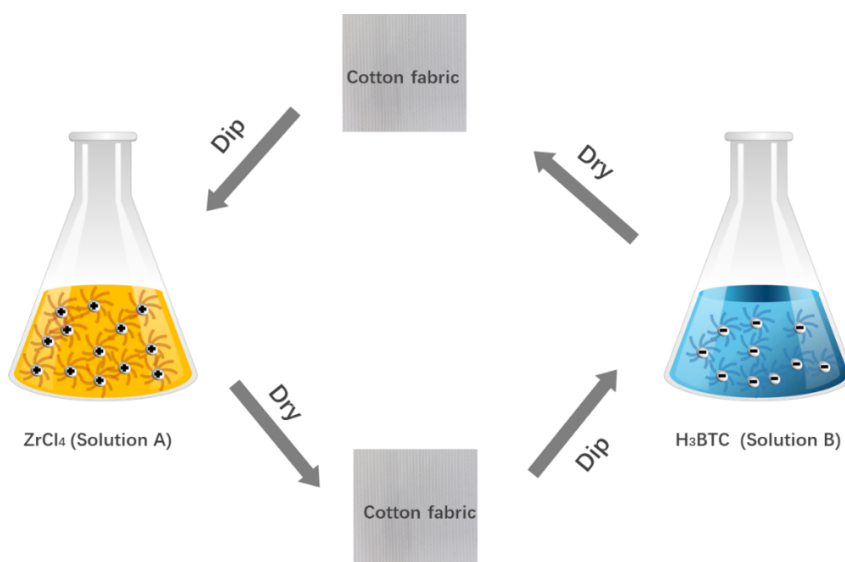


**Figure 2.15** Schematic of layer-by-layer synthesis of UIO-66-COOH on cotton substrates



## SEM

The UIO-66-COOH coating were obtained by layer-by-layer method for 1 BL and 2 BL respectively. SEM was used to observe the growth of UIO-66-COOH onto cotton substrates and to compare it with pure cotton fabric. Figure 2.16 below showed the surface morphology images of pristine cotton, sample UIO-66-COOH (1BL) and UIO-66-COOH (2BL).

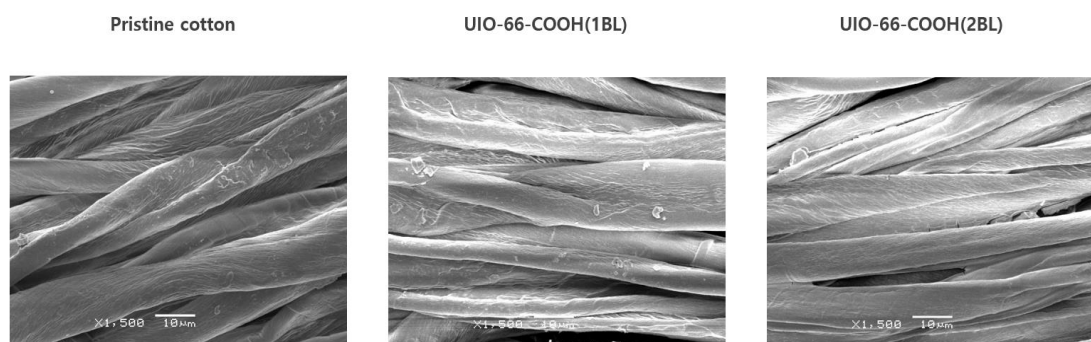


**Figure 2.16** The SEM image analysis of pristine cotton and treated samples

Judging by the SEM photographs, it was clear that the quantity of UIO-66-COOH particles successfully synthesized by the LBL method growing on cotton fibers was insignificant. It could be assumed that some  $ZrCl_4$  and  $H_3BTC$  finishing liquids were only absorbed by the cotton fibers individually, instead of generating UIO-66-COOH particles as expected. However, the possibility of using this approach for the construction of fire barriers onto cotton fabrics had yet to be analyzed in terms of thermal behavior.

## Thermal analysis

Thermogravimetric analysis (TGA) and derivative thermogravimetry (DTG) curves of all the samples were drawn in order to clearly identify the differences in thermal properties before and after treatment as seen in Figure 2.17. Table 2.8 exhibited the correlating data extracted from TGA and DTG curves.

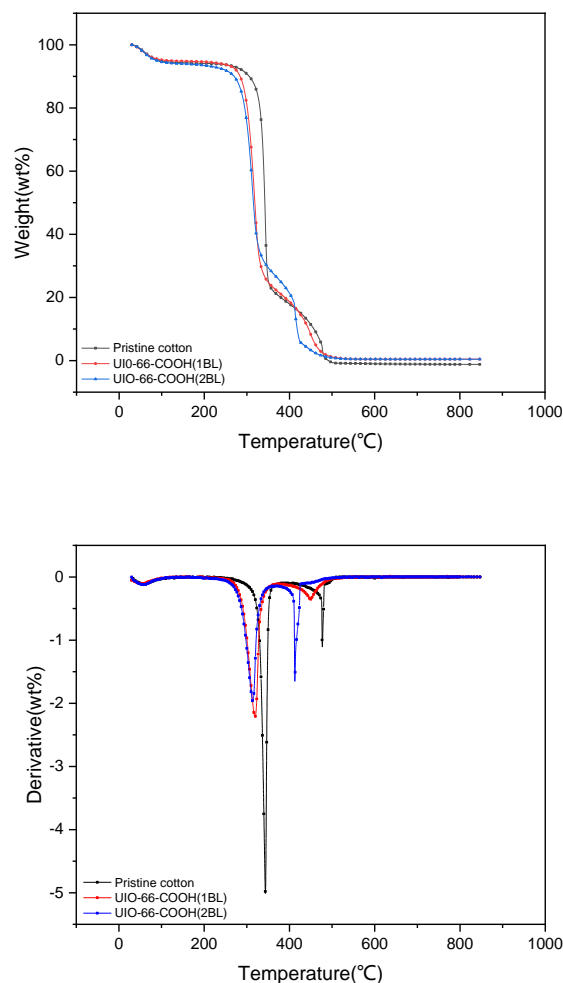


**Figure 2.17** TGA and DTG curves of (a) pristine cotton sample, (b) UIO-66-COOH (1BL) sample and (c) UIO-66-COOH (2BL) sample

**Table 2.8** TGA data of cotton samples under air atmosphere

Sample	$T_{10\%}$ (°C)	Stage1		Stage2		Residue at 800 °C (wt%)
		$T_{max}$ (°C)	$R_{max}$ (wt%/min)	$T_{max}$ (°C)	$R_{max}$ (wt%/min)	
Pristine cotton	318.5	341.6	37.6	479	93.4	-1.21
UIO-66-COOH (1BL)	291.3	320	31.7	458.1	90.9	0.4427
UIO-66-COOH (2BL)	280.1	317.4	39.2	420.8	87	0.4245

\* The heating rate is fixed by 10 °C/min.  $T_{10\%}$  is the initial decomposition temperature at which 10% sample weight is lost.  $T_{max}$  is the temperature of maximum rate of weight loss.  $R_{max}$  is weight loss rate at the maximal peak ( $T_{max}$ ).

According to the DTG curves, it was easily found that all cotton samples performed two-step degradation behavior. The cotton fabric first undergone a series of dehydration and degradation. At higher temperatures, the resulting L-glucose would break down into small molecules, while residual char was formed. As the temperature continued to rise, the unstable char layers went through oxidative degradation. From Figure 2.17 and Table 2.8, it could be seen the residual char content of treated samples at 500 - 800 °C was increased than that of pristine cotton fabric. The more layers of UIO-66-COOH were constructed on the surface of cotton fabric, the more char yielded. Compared to the pure cotton, the initial decomposition temperature ( $T_{10\%}$ ) of treated samples became lower, which may be caused by evaporating liquids and the early decomposition of UIO-66-COOH for releasing heat to protect the cotton fibers underneath. Probably due to the insufficient amount of UIO-66-COOH particles growing onto cotton fabrics, there was no increase in  $T_{max}$  for both sample UIO-66-COOH (1BL) and UIO-66-COOH (2BL) despite resulting in a slight reduction in  $R_{max}$  at high temperatures.

### **2.2.3.2 The application of UIO-66-COOH (LBL) in combination with BPEI**

3 wt% BPEI finishing solution was made by dissolving 3 g BPEI into 97 ml distilled water with magnetic stirring under 70 °C for 6h. The cotton substrate was firstly incorporated with 2BL UIO-66-COOH by LBL assembly and then with 3 wt% BPEI finishing solution via dip-pad-dry process. The treated cotton samples were respectively denoted as U2BL-P1, U2BL-P2 and U2BL-P3 depending on the deposition layers of BPEI.

### **SEM**

SEM was utilized to display the surface morphology of cotton sample U2BL-P1, U2BL-P2 and U2BL-P3 for comparison. Because of the good film-forming properties of hydrophilic BPEI, the cotton fibers were entirely coated as seen in Figure 2.18. With more layers of BPEI applied to cotton fabrics, the composite material formed by UIO-66-COOH and BPEI had become denser and thicker, covering the surface of cotton fabrics to protect them from fire. Additionally, BPEI could act as a blowing agent, releasing low molecular weight molecules like  $NH_3$  and causing the carbonaceous residues to become porous. The differences

between these three cotton samples treated by varying numbers of finishing layers still required TGA to further analyze their thermal behavior and compared them with the pristine cotton.

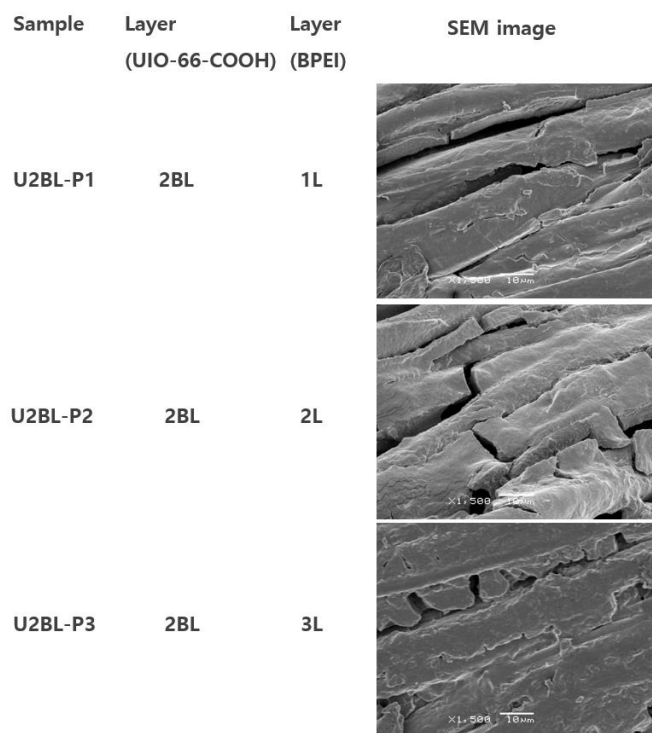


**Figure 2.18** The SEM image analysis of treated samples

### Thermal analysis

Figure 2.19 showed the TGA and DTG curves of cotton samples before and after treatment, while Table 2.9 exhibited the crucial information derived from the DTG and TGA. Firstly, the initial decomposition temperature ( $T_{10\%}$ ) of all treated samples was lower than that of pristine cotton fabric, which may be caused by the evaporation of water and early decomposition of the incorporated composites material covering cotton surface. At both stage 1 and stage 2 of cotton degradation, the finished samples succeeded in reducing  $R_{max}$  but neither improved  $T_{max}$ . Meanwhile, the residuals content of all treated samples was higher than that of pristine cotton, which indicated that BPEI was contributed to increasing protective char yield. However, sample U2BL-P1 ultimately yielded residues of 1.1708 wt%, while sample U2BL-P3 yielded only 0.6855 wt%. There

was some possibility that the UIO-66-CCOH synthesized by LBL assembly didn't interact well with BPEI.

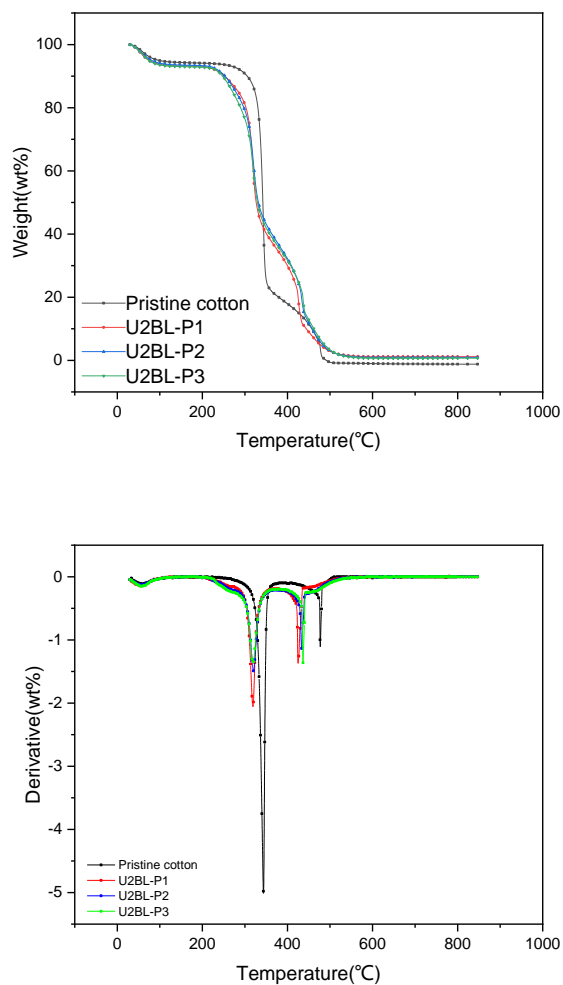


**Figure 2.19** TGA and DTG curves of (a) pristine cotton sample, (b) U2BL-P1 sample, (c) U2BL-P2 sample and (d) U2BL-P3 sample

**Table 2.9** TGA data of cotton samples under air atmosphere

Sample	$T_{10\%}$ (°C)	Stage1		Stage2		Residue at 800 °C (wt%)
		$T_{max}$ (°C)	$R_{max}$ (wt%/min)	$T_{max}$ (°C)	$R_{max}$ (wt%/min)	
Pristine cotton	318.5	341.6	37.6	479	93.4	-1.21
U2BL-P1	259	321.5	24.1	426.8	73.5	1.1708
U2BL-P2	259.8	322	25.1	432.1	75.4	0.9231
U2BL-P3	257.9	321.1	28.3	432.6	75	0.6855

\* The heating rate is fixed by 10 °C/min.  $T_{10\%}$  is the initial decomposition temperature at which 10% sample weight is lost.  $T_{max}$  is the temperature of maximum rate of weight loss.  $R_{max}$  is weight loss rate at the maximal peak ( $T_{max}$ ).

### 2.2.3.3 Hydrothermal synthesis of UIO-66-COOH homogeneous dispersion

The synthesis of MOFs is usually achieved by the conventional solvothermal technique that is using organic solvents with strong polarity at the condition of high pressure and temperature. When the organic solvents are replaced by water in the process, it is known as hydrothermal synthesis (González et al., 2021).

The whole synthesis route of UIO-66-COOH homogeneous dispersion was inspired from Jia et al. and described as follows (Xiangze et al., 2021). The same chemical amount of  $ZrCl_4$  and  $H_3BTC$  powder were respectively dissolved in deionized water with the help of Turrax digital homogenizer. The two were mixed and added to the sealed reactor with refluxed condenser for magnetic stirring. 1:1 mixture of ethanol and water was then added to produce the dispersion by homogenizer or ultrasonication treatment, the particle size and zeta potential of the samples were measured after magnetic stirring at room temperature overnight (Table 2.10).

**Table 2.10** The properties of UIO-66-COOH homogeneous dispersion

Sample	Homogenization time /min	Ultrasonication time/min	Size/nm	Zeta potential/mv
1	1		2190	10.5
2	2		1530	9.63
3	3		1040	9.14
4	4		1510	10.3
5	5		1302	8.87
6		3	810	10.85
7		6	623	11.99
8		10	322	11.8
9		15	356	11.3

In order to obtain homogeneous and fine UIO-66-COOH dispersion, the effect of the Turrax digital homogenizer was compared with that of the ultrasonic machine. The particle size and zeta potential data for UIO-66-COOH samples were presented in Table 2.10, and it was determined that the particle size could be reduced to 322 nm and stay good stability with the assistance of ultrasonication technology.

### Synthesis rote of UIO-66-COOH homogeneous dispersion

The specific procedure for the eco-friendly hydrothermal synthesis of UIO-66-COOH homogeneous dispersion was finalized: Firstly,  $ZrCl_4$  (2.4 g) and  $H_3BTC$  (2.2 g) were dissolved in DI (50 ml), respectively. The two were mixed and refluxed in a sealed reactor at 100 °C for 16 hours. A mixture of 170 ml of ethanol and water (1:1) was then added and sonicated for 10 minutes. After overnight magnetic stirring at room temperature, the homogeneous dispersion of UIO-66-COOH would be achieved (Figure 2.20). With the resultant nano-sized particles (322 nm), it was enabled to uniformly incorporate and distribute UIO-66-COOH onto cotton fibers and improve the add-on.

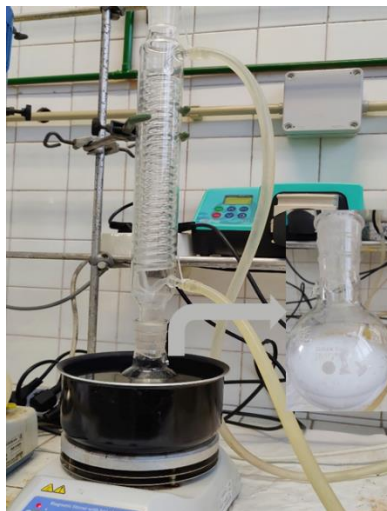


**Figure 2.20** Hydrothermal synthesis of UIO-66-COOH

### The visible stability of UIO-66-COOH dispersion

The resultant UIO-66-COOH dispersion sample was observed at room temperature for an extended period of time. The evolution of the dispersion stability of UIO-66-COOH with time could be intuitively seen from the digital photos shown in Figure 2.21 below. It was quite clear that the sample maintained homogeneous dispersion and that gravitational phase separation at room temperature would progressively appear after 12 hours or more.

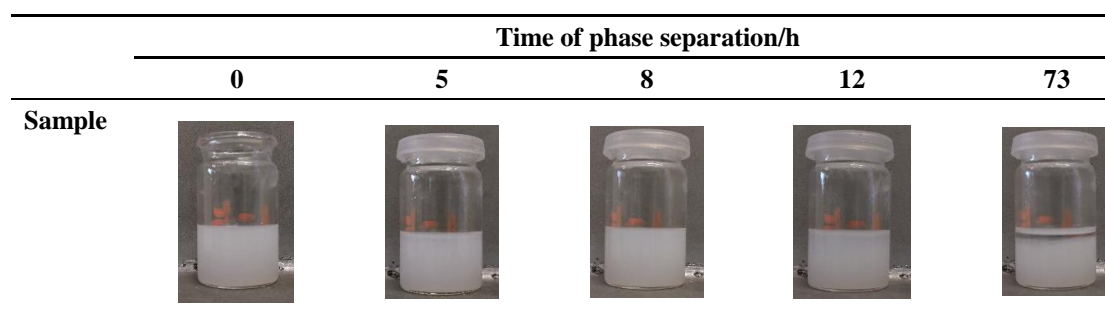


**Figure 2.21** Digital photos of UIO-66-COOH homogeneous dispersion at different time

#### 2.2.3.4 The application of UIO-66-COOH homogeneous dispersion

UIO-66-COOH homogeneous dispersion was applied onto cotton substrates at room temperature by a two-dip-two-nip padding process, which could achieve 100% wet pick-up with pressure of 0.6 kg/m<sup>2</sup> and velocity of 3.5 m/s. And the



treated cotton fabric was able to obtain approximately 6 wt% add-on after drying at 75 °C for 4 min, which was considered as one dip-pad-dry cycle (1L). The relevant data of cotton fabrics after finishing were shown in Table 2.11 below. It was clarified that the cotton substrates after depositing one-layer and two-layer of UIO-66-COOH respectively, were denoted as sample UIO-66-COOH (1L) and UIO-66-COOH (2L) with the corresponding weight gain of 6.17 wt% and 10.72 wt%. The quantity of UIO-66-COOH particles that was incorporated into the cotton substrates increased with the cycles of dip-pad-dry application. Nevertheless, the add-on of UIO-66-COOH needed to be balanced to prevent a highly substantial influence on the physical properties of cotton fibers.

**Table 2.11** The treatment data of cotton sample

Sample	W <sub>0</sub> /g	W <sub>1</sub> /g	Add-on/wt%
UIO-66-COOH (1L)	0.681	0.723	6.17
UIO-66-COOH (2L)	0.681	0.754	10.72

\* W<sub>0</sub> and W<sub>1</sub> refer to initial and final weight of specimen, respectively.

## SEM

As shown in Figure 2.22 below, the morphology of cotton fabrics before and after treatment was characterized through SEM photos. It was seen that the surface of the pristine cotton fiber was relatively smooth, flat and clean. For the treated samples, UIO-66-COOH was adsorbed on the fiber surface in the form of rough structure at the nano-micron scale, while partially UIO-66-COOH was agglomerated into larger-sized particles that may generate certain fiber defects. Additionally, compared to sample UIO-66-COOH (1L), the denser and thicker shielding layers were formed on sample UIO-66-COOH (2L).

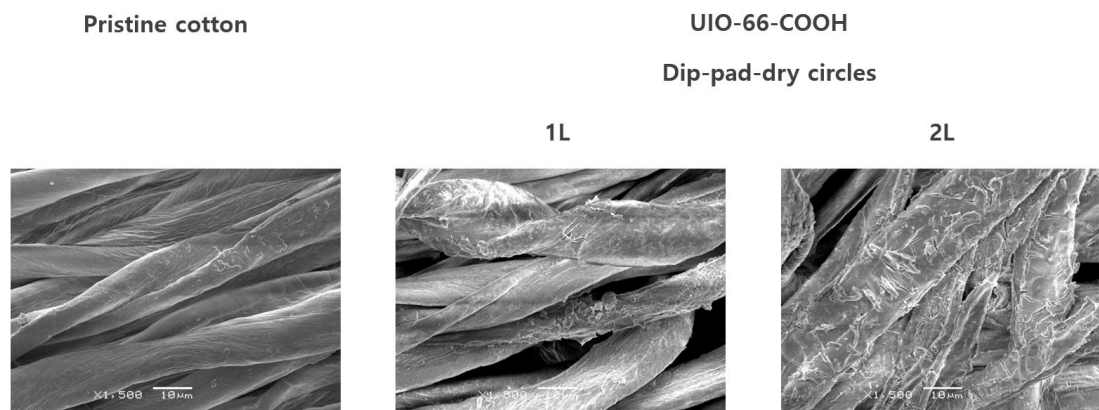


**Figure 2.22** The SEM image analysis of pristine cotton and treated samples

### Thermal analysis

The TGA and DTG curves of pristine cotton, sample UIO-66-COOH (1L) and UIO-66-COOH (2L) were displayed in Figure 2.23, and critical data from Table 2.12 was presented based on TGA and DTG. It was found that the residual char content of treated samples at 500 - 800 °C was increased compared to pristine cotton fabric. The more layer of UIO-66-COOH, the higher amount of char residues, which indicated that the UIO-66-COOH constructed on the surface of cotton fabrics had obvious protective effects. Besides, the initial decomposition temperature ( $T_{10\%}$ ) of treated samples was slightly lower than that of pristine cotton fabric, which caused by the decomposition of the incorporated UIO-66-COOH and the evaporation of liquid. The whole thermal degradation of the cotton fabrics could be considered as two stages. The  $R_{\max}$  of pristine cotton at stage 1 was 37.6 wt%/min, whereas the  $R_{\max}$  of sample UIO-66-COOH (1L) and UIO-66-COOH (2L) at stage 1 were respectively 40.8 wt%/min and 45.7 wt%/min. Likewise, compared to the pristine sample, the  $R_{\max}$  of treated samples at stage 2 wasn't decreased much, either. But, the  $T_{\max}$  of cotton was managed to raise from 479 °C to 500.9 °C with the aid of UIO-66-COOH. Thereby inferring that the introduction of individual UIO-66-COOH wasn't able to crucially enhance the thermal stability of cotton fabrics at elevated temperature and that was required to collaborate with additional flame-retardancy chemicals.

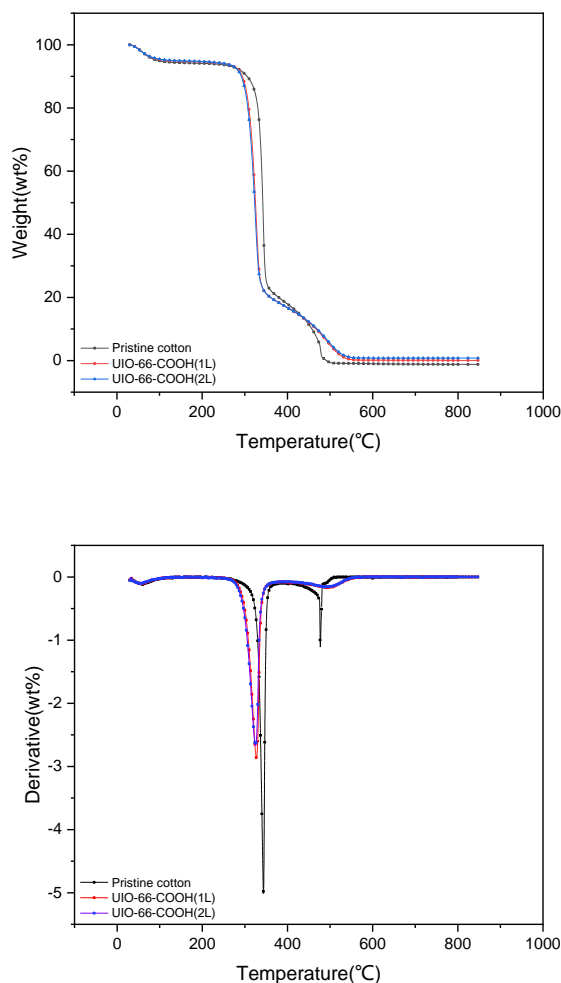


**Figure 2.23** TGA and DTG curves of (a) pristine cotton sample, (b) UIO-66-COOH (1L) sample and (c) UIO-66-COOH (2L) sample

**Table 2.12** TGA data of cotton samples under air atmosphere

Sample	$T_{10\%}$ (°C)	Stage1		Stage2		Residue at 800 °C (wt%)
		$T_{max}$ (°C)	$R_{max}$ (wt%/min)	$T_{max}$ (°C)	$R_{max}$ (wt%/min)	
Pristine cotton	318.5	341.6	37.6	479	93.4	-1.21
UIO-66-COOH (1L)	310.8	325.7	40.8	500.9	92.8	0.0573
UIO-66-COOH (2L)	308.3	324.8	45.7	501.5	95.8	0.7812

\* The heating rate is fixed by 10 °C/min.  $T_{10\%}$  is the initial decomposition temperature at which 10% sample weight is lost.  $T_{max}$  is the temperature of maximum rate of weight loss.  $R_{max}$  is weight loss rate at the maximal peak ( $T_{max}$ ).

### **2.2.3.5 The application of UIO-66-COOH homogeneous dispersion in combination with BPEI**

3 wt% BPEI solution was prepared and its pH value was measured to be 11.33, which was able to be adjusted to 6.75 with dilute hydrochloric acid, and it was referred as A-BPEI. The cotton fabrics were treated by UIO-66-COOH homogeneous dispersion and 3 wt% BPEI (A-BPEI) solution by multiple dip-pad-dry processes. Depending on the finishing agents and the number of layers, the resulting cotton samples were denoted as U2P1, U2P1, U2AP1 and U2AP2 respectively.

#### **SEM**

Figure 2.24 below exhibited the composition of various finishing layers for sample U2P1, U2P1, U2AP1 and U2AP2. The differences between all samples could be analyzed in relation to the surface morphology of cotton fabrics. From the SEM photos of treated samples, it was observed that UIO-66-COOH was able to penetrate into the interstices of cotton fibers and formed uniform and continuous film with the assistance of BPEI. The composites of UIO-66-COOH and BPEI have been incorporated and well distributed onto cotton substrates, reducing the surface roughness of the fabric and obtaining strong bonding effects against fire. However, more investigation was required to find the impacts of the quantity of finishing layers and pH level of BPEI.

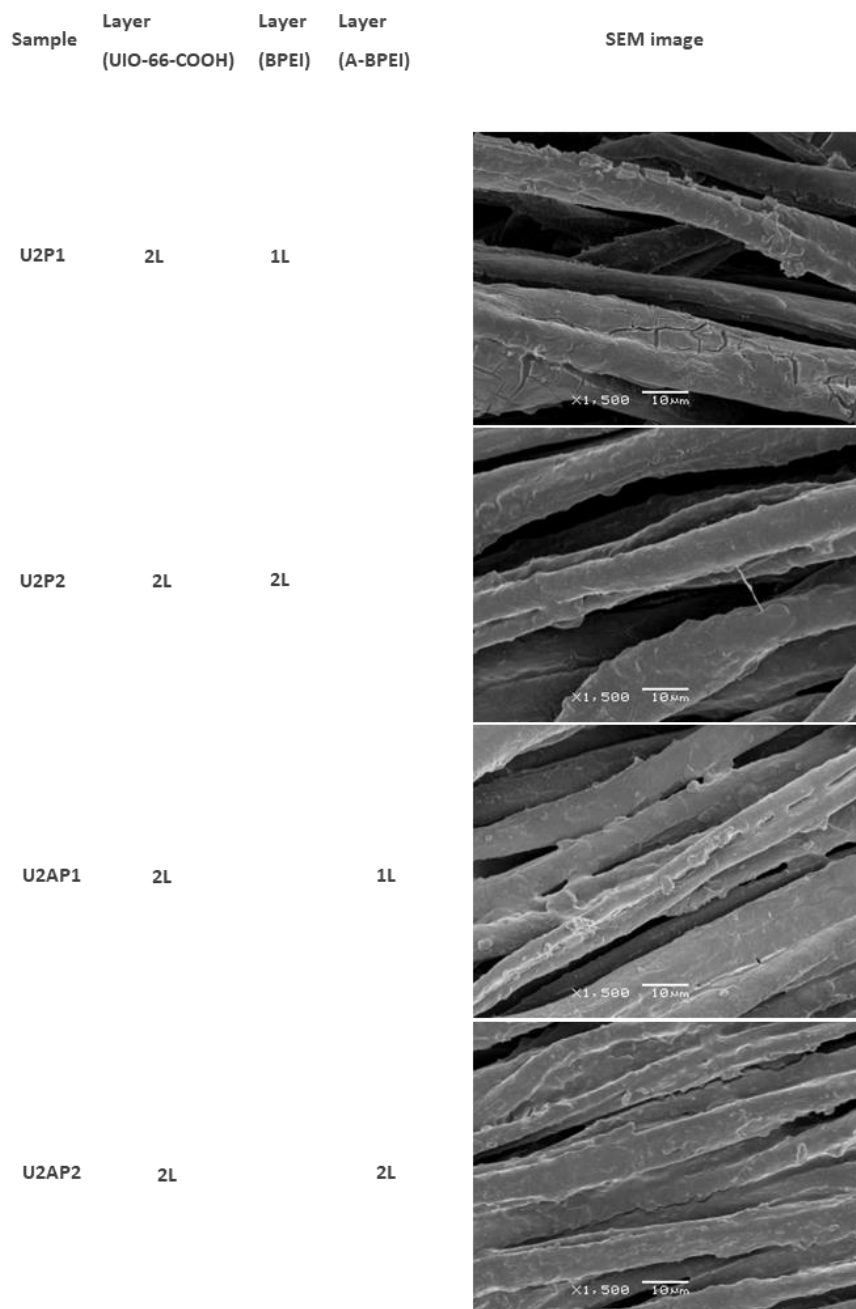


**Figure 2.24** The SEM image analysis of treated samples

### Thermal analysis

Figure 2.25 showed the TGA and DTG curves of sample U2P1, U2P1, U2AP1 and U2AP2, and matched them with pristine cotton fabric. Also, Table 2.13 included the relevant key data. At 500°C - 800 °C, sample U2AP1 and U2AP2 produced larger amounts of protective char residues than sample U2P1 and U2P2, which suggested that pH-adjusted BPEI may be helpful for increasing final char yield. The initial decomposition temperature ( $T_{10\%}$ ) of all treated samples

was lower than that of pristine cotton fabric. It was probably caused by evaporating liquid and the early decomposition of finishing chemicals. Since BPEI functioned as blowing agent, it could release low molecular weight molecules like  $\text{NH}_3$ , making the carbonaceous residue become porous. The degradation process of cotton fabrics was divided into two stages. Compared to utilizing UIO-66-COOH alone, the  $R_{\text{max}}$  was reduced at both stage 1 and stage 2 when the combination of UIO-66-COOH and BPEI was applied to cotton fabrics. Thereby it could be explained that there was a synergistic barrier effect between UIO-66-COOH and BPEI that contributed to improving the thermal degradation stability of cotton fabrics.

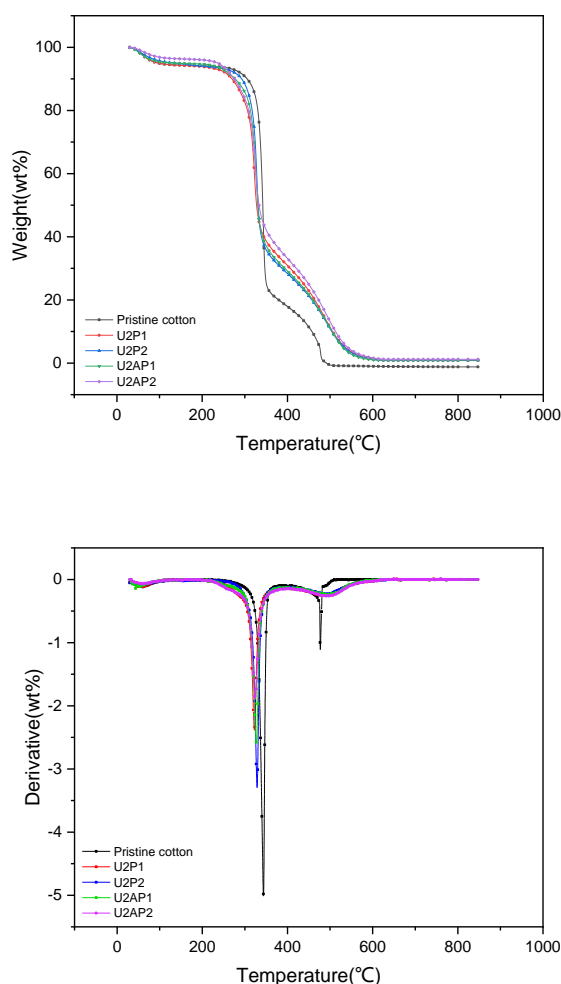


**Figure 2.25** TGA and DTG curves of (a) pristine cotton sample, (b) U2P1 sample, (c) U2P2 sample, (d) U2AP1 sample and (e) U2AP2 sample

**Table 2.13** TGA data of cotton samples under air atmosphere

Sample	$T_{10\%}$ (°C)	Stage1		Stage2		Residue at 800 °C (wt%)
		$T_{max}$ (°C)	$R_{max}$ (wt%/min)	$T_{max}$ (°C)	$R_{max}$ (wt%/min)	
Pristine cotton	318.5	341.6	37.6	479	93.4	-1.21
U2P1	274.9	322.6	36.9	500.3	87	0.8097
U2P2	303.5	326.2	25.6	499	88.1	0.9052
U2AP1	283.8	325.1	30.7	499.2	87.9	0.905
U2AP2	282.5	324	32.4	500.9	85.2	1.2102

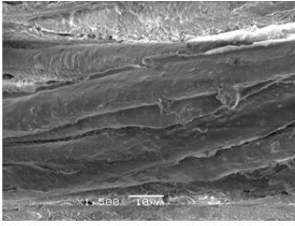
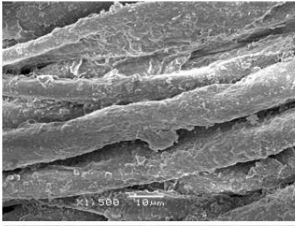
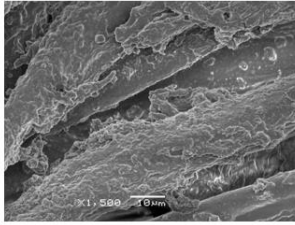
\* The heating rate is fixed by 10 °C/min.  $T_{10\%}$  is the initial decomposition temperature at which 10% sample weight is lost.  $T_{max}$  is the temperature of maximum rate of weight loss.  $R_{max}$  is weight loss rate at the maximal peak ( $T_{max}$ ).

### 2.2.3.6 The application of UIO-66-COOH homogeneous dispersion in combination with BPEI and VTES

8 g of VTES were dissolved in 92 ml of distilled water, ultrasonicated for 5 min and then stirred magnetically for 8h at room temperature to obtain the 8 wt% VTES finishing solution. The cotton fabrics were treated by UIO-66-COOH homogeneous dispersion at first, followed by 3 wt% A-BPEI and 8 wt% VTES solution via multiple dip-pad-dry processes. The resultant cotton samples were labeled as U1AP1V1, U2AP1V1 and U1AP1V2 accordingly, relying on the finishing solution and the number of layers.

### SEM

As shown in Figure 2.26, it was the SEM photographs of sample U1AP1V1, U2AP1V1 and U1AP1V2. In comparison to pure cotton, the surface morphology of treated cotton was rougher because some chemicals would migrate to the fibers surface. In the presence of VTES, the cotton fibers were fully coated via strong cross-linking through the Si–O–Si network, allowing the UIO-66-COOH and BPEI to be firmly retained inside. During the combustion process, the VTES coating could efficiently accelerate the dehydration and carbonization of cotton substrates, considerably increasing the protective char yield and reducing the overflow of combustible gases.

Sample	Layer (UIO-66-COOH)	Layer (A-BPEI)	Layer (VTES)	SEM image
U1AP1V1	1L	1L	1L	
U2AP1V1	2L	1L	1L	
U1AP1V2	1L	1L	2L	

**Figure 2.26** The SEM image analysis of cotton samples

### Thermal analysis

Figure 2.27 displayed the TGA and DTG curves of pristine cotton, sample U1AP1V1, U2AP1V1 and U1AP1V2, while Table 2.14 supplied a summary of the meaningful data. Firstly, it was obvious that there was no discernible difference between sample U1AP1V1 and U2AP1V1 in terms of their general trending of TGA curves. These treated samples showed a significant increase in residual char content at 500 - 800 °C when compared with pristine cotton fabric and other previously studied samples, indicating that VTES was with strong ability to promote fire retardancy and produce siliceous carbon for cotton substrates, which was mainly due to the formation of Si-O-C and Si-C bonds between the generated silica and cellulose in combustion (Zhang et al. 2022). Meanwhile, the initial decomposition temperature ( $T_{10\%}$ ) of treated samples was higher than that of pristine cotton fabric, which was attributed to the good thermal stability of silicon-based compounds. After finishing, the  $R_{max}$  for the first and second stages of cotton degradation was drastically decreased to 17.2 wt% and 84.6 wt%/min. It was therefore concluded that the combination of UIO-66-COOH, BPEI and VTES



was beneficial to facilitating the generation of carbon layers and inhibiting the thermal degradation of cotton fabrics.

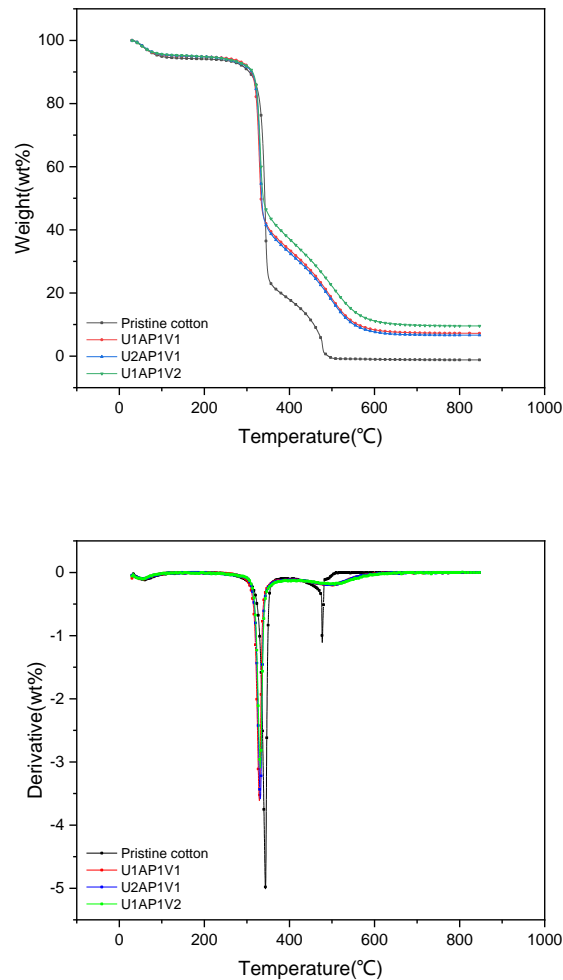


**Figure 2.27** TGA and DTG curves of (a) pristine cotton sample, (b) U1AP1V1 sample, (c) U2AP1V1 sample and (d) U1AP1V2 sample

**Table 2.14** TGA data of cotton samples under air atmosphere

Sample	$T_{10\%}$ (°C)	Stage1		Stage2		Residue at 800 °C (wt%)
		$T_{max}$ (°C)	$R_{max}$ (wt%/min)	$T_{max}$ (°C)	$R_{max}$ (wt%/min)	
Pristine cotton	318.5	341.6	37.6	479	93.4	-1.21
U1AP1V1	319.3	330.8	17.2	523.3	84.6	7.2355
U2AP1V1	320.9	332.5	14.8	522.7	85.3	6.6315
U1AP1V2	322	334.1	13.5	523.9	81	9.5643

\* The heating rate is fixed by 10 °C/min.  $T_{10\%}$  is the initial decomposition temperature at which 10% sample weight is lost.  $T_{max}$  is the temperature of maximum rate of weight loss.  $R_{max}$  is weight loss rate at the maximal peak ( $T_{max}$ ).

### 2.2.3.7 Conclusions

Firstly, these two synthetic approaches, layer-by-layer and hydrothermal synthesis, were evaluated and the latter was found to provide more efficient introduction and production of UIO-66-COOH for the fire barriers assembled onto cotton fabrics. Then after investigating and comparing different treatments, the organic–inorganic composite consisting of UIO-66-COOH, BPEI (pH 6.75) and VTES was considered promising to build the structural fire barriers for cotton fabrics.

The detailed finishing procedure was illustrated as Figure 2.28. UIO-66-COOH, BPEI and VTES were successively deposited onto cotton substrates. After finishing, the gained add-on of sample UIO-66-COOH, UIO-66-COOH/BPEI and UIO-66-COOH/BPEI/VTES were 2.9 wt%, 5.6 wt% and 10.9 wt% respectively.

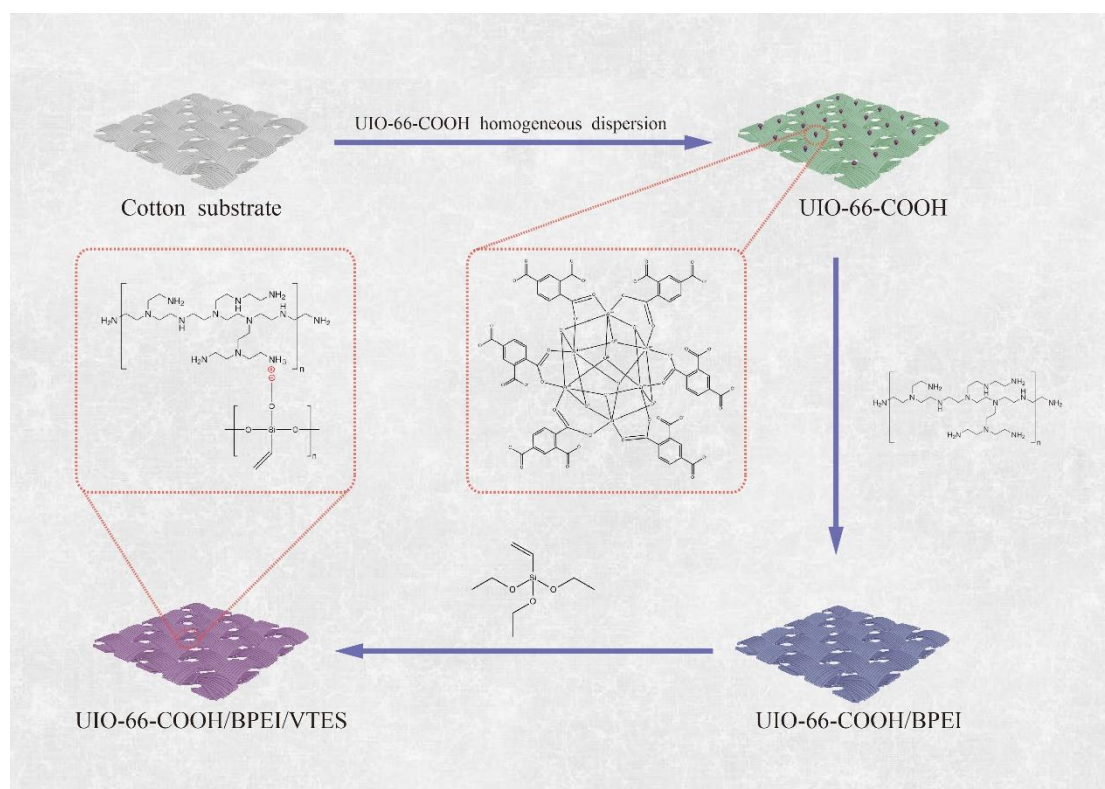


**Figure 2.28** Graphical representation of hybrid coating assembled onto cotton fabrics

## Vertical burning test

To evaluate the flammability and fire resistance of cotton samples, vertical burning tests were conducted. Given cotton fiber was highly flammable, these samples were exposed to a naked flame for 10 seconds before the ignition source was removed in order to record the combustion process. In Figure 2.29, the pristine cotton was vigorously burning and flame spread extremely rapid after ignition. During the burning, the fabric was entirely consumed without remaining chars. As sample UIO-66-COOH with very low add-on (2.9 wt%), the combustion duration was shortened accompanied by the formation of small amount of chars. And because BPEI acted as an effective carbon source, more dense char layers of sample UIO-66-COOH/BPEI was found. Apparently neither sample UIO-66-COOH nor sample UIO-66-COOH/BPEI appeared to slow the flame-spread, suggesting that other flame-retardant elements should be introduced for synergetic system. From the combustion behavior of sample UIO-66-COOH/BPEI/VTES, it performed better barrier effects by reducing the flame-spread speed and generating more protective char layers at the same time.

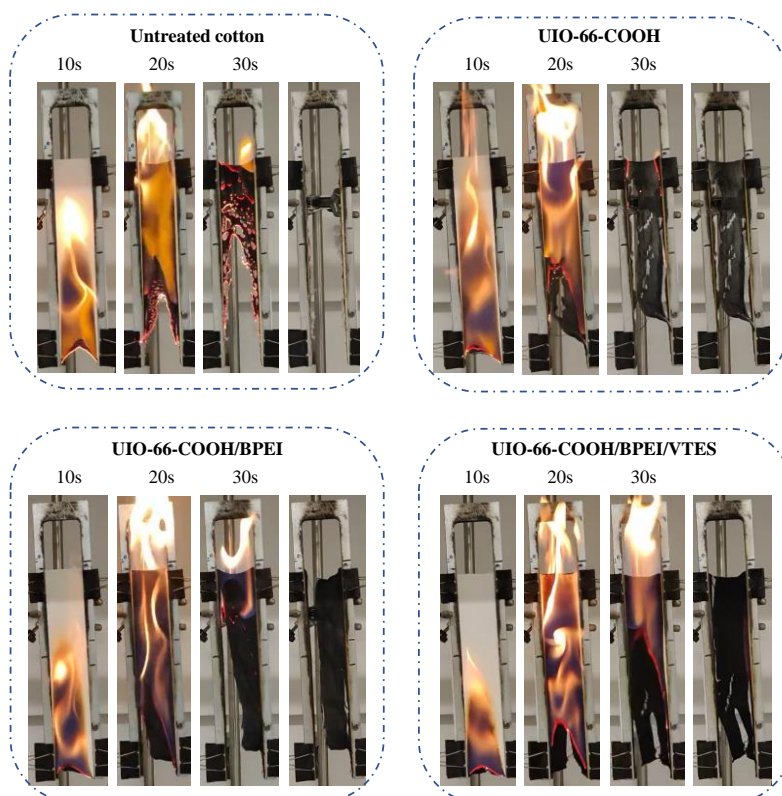


**Figure 2.29** Digital photos of cotton samples in the vertical burning test after ignition

## SEM

To study the surface morphology of cotton fabrics before and after combustion, all samples were observed by using SEM. The morphology of pristine cotton, sample UIO-66-COOH, UIO-66-COOH/BPEI and UIO-66-COOH/BPEI/VTES were exhibited in (a)-(d) photos of Figure 2.30. It was seen that the surface of the pure cotton fabrics was relatively smooth, flat and clean (Fig. 2.30a). For treated samples, UIO-66-COOH was adsorbed to form a micro-nano rough structure on the fibers, while some of the UIO-66-COOH was agglomerated into larger-sized particles that may generate certain defects (Fig. 2.30b). As hyperbranched polymer, BPEI was able to help UIO-66-COOH to penetrate into the interstices of cotton fibers, making them evenly distributed and forming the uniform and continuous film-like structure with the bonding effects (Fig. 2.30c). In the presence of VTES, the cotton fibers were fully coated due to strong cross-linking through Si–O–Si network, allowing UIO-66-COOH and BPEI to adhere and be trapped inside. During the burning process, the VTES coating could efficiently accelerate the carbonization of cotton fibers, increasing the protective char yield to a great extent (Fig. 2.30d). After combustion, the produced carbonized residuals of cotton samples retained the original cellulosic fiber structure to varying degrees as shown in (e)-(g) photos of Figure 2.30. Particularly for sample UIO-66-COOH/BPEI/VTES, the coated organic–inorganic composites contributed to denser and thicker carbon layers that protected the fibers in combustion (Fig. 2.30g).

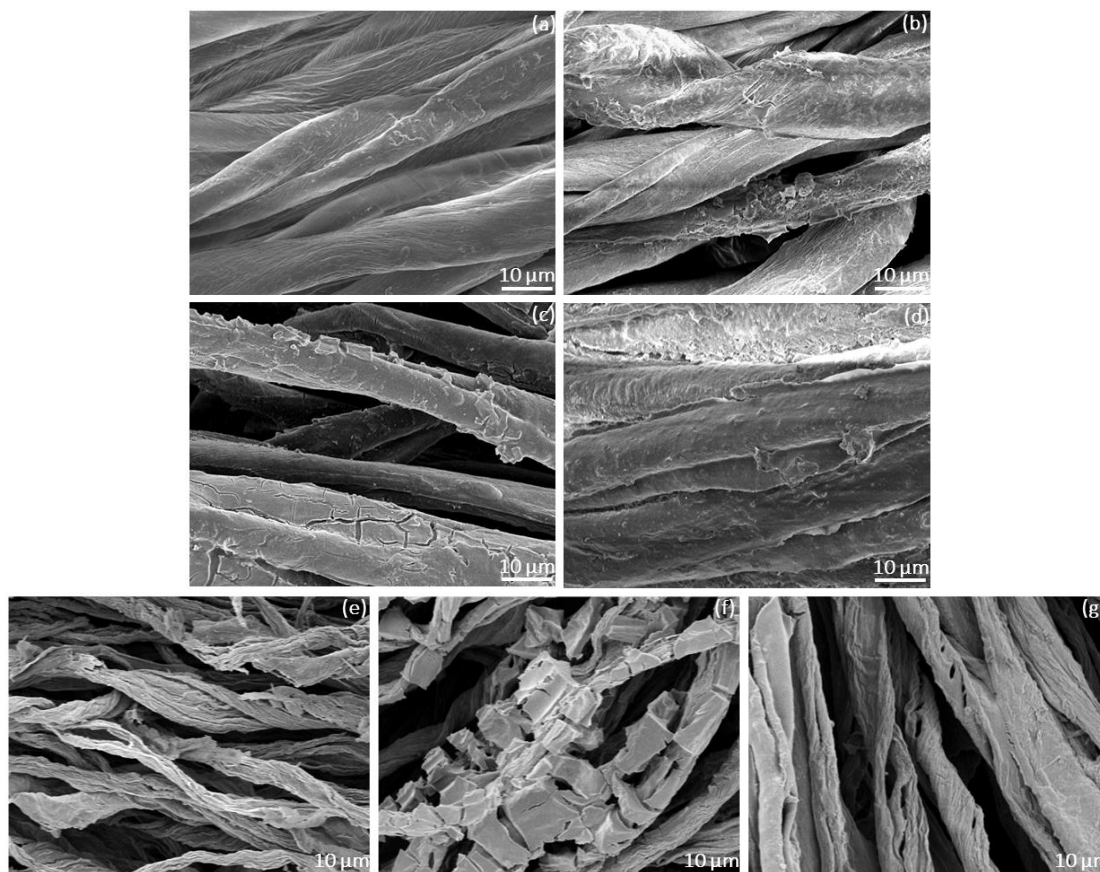


**Figure 2.30** The SEM images of (a) pristine cotton, (b) UIO-66-COOH sample, (c) UIO-66-COOH/BPEI sample (d) UIO-66-COOH/BPEI/VTES sample, (e) UIO-66-COOH residual chars, (f) UIO-66-COOH/BPEI residual chars and (g) UIO-66-COOH/BPEI/VTES residual chars

## FTIR

The infrared spectra of pristine cotton and sample UIO-66-COOH/BPEI/VTES were measured by FTIR spectrometer as presented in Figure 2.31. For untreated cotton, the peaks at  $1025\text{ cm}^{-1}$ ,  $1315\text{ cm}^{-1}$ ,  $1363\text{ cm}^{-1}$ ,  $1430\text{ cm}^{-1}$  and  $2889\text{ cm}^{-1}$  were respectively related to (CO) and (OH) stretching of the polysaccharide, C-O bending, C-H bending,  $\text{CH}_2$  bending and C-H stretching vibration (Portella et al., 2016). The broad band approximately  $3300\text{ cm}^{-1}$  of pristine cotton was assigned to -OH group and weakened after treatment (Chung et al., 2004; Wang et al., 2020). Also, the peak near  $1703\text{ cm}^{-1}$  represented as free carboxylate group was eliminated in UIO-66-COOH/BPEI/VTES sample, which demonstrated the formation of cross-link between cellulose and incorporated composites. There were some new characteristic peaks could be noticed in sample UIO-66-

COOH/BPEI/VTES compared with pristine cotton. The asymmetric stretching vibrations at  $1620\text{ cm}^{-1}$  and symmetric stretching vibrations at  $1380\text{ cm}^{-1}$  were corresponded to  $-\text{COO}-\text{Zr}$  group from UIO-66-COOH (Ren et al., 2021), confirming the deposition of UIO-66-COOH on the cotton substrates. While the absorption peak at  $1560\text{ cm}^{-1}$  and  $755\text{ cm}^{-1}$  were due to N-H bending and N-H wagging from the available BPEI (Zhao et al., 2021), the prominent absorption band located at  $1010\text{ cm}^{-1}$  was identified the presence of Si-O-Si (Lin et al., 2018). These emerging peaks indicated UIO-66-COOH, BPEI and VTES were successfully assembled onto cotton fabrics.

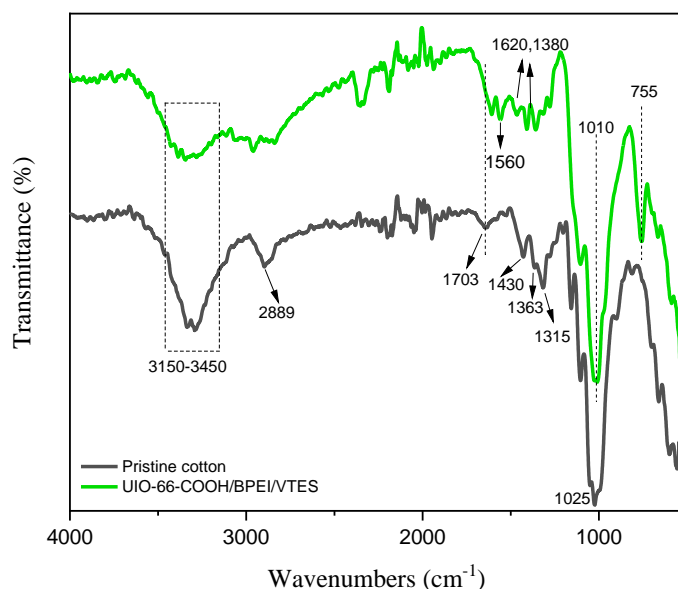


**Figure 2.31** The FTIR spectra of pristine cotton and sample UIO-66-COOH/BPEI/VTES

### Thermal properties

Because of the hydrophilic nature of cotton fibers, the weight loss at around  $100\text{ }^{\circ}\text{C}$  was related to moisture evaporation (Salmeia et al., 2016). The thermal decomposition process of each cotton sample was composed of two main stages (Figure 2.32). The dehydration of pristine cotton occurred accompanied by char formation at temperatures ranging from  $318\text{ }^{\circ}\text{C}$  to  $380\text{ }^{\circ}\text{C}$  in first stage (Hsieh, 2007), and the chars were further oxidized to produce more gaseous combustible products at higher temperatures in second stage (Y. Li et al., 2018). As evidenced

by the TGA data in Table 2.15, the  $T_{max}$  of cotton sample was raised from 479 °C to 500.9 °C with the aid of UIO-66-COOH in stage 1. However, for sample UIO-66-COOH, it was clear that the  $R_{max}$  did not decrease explicitly in either stage 1 or stage 2. As a result, the introduction of individual UIO-66-COOH wasn't able to greatly improve the thermal stability of cotton at elevated temperatures. BPEI was regarded as blowing agent, releasing low molecular weight molecules like  $NH_3$  and causing the carbonaceous residue to become porous (Wang et al., 2014). The  $R_{max}$  of sample UIO-66-COOH/BPEI was lower in both stage 1 and stage 2 compared to utilizing UIO-66-COOH alone. In addition, after assembling the composites material of UIO-66-COOH, BPEI and VTES onto cotton fabrics, the formed siliceous carbon layer of VTES in combustion was the first barrier that could suppress fire by oxygen and heat insulation (Hamdani - Devarenes et al., 2009). Consequentially, the  $R_{max}$  was further reduced from 37.6 wt%/min to 17.2 wt%/min in stage 1, the  $T_{max}$  was developed from 479 °C to 523.3 °C in stage 2. There was no residue left for pristine cotton at 800 °C, whereas the residual char content of sample UIO-66-COOH/BPEI/VTES was up to 7.2355 wt%. Thereby it could be concluded that the synergistic barrier effects between UIO-66-COOH, BPEI and VTES were more conducive to inhibiting the thermal degradation of cotton fabrics and improving their thermal stability at elevated temperatures.

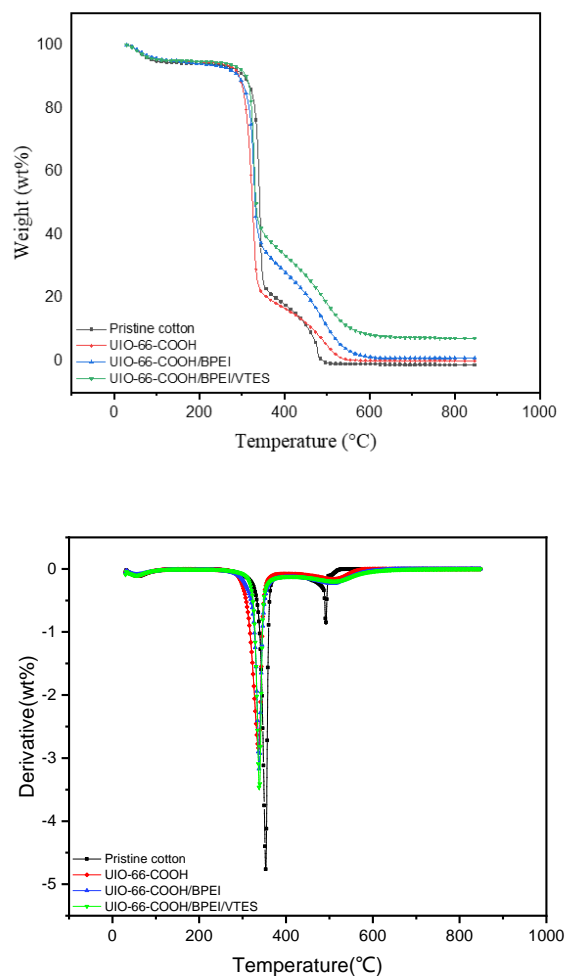


**Figure 2.32** TGA and DTG curves of (a) pristine cotton sample (b) UIO-66-COOH sample, (c) UIO-66-COOH/BPEI sample and (d) UIO-66-COOH/BPEI/VTES sample

**Table 2.15** TGA data of cotton samples under air atmosphere

Sample	$T_{10\%}$ (°C)	Stage1		Stage2		Residue at 800 °C (wt%)
		$T_{max}$ (°C)	$R_{max}$ (wt%/min)	$T_{max}$ (°C)	$R_{max}$ (wt%/min)	
Pristine cotton	318.5	341.6	37.6	479	93.4	-1.21
UIO-66-COOH	310.8	325.7	40.8	500.9	92.8	0.0573
UIO-66-COOH/BPEI	303.5	326.2	25.6	499	88.1	0.9052
UIO-66-COOH/BPEI/VTES	319.3	330.8	17.2	523.3	84.6	7.2355

\* The heating rate is fixed by 10 °C/min.  $T_{10\%}$  is the initial decomposition temperature at which 10% sample weight is lost.  $T_{max}$  is the temperature of maximum rate of weight loss.  $R_{max}$  is weight loss rate at the maximal peak ( $T_{max}$ ).



### 2.2.4 Fire barrier investigation of DOPO-HQ@UIO-66-COOH composites

Considering that MOFs own permanent porous structure, the diverse functional materials are able to incorporate with MOFs to produce stable metal–organic framework composites with additional advantages (Yu et al., 2017). With a variety of promising uses in fields including gas storage/separation, sensing, protective and functional coatings, MOF-based composites can be employed either as innovative materials or as precursors for solids (Lian et al., 2017; Xue et al., 2019). In contrast to other porous solids, MOFs could act as matrix materials in composites, allowing direct reactions with externally sourced reactants and the formation of active substances inside the frameworks. Additionally, the interior surfaces of MOFs can be tunable to further enhance chemical reactions and molecular adsorption/binding (Lian et al., 2017). Angus et al. successfully synthesized TiO<sub>2</sub>/NH<sub>2</sub>-UiO-66 composites for the photoreduction of carbon dioxide (Crake et al., 2019). Some researchers prepared silica–MOF composites that demonstrated good separation ability of [Cu<sub>3</sub>(BTC)<sub>2</sub>] and column packing performance of silica (Ameloot et al., 2010). In aiming to impart more efficient fire barrier properties to cotton fabrics, it's intended to design the MOF-based composites by combining DOPO-HQ with Zr-MOF (UIO-66-COOH). To the best of our knowledge, there is no literature reporting that DOPO-HQ is incorporated into porous Zr-based MOF support for applications onto cotton substrates.

#### 2.2.4.1 Sample preparation of DOPO-HQ@UIO-66-COOH dispersion

The following steps were used to prepare DOPO-HQ@UIO-66-COOH composites dispersion: 2.4 g (10 mmol) ZrCl<sub>4</sub> was completely dissolved in 50 ml deionized water, while 2.2 g (10 mmol) H<sub>3</sub>BTC was dissolved in 50 ml deionized water with the help of Turrax digital homogenizer (16000 rpm \* 1 min), the two were mixed and refluxed in a sealed reactor at 100 °C for 16 hours. Then 6.5 g (20 mmol) DOPO-HQ powder was added with 170 ml of ethanol/water mixture (1:1), and followed by ultrasonication treatment for 15 min and overnight vigorous magnetic stirring at room temperature. The resultant sample (Figure 2.33) was subsequently verified with particle size of 401 nm by Malvern Zetasizer Nano ZS90. With particle size of nano-level, it was beneficial for DOPO-HQ@UIO-66-COOH composites to be absorbed and uniformly distributed onto cotton fibers.

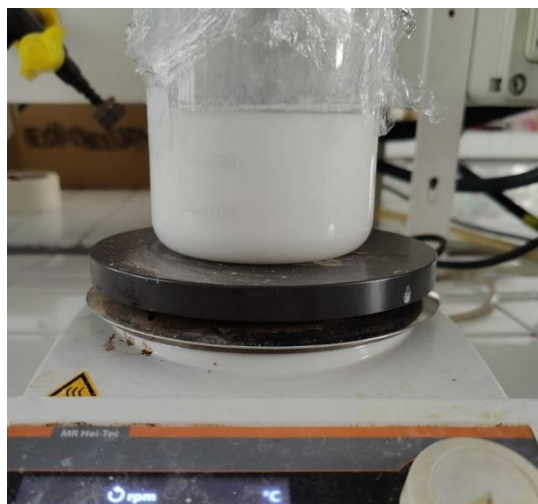


**Figure 2.33** DOPO-HQ@UIO-66-COOH composites dispersion

#### 2.2.4.2 The visible stability of DOPO-HQ@UIO-66-COOH dispersion

In order to access the gravitational stability of DOPO-HQ@UIO-66-COOH dispersion, the resultant sample was observed for an extended period of time as shown in Figure 2.34. With the digital photographs, it was intuitively to visualize the evolution of sample stability over time. At ambient condition, the DOPO-HQ@UIO-66-COOH sample remained homogeneously dispersed until phase separation progressively occurred after 8 hours.

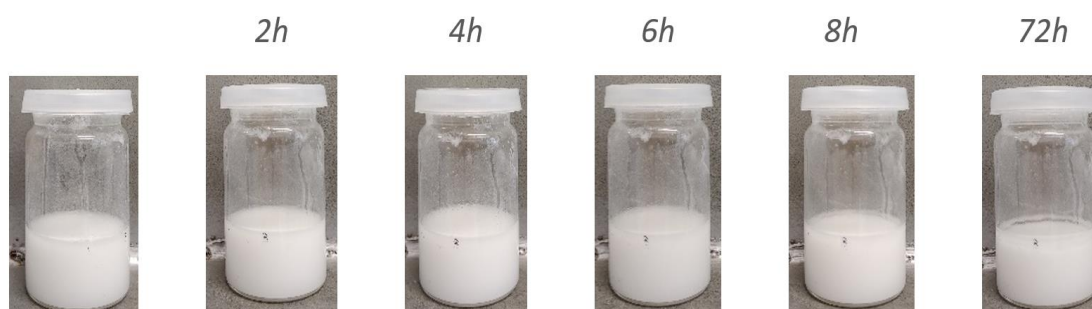


**Figure 2.34** Digital photos of DOPO-HQ@UIO-66-COOH dispersion at different time

#### 2.2.4.3 Analysis of DOPO-HQ@UIO-66-COOH composites

From the above results it was clear that immiscible DOPO-HQ was appropriately incorporated into porous Zr-MOF support. And for further analysis of DOPO-HQ@UIO-66-COOH composites, the obtained dispersion sample was dried to

remove the solvent, which was then used to compare with pure DOPO-HQ powder by the results of SEM images and XRD patterns (Figure 2.35).

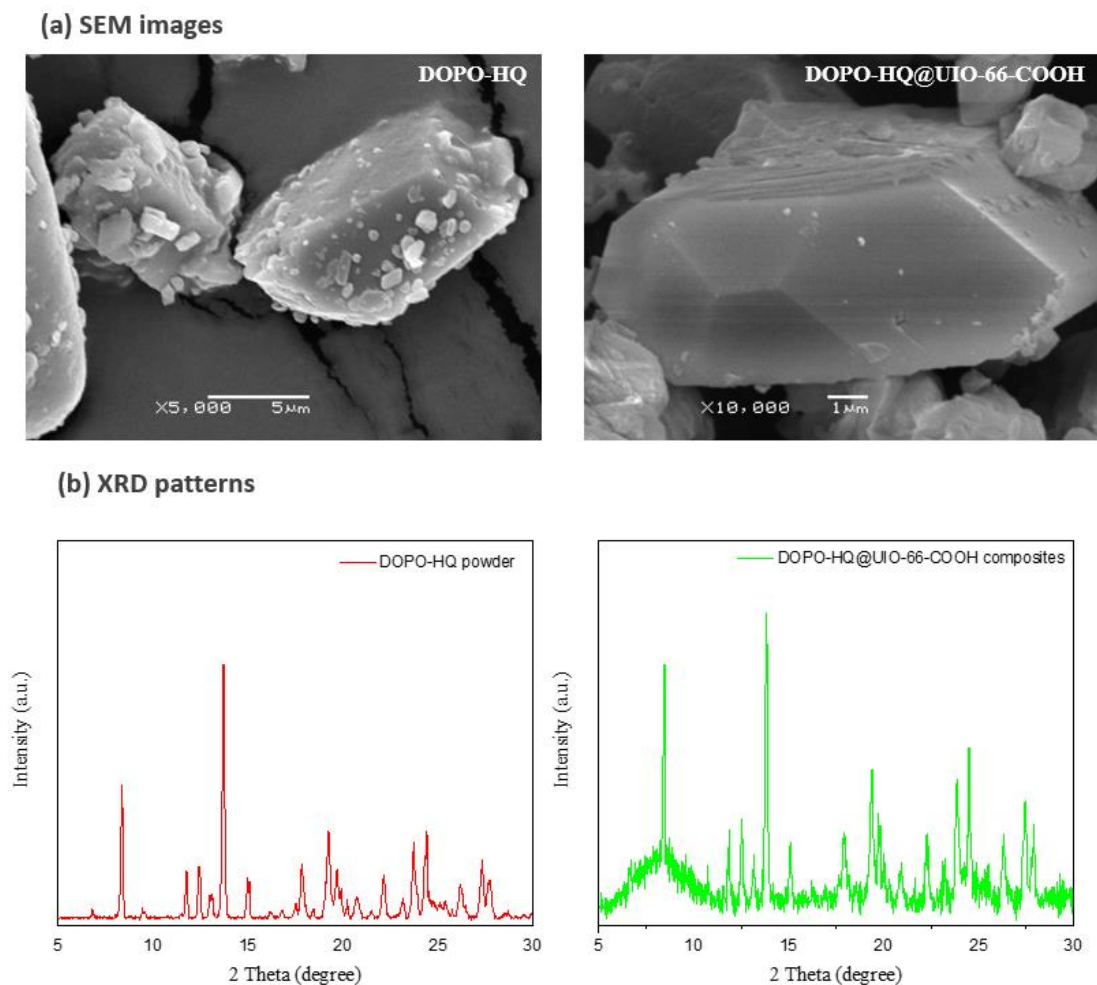


**Figure 2.35** The comparison results of (a) SEM images and (b) XRD patterns

From the surface morphology of DOPO-HQ powder, it appeared that the solid DOPO-HQ tended to be agglomerated and showed a highly ordered shape. Since the preferred orientation, the XRD pattern of DOPO-HQ had several strong and sharp peaks that usually found in crystalline components. Accordingly, since the DOPO-HQ@UIO-66-COOH composites were not homogeneously dispersed in the aqueous media, their surfaces were apparently covered by a large amount of agglomerated DOPO-HQ as judged from the SEM image analysis. In the light of the XRD result of DOPO-HQ@UIO-66-COOH composites material, it could therefore be assumed that the similar behavior to that of DOPO-HQ was caused by the DOPO-HQ surrounded on UIO-66-COOH, which intensely affected the X-rays path accompanied with scattering.

### 2.2.4.4 The application of DOPO-HQ@UIO-66-COOH composites dispersion

The cotton fabrics were treated with finishing solution by means of dipping-drying process. Explicitly, the cotton substrates were firstly dipped in resultant DOPO-HQ@UIO-66-COOH composites dispersion for 5 minutes, then dried in an oven at 75 °C for 4 minutes, which was considered one dipping-drying cycle (1L). The more dipping-drying cycles were applied, the higher amount of DOPO-HQ@UIO-66-COOH composites would be introduced to the cotton substrates. The whole operation route was illustrated in Figure 2.36.

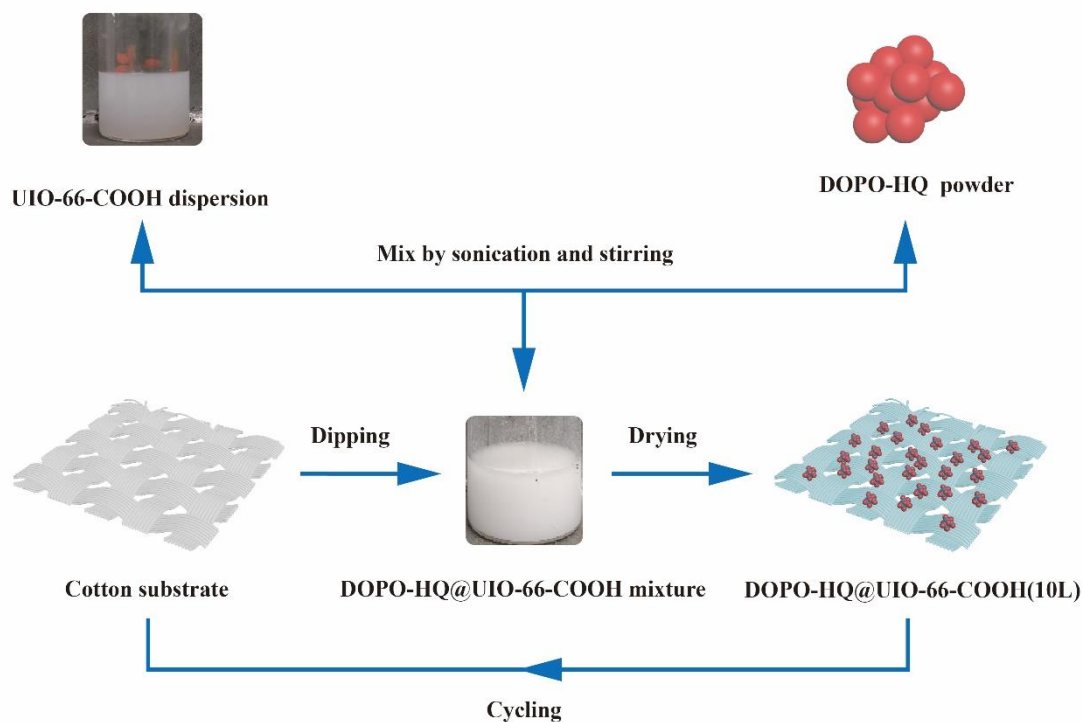


**Figure 2.36** Graphical representation of functionalization treatment process for cotton fabric

The treated cotton fabrics were accordingly denoted as DOPO-HQ@UIO-66-COOH (1L) and DOPO-HQ@UIO-66-COOH (10L) with reference to the dipping-drying finishing cycles. Weighing was conducted on all samples both before and after the finishing process. As stated by the following equation, the corresponding add-on values (wt%) of cotton samples were calculated and the results were summarized in Table 2.16. It was noticeable that after depositing 1 layer and 10

multilayer of DOPO-HQ@UIO-66-COOH composites dispersion, the cotton substrates attained weight of 2.82 wt% and 12.03 wt%, respectively.

$$\text{Add-on (wt\%)} = \frac{\text{Last weight of specimen(g)} - \text{Initial weight of specimen(g)}}{\text{Initial weight of specimen(g)}} * 100$$

**Table 2.16** The treatment data of cotton sample

Sample	W <sub>0</sub> /g	W <sub>1</sub> /g	Add-on/wt%
DOPO-HQ@UIO-66-COOH (1L)	5.68	5.84	2.82
DOPO-HQ@UIO-66-COOH (10L)	5.82	6.52	12.03

\* W<sub>0</sub> and W<sub>1</sub> refer to initial and final weight of specimen, respectively.

## SEM

In Figure 2.37 below, the surface morphology of cotton fabrics was characterized through SEM photos. It was distinctly seen that the DOPO-HQ@UIO-66-COOH composites were absorbed and distributed on the treated cotton substrates in the form of micron-nanometer sized particles. When more DOPO-HQ@UIO-66-COOH composites were successfully deposited and assembled onto cotton fibers, they would work as thick heat-insulating layers to protect the substrates during combustion, leading to forming more non-flammable carbonized residuals. It could be observed that the fibers of sample DOPO-HQ@UIO-66-COOH (10L) were still adhered together and maintained some structural integrity even after burning, suggesting that the treated cotton fabric was not fully degraded (Wan et al. 2021).

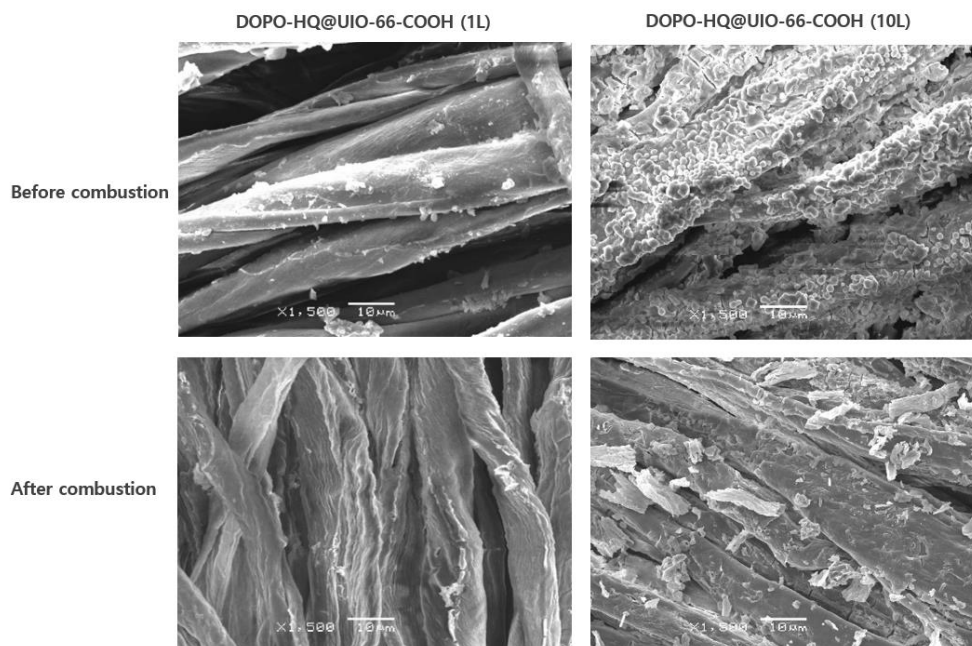


**Figure 2.37** The SEM images of cotton samples before and after combustion

### Vertical burning test

Vertical burning tests were performed on pristine cotton, sample DOPO-HQ@UIO-66-COOH (1L) and DOPO-HQ@UIO-66-COOH (10L) to analyze their burning behavior. These samples were exposed to a naked flame for 10 seconds before the ignition source was removed, the whole combustion process would be recorded as Figure 2.38 shown.

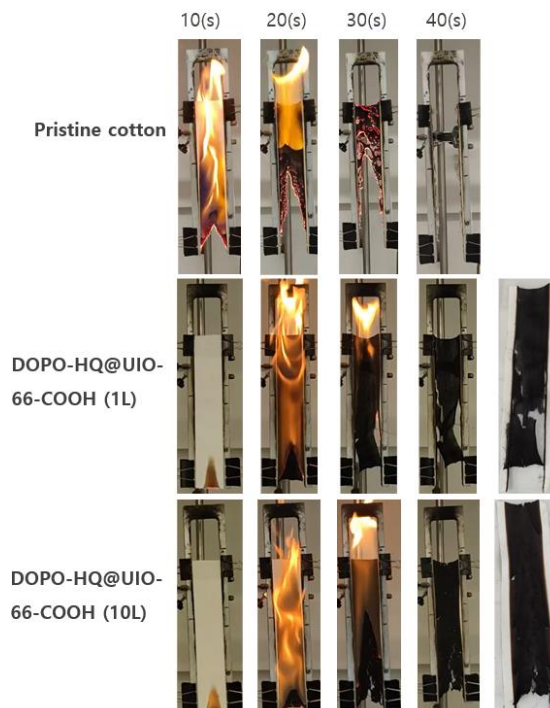


**Figure 2.38** Digital photos of cotton samples in the vertical burning test after ignition

In view of the results of vertical burning tests, it was clear to find that the pristine cotton was violently burning and totally consumed without generating residual chars. With only one-layer deposition of DOPO-HQ@UIO-66-COOH composites, the treated cotton fabric was endowed with good char-forming properties, and consequently the duration of combustion was productively shortened. Besides, it exhibited more positive effects on smoke suppression when a large amount of DOPO-HQ@UIO-66-COOH composites were introduced to cotton substrates. The denser and thicker carbon layer on the surface of cotton fabrics was formed to protect the intact structure of fibers in the combustion process. However, as seen visually, the differences between sample DOPO-HQ@UIO-66-COOH (1L) and DOPO-HQ@UIO-66-COOH (10L) in inhibiting flame spreading didn't appear significant. It was expected to apply thermogravimetric technique for gathering quantifiable information that could be additionally utilized to investigate the fire performances of cotton samples.

## Thermal analysis

For better knowledge of the thermal properties of cotton fabrics, TGA and DTG were applied to found out the weight loss situation of samples with the increasing temperature in a controlled atmosphere (Figure 2.39), and some key data from Table 2.17 were listed based on TGA and DTG.

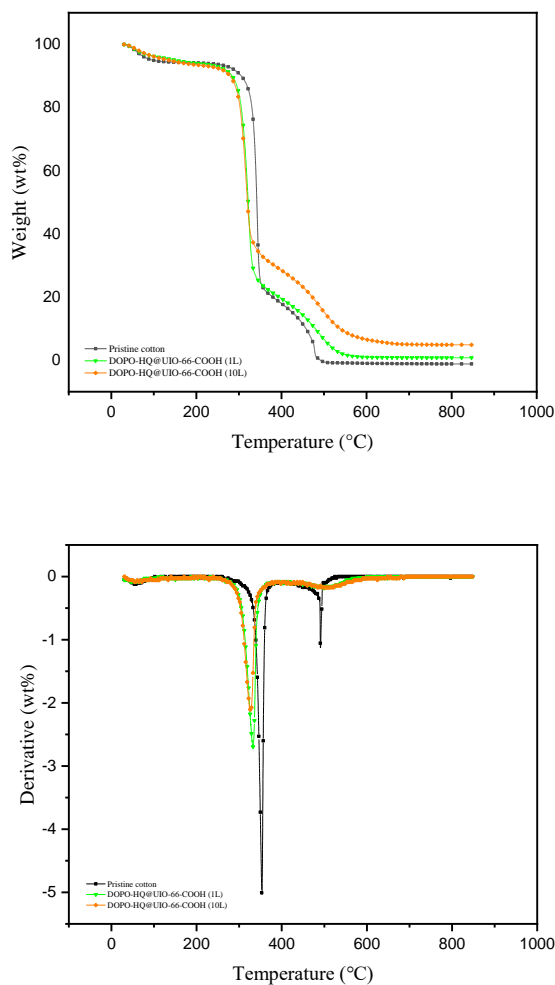


**Figure 2.39** TGA and DTG curves of (a) pristine cotton sample, (b) DOPO-HQ@UIO-66-COOH (1L) sample and (c) DOPO-HQ@UIO-66-COOH (10L) sample



**Table 2.17** TGA data of cotton samples under air atmosphere

Sample	$T_{10\%}$ (°C)	Stage1		Stage2		Residue at 800°C (wt%)
		$T_{max}$ (°C)	$R_{max}$ (wt%/min)	$T_{max}$ (°C)	$R_{max}$ (wt%/min)	
Pristine cotton	318.5	341.6	37.6	479	93.4	-1.21
DOPO-HQ@UIO-66-COOH (1L)	305.9	321.9	37.8	485	90	0.7689
DOPO-HQ@UIO-66-COOH (10L)	296.8	320.2	38.8	484.5	76.4	4.8478

\* The heating rate is fixed by 10 °C/min.  $T_{10\%}$  is the initial decomposition temperature at which 10% sample weight is lost.  $T_{max}$  is the temperature of maximum rate of weight loss.  $R_{max}$  is weight loss rate at the maximal peak ( $T_{max}$ ).

The initial decomposition temperature ( $T_{10\%}$ ) of sample DOPO-HQ@UIO-66-COOH (1L) and DOPO-HQ@UIO-66-COOH (10L) were 305.9 °C and 296.8 °C, which were both lower than pure cotton because of the early decomposition of DOPO-HQ@UIO-66-COOH composites. The phosphorus-containing component was preferentially decomposed to generate derivatives such as phosphoric acid by heat, which could phosphorylate the primary hydroxyl group at the C6 position on the cellulosic chain to make the cracking of cellulose to lower temperatures and thus inhibit the production of L-glucose and combustibles, catalyzing the dehydration and carbonization of cotton fabrics (Cheng and Gao 2016; Li and Jiang 2021; Ma et al. 2021). The whole thermal degradation of cotton fabrics under air atmosphere could be typically considered as two stages of mass loss processes (Moltó et al. 2006). Also, it was straightforward to detect that the fire performances of cotton fabrics incorporating DOPO-HQ@UIO-66-COOH composites were primarily developed at elevated temperatures (stage 2). At 500 - 800 °C, the pure cotton fabric was burned out with no residuals. In contrast, the protective char formation of sample DOPO-HQ@UIO-66-COOH (1L) and DOPO-HQ@UIO-66-COOH (10L) were respectively yielded to 0.77 wt% and 4.85 wt%. Compared to sample DOPO-HQ@UIO-66-COOH (1L), sample DOPO-HQ@UIO-66-COOH (10L) exhibited with more retardancy effects and final char residues. For sample DOPO-HQ@UIO-66-COOH (10L), the  $T_{max}$  was successfully enhanced from 479 °C to 484.5 °C and  $R_{max}$  was decreased from 93.4 wt%/min to 76.4 wt%/min, both of which were revealed based on the thermal behavior of cotton samples at the second stage. As a result of the simultaneous

mode of actions in gas and condensed phase, the overall thermal stability of cotton samples with the incorporation of DOPO-HQ@UIO-66-COOH composites was higher than pristine cotton fabric. But given the behavior of treated cotton at initial thermal degradation stage, other flame-retardancy elements were expected to be selected and collaborated with DOPO-HQ@UIO-66-COOH composites for suppressing fire.

## FTIR

To further investigate the incorporation of DOPO-HQ@UIO-66-COOH with cotton substrate, Nicolet iS10 Spectrometer (Thermo Fisher, Waltham, USA) was used to perform FTIR analysis for determining functional groups of samples as presented in Figure 2.40.

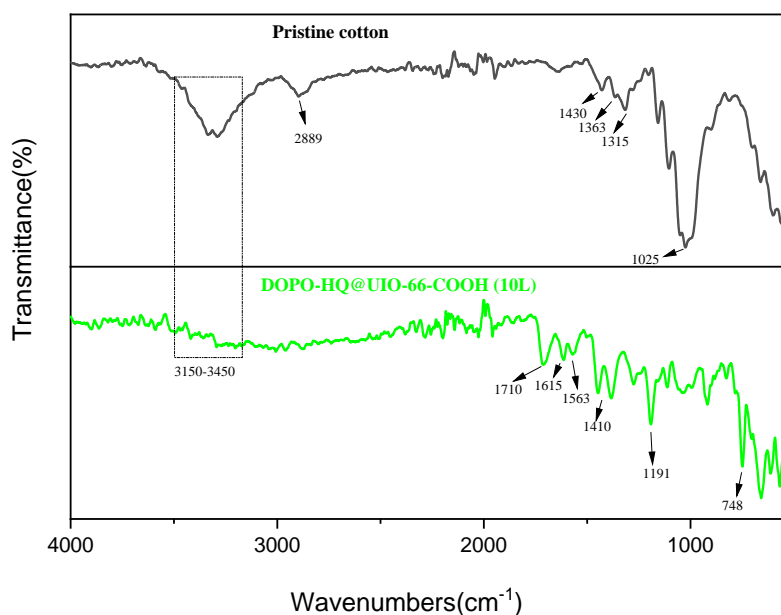


**Figure 2.40** The FTIR spectra of pristine cotton and DOPO-HQ@UIO-66-COOH (10L)

The FTIR absorbance spectra taken from cotton samples before and after treatment convincingly verified the effective interaction between DOPO-HQ@UIO-66-COOH composites material and cotton substrates. Peaks at 1025  $\text{cm}^{-1}$ , 1315  $\text{cm}^{-1}$ , 1363  $\text{cm}^{-1}$ , 1430  $\text{cm}^{-1}$ , and 2889  $\text{cm}^{-1}$  for pristine cotton were associated to (CO) and (OH) stretching of the polysaccharide, C-O bending, C-H bending,  $\text{CH}_2$  bending, and C-H stretching vibration, respectively (Portella et al.,

2016). The broad band at approximately  $3300\text{ cm}^{-1}$  of pristine cotton was assigned to the  $-\text{OH}$  group and weakened after treatment due to the hybrid composites coating (Chung et al., 2004; Wang et al., 2020). The peak observed at  $1710\text{ cm}^{-1}$  was derived from  $\text{C}=\text{O}$  stretching of DOPO-HQ@UIO-66-COOH composites. The peaks at  $748\text{ cm}^{-1}$ ,  $1191\text{ cm}^{-1}$  and  $1563\text{ cm}^{-1}$  were correspondingly ascribed to the P-C stretching, P=O vibration and P-Ph stretching of DOPO-HQ (Beg and Clark, 1962; Shi et al., 2018; Zhang et al., 2019), while the asymmetric stretching vibrations at  $1615\text{ cm}^{-1}$  and symmetric stretching vibrations at  $1410\text{ cm}^{-1}$  were assigned to the  $-\text{COO}-\text{Zr}$  group of UIO-66-COOH (Ren et al., 2021).

#### 2.2.4.5 The application of DOPO-HQ@UIO-66-COOH composites dispersion in combination with CS

As previously described, chitosan (CS) and its derivatives are water-soluble polymers that are typically applied in conjunction with other flame retardants to construct fire barrier system (Malucelli, 2020). Thus, it was attempted to treat cotton fabrics with the incorporation of CS and DOPO-HQ@UIO-66-COOH to investigate how they performed in fire. The detailed protocol was given below:

Firstly, CS solution was prepared by dissolving 1 wt% low molecular chitosan into 1% acetic acid solvent by magnetic stirring at room temperature for 24h. Then the obtained CS and DOPO-HQ@UIO-66-COOH finishing liquids were alternatively deposited onto cotton substrates by the dipping-drying process mentioned above. The corresponding treatment data were calculated and shown in Table 2.18. According to the number of deposition layers, the treated cotton samples were named CS/DOPO-HQ@UIO-66-COOH (1BL) and CS/DOPO-HQ@UIO-66-COOH (3BL), respectively with the gained add-on of 7.02 wt% and 11.93 wt%.

**Table 2.18** The treatment data of cotton sample

Sample	$W_0/\text{g}$	$W_1/\text{g}$	Add-on/wt%
CS/DOPO-HQ@UIO-66-COOH (1BL)	5.84	6.25	7.02
CS/DOPO-HQ@UIO-66-COOH (3BL)	5.93	6.64	11.97

\*  $W_0$  and  $W_1$  refer to initial and final weight of specimen, respectively.

## Vertical burning test

As shown in Figure 2.41, pristine cotton fabric, sample CS/DOPO-HQ@UIO-66-COOH (1BL) and CS/DOPO-HQ@UIO-66-COOH (3BL) were all subjected to vertical burning test to investigate their burning behavior.

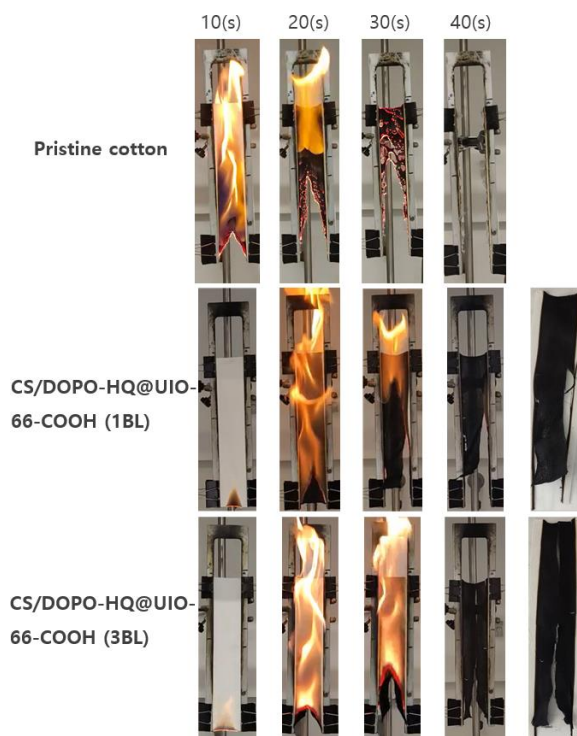


**Figure 2.41** Digital photos of cotton samples in the vertical burning test after ignition

The results of vertical burning tests exhibited that the pristine cotton was aggressively burning and completely destroyed, with no char residuals. For the treated samples, it seemed feasible to establish a protective carbon layer on the surface of cotton fabric using only 1 BL deposition of CS/DOPO-HQ@UIO-66-COOH, retaining the integrity of the fiber structure in combustion. When a considerable amount of CS/DOPO-HQ@UIO-66-COOH composites were incorporated with cotton matrix, it had the effect of slightly slowing down the spread of flame and fire suppression. It was desired to reveal the thermal behavior of cotton samples in detail by thermogravimetric techniques.

## Thermal analysis

Thermogravimetric analysis (TGA) was conducted to study the thermal properties between treated samples and pristine cotton. Figure 2.42 showed that the thermal degradation curves of pristine cotton, sample CS/DOPO-HQ@UIO-66-COOH (1BL) and CS/DOPO-HQ@UIO-66-COOH (3BL) under air gas atmosphere, and Table 2.19 listed the significant data.

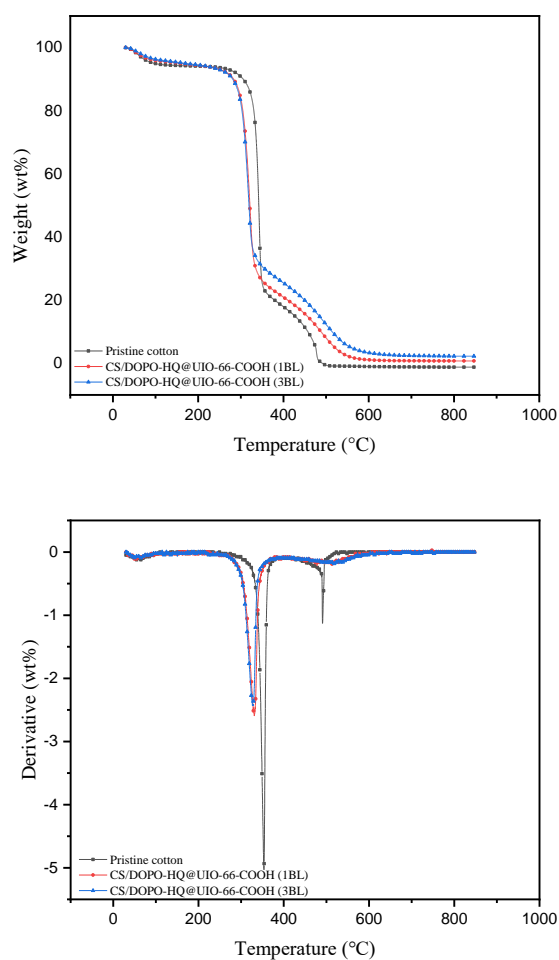


**Figure 2.42** TGA and DTG curves of (a) pristine cotton sample, (b) CS/DOPO-HQ@UIO-66-COOH (1BL) sample and (c) CS/DOPO-HQ@UIO-66-COOH (3BL) sample

**Table 2.19** TGA data of cotton samples under air atmosphere

Sample	$T_{10\%}$ (°C)	Stage1		Stage2		Residue at 800°C (wt%)
		$T_{max}$ (°C)	$R_{max}$ (wt%/min)	$T_{max}$ (°C)	$R_{max}$ (wt%/min)	
Pristine cotton	318.5	341.6	37.6	479	93.4	-1.21
CS/DOPO-HQ@UIO-66-COOH (1BL)	297.9	321.1	35.9	499.8	90.3	0.748
CS/DOPO-HQ@UIO-66-COOH (3BL)	297.2	320.8	36.2	500.2	82.5	2.2486

\* The heating rate is fixed by 10 °C/min.  $T_{10\%}$  is the initial decomposition temperature at which 10% sample weight is lost.  $T_{max}$  is the temperature of maximum rate of weight loss.  $R_{max}$  is weight loss rate at the maximal peak ( $T_{max}$ ).

The initial decomposition temperature ( $T_{10\%}$ ) of treated cotton samples was lower than that of pure cotton due to water evaporation and early decomposition of the composites coated on the surface of cotton fabrics. Comparing the char residuals of cotton samples at 800 °C demonstrated that the incorporation of CS/DOPO-HQ@UIO-66-COOH was helpful to promote the formation of carbon layers for insulating oxygen and heat during the combustion process. However, on the basis of the overall thermogravimetric curve trend and the amount of resulting carbon residues, samples with multilayer treatment of CS/DOPO-HQ@UIO-66-COOH didn't exhibit significant barrier effects.

#### 2.2.4.6 The application of DOPO-HQ@UIO-66-COOH composites dispersion in combination with TEOS

As a kind of small molecule silicone, tetraethyl orthosilicate (TEOS) owns good permeability (Figure 2.43). Because of the present immiscible gap in the TEOS-water system, homogenizing media (e.g. alcoholic solvents) is required to speed up the hydrolysis of TEOS (Donatti et al., 2002; Donatti and Vollet, 2000). The use of TEOS would help to generate a large number of strong Si-OH bonds on the surface of cotton, without seriously damaging the hydrophilicity of the pristine fabric (Yan et al., 2015). TEOS, it could collaborate with DOPO-HQ for P/Si synergistic effects and cross-link cotton fibers through Si-O-Si network. During combustion, it will work as heat insulation and oxygen barrier by forming siliceous carbon layer and reduce the overflow of flammable gases. Yu et al. designed organic-inorganic hybrid aerogel with fire protection by using TEOS and phenol-formaldehyde-resin for prospective uses in aerospace, transport and architecture (Yu et al., 2018). In the previous released study, researchers discovered that when high concentration of TEOS was applied onto cotton fabrics by depositing six consecutive layers, it demonstrated good fire performances with yielding 17% char residuals. Even after washing for 5 times, the treated cotton sample was still managed to maintain the good carbon formation ability (Colleoni et al., 2013).

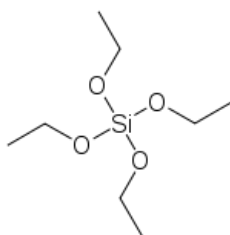


**Figure 2.43** Chemical structure of TEOS

#### Preparation of TEOS finishing solution

With the aim of making TEOS finishing solution, 10 g of TEOS was firstly dissolved in 8.8 g of ethanol and then 51.2 ml of deionized water was slowly added and followed by vigorous stirring for varying time. The corresponding particle size of TEOS finishing solution at the different stirring time was measured and summarized in the following Table 2.20. On all accounts, the stirring time for

preparing TEOS solution was set at 44h to obtain the particle size of 160 nm, which enabled its distribution and penetration on the cotton fibers.

**Table 2.20** The particle size of TEOS finishing solution

Stirring time/h	2	4	7	9	24	32	40	44	48
Particle size/nm	4040	4900	4380	4250	4050	2650	680	160	168

### Finishing of cotton substrates with DOPO-HQ@UIO-66-COOH and TEOS

The finishing procedure was described as Figure 2.44. The cotton substrate was first dipped in DOPO-HQ@UIO-66-COOH dispersion for 5 minutes, then dried at 75 °C for 4 minutes, then it was treated with TEOS finishing solution by the same dipping-drying method. The resulting sample was acquired by simple successive deposition of DOPO-HQ@UIO-66-COOH and TEOS. The structural barrier system against fire was assembled onto cotton fabrics, with the advantage of significantly reducing the redundancy of the application process. In order to further investigate the synergistic barrier effects of DOPO-HQ@UIO-66-COOH and TEOS, the cotton sample treated with individual TEOS was also prepared for comparison using SEM and thermal analysis.

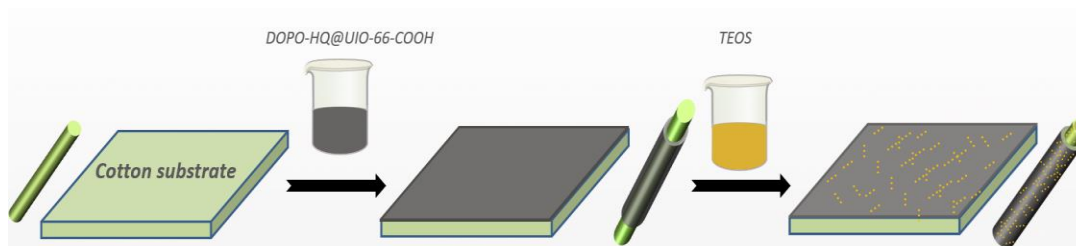


**Figure 2.44** Finishing procedure for applying DOPO-HQ@UIO-66-COOH and TEOS onto cotton substrates



## SEM

The cotton samples after treatment were respectively denoted as TEOS and DOPO-HQ@UIO-66-COOH/TEOS with regard to the finishing solution. The surface morphology of cotton fabrics was determined by SEM images as seen in Figure 2.45 below. The application of individual TEOS to cotton substrates resulted in producing micron-nanometer particles that adhered to fibers and acted as a fire barrier. Furthermore, when TEOS was combined with DOPO-HQ@UIO-66-COOH to be incorporated in cotton, each cotton fiber was fully coated to provide fire protection through strong binding effects. The crystalline structure generated on the fiber surface also had the potential to help protect the cotton from burning and welding, as discovered by SEM images of sample DOPO-HQ@UIO-66-COOH/TEOS after combustion.

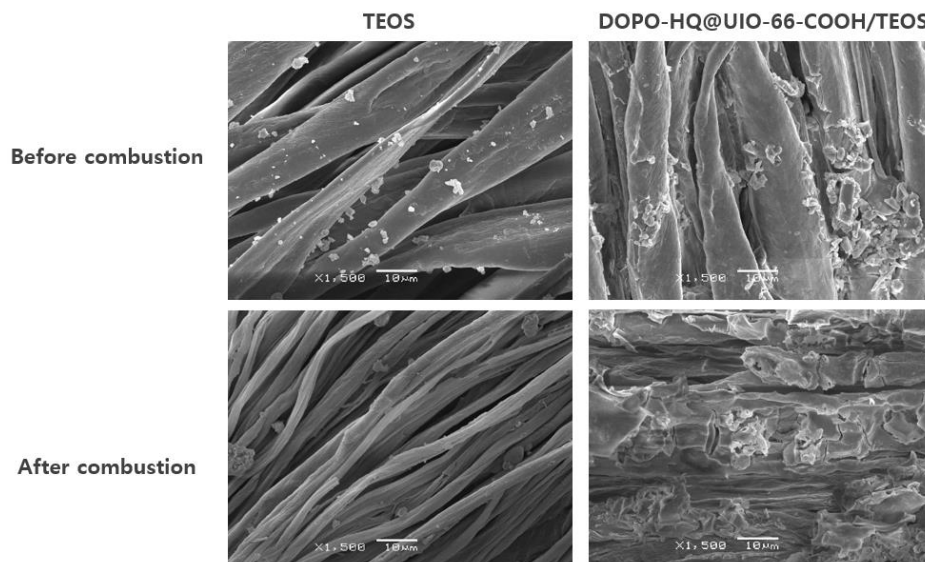


**Figure 2.45** The SEM images of cotton samples before and after combustion

## Thermal analysis

To explicitly explain the thermal characteristics of cotton fabrics after different treatments, the TGA (DTG) results of pristine cotton, sample DOPO-HQ@UIO-66-COOH, TEOS and DOPO-HQ@UIO-66-COOH/TEOS were acquired. The significant data derived from TGA and DTG curves was displayed in Table 2.21. As Figure 2.46 shown, the whole thermal degradation of cotton fabric could be

considered as two stages. In combustion, TEOS was heated to produce a silicon carbon layer for developing the fire performances of cotton substrates by enhancing the thickness and oxidation resistance of insulation layers (Wang et al. 2021; Wei et al. 2019). When single layer TEOS was applied onto the cotton substrate, it performed positive fire resistance by decreasing  $R_{\max}$  from 37.6 wt%/min to 18.8 wt%/min at stage 1. Meanwhile, sample TEOS had developed the protective char residuals from -1.21 wt% to 0.9022 wt%. In addition, sample DOPO-HQ@UIO-66-COOH proved its retardancy ability at high temperatures by increasing  $T_{\max}$  from 479 °C to 485 °C, reducing  $R_{\max}$  from 93.4 wt%/min to 90.5 wt%/min at stage 2, and generating the carbon yield of 0.7689 wt% at 800°C. Although compared to pristine cotton, both sample DOPO-HQ@UIO-66-COOH and TEOS performed well, sample DOPO-HQ@UIO-66-COOH/TEOS functioned substantially differently owing to the excellent synergistic barrier effects. It helped to enhance the initial decomposition temperature ( $T_{10\%}$ ) from 318.5 °C to 321.6 °C and increase the final carbon residuals from -1.21 wt% to 6.7143 wt%. At stage 2, the  $T_{\max}$  of sample DOPO-HQ@UIO-66-COOH was developed to 494.8 °C and  $R_{\max}$  was decreased to 79.3 wt%/min, which demonstrated the effectiveness of the combination of DOPO-HQ@UIO-66-COOH and TEOS in developing fire performances of cotton fabrics. At 800 °C, the pure cotton fabric was totally consumed without residues whereas sample DOPO-HQ@UIO-66-COOH/TEOS ended up generating protective chars of 6.7143 wt%.

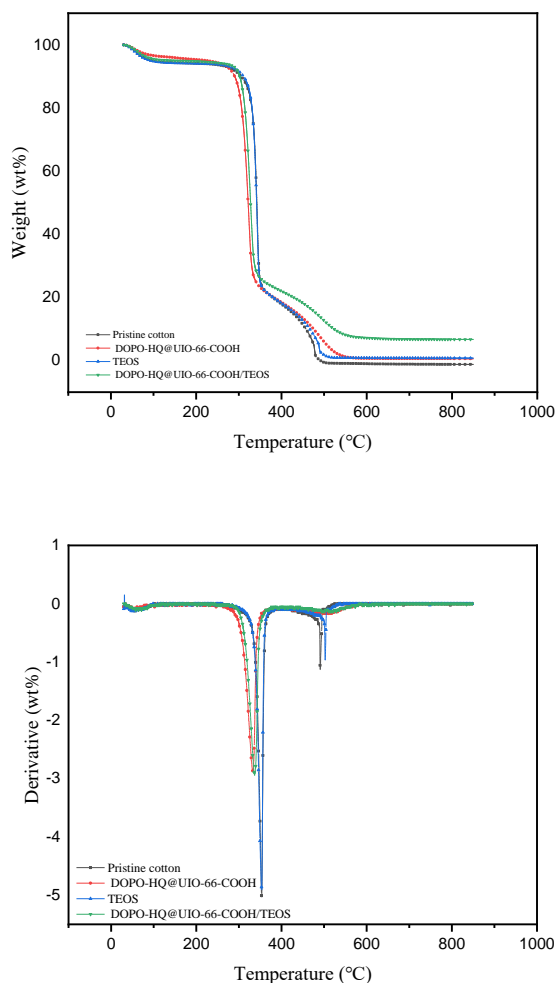


**Figure 2.46** TGA and DTG curves of (a) pristine cotton sample, (b) DOPO-HQ@UIO-66-COOH sample, (c) TEOS sample and (d) DOPO-HQ@UIO-66-COOH/TEOS sample

**Table 2.21** TGA data of cotton samples under air atmosphere

Sample	$T_{10\%}$ (°C)	Stage1		Stage2		Residue 800°C (wt%)
		$T_{max}$ (°C)	$R_{max}$ (wt%/min)	$T_{max}$ (°C)	$R_{max}$ (wt%/min)	
Pristine cotton	318.5	341.6	37.6	479	93.4	-1.21
DOPO-HQ@UIO-66-COOH	305.9	321.9	37.8	485	90	0.7689
TEOS	319.8	334.5	18.8	479	90.5	0.9022
DOPO-HQ@UIO-66-COOH/TEOS	321.6	342	33.1	494.8	79.3	6.7143

\* The heating rate is fixed by 10 °C/min.  $T_{10\%}$  is the initial decomposition temperature at which 10% sample weight is lost.  $T_{max}$  is the temperature of maximum rate of weight loss.  $R_{max}$  is weight loss rate at the maximal peak ( $T_{max}$ ).

## FTIR

To further investigate the incorporation of the finishing reagents with cotton substrates, the FTIR spectra of pure cotton and sample DOPO-HQ@UIO-66-COOH/TEOS were measured to identify the functional groups. According to the outcomes of Figure 2.47, the broad band at approximately  $3300\text{ cm}^{-1}$  of pristine cotton was assigned to the  $-\text{OH}$  group and weakened after treatment due to the coating formation of DOPO-HQ@UIO-66-COOH/TEOS (Chung et al., 2004; Wang et al., 2020). Because of abundant  $\text{C}=\text{O}$  from DOPO-HQ@UIO-66-COOH composites, the peak at  $1702\text{ cm}^{-1}$  was obtained. The asymmetric stretching vibrations at  $1615\text{ cm}^{-1}$  and symmetric stretching vibrations at  $1410\text{ cm}^{-1}$  were derived from  $-\text{COO}-\text{Zr}$  group of UIO-66-COOH (Ren et al., 2021). In addition, the P-C stretching, P=O vibration and P-Ph stretching of DOPO-HQ were attributed to the bands at  $748\text{ cm}^{-1}$ ,  $1191\text{ cm}^{-1}$  and  $1563\text{ cm}^{-1}$  (Beg and Clark, 1962; Shi et al., 2018; Zhang et al., 2019). The characteristic peak at  $2335\text{ cm}^{-1}$  was corresponded to Si-H vibration (Bugaev et al., 2011; Lin et al., 2000), and the peaks at  $1049\text{ cm}^{-1}$ ,  $786\text{ cm}^{-1}$  were indicated the formation of Si-O-Si (Aroke et al., 2013; Kaya et al., 2020), confirming the reliable interactions between TEOS and cotton fabric. Taking into account the FTIR analysis results, it was demonstrated that DOPO-HQ@UIO-66-COOH and TEOS were effectively deposited and assembled onto the cotton substrate.

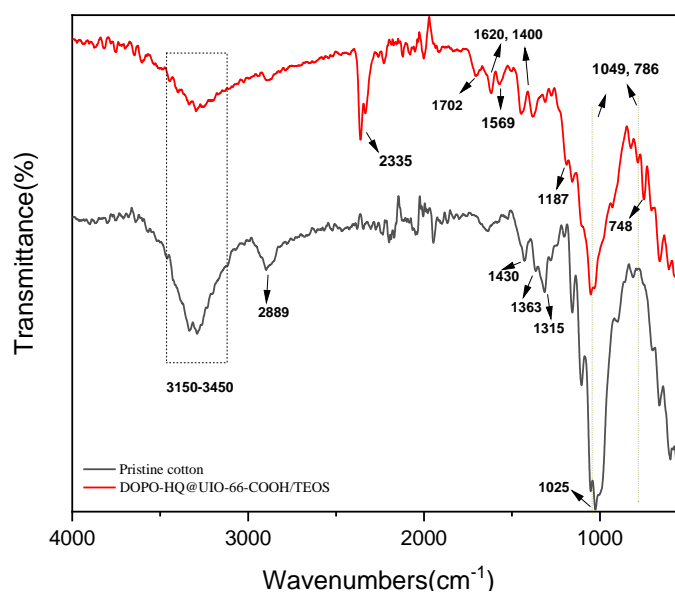


**Figure 2.47** The FTIR spectra of pristine cotton and sample DOPO-HQ@UIO-66-COOH/TEOS

### 2.2.4.7 Conclusions

The DOPO-HQ@UIO-66-COOH composites dispersion was successfully prepared with ultrasonic assistance and then introduced onto cotton fabrics through the facile dipping-drying method. It could facilitate the formation of carbonaceous insulation layer and thereby retained the original morphology of cotton fabrics in the burning process. In comparison with pristine cotton, the results of vertical burning test and thermal analysis positively clarified that the treated cotton fabric with the incorporation of DOPO-HQ@UIO-66-COOH composites were provided with advantageous thermal stability and smoke suppression properties. Clearly, DOPO-HQ@UIO-66-COOH composites was anticipated to work as a potential flame-retardant for cotton textiles. More importantly, when DOPO-HQ@UIO-66-COOH composites were used in combination with TEOS for cotton substrates, it could substantially reduce the redundancy of application process and realize synergistic fire barrier effects. At stage 2 of cotton degradation, the  $T_{\max}$  of sample DOPO-HQ@UIO-66-COOH/TEOS was increased from 479 °C to 494.8 °C and the  $R_{\max}$  was decreased from 93.4 wt%/min to 79.3 wt%/min. Meanwhile, the initial decomposition temperature ( $T_{10\%}$ ) was slightly enhanced from 318.5 °C to 321.6 °C, and the final char yield at 800 °C was proved a significant increase from -1.21 wt% to 6.7143 wt%. Conclusively, the structural barriers composed of DOPO-HQ@UIO-66-COOH and TEOS presented broad prospects regarding the eco-friendly development of fire protection for cotton fabrics.

## 2.3 Summary

It was discovered that UIO-66-COOH was more advantageous for developing fire performances when UIO-66-COOH and ZIF-8 were investigated to be introduced to cotton fabrics. DOPO-HQ was adequately incorporated into porous UIO-66-COOH support, which formed the DOPO-HQ@UIO-66-COOH composites that had the potential to be a novel halogen-free flame retardant. Therefore, it was of interest to further study the absorption behavior of cotton fabrics to DOPO-HQ@UIO-66-COOH composites. When DOPO-HQ@UIO-66-COOH composites were used in combination with TEOS, it provided efficient barrier effects for cotton fabrics while greatly reducing the redundancy of the application process.

## 2.4 References

- Al-Kutubi, H., Gascon, J., Sudhölter, E.J.R., Rassaei, L., 2015. Electrosynthesis of Metal–Organic Frameworks: Challenges and Opportunities. *ChemElectroChem* 2, 462–474. <https://doi.org/10.1002/celec.201402429>
- Ameloot, R., Liekens, A., Alaerts, L., Maes, M., Galarneau, A., Coq, B., Desmet, G., Sels, B.F., Denayer, J.F.M., De Vos, D.E., 2010. Silica–MOF Composites as a Stationary Phase in Liquid Chromatography. *European Journal of Inorganic Chemistry* 2010, 3735–3738. <https://doi.org/10.1002/ejic.201000494>
- Andrés, M.A., Sicard, C., Serre, C., Roubeau, O., Gascón, I., 2019. Ultrathin hydrophobic films based on the metal organic framework UiO-66-COOH(Zr). *Beilstein J. Nanotechnol.* 10, 654–665. <https://doi.org/10.3762/bjnano.10.65>
- Ardila-Suárez, C., Rodríguez-Pereira, J., Baldovino-Medrano, V.G., Ramírez-Caballero, G.E., 2019. An analysis of the effect of zirconium precursors of MOF-808 on its thermal stability, and structural and surface properties. *CrystEngComm* 21, 1407–1415. <https://doi.org/10.1039/C8CE01722K>
- Aroke, U.O., Abdulkarim, A., Ogubunka, R.O., 2013. Fourier-transform Infrared Characterization of Kaolin, Granite, Bentonite and Barite. *ATBU Journal of Environmental Technology* 6, 42–53.
- Bakshia, P., Selvakumara, D., Kadirvelub, K., Kumara, N.S., 2019. Chitosan as an environment friendly biomaterial - a review on recent modifications and applications. *International Journal of Biological Macromolecules* 150. <https://doi.org/10.1016/j.ijbiomac.2019.10.113>
- Barton, H.F., Jamir, J.D., Davis, A.K., Peterson, G.W., Parsons, G.N., 2021. Doubly Protective MOF-Photo-Fabrics: Facile Template-Free Synthesis of PCN-222-Textiles Enables Rapid Hydrolysis, Photo-Hydrolysis and Selective Oxidation of Multiple Chemical Warfare Agents and Simulants. *Chemistry – A European Journal* 27, 1465–1472. <https://doi.org/10.1002/chem.202003716>
- Beg, M.A.A., Clark, H.C., 1962. CHEMISTRY OF THE TRIFLUOROMETHYL GROUP: PART V. INFRARED SPECTRA OF SOME PHOSPHORUS COMPOUNDS CONTAINING CF<sub>3</sub>. *Can. J. Chem.* 40, 393–398. <https://doi.org/10.1139/v62-063>
- Beulah, P., Jinu, U., Ghorbanpour, M., Venkatachalam, P., 2019. Chapter 14 - Green Engineered Chitosan Nanoparticles and Its Biomedical Applications—An Overview, in: Ghorbanpour, M., Wani, S.H. (Eds.), *Advances in Phytotechnology*. Academic Press, pp. 329–341. <https://doi.org/10.1016/B978-0-12-815322-2.00015-8>
- Bugaev, K.O., Zelenina, A.A., Volodin, V.A., 2011. Vibrational Spectroscopy of Chemical Species in Silicon and Silicon-Rich Nitride Thin Films. *International Journal of Spectroscopy* 2012, e281851. <https://doi.org/10.1155/2012/281851>
- Carosio, F., Laufer, G., Alongi, J., Camino, G., Grunlan, J.C., 2011. Layer-by-layer assembly of silica-based flame retardant thin film on PET fabric. *Polymer Degradation and Stability* 96, 745–750. <https://doi.org/10.1016/j.polymdegradstab.2011.02.019>

- Chen, Gu, X., Jin, X., Sun, J., Zhang, S., 2016. The effect of chitosan on the flammability and thermal stability of polylactic acid/ammonium polyphosphate biocomposites. *Carbohydrate Polymers* 157. <https://doi.org/10.1016/j.carbpol.2016.11.035>
- Chen, L., Xu, Q., 2019. Metal-Organic Framework Composites for Catalysis. *Matter* 1, 57–89. <https://doi.org/10.1016/j.matt.2019.05.018>
- Chen, T., Hong, J., Peng, C., Chen, G., Yuan, C., Xu, Y., Zeng, B., Dai, L., 2019. Superhydrophobic and flame retardant cotton modified with DOPO and fluorine-silicon-containing crosslinked polymer. *Carbohydrate Polymers* 208, 14–21. <https://doi.org/10.1016/j.carbpol.2018.12.023>
- Chen, Z., Li, X., Yang, C., Cheng, K., Tan, T., Lv, Y., Liu, Y., 2021. Hybrid Porous Crystalline Materials from Metal Organic Frameworks and Covalent Organic Frameworks. *Advanced Science* 8, 2101883. <https://doi.org/10.1002/advs.202101883>
- Chen, Z., Ma, K., Mahle, J.J., Wang, H., Syed, Z.H., Atilgan, A., Chen, Y., Xin, J.H., Islamoglu, T., Peterson, G.W., Farha, O.K., 2019. Integration of Metal–Organic Frameworks on Protective Layers for Destruction of Nerve Agents under Relevant Conditions. *J. Am. Chem. Soc.* 141, 20016–20021. <https://doi.org/10.1021/jacs.9b11172>
- Cheng, B., Pei, B., Wang, Z., Hu, Q., 2017. Advances in chitosan-based superabsorbent hydrogels. *RSC Adv.* 7, 42036–42046. <https://doi.org/10.1039/C7RA07104C>
- Cheng, C., Xu, J., Gao, W., Jiang, S., Guo, R., 2019. Preparation of flexible supercapacitor with RGO/Ni-MOF film on Ni-coated polyester fabric. *Electrochimica Acta* 318, 23–31. <https://doi.org/10.1016/j.electacta.2019.06.055>
- Cheng, Genyin, and Ming Gao. 2016. 'Thermal Stability of Cotton Cellulose Modified with Dysprosium Complexes'. In *Proceedings of the 2016 6th International Conference on Machinery, Materials, Environment, Biotechnology and Computer*. Tianjin, China: Atlantis Press. <https://doi.org/10.2991/mmebc-16.2016.386>
- Chernyy, S., Ulah, S., Sørensen, G., Tordrup, S.W., Pedersen, P.B., Almdal, K., 2015. DOPO-VTS-based coatings in the realm of fire retardants for cotton textile. *J. Appl. Polym. Sci.* 132, n/a-n/a. <https://doi.org/10.1002/app.41955>
- Cheung, Y.H., Ma, K., van Leeuwen, H.C., Wasson, M.C., Wang, X., Idrees, K.B., Gong, W., Cao, R., Mahle, J.J., Islamoglu, T., Peterson, G.W., de Koning, M.C., Xin, J.H., Farha, O.K., 2021. Immobilized Regenerable Active Chlorine within a Zirconium-Based MOF Textile Composite to Eliminate Biological and Chemical Threats. *J. Am. Chem. Soc.* 143, 16777–16785. <https://doi.org/10.1021/jacs.1c08576>
- Chung, C., Lee, M., Choe, E., 2004. Characterization of cotton fabric scouring by FT-IR ATR spectroscopy. *Carbohydrate Polymers* 58, 417–420. <https://doi.org/10.1016/j.carbpol.2004.08.005>
- Colleoni, C., Donelli, I., Freddi, G., Guido, E., Migani, V., Rosace, G., 2013. A novel sol-gel multi-layer approach for cotton fabric finishing by tetraethoxysilane precursor. *Surface and Coatings Technology* 235, 192–203. <https://doi.org/10.1016/j.surfcoat.2013.07.033>
- Cortés, P.H., Macías, S.R., 2021. *Metal-Organic Frameworks in Biomedical and Environmental Field*. Springer Nature.



- Crake, A., Christoforidis, K.C., Gregg, A., Moss, B., Kafizas, A., Petit, C., 2019. The Effect of Materials Architecture in TiO<sub>2</sub>/MOF Composites on CO<sub>2</sub> Photoreduction and Charge Transfer. *Small* 15, 1805473. <https://doi.org/10.1002/sml.201805473>
- D'Amato, R., Bondi, R., Moghdad, I., Marmottini, F., McPherson, M.J., Naïli, H., Taddei, M., Costantino, F., 2021. "Shake 'n Bake" Route to Functionalized Zr-Uio-66 Metal-Organic Frameworks. *Inorg Chem* 60, 14294–14301. <https://doi.org/10.1021/acs.inorgchem.1c01839>
- Donatti, D.A., Ruiz, A.I., Vollet, D.R., 2002. A dissolution and reaction modeling for hydrolysis of TEOS in heterogeneous TEOS–water–HCl mixtures under ultrasound stimulation. *Ultrasonics Sonochemistry* 9, 133–138. [https://doi.org/10.1016/S1350-4177\(01\)00120-1](https://doi.org/10.1016/S1350-4177(01)00120-1)
- Donatti, D.A., Vollet, D.R., 2000. Effects of the Water Quantity on the Solventless TEOS Hydrolysis Under Ultrasound Stimulation. *Journal of Sol-Gel Science and Technology* 17, 19–24. <https://doi.org/10.1023/A:1008748702656>
- Duan, H., Ji, S., Yin, T., Tao, X., Chen, Y., Ma, H., 2019. Phosphorus–nitrogen - type fire - retardant vinyl ester resin with good comprehensive properties. *J Appl Polym Sci* 136, 47997. <https://doi.org/10.1002/app.47997>
- Férey, G., Mellot-Draznieks, C., Serre, C., Millange, F., Dutour, J., Surlé, S., Margiolaki, I., 2005. A Chromium Terephthalate-Based Solid with Unusually Large Pore Volumes and Surface Area. *Science* 309, 2040–2042. <https://doi.org/10.1126/science.1116275>
- Férey, G., Serre, C., Mellot-Draznieks, C., Millange, F., Surlé, S., Dutour, J., Margiolaki, I., 2004. A Hybrid Solid with Giant Pores Prepared by a Combination of Targeted Chemistry, Simulation, and Powder Diffraction. *Angewandte Chemie* 116, 6456–6461. <https://doi.org/10.1002/ange.200460592>
- Gao, M., Zeng, L., Nie, J., Ma, G., 2016. Polymer–metal–organic framework core–shell framework nanofibers via electrospinning and their gas adsorption activities. <https://doi.org/10.1039/C5RA23147G>
- Gaspar, V.M., Moreira, A.F., de Melo-Diogo, D., Costa, E.C., Queiroz, J.A., Sousa, F., Pichon, C., Correia, I.J., 2016. Chapter 6 - Multifunctional nanocarriers for codelivery of nucleic acids and chemotherapeutics to cancer cells, in: Grumezescu, A.M. (Ed.), *Nanobiomaterials in Medical Imaging*. William Andrew Publishing, pp. 163–207. <https://doi.org/10.1016/B978-0-323-41736-5.00006-6>
- González, C.M.O., Morales, E.M.C., Tellez, A. de M.N., Quezada, T.E.S., Kharissova, O.V., Méndez-Rojas, M.A., 2021. Chapter 18 - CO<sub>2</sub> capture by MOFs, in: Kharisov, B., Kharissova, O. (Eds.), *Handbook of Greener Synthesis of Nanomaterials and Compounds*. Elsevier, pp. 407–448. <https://doi.org/10.1016/B978-0-12-822446-5.00018-6>
- Guo, D.-M., An, Q.-D., Xiao, Z.-Y., Zhai, S.-R., Shi, Z., 2017. Polyethylenimine-functionalized cellulose aerogel beads for efficient dynamic removal of chromium( vi ) from aqueous solution. *RSC Advances* 7, 54039–54052. <https://doi.org/10.1039/C7RA09940A>
- Halima, N.B., 2016. Poly(vinyl alcohol): review of its promising applications and insights into biodegradation. *RSC Adv.* 6, 39823–39832. <https://doi.org/10.1039/C6RA05742J>

- Hamdani - Devarenes, S., Longuet, C., Perrin, D., Lopez-cuesta, J.-M., Ganachaud, F., 2009. Flame retardancy of silicone-based materials. *Polymer Degradation and Stability* 94, 465–495. <https://doi.org/10.1016/j.polymdegradstab.2008.11.019>
- He, M., Zhang, D., Zhao, W., Qin, S., Yu, J., 2019. Flame retardant and thermal decomposition mechanism of poly(butylene terephthalate)/DOPO-HQ composites. *Polym. Compos.* 40, 974–985. <https://doi.org/10.1002/pc.24772>
- Hergenrother, P.M., Thompson, C.M., Smith, J.G., Connell, J.W., Hinkley, J.A., Lyon, R.E., Moulton, R., 2005. Flame retardant aircraft epoxy resins containing phosphorus. *Polymer* 46, 5012–5024. <https://doi.org/10.1016/j.polymer.2005.04.025>
- Hou, Y., Hu, W., Gui, Z., Hu, Y., 2017. Preparation of Metal-Organic Frameworks and Their Application as Flame Retardants for Polystyrene. *Industrial & Engineering Chemistry Research* 56. <https://doi.org/10.1021/acs.iecr.6b04920>
- Hsieh, Y.L., 2007. Chemical structure and properties of cotton, in: *Cotton*. Elsevier, pp. 3–34. <https://doi.org/10.1533/9781845692483.1.3>
- Hu, S., Hu, Y., Song, L., Lu, H., 2011. Effect of modified organic–inorganic hybrid materials on thermal properties of cotton fabrics. *J Therm Anal Calorim* 103, 423–427. <https://doi.org/10.1007/s10973-010-1093-1>
- J. Katz, M., J. Brown, Z., J. Colón, Y., W. Siu, P., A. Scheidt, K., Q. Snurr, R., T. Hupp, J., K. Farha, O., 2013. A facile synthesis of UiO-66, UiO-67 and their derivatives. *Chemical Communications* 49, 9449–9451. <https://doi.org/10.1039/C3CC46105J>
- Jiang, X., Zhao, C., Zhong, C., Li, J., 2017. The Electrochemical Sensors Based on MOF and Their Applications. *Progress in Chemistry* 29, 1206–1214. <https://doi.org/10.7536/PC170619>
- Jiang, Zhiming, Hao Li, Yewei He, Yun Liu, Chaohong Dong, and Ping Zhu. 2019. Flame Retardancy and Thermal Behavior of Cotton Fabrics Based on a Novel Phosphorus-Containing Siloxane. *Applied Surface Science* 479 (June): 765–775. <https://doi.org/10.1016/j.apsusc.2019.02.159>
- Kaya, H., Ngo, D., Gin, S., Kim, S.H., 2020. Spectral changes in Si–O–Si stretching band of porous glass network upon ingress of water. *Journal of Non-Crystalline Solids* 527, 119722. <https://doi.org/10.1016/j.jnoncrysol.2019.119722>
- Kayal, S., Sun, B., Chakraborty, A., 2015. Study of metal-organic framework MIL-101(Cr) for natural gas (methane) storage and compare with other MOFs (metal-organic frameworks). *Energy* 91, 772–781. <https://doi.org/10.1016/j.energy.2015.08.096>
- Khabzina, Y., Dhainaut, J., Ahlhelm, M., Richter, H.-J., Reinsch, H., Stock, N., Farrusseng, D., 2018. Synthesis and Shaping Scale-up Study of Functionalized UiO-66 MOF for Ammonia Air Purification Filters. *Ind. Eng. Chem. Res.* 57, 8200–8208. <https://doi.org/10.1021/acs.iecr.8b00808>
- Khanjani, S., Morsali, A., 2014. Ultrasound-promoted coating of MOF-5 on silk fiber and study of adsorptive removal and recovery of hazardous anionic dye “congo red.” *Ultrasonics Sonochemistry* 21, 1424–1429. <https://doi.org/10.1016/j.ultsonch.2013.12.012>

- Klinowski, J., Paz, F.A.A., Silva, P., Rocha, J., 2010. Microwave-Assisted Synthesis of Metal–Organic Frameworks. *Dalton Trans.* 40, 321–330. <https://doi.org/10.1039/C0DT00708K>
- Kwon, H.T., Jeong, H.-K., 2013. In situ synthesis of thin zeolitic-imidazolate framework ZIF-8 membranes exhibiting exceptionally high propylene/propane separation. *J Am Chem Soc* 135, 10763–10768. <https://doi.org/10.1021/ja403849c>
- Laufer, G., Kirkland, C., Morgan, A.B., Grunlan, J.C., 2012. Intumescent Multilayer Nanocoating, Made with Renewable Polyelectrolytes, for Flame-Retardant Cotton [WWW Document]. ACS Publications. <https://doi.org/10.1021/bm300873b>
- Lee, Y.-R., Kim, J., Ahn, W.-S., 2013. Synthesis of metal-organic frameworks: A mini review. *Korean J. Chem. Eng.* 30, 1667–1680. <https://doi.org/10.1007/s11814-013-0140-6>
- Li, D., Zhou, Q., Hu, X., Mu, L., Zeng, H., Luo, J., 2022. Environmental decomposition and remodeled phytotoxicity of framework-based nanomaterials. *J Hazard Mater* 422, 126846. <https://doi.org/10.1016/j.jhazmat.2021.126846>
- Li, D.-J., Lei, S., Wang, Y.-Y., Chen, S., Kang, Y., Gu, Z.-G., Zhang, J., 2018. Helical carbon tubes derived from epitaxial Cu-MOF coating on textile for enhanced supercapacitor performance. *Dalton Trans.* 47, 5558–5563. <https://doi.org/10.1039/C8DT00761F>
- Li, G., Xia, L., Dong, J., Chen, Y., Li, Y., 2020. 10 - Metal-organic frameworks, in: Poole, C.F. (Ed.), *Solid-Phase Extraction, Handbooks in Separation Science*. Elsevier, pp. 285–309. <https://doi.org/10.1016/B978-0-12-816906-3.00010-8>
- Li, H., Li, L., Lin, R.-B., Zhou, W., Zhang, Z., Xiang, S., Chen, B., 2019. Porous metal-organic frameworks for gas storage and separation: Status and challenges. *EnergyChem* 1, 100006. <https://doi.org/10.1016/j.enchem.2019.100006>
- Li, H., Wang, K., Sun, Y., Lollar, C.T., Li, J., Zhou, H.-C., 2018. Recent advances in gas storage and separation using metal–organic frameworks. *Materials Today* 21, 108–121. <https://doi.org/10.1016/j.mattod.2017.07.006>
- Li, Jinfeng, and Wei Jiang. 2021. 'Synthesis of a Novel P-N Flame Retardant for Preparing Flame Retardant and Durable Cotton Fabric'. *Industrial Crops and Products* 174 (December): 114205. <https://doi.org/10.1016/j.indcrop.2021.114205>.
- Li, N., Ming, J., Yuan, R., Fan, S., Liu, L., Li, F., Wang, X., Yu, J., Wu, D., 2020. Novel Eco-Friendly Flame Retardants Based on Nitrogen–Silicone Schiff Base and Application in Cellulose. *ACS Sustainable Chem. Eng.* 8, 290–301. <https://doi.org/10.1021/acssuschemeng.9b05338>
- Li, P., Wang, B., Liu, Y.-Y., Xu, Y.-J., Jiang, Z.-M., Dong, C.-H., Zhang, L., Liu, Y., Zhu, P., 2020. Fully bio-based coating from chitosan and phytate for fire-safety and antibacterial cotton fabrics. *Carbohydrate Polymers* 237, 116173. <https://doi.org/10.1016/j.carbpol.2020.116173>
- Li, Y., Wang, B., Sui, X., Xie, R., Xu, H., Zhang, L., Zhong, Y., Mao, Z., 2018. Durable flame retardant and antibacterial finishing on cotton fabrics with cyclotriphosphazene/polydopamine/silver nanoparticles hybrid coatings. *Applied Surface Science* 435, 1337–1343. <https://doi.org/10.1016/j.apsusc.2017.11.269>

- Lian, X., Fang, Y., Joseph, E., Wang, Q., Li, J., Banerjee, S., Lollar, C., Wang, X., Zhou, H.-C., 2017. Enzyme–MOF (metal–organic framework) composites. *Chem. Soc. Rev.* 46, 3386–3401. <https://doi.org/10.1039/C7CS00058H>
- Liang, J., Huang, Y.-B., Cao, R., 2019. Metal–organic frameworks and porous organic polymers for sustainable fixation of carbon dioxide into cyclic carbonates. *Coordination Chemistry Reviews, Special issue on the 8th Chinese Coordination Chemistry Conference* 378, 32–65. <https://doi.org/10.1016/j.ccr.2017.11.013>
- Lin, C.-F., Tseng, W., Feng, M., 2000. Formation and characteristics of silicon nanocrystals in plasma-enhanced chemical-vapor-deposited silicon-rich oxide. *Journal of Applied Physics - J APPL PHYS* 87, 2808–2815. <https://doi.org/10.1063/1.372260>
- Lin, D., Zeng, X., Li, H., Lai, X., Wu, T., 2018. One-pot fabrication of superhydrophobic and flame-retardant coatings on cotton fabrics via sol-gel reaction. *Journal of Colloid and Interface Science* 533. <https://doi.org/10.1016/j.jcis.2018.08.060>
- Liu, G., Han, Y., Zhao, Y., Zheng, H., Zheng, L., 2020. Development of CO<sub>2</sub> utilized flame retardant finishing: Solubility measurements of flame retardants and application of the process to cotton. *Journal of CO<sub>2</sub> Utilization* 37, 222–229. <https://doi.org/10.1016/j.jcou.2019.12.015>
- Liu, M., Yin, H., Chen, X., Yang, J., Liang, Y., Zhang, J., Yang, F., Deng, Y., Lu, S., 2018. Preliminary ecotoxicity hazard evaluation of DOPO-HQ as a potential alternative to halogenated flame retardants. *Chemosphere* 193, 126–133. <https://doi.org/10.1016/j.chemosphere.2017.10.142>
- Liu, S., Fang, Z., Yan, H., Chevali, V.S., Wang, H., 2016. Synergistic flame retardancy effect of graphene nanosheets and traditional retardants on epoxy resin. *Composites Part A: Applied Science and Manufacturing* 89, 26–32. <https://doi.org/10.1016/j.compositesa.2016.03.012>
- Liu, Y., He, J., Yang, R., 2016. The preparation and properties of flame-retardant polyisocyanurate–polyurethane foams based on two DOPO derivatives. *Journal of Fire Sciences* 34, 431–444. <https://doi.org/10.1177/0734904116662667>
- Lu, A.X., McEntee, M., Browe, M.A., Hall, M.G., DeCoste, J.B., Peterson, G.W., 2017. MOFfabric: Electrospun Nanofiber Mats from PVDF/UiO-66-NH<sub>2</sub> for Chemical Protection and Decontamination. *ACS Appl Mater Interfaces* 9, 13632–13636. <https://doi.org/10.1021/acsami.7b01621>
- Ma, K., Idrees, K.B., Son, F.A., Maldonado, R., Wasson, M.C., Zhang, X., Wang, X., Shehayeb, E., Merhi, A., Kaafarani, B.R., Islamoglu, T., Xin, J.H., Farha, O.K., 2020. Fiber Composites of Metal–Organic Frameworks. *Chem. Mater.* 32, 7120–7140. <https://doi.org/10.1021/acs.chemmater.0c02379>
- Ma, K., Wang, Y., Chen, Z., Islamoglu, T., Lai, C., Wang, X., Fei, B., Farha, O.K., Xin, J.H., 2019. Facile and Scalable Coating of Metal–Organic Frameworks on Fibrous Substrates by a Coordination Replication Method at Room Temperature. *ACS Appl. Mater. Interfaces* 11, 22714–22721. <https://doi.org/10.1021/acsami.9b04780>
- Ma, T., Li, H., Ma, J.-G., Cheng, P., 2020. Application of MOF-based materials in electrochemical sensing. *Dalton Trans.* 49, 17121–17129. <https://doi.org/10.1039/D0DT03388J>
- Ma, Yanan, Xiaolei Luo, Lin Liu, Cong Zhang, Xiaolei Shang, and Juming Yao. 2021. ‘Eco-Friendly, Efficient and Durable Fireproof Cotton Fabric

- Prepared by a Feasible Phytic Acid Grafting Route'. *Cellulose* 28 (6): 3887–99. <https://doi.org/10.1007/s10570-021-03767-0>.
- Mahmoodi, N.M., Abdi, J., Oveisi, M., Alinia Asli, M., Vossoughi, M., 2018. Metal-organic framework (MIL-100 (Fe)): Synthesis, detailed photocatalytic dye degradation ability in colored textile wastewater and recycling. *Materials Research Bulletin* 100, 357 – 366. <https://doi.org/10.1016/j.materresbull.2017.12.033>
- Malucelli, G., 2020. Flame-Retardant Systems Based on Chitosan and Its Derivatives: State of the Art and Perspectives. *Molecules* 25, 4046. <https://doi.org/10.3390/molecules25184046>
- Martínez-Ahumada, E., Díaz-Ramírez, M.L., Velásquez-Hernández, M. de J., Jancik, V., Ibarra, I.A., 2021. Capture of toxic gases in MOFs: SO<sub>2</sub>, H<sub>2</sub>S, NH<sub>3</sub> and NO<sub>x</sub>. *Chem. Sci.* 12, 6772–6799. <https://doi.org/10.1039/D1SC01609A>
- Mehra, S., Polisetti, V., Damarla, K., Ray, P., Kumar, A., 2021. Ionic Liquid-Based Colloidal Formulations for the Synthesis of Nano-MOFs: Applications in Gas Adsorption and Water Desalination. *ACS Appl. Mater. Interfaces* 13, 41249–41261. <https://doi.org/10.1021/acsami.1c10184>
- Mercado, L.A., Galià, M., Reina, J.A., 2006. Silicon-containing flame retardant epoxy resins: Synthesis, characterization and properties. *Polymer Degradation and Stability* 91, 2588–2594. <https://doi.org/10.1016/j.polymdegradstab.2006.05.007>
- Moltó, Julia, Rafael Font, Juan A. Conesa, and Ignacio Martín-Gullón. 2006. 'Thermogravimetric Analysis during the Decomposition of Cotton Fabrics in an Inert and Air Environment'. *Journal of Analytical and Applied Pyrolysis* 76 (1): 124–31. <https://doi.org/10.1016/j.jaap.2005.09.001>.
- Mukherjee, S., Kumar, A., Zaworotko, M.J., 2019. 2 - Metal-organic framework based carbon capture and purification technologies for clean environment, in: Ghosh, S.K. (Ed.), *Metal-Organic Frameworks (MOFs) for Environmental Applications*. Elsevier, pp. 5–61. <https://doi.org/10.1016/B978-0-12-814633-0.00003-X>
- Nabipour, H., Nie, S., Wang, X., Song, L., Hu, Y., 2020a. Highly flame retardant zeolitic imidazole framework-8@cellulose composite aerogels as absorption materials for organic pollutants. *Cellulose* 27, 2237–2251. <https://doi.org/10.1007/s10570-019-02860-9>
- Nabipour, H., Wang, X., Song, L., Hu, Y., 2020b. Metal-organic frameworks for flame retardant polymers application: A critical review. *Composites Part A: Applied Science and Manufacturing* 139, 106113. <https://doi.org/10.1016/j.compositesa.2020.106113>
- Nabipour, H., Wang, X., Song, L., Hu, Y., 2020c. Graphene oxide/zeolitic imidazolate frameworks-8 coating for cotton fabrics with highly flame retardant, self-cleaning and efficient oil/water separation performances. *Materials Chemistry and Physics* 256, 123656. <https://doi.org/10.1016/j.matchemphys.2020.123656>
- Ozer, D., 2020. Fabrication and Functionalization Strategies of MOFs and Their Derived Materials "MOF Architecture," in: *Applications of Metal–Organic Frameworks and Their Derived Materials*. John Wiley & Sons, Ltd, pp. 63–100. <https://doi.org/10.1002/9781119651079.ch3>
- Pan, Y.-T., Zhang, Z., Yang, R., 2020. The rise of MOFs and their derivatives for flame retardant polymeric materials: A critical review. *Composites Part B:*

- Engineering 199, 108265.  
<https://doi.org/10.1016/j.compositesb.2020.108265>
- Park, K.S., Ni, Z., Côté, A.P., Choi, J.Y., Huang, R., Uribe-Romo, F.J., Chae, H.K., O'Keeffe, M., Yaghi, O.M., 2006. Exceptional chemical and thermal stability of zeolitic imidazolate frameworks. *Proceedings of the National Academy of Sciences* 103, 10186–10191.  
<https://doi.org/10.1073/pnas.0602439103>
- Pascanu, V., González Miera, G., Inge, A.K., Martín-Matute, B., 2019. Metal–Organic Frameworks as Catalysts for Organic Synthesis: A Critical Perspective. *J. Am. Chem. Soc.* 141, 7223–7234.  
<https://doi.org/10.1021/jacs.9b00733>
- Peng, C., Li, J., Wu, Z., Peng, W., Zhou, D., 2016. Investigating into the liquid oxygen compatibility of a modified epoxy resin containing silicon/phosphorus and its mechanical behavior at cryogenic temperature. *RSC Adv.* 6, 38300–38309. <https://doi.org/10.1039/C6RA06033A>
- Pirzadeh, K., Ghoreyshi, A.A., Rahimnejad, M., Mohammadi, M., 2018. Electrochemical synthesis, characterization and application of a microstructure Cu<sub>3</sub>(BTC)<sub>2</sub> metal organic framework for CO<sub>2</sub> and CH<sub>4</sub> separation. *Korean Journal of Chemical Engineering* 35.  
<https://doi.org/10.1007/s11814-017-0340-6>
- Portella, E.H., Romanzini, D., Angrizani, C.C., Amico, S.C., Zattera, A.J., 2016. Influence of Stacking Sequence on the Mechanical and Dynamic Mechanical Properties of Cotton/Glass Fiber Reinforced Polyester Composites. *Mat. Res.* 19, 542–547. <https://doi.org/10.1590/1980-5373-MR-2016-0058>
- Qi, X.-L., Zhou, D.-D., Zhang, J., Hu, S., Haranczyk, M., Wang, D.-Y., 2019. Simultaneous Improvement of Mechanical and Fire-Safety Properties of Polymer Composites with Phosphonate-Loaded MOF Additives. *ACS Appl. Mater. Interfaces* 11, 20325–20332.  
<https://doi.org/10.1021/acsami.9b02357>
- Rakotomalala, M., Wagner, S., Döring, M., 2010. Recent Developments in Halogen Free Flame Retardants for Epoxy Resins for Electrical and Electronic Applications. *Materials* 3, 4300–4327.  
<https://doi.org/10.3390/ma3084300>
- Ren, L., Zhao, X., Liu, B., Huang, H., 2021. Synergistic effect of carboxyl and sulfate groups for effective removal of radioactive strontium ion in a Zr-metal-organic framework. *Water Science and Technology* 83, 2001–2011.  
<https://doi.org/10.2166/wst.2021.103>
- Rodríguez, H.S., Hinestroza, J.P., Ochoa-Puentes, C., Sierra, C.A., Soto, C.Y., 2014. Antibacterial activity against *Escherichia coli* of Cu-BTC (MOF-199) metal-organic framework immobilized onto cellulosic fibers. *Journal of Applied Polymer Science* 131. <https://doi.org/10.1002/app.40815>
- Rowsell, J.L.C., Yaghi, O.M., 2004. Metal–organic frameworks: a new class of porous materials. *Microporous and Mesoporous Materials* 73, 3–14.  
<https://doi.org/10.1016/j.micromeso.2004.03.034>
- Rubio-Martinez, M., Avci-Camur, C., Thornton, A.W., Imaz, I., Maspoch, D., Hill, M.R., 2017. New synthetic routes towards MOF production at scale. *Chem. Soc. Rev.* 46, 3453–3480. <https://doi.org/10.1039/C7CS00109F>
- Salmeia, K.A., Jovic, M., Ragaisiene, A., Rukuiziene, Z., Milasius, R., Mikucioniene, D., Gaan, S., 2016. Flammability of Cellulose-Based Fibers

- and the Effect of Structure of Phosphorus Compounds on Their Flame Retardancy. *Polymers (Basel)* 8, 293. <https://doi.org/10.3390/polym8080293>
- Samuel, M.S., Bhattacharya, J., Parthiban, C., Viswanathan, G., Pradeep Singh, N.D., 2018. Ultrasound-assisted synthesis of metal organic framework for the photocatalytic reduction of 4-nitrophenol under direct sunlight. *Ultrasonics Sonochemistry* 49, 215–221. <https://doi.org/10.1016/j.ultsonch.2018.08.004>
- Schelling, M., Kim, M., Otal, E., Aguirre, M., Hinestroza, J.P., 2020. Synthesis of a zinc–imidazole metal–organic framework (ZIF-8) using ZnO rods grown on cotton fabrics as precursors: arsenate absorption studies. *Cellulose* 27, 6399–6410. <https://doi.org/10.1007/s10570-020-03216-4>
- Schelling, M., Kim, M., Otal, E., Hinestroza, J., 2018. Decoration of Cotton Fibers with a Water-Stable Metal-Organic Framework (UiO-66) for the Decomposition and Enhanced Adsorption of Micropollutants in Water. *Bioengineering (Basel)* 5. <https://doi.org/10.3390/bioengineering5010014>
- Shang, M., Zhang, X., Zhang, J., Sun, J., Zhao, X., Yu, S., Liu, X., Liu, B., Yi, X., 2021. Nitrogen-doped carbon composite derived from ZIF-8/polyaniline@cellulose-derived carbon aerogel for high-performance symmetric supercapacitors. *Carbohydrate Polymers* 262, 117966. <https://doi.org/10.1016/j.carbpol.2021.117966>
- Shekhah, O., Fu, L., Sougrat, R., Belmabkhout, Y., Cairns, A.J., Giannelis, E.P., Eddaoudi, M., 2012. Successful implementation of the stepwise layer-by-layer growth of MOF thin films on confined surfaces: mesoporous silica foam as a first case study. *Chem. Commun.* 48, 11434–11436. <https://doi.org/10.1039/C2CC36233C>
- Shekhah, O., Liu, J., Fischer, R.A., Wöll, C., 2011. MOF thin films: existing and future applications. *Chem. Soc. Rev.* 40, 1081–1106. <https://doi.org/10.1039/C0CS00147C>
- Shi, X., Peng, X., Zhu, J., Lin, G., Kuang, T., 2018. Synthesis of DOPO-HQ-functionalized graphene oxide as a novel and efficient flame retardant and its application on polylactic acid: Thermal property, flame retardancy, and mechanical performance. *Journal of Colloid and Interface Science* 524, 267–278. <https://doi.org/10.1016/j.jcis.2018.04.016>
- Singh, R., Gautam, S., Sharma, B., Jain, P., Chauhan, K.D., 2021. Chapter 2 - Biopolymers and their classifications, in: Thomas, S., Gopi, S., Amalraj, A. (Eds.), *Biopolymers and Their Industrial Applications*. Elsevier, pp. 21–44. <https://doi.org/10.1016/B978-0-12-819240-5.00002-X>
- So, M.C., Beyzavi, M.H., Sawhney, R., Shekhah, O., Eddaoudi, M., Al-Juaid, S.S., Hupp, J.T., Farha, O.K., 2014. Post-assembly transformations of porphyrin-containing metal–organic framework (MOF) films fabricated via automated layer-by-layer coordination. *Chem. Commun.* 51, 85–88. <https://doi.org/10.1039/C4CC05727A>
- Su, Z., Zhang, M., Lu, Z., Song, S., Zhao, Y., Hao, Y., 2018. Functionalization of cellulose fiber by in situ growth of zeolitic imidazolate framework-8 (ZIF-8) nanocrystals for preparing a cellulose-based air filter with gas adsorption ability. *Cellulose* 25, 1997–2008. <https://doi.org/10.1007/s10570-018-1696-4>
- Sun, Y., Zheng, L., Yang, Y., Qian, X., Fu, T., Li, X., Yang, Z., Yan, H., Cui, C., Tan, W., 2020. Metal–Organic Framework Nanocarriers for Drug Delivery

- in Biomedical Applications. *Nano-Micro Lett.* 12, 103. <https://doi.org/10.1007/s40820-020-00423-3>
- Tanaka, S., 2020. Chapter 10 - Mechanochemical synthesis of MOFs, in: Mozafari, M. (Ed.), *Metal-Organic Frameworks for Biomedical Applications*. Woodhead Publishing, pp. 197–222. <https://doi.org/10.1016/B978-0-12-816984-1.00012-3>
- Tang, H., Zhu, Z., Chen, R., Wang, J., Zhou, H., 2019. Synthesis of DOPO - based pyrazine derivative and its effect on flame retardancy and thermal stability of epoxy resin. *Polym Adv Technol* 30, 2331–2339. <https://doi.org/10.1002/pat.4674>
- Vasiljević, J., Jerman, I., Jakša, G., Alongi, J., Malucelli, G., Zorko, M., Tomšič, B., & Simončič, B., 2015. Functionalization of cellulose fibres with DOPO-polysilsesquioxane flame retardant nanocoating. *Cellulose* 22, 1893–1910. <https://doi.org/10.1007/s10570-015-0599-x>
- Wan, Caiyan, Mingsheng Liu, Shidong Liu, Yv Chen, Guangxian Zhang, and Fengxiu Zhang. 2021. 'An Efficient and Durable DOPO/H3PO4-Based Flame Retardant for Cotton Fabric'. *Cellulose* 28 (11): 7421–34. <https://doi.org/10.1007/s10570-021-03981-w>.
- Wang, H., Qiao, H., Guo, J., Sun, J., Li, H., Zhang, S., Gu, X., 2019. Preparation of cobalt-based metal organic framework and its application as synergistic flame retardant in thermoplastic polyurethane (TPU). *Composites Part B: Engineering* 182, 107498. <https://doi.org/10.1016/j.compositesb.2019.107498>
- Wang, L., Zhang, T., Yan, H., Peng, M., Fang, Z., Li, Y., Hao, W., 2014. Flame-retardant coating by alternate assembly of poly(vinylphosphonic acid) and polyethylenimine for ramie fabrics. *Chin J Polym Sci* 32, 305–314. <https://doi.org/10.1007/s10118-014-1408-y>
- Wang, P., Cai, Z., 2017. Highly efficient flame-retardant epoxy resin with a novel DOPO-based triazole compound: Thermal stability, flame retardancy and mechanism. *Polymer Degradation and Stability* 137, 138–150. <https://doi.org/10.1016/j.polymdegradstab.2017.01.014>
- Wang, Shihao, Ling Sun, Yuyang Li, Huixin Wang, Jie Liu, Ping Zhu, and Chaohong Dong. 2021. 'Properties of Flame-Retardant Cotton Fabrics: Combustion Behavior, Thermal Stability and Mechanism of Si/P/N Synergistic Effect'. *Industrial Crops and Products* 173 (December): 114157. <https://doi.org/10.1016/j.indcrop.2021.114157>.
- Wang, X., Lu, Y., Zhang, Q., Wang, K., Carmalt, C., Parkin, I., Zhang, Z., Zhang, X., 2020. Durable Fire Retardant, Superhydrophobic, Abrasive Resistant and Air/UV Stable Coatings. *Journal of Colloid and Interface Science* 582. <https://doi.org/10.1016/j.jcis.2020.07.084>
- Wei, Dongdong, Chaohong Dong, Jian Liu, Zheng Zhang, and Zhou Lu. 2019. 'A Novel Cyclic Polysiloxane Linked by Guanidyl Groups Used as Flame Retardant and Antimicrobial Agent on Cotton Fabrics'. *Fibers and Polymers* 20 (7): 1340–46. <https://doi.org/10.1007/s12221-019-9008-7>.
- Wei, Z., Gu, X., Wu, J., Wei, M., Yu, Q., Xiujian, T., Wang, Z., 2019. Performance comparison of epoxy resins modified with diphenylphosphine oxide and DOPO. *Fire and Materials* 43, 892–902. <https://doi.org/10.1002/fam.2749>
- Wilkie, C.A., Morgan, A.B., 2009. *Fire Retardancy of Polymeric Materials*, Second Edition. CRC Press.



- Williams, B.L., Ding, H., Hou, Z., Paul, P.O., Lewis, F.A., Smith, A.T., Sun, L., 2021. Highly efficient polyvinyl alcohol/montmorillonite flame retardant nanocoating for corrugated cardboard. *Adv Compos Hybrid Mater* 4, 662–669. <https://doi.org/10.1007/s42114-021-00299-w>
- Wolff, S., 1996. Chemical Aspects of Rubber Reinforcement by Fillers. *Rubber Chemistry and Technology* 69, 325–346. <https://doi.org/10.5254/1.3538376>
- Wu, M.-X., Yang, Y.-W., 2017. Metal–Organic Framework (MOF)-Based Drug/Cargo Delivery and Cancer Therapy. *Advanced Materials* 29, 1606134. <https://doi.org/10.1002/adma.201606134>
- Xiangze, J., Bin, Z., Bin, Z., Bin, Z., Bin, Z., Chun, C., Chun, C., Chun, C., Xiong, F., Xiong, F., Xiong, F., Qiang, H., Qiang, H., Qiang, H., 2021. Immobilization of chitosan grafted carboxylic Zr-MOF to porous starch for sulfanilamide adsorption. *Carbohydrate Polymers* 253.
- Xue, Y., Zheng, S., Xue, H., Pang, H., 2019. Metal–organic framework composites and their electrochemical applications. *Journal of Materials Chemistry A* 7, 7301–7327. <https://doi.org/10.1039/C8TA12178H>
- Yan, H., Yuanhao, W., Hongxing, Y., 2015. TEOS/Silane-Coupling Agent Composed Double Layers Structure: A Novel Super-hydrophilic Surface. *Energy Procedia, Clean, Efficient and Affordable Energy for a Sustainable Future: The 7th International Conference on Applied Energy (ICAE2015)* 75, 349–354. <https://doi.org/10.1016/j.egypro.2015.07.384>
- Yang, D., Odoh, S., Wang, T., Farha, O., Hupp, J., Cramer, C., Prof. Dr, L., Gates, B., 2015. Metal–Organic Framework Nodes as Nearly Ideal Supports for Molecular Catalysts: NU-1000- and UiO-66-Supported Iridium Complexes. *Journal of the American Chemical Society* 137. <https://doi.org/10.1021/jacs.5b02956>
- Yi, S., Su, Y., Wan, Y., 2010. Preparation and characterization of vinyltriethoxysilane (VTES) modified silicalite-1/PDMS hybrid pervaporation membrane and its application in ethanol separation from dilute aqueous solution. *Journal of Membrane Science* 11.
- Yu, J., Mu, C., Yan, B., Qin, X., Shen, C., Xue, H., Pang, H., 2017. Nanoparticle/MOF composites: preparations and applications. *Mater. Horiz.* 4, 557–569. <https://doi.org/10.1039/C6MH00586A>
- Yu, M., Li, W., Wang, Z., Zhang, B., Ma, H., Li, L., Li, J., 2016. Covalent immobilization of metal–organic frameworks onto the surface of nylon—a new approach to the functionalization and coloration of textiles. *Sci Rep* 6, 22796. <https://doi.org/10.1038/srep22796>
- Yu, Z.-L., Yang, N., Apostolopoulou-Kalkavoura, V., Qin, B., Ma, Z.-Y., Xing, W.-Y., Qiao, C., Bergström, L., Antonietti, M., Yu, S.-H., 2018. Fire-Retardant and Thermally Insulating Phenolic-Silica Aerogels. *Angewandte Chemie International Edition* 57, 4538–4542. <https://doi.org/10.1002/anie.201711717>
- Zhang, J., Li, Z., Qi, X.-L., Wang, D.-Y., 2020. Recent Progress on Metal–Organic Framework and Its Derivatives as Novel Fire Retardants to Polymeric Materials. *Nano-Micro Lett.* 12, 173. <https://doi.org/10.1007/s40820-020-00497-z>
- Zhang, Y., Chang, C., Tan, B., Xu, D., Wang, Y., Qi, T., 2019. Application of a Sustainable Bioderived Solvent (Biodiesel) for Phenol Extraction. *ACS Omega* 4, 10431–10437. <https://doi.org/10.1021/acsomega.9b00977>

- Zhang, Yingnan, Mingju Jing, Shuya Hou, Yawen Gong, Zhi Wang, Juncheng Jiang, and Bin Zhang. 2022. 'Preparation and Fire-Retardant Mechanism of Self-Hardening Silica Foam for Wood Fire Prevention'. *Silicon*, June. <https://doi.org/10.1007/s12633-022-01975-2>.
- Zhang, Z., Dong, C., Liu, J., Kong, D., Sun, L., Lu, Z., 2020. Preparation of a synergistic reactive flame retardant based on silicon, phosphorus and nitrogen and its application to cotton fabrics. *Cellulose* 27, 1799–1815. <https://doi.org/10.1007/s10570-019-02900-4>
- Zhao, B., Kolibaba, T.J., Lazar, S., Grunlan, J.C., 2021. Environmentally-benign, water-based covalent polymer network for flame retardant cotton. *Cellulose* 28, 5855–5866. <https://doi.org/10.1007/s10570-021-03874-y>
- Zhou, S., Huangfu, W., You, F., Li, D., Fan, D., 2019. Flame Retardancy and Mechanism of Cotton Fabric Finished by Phosphorus Containing SiO<sub>2</sub> Hybrid Sol, in: 2019 9th International Conference on Fire Science and Fire Protection Engineering (ICFSFPE). Presented at the 2019 9th International Conference on Fire Science and Fire Protection Engineering (ICFSFPE), IEEE, Chengdu, China, pp. 1–5. <https://doi.org/10.1109/ICFSFPE48751.2019.9055847>
- Zhou, W., Yang, C.Q., Lickfield, G.C., 2004. Mechanical strength of durable press finished cotton fabric part V: Poly(vinyl alcohol) as an additive to improve fabric abrasion resistance. *Journal of Applied Polymer Science* 91, 3940–3946. <https://doi.org/10.1002/app.13606>
- Zia, K.M., Zuber, M., Rizwan, A., Jamil, T., Tabasum, S., Shahid, M., 2012. Modification of cellulosic fabric using polyvinyl alcohol—Part-I: Physicochemical properties. *Carbohydrate Polymers* 87, 2063–2067. <https://doi.org/10.1016/j.carbpol.2011.10.021>

## **Chapter III. Absorption behavior analysis of cotton fabrics to DOPO-HQ@UIO-66-COOH composites**

### 3.1 Introduction

The DOPO-HQ@Zr-MOF composites featured the benefits of DOPO-HQ in addition to retaining the characteristics of the zirconium metal-organic framework. Furthermore, the KILBY mathematical model was utilized to analyze the adsorption behavior of cotton fabrics in UIO-66-COOH, DOPO-HQ and DOPO-HQ@Zr-MOF finishing solution, respectively. The factors such as sample concentration, dipping time and bath temperature were observed during experimental process.

E is exhaustion rate

$$E = \frac{C_0 - C_\infty}{C_0}$$

$\alpha$  is exhaustion coefficient

$$\alpha = \frac{1-E}{E}$$

The Mathematical model of adsorption of reagents and their diffusion on fabrics is referred to Manel Lis doctoral dissertation (Lis Arias, 2002), which is particularly suitable for adsorption studies on specific cylinder fiber materials with finite bath. The detailed model derivation basis is presented as follows.

Firstly, Professor John Crank put forward the mathematics of diffusion based on infinite cylinder and finite bath (Crank, 1980):

$$\frac{C_t}{C_\infty} = \frac{1+\alpha}{1+\frac{\alpha}{4}} \left[ 1 - \exp \left\{ 4 \left\{ 1 + \frac{\alpha}{4} \right\}^2 \frac{Dt}{r^2 \alpha^2} \right\} \operatorname{erfc} \left\{ 2 \left\{ 1 + \frac{\alpha}{4} \right\} \frac{1}{\alpha} \left\{ \frac{Dt}{r^2} \right\}^{1/2} \right\} \right]$$

*t* - dipping time

*r* - cylinder fiber radius

$\alpha$  - exhaustion coefficient

*D* - diffusion coefficient

$C_t$  - reagents concentration on textile fabrics at time *t*

$C_\infty$  - the maximum concentration of reagents on cotton fabrics

The equation can be simplified as below:

$$\frac{C_t}{C_\infty} = \frac{1+\alpha}{1+\frac{\alpha}{4}} [1 - \exp\{4x^2\} \operatorname{erfc}\{2x\}]$$

$$x = \left(\frac{1}{\alpha} + 0.25\right) \left(\frac{Dt}{r^2}\right)^{1/2}$$

Then Kilby further expanded the function equation (Kilby, 1960):

$$\exp = 1 + x + \frac{x^2}{2} + \dots$$

$$\operatorname{erfc} = 1 - \left\{ \frac{2}{\pi^{1/2}} \right\} \left\{ x - \frac{x^3}{3} + \dots \right\}$$

When the value of  $Dt/r^2$  tends to be 0 (time  $t \rightarrow 0$ ), the above equation can be defined as below to obtain the diffusion model for fabric fibers over a short period of time.

$$\frac{C_t}{C_\infty} = \frac{4(1+\alpha)x}{(1+\frac{\alpha}{4})\pi^{1/2}} = \frac{4(1+\alpha)}{(1+\frac{\alpha}{4})\pi^{1/2}} \left(\frac{1}{\alpha} + 0.25\right) \left(\frac{Dt}{r^2}\right)^{1/2} = A \left(\frac{D}{r^2}\right)^{1/2} t^{1/2}$$

$$\text{Where: } A = \frac{4(1+\alpha)}{(1+\frac{\alpha}{4})\pi^{1/2}} \left(\frac{1}{\alpha} + 0.25\right)$$

From the above derivation, it can be simply concluded that the diffusion state between reagents and textile fibers are only related to diffusion coefficient  $D/r^2$  besides factor of time  $t$ .

## 3.2 Absorption behavior analysis of cotton fabrics

### 3.2.1 Absorption of DOPO-HQ

DOPO-HQ powder was dissolved in ethanol with DOPO-HQ with different concentration (0.5 wt%, 1 wt%, 1.5 wt%), the cotton tissue was immersed in corresponding water bath at different temperature (30 °C, 60 °C, 90 °C). Every 10 minutes 1 mL sample was taken out from the bath, and 1mL distilled water was added at same time. The sample solution was diluted to a suitable concentration and its associated UV-vis spectrum was measured. The actual sample concentration was then calculated from the absorbance at the maximum absorption wavelength ( $\lambda_{max}$ ) based on calibration curve prepared previously.

The calibration curve of DOPO-HQ was  $y = 0.18545x$  (ppm)+ 0.06523 (Figure 3.1). According to this equation, the relevant concentration of samples could be calculated.

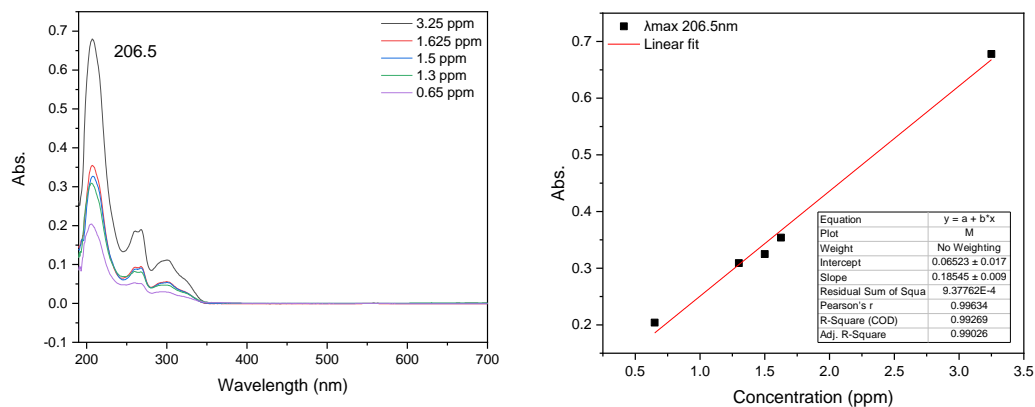


**Figure 3.1** Calibration curve for UV-vis spectrophotometric determination of DOPO-HQ in aqueous solution ( $\lambda_{max} = 206.5$  nm)

After the above measurements, relevant parameters  $C_t$  (DOPO-HQ concentration on textile fabrics at time  $t$ ), constant  $t^{1/2}$  and  $C_t/C_\infty$  were calculated and listed in the following tables.

**30 °C****Table 3.1** The relevant data of 0.5 wt% DOPO-HQ (30 °C)

Sample	t/min	C <sub>t</sub> /ppm	C <sub>t</sub> /C <sub>∞</sub>	t <sup>1/2</sup>
1	0	0.00	0.00	0.00
2	10	4793.29	1.00	3.16
3	20	4793.29	1.00	4.47
4	30	3293.69	0.69	5.48
5	40	961.53	0.20	6.33
6	50	704.85	0.15	7.07
7	60	1350.85	0.28	7.75
8	70	1574.09	0.33	8.37
9	80	2509.11	0.52	8.94
10	90	2046.46	0.43	9.49
11	100	1868.51	0.39	10.00
12	110	2364.60	0.49	10.49
13	120	1512.62	0.32	10.95

**Table 3.2** The relevant data of 1 wt% DOPO-HQ (30 °C)

Sample	t/min	$C_t$ /ppm	$C_t/C_\infty$	$t^{1/2}$
1	0	0.00	0.00	0.00
2	10	9232.49	0.92	3.16
3	20	6486.74	0.65	4.47
4	30	4004.13	0.40	5.48
5	40	3896.28	0.39	6.33
6	50	1433.08	0.14	7.07
7	60	5138.66	0.51	7.75
8	70	5013.56	0.50	8.37
9	80	3963.15	0.40	8.94
10	90	2709.98	0.27	9.49
11	100	4946.70	0.50	10.00
12	110	10000.00	1.00	10.49

**Table 3.3** The relevant data of 1.5 wt% DOPO-HQ (30 °C)

Sample	t/min	$C_t$ /ppm	$C_t/C_\infty$	$t^{1/2}$
1	0	0.00	0.00	0.00
2	10	6338.18	0.63	3.16
3	20	7850.18	0.78	4.47
4	30	8583.53	0.85	5.48
5	40	0.00	0.00	6.33
6	50	4750.69	0.47	7.07
7	60	7753.12	0.77	7.75
8	70	8712.94	0.86	8.37
9	80	8943.73	0.88	8.94
10	90	8999.81	0.89	9.49
11	100	8870.40	0.88	10.00
12	110	9176.68	0.91	10.49
13	120	8270.78	0.82	10.95



According to the calculated data above, the corresponding  $C_t/C_\infty$  with  $t^{1/2}$  curves of DOPO-HQ in different concentration were achieved as Figure 3.2.

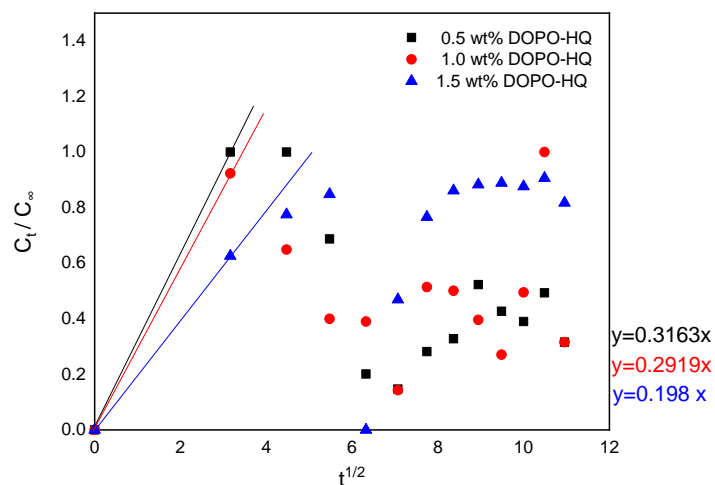


**Figure 3.2** Evolution of DOPO-HQ in different concentration with  $t^{1/2}$  at 30 °C

At the temperature of 30 °C, it was clear that the cotton tissues reached the maximum absorption in a very short time with lower concentration of DOPO-HQ (0.5 wt%, 1 wt%). As the dipping time increased, all cotton tissues at different concentration (0.5 wt%, 1 wt%, 1.5 wt%) exhibited the progressive absorption of DOPO-HQ at first, which was gradually decreased and then increased again until the equilibrium was achieved.

**60 °C****Table 3.4** The relevant data of 0.5 wt% DOPO-HQ (60 °C)

Sample	t/min	$C_t$ /ppm	$C_t/C_\infty$	$t^{1/2}$
1	0	0.00	0.00	0.00
2	10	4999.05	1.00	3.16
3	20	4998.54	1.00	4.47
4	30	4998.34	0.69	5.48
5	40	4999.07	0.20	6.33
6	50	4999.07	0.15	7.07
7	60	4998.57	0.28	7.75
8	70	4999.56	0.33	8.37
9	80	4998.42	0.52	8.94
10	90	4998.63	0.43	9.49
11	100	4998.89	0.39	10.00
12	110	4996.84	0.49	10.49
13	120	4998.08	0.32	10.95

**Table 3.5** The relevant data of 1 wt% DOPO-HQ (60 °C)

Sample	t/min	$C_t$ /ppm	$C_t/C_\infty$	$t^{1/2}$
1	0	0.00	0.00	0.00
2	10	9997.80	1.00	3.16
3	20	9998.36	1.00	4.47
4	30	9998.32	1.00	5.48
5	40	9997.31	1.00	6.33
6	50	9997.71	1.00	7.07
7	60	9996.65	1.00	7.75
8	70	9998.17	1.00	8.37
9	80	9997.33	1.00	8.94
10	90	9997.06	1.00	9.49
11	100	9997.49	1.00	10.00
12	110	9998.63	1.00	10.49

**Table 3.6** The relevant data of 1.5 wt% DOPO-HQ (60 °C)

Sample	t/min	$C_t$ /ppm	$C_t/C_\infty$	$t^{1/2}$
1	0	0.00	0.00	0.00
2	10	8907.07	0.76	3.16
3	20	5606.98	0.48	4.47
4	30	3598.90	0.31	5.48
5	40	8734.51	0.74	6.33
6	50	9823.75	0.84	7.07
7	60	8909.22	0.76	7.75
8	70	5164.82	0.44	8.37
9	80	4886.57	0.42	8.94
10	90	11739.10	1.00	9.49
11	100	11161.04	0.95	10.00
12	110	11441.44	0.98	10.49
13	120	10664.95	0.91	10.95

According to the calculated data above, the corresponding  $C_t/C_\infty$  with  $t^{1/2}$  curves of DOPO-HQ in different concentration were achieved as Figure 3.3.

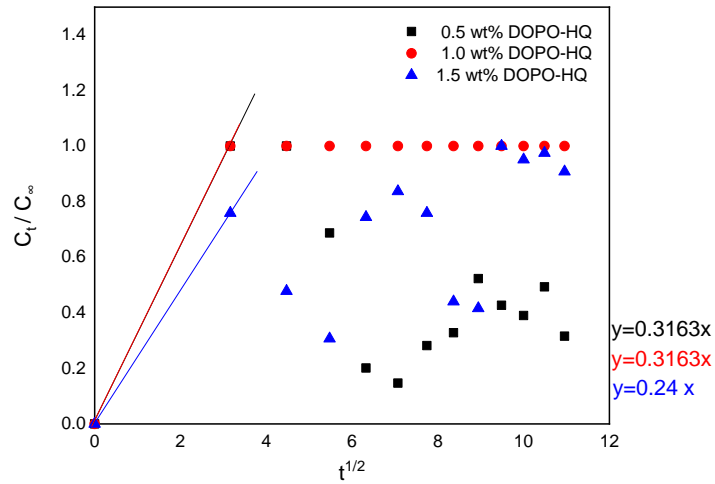


**Figure 3.3** Evolution of DOPO-HQ in different concentration with  $t^{1/2}$  at 60 °C

At the temperature of 60 °C, the cotton tissue immersed in 0.5 wt% DOPO-HQ water bath achieved the maximum absorption and maintained the equilibrium for a shorter time than under 30 °C, which demonstrated that the elevated temperatures within a certain range contributed to the uptake of DOPO-HQ by cotton fabric. In contrast, the absorption behavior of cotton fabrics in higher concentration (1 wt% and 1.5 wt%) DOPO-HQ water bath still followed the repeated process of uptake and release.

**90 °C****Table 3.7** The relevant data of 0.5 wt% DOPO-HQ (90 °C)

Sample	t/min	C <sub>t</sub> /ppm	C <sub>t</sub> /C <sub>∞</sub>	t <sup>1/2</sup>
1	0	0.00	0.00	0.00
2	10	5000.00	1.00	3.16
3	20	1463.01	0.29	4.47
4	30	5000.00	1.00	5.48
5	40	837.50	0.17	6.33
6	50	5000.00	1.00	7.07
7	60	5000.00	1.00	7.75
8	70	410.44	0.08	8.37
9	80	2871.48	0.57	8.94
10	90	1935.37	0.39	9.49
11	100	1799.49	0.36	10.00
12	110	3626.40	0.73	10.49
13	120	3113.05	0.62	10.95

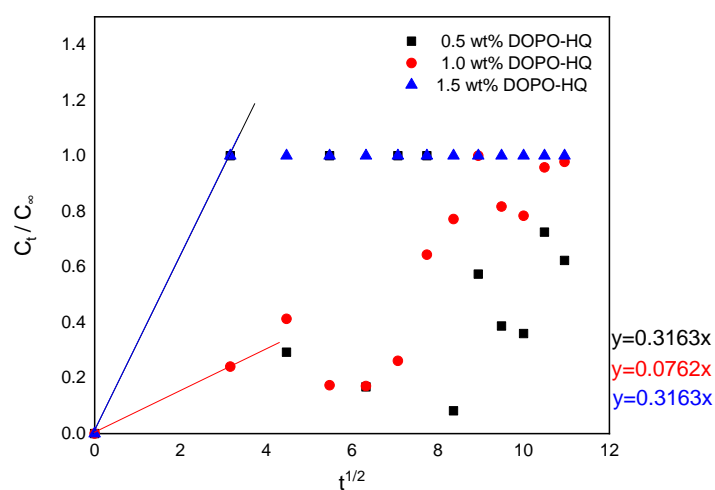
**Table 3.8** The relevant data of 1 wt% DOPO-HQ (90 °C)

Sample	t/min	C <sub>t</sub> /ppm	C <sub>t</sub> /C <sub>∞</sub>	t <sup>1/2</sup>
1	0	0.00	0.00	0.00
2	10	2310.95	0.24	3.16
3	20	3960.99	0.41	4.47
4	30	1666.03	0.17	5.48
5	40	1635.83	0.17	6.33
6	50	2511.54	0.26	7.07
7	60	6180.45	0.64	7.75
8	70	7403.43	0.77	8.37
9	80	9592.70	1.00	8.94
10	90	7841.28	0.82	9.49
11	100	7524.21	0.78	10.00
12	110	9185.04	0.96	10.49
13	120	9381.32	0.98	10.95

**Table 3.9** The relevant data of 1.5 wt% DOPO-HQ (90 °C)

Sample	t/min	$C_t$ /ppm	$C_t/C_\infty$	$t^{1/2}$
1	0	0.00	0.00	0.00
2	10	14994.31	1.00	3.16
3	20	14997.93	1.00	4.47
4	30	14997.18	1.00	5.48
5	40	14998.57	1.00	6.33
6	50	14999.80	1.00	7.07
7	60	14999.81	1.00	7.75
8	70	14999.69	1.00	8.37
9	80	15000.00	1.00	8.94
10	90	15000.00	1.00	9.49
11	100	15000.00	1.00	10.00
12	110	15000.00	1.00	10.49
13	120	15000.00	1.00	10.95

According to the calculated data above, the corresponding  $C_t/C_\infty$  with  $t^{1/2}$  curves of DOPO-HQ in different concentration were achieved as Figure 3.4.

**Figure 3.4** Evolution of DOPO-HQ in different concentration with  $t^{1/2}$  at 90 °C

At the temperature of 90 °C, the diffusion of DOPO-HQ at the interface between water bath (0.5 wt% and 1 wt%) and cotton substrate was more intense and uncontrolled. Furthermore, it was obvious that higher temperature (90 °C) was more advantageous for the absorption of DOPO-HQ in higher concentration by cotton tissues.

### 3.2.2 Absorption of UIO-66-COOH

After preparing different concentration of 0.5 wt%, 1 wt%, 1.5 wt% UIO-66-COOH samples, the cotton tissue was immersed in corresponding water bath at different temperature (30 °C, 60 °C, 90 °C). Every 10 minutes 1 mL sample was taken out from the bath, and 1 mL distilled water was added at same time. The sample solution was diluted to a suitable concentration and its associated UV-vis spectrum was measured. The actual sample concentration was then calculated from the absorbance at the maximum absorption wavelength ( $\lambda_{\max}$ ) based on calibration curve prepared previously.

The calibration curve of UIO-66-COOH was  $y = 0.0052x$  (ppm)+ 0.02108 (Figure 3.5). According to this equation, the relevant concentration of samples could be calculated.

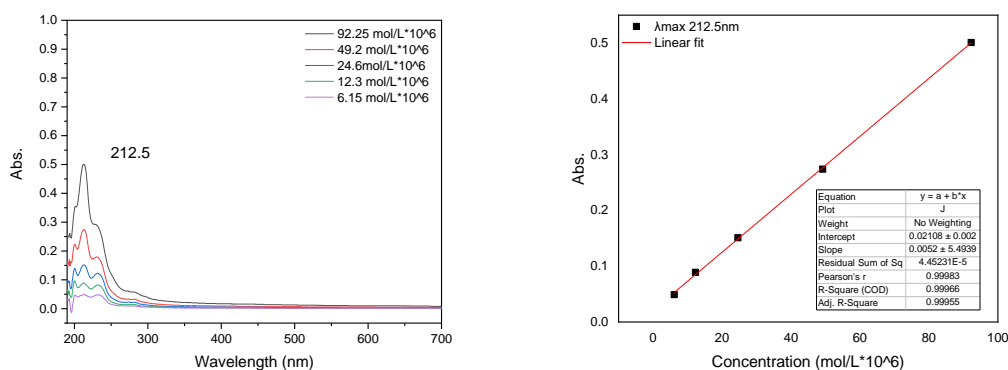


**Figure 3.5** Calibration curve for UV-vis spectrophotometric determination of UIO-66-COOH in aqueous solution ( $\lambda_{\max} = 212.5$  nm)

After the above measurements, relevant parameters  $C_t$  (UIO-66-COOH concentration on textile fabrics at time  $t$ ), constant  $t^{1/2}$  and  $C_t/C_\infty$  were calculated and listed in the following tables.



**30 °C****Table 3.10** The relevant data of 0.5 wt% UIO-66-COOH (30 °C)

Sample	t/min	C <sub>t</sub> /ppm	C <sub>t</sub> /C <sub>∞</sub>	t <sup>1/2</sup>
1	0	0.00	0.00	0.00
2	10	14994.31	1.00	3.16
3	20	14997.93	1.00	4.47
4	30	14997.18	1.00	5.48
5	40	14998.57	1.00	6.33
6	50	14999.80	1.00	7.07
7	60	14999.81	1.00	7.75
8	70	14999.69	1.00	8.37
9	80	15000.00	1.00	8.94
10	90	15000.00	1.00	9.49
11	100	15000.00	1.00	10.00
12	110	15000.00	1.00	10.49
13	120	15000.00	1.00	10.95

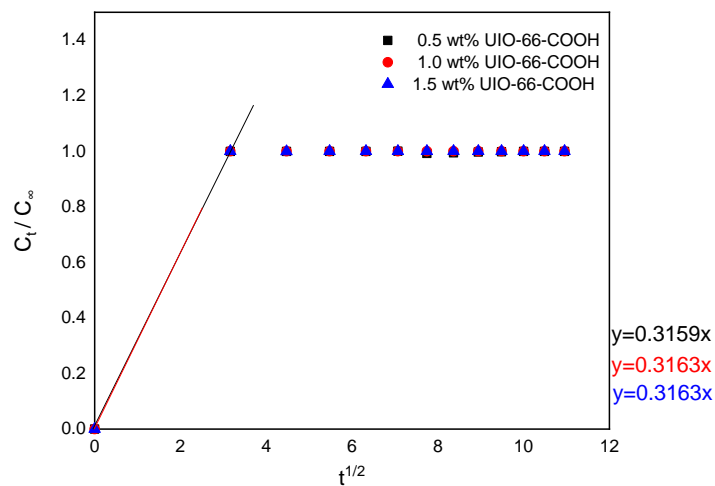
**Table 3.11** The relevant data of 1 wt% UIO-66-COOH (30 °C)

Sample	t/min	C <sub>t</sub> /ppm	C <sub>t</sub> /C <sub>∞</sub>	t <sup>1/2</sup>
1	0	0.00	0.00	0.00
2	10	10000.00	1.00	3.16
3	20	9998.29	1.00	4.47
4	30	10000.00	1.00	5.48
5	40	10000.00	1.00	6.33
6	50	9997.71	1.00	7.07
7	60	10000.00	1.00	7.75
8	70	10000.00	1.00	8.37
9	80	10000.00	1.00	8.94
10	90	10000.00	1.00	9.49
11	100	10000.00	1.00	10.00
12	110	10000.00	1.00	10.49
13	120	10000.00	1.00	10.95

**Table 3.12** The relevant data of 1.5 wt% UIO-66-COOH (30 °C)

Sample	t/min	$C_t$ /ppm	$C_t/C_\infty$	$t^{1/2}$
1	0	0.00	0.00	0.00
2	10	14992.71	1.00	3.16
3	20	14978.48	1.00	4.47
4	30	14997.71	1.00	5.48
5	40	15000.00	1.00	6.33
6	50	14999.82	1.00	7.07
7	60	15000.00	1.00	7.75
8	70	15000.00	1.00	8.37
9	80	14998.29	1.00	8.94
10	90	14997.32	1.00	9.49
11	100	15000.98	1.00	10.00
12	110	15000.00	1.00	10.49
13	120	14998.86	1.00	10.95

According to the calculated data above, the corresponding  $C_t/C_\infty$  with  $t^{1/2}$  curves of UIO-66-COOH in different concentration were achieved as Figure 3.6.

**Figure 3.6** Evolution of UIO-66-COOH in different concentration with  $t^{1/2}$  at 30 °C

At the temperature of 30 °C, it was evident that it only took very short time for cotton tissues to reach the maximum absorption of UIO-66-COOH (0.5 wt%, 1 wt%, 1.5 wt%) and maintain the equilibrium.

### 60 °C

**Table 3.13** The relevant data of 0.5 wt% UIO-66-COOH (60 °C)

Sample	t/min	C <sub>t</sub> /ppm	C <sub>t</sub> /C <sub>∞</sub>	t <sup>1/2</sup>
1	0	0.00	0.00	0.00
2	10	5000.00	1.00	3.16
3	20	5000.00	1.00	4.47
4	30	5000.00	1.00	5.48
5	40	4968.29	0.99	6.33
6	50	5000.00	1.00	7.07
7	60	5000.00	1.00	7.75
8	70	5000.00	1.00	8.37
9	80	5000.00	1.00	8.94
10	90	5000.00	1.00	9.49
11	100	5000.00	1.00	10.00
12	110	5000.00	1.00	10.49
13	120	5000.00	1.00	10.95

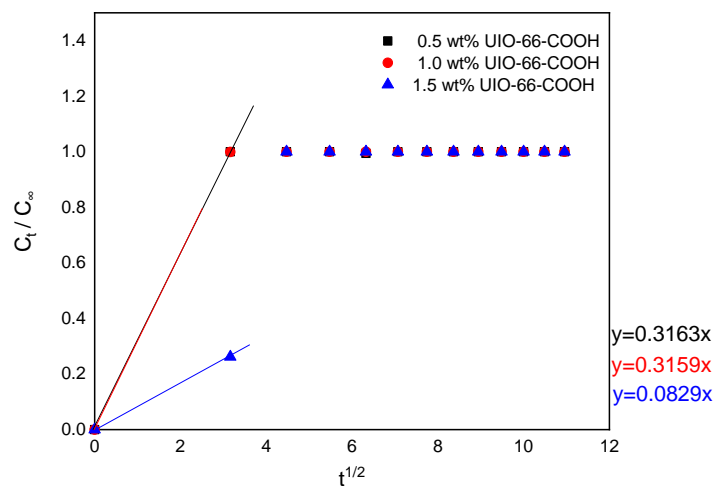
**Table 3.14** The relevant data of 1 wt% UIO-66-COOH (60 °C)

Sample	t/min	C <sub>t</sub> /ppm	C <sub>t</sub> /C <sub>∞</sub>	t <sup>1/2</sup>
1	0	0.00	0.00	0.00
2	10	9989.05	1.00	3.16
3	20	10000.00	1.00	4.47
4	30	10000.00	1.00	5.48
5	40	10000.00	1.00	6.33
6	50	10000.00	1.00	7.07
7	60	10000.00	1.00	7.75
8	70	10000.00	1.00	8.37
9	80	9998.48	1.00	8.94
10	90	10000.00	1.00	9.49
11	100	10000.00	1.00	10.00
12	110	10000.00	1.00	10.49
13	120	10000.00	1.00	10.95

**Table 3.15** The relevant data of 1.5 wt% UIO-66-COOH (60 °C)

Sample	t/min	$C_t$ /ppm	$C_t/C_\infty$	$t^{1/2}$
1	0	0.00	0.00	0.00
2	10	3927.13	0.26	3.16
3	20	15000.00	1.00	4.47
4	30	15000.00	1.00	5.48
5	40	15000.00	1.00	6.33
6	50	15000.00	1.00	7.07
7	60	15000.00	1.00	7.75
8	70	15000.00	1.00	8.37
9	80	15000.00	1.00	8.94
10	90	15000.00	1.00	9.49
11	100	15000.00	1.00	10.00
12	110	15000.00	1.00	10.49
13	120	15000.00	1.00	10.95

According to the calculated data above, the corresponding  $C_t/C_\infty$  with  $t^{1/2}$  curves of UIO-66-COOH in different concentration were achieved as Figure 3.7.

**Figure 3.7** Evolution of UIO-66-COOH in different concentration with  $t^{1/2}$  at 60 °C

At the temperature of 60 °C, the absorption behavior of cotton tissues immersed in 0.5 wt% and 1 wt% UIO-66-COOH water bath remained consistent. And it took slightly longer for cotton tissue to reach the maximum absorption in higher concentration (1.5 wt%) water bath. However, raising the temperature from 30 °C to 60 °C didn't seem to have a major effect on cotton fabrics in terms of achieving maximum absorption in a shorter period of time.

### 90 °C

**Table 3.16** The relevant data of 0.5 wt% UIO-66-COOH (90 °C)

Sample	t/min	$C_t$ /ppm	$C_t/C_\infty$	$t^{1/2}$
1	0	0.00	0.00	0.00
2	10	3273.29	1.00	3.16
3	20	0.00	0.00	4.47
4	30	0.00	0.00	5.48
5	40	0.00	0.00	6.33
6	50	580.98	0.18	7.07
7	60	196.36	0.06	7.75
8	70	0.00	0.00	8.37
9	80	0.00	0.00	8.94
10	90	0.00	0.00	9.49
11	100	0.00	0.00	10.00
12	110	0.00	0.00	10.49
13	120	0.00	0.00	10.95

**Table 3.17** The relevant data of 1 wt% UIO-66-COOH (90 °C)

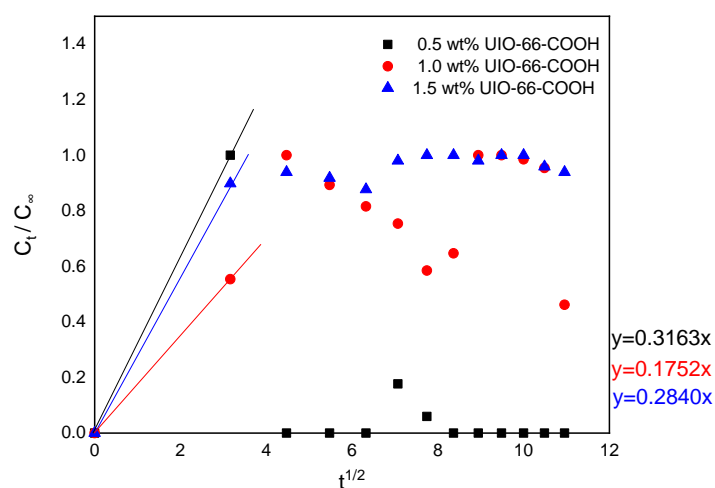
Sample	t/min	C <sub>t</sub> /ppm	C <sub>t</sub> /C <sub>∞</sub>	t <sup>1/2</sup>
1	0	0.00	0.00	0.00
2	10	5542.52	0.55	3.16
3	20	10000.00	1.00	4.47
4	30	8927.13	0.89	5.48
5	40	8157.90	0.82	6.33
6	50	7542.52	0.75	7.07
7	60	5850.21	0.59	7.75
8	70	6465.59	0.65	8.37
9	80	10000.00	1.00	8.94
10	90	10000.00	1.00	9.49
11	100	9850.21	0.99	10.00
12	110	9542.52	0.95	10.49
13	120	4619.44	0.46	10.95



**Table 3.18** The relevant data of 1.5 wt% UIO-66-COOH (90 °C)

Sample	t/min	$C_t$ /ppm	$C_t/C_\infty$	$t^{1/2}$
1	0	0.00	0.00	0.00
2	10	13465.59	0.90	3.16
3	20	14080.98	0.94	4.47
4	30	13773.29	0.92	5.48
5	40	13157.90	0.88	6.33
6	50	14696.36	0.98	7.07
7	60	15000.00	1.00	7.75
8	70	15000.00	1.00	8.37
9	80	14696.36	0.98	8.94
10	90	15000.00	1.00	9.49
11	100	15000.00	1.00	10.00
12	110	14388.67	0.96	10.49
13	120	14080.98	0.94	10.95

According to the calculated data above, the corresponding  $C_t/C_\infty$  with  $t^{1/2}$  curves of UIO-66-COOH in different concentration were achieved as Figure 3.8.

**Figure 3.8** Evolution of UIO-66-COOH in different concentration with  $t^{1/2}$  at 90 °C

At the temperature of 90 °C, the diffusion of UIO-66-COOH at the interface between water bath (0.5 wt% and 1 wt%) and cotton tissue was more intense and uncontrolled. But still all cotton tissues were able to reach the maximum absorption in a short time.

### 3.2.3 Absorption of DOPO-HQ@UIO-66-COOH

After preparing different concentration of 0.5 wt%, 1 wt%, 1.5 wt% UIO-66- DOPO-HQ@UIO-66-COOH samples, the cotton tissue was immersed in corresponding water bath at different temperature (30 °C, 60 °C, 90 °C). Every 10 minutes 1 mL sample was taken out from the bath, and 1 mL distilled water was added at same time. The sample solution was diluted to a suitable concentration and its associated UV-vis spectrum was measured. The actual sample concentration was then calculated from the absorbance at the maximum absorption wavelength ( $\lambda_{max}$ ) based on calibration curve prepared previously.

The calibration curve of DOPO-HQ@UIO-66-COOH was  $y = 0.11209x$  (ppm)+ 0.14957 (Figure 3.9). According to this equation, the relevant concentration of samples could be calculated.

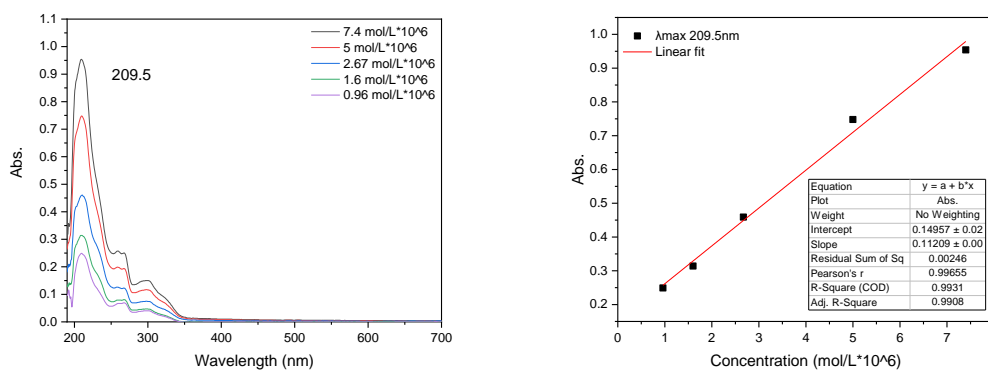


**Figure 3.9** Calibration curve for UV-vis spectrophotometric determination of DOPO-HQ@UIO-66-COOH in aqueous solution ( $\lambda_{max} = 209.5$  nm)

After the above measurements, relevant parameters  $C_t$  (DOPO-HQ@UIO-66-COOH concentration on textile fabrics at time  $t$ ), constant  $t^{1/2}$  and  $C_t/C_\infty$  were calculated and listed in the following tables.

**30 °C****Table 3.19** The relevant data of 0.5 wt% DOPO-HQ@UIO-66-COOH (30 °C)

Sample	t/min	C <sub>t</sub> /ppm	C <sub>t</sub> /C <sub>∞</sub>	t <sup>1/2</sup>
1	0	0.00	0.00	0.00
2	10	4901.42	0.98	3.16
3	20	4951.38	0.99	4.47
4	30	4851.46	0.97	5.48
5	40	4951.38	0.99	6.33
6	50	4972.79	1.00	7.07
7	60	4937.10	0.99	7.75
8	70	4951.38	0.99	8.37
9	80	4958.51	1.00	8.94
10	90	4965.65	1.00	9.49
11	100	4944.24	0.99	10.00
12	110	4979.92	1.00	10.49
13	120	4944.24	0.99	10.95

**Table 3.20** The relevant data of 1 wt% DOPO-HQ@UIO-66-COOH (30 °C)

Sample	t/min	C <sub>t</sub> /ppm	C <sub>t</sub> /C <sub>∞</sub>	t <sup>1/2</sup>
1	0	0.00	0.00	0.00
2	10	9637.34	0.99	3.16
3	20	9508.87	0.98	4.47
4	30	9644.48	0.99	5.48
5	40	9694.44	1.00	6.33
6	50	9416.09	0.97	7.07
7	60	9673.03	1.00	7.75
8	70	9516.01	0.98	8.37
9	80	9587.38	0.99	8.94
10	90	9701.58	1.00	9.49
11	100	9530.28	0.98	10.00
12	110	9601.66	0.99	10.49
13	120	9615.93	0.99	10.95

**Table 3.21** The relevant data of 1.5 wt% DOPO-HQ@UIO-66-COOH (30 °C)

Sample	t/min	$C_t$ /ppm	$C_t/C_\infty$	$t^{1/2}$
1	0	0.00	0.00	0.00
2	10	14630.20	0.99	3.16
3	20	14740.83	1.00	4.47
4	30	14662.32	0.99	5.48
5	40	14726.56	1.00	6.33
6	50	14658.75	0.99	7.07
7	60	14790.79	1.00	7.75
8	70	14658.75	0.99	8.37
9	80	14637.34	0.99	8.94
10	90	14619.50	0.99	9.49
11	100	14705.14	0.99	10.00
12	110	14722.99	1.00	10.49
13	120	14637.34	0.99	10.95

According to the calculated data above, the corresponding  $C_t/C_\infty$  with  $t^{1/2}$  curves of DOPO-HQ@UIO-66-COOH in different concentration were achieved as Figure 3.10.

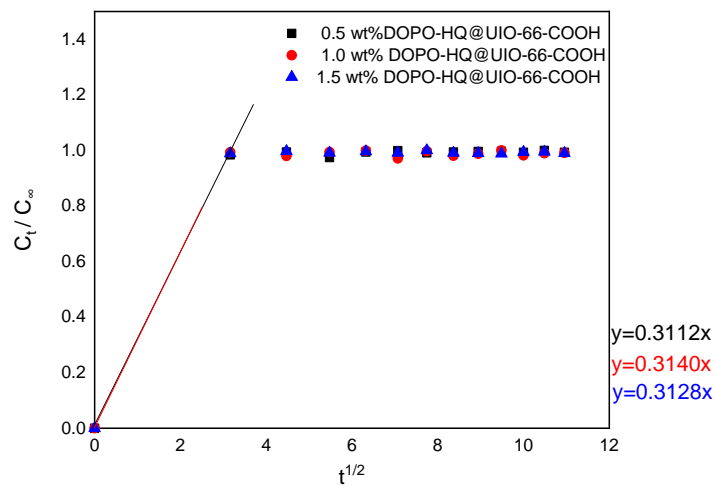


**Figure 3.10** Evolution of DOPO-HQ@UIO-66-COOH in different concentration with  $t^{1/2}$  at 30 °C

At the temperature of 30 °C, it was clear that it only took very short time for cotton tissues to reach the maximum absorption of DOPO-HQ@UIO-66-COOH (0.5 wt%, 1 wt%, 1.5 wt%) and maintain the equilibrium, and their absorption behavior were in line with that for UIO-66-COOH.

### 60 °C

**Table 3.22** The relevant data of 0.5 wt% DOPO-HQ@UIO-66-COOH (60 °C)

Sample	t/min	$C_t$ /ppm	$C_t/C_\infty$	$t^{1/2}$
1	0	0.00	0.00	0.00
2	10	4715.85	0.98	3.16
3	20	4680.16	0.98	4.47
4	30	4751.54	0.99	5.48
5	40	4737.26	0.99	6.33
6	50	4794.36	1.00	7.07
7	60	4758.67	0.99	7.75
8	70	4772.95	0.99	8.37
9	80	4801.50	1.00	8.94
10	90	4801.50	1.00	9.49
11	100	4772.95	0.99	10.00
12	110	4751.54	0.99	10.49
13	120	4765.81	0.99	10.95

**Table 3.23** The relevant data of 1 wt% DOPO-HQ@UIO-66-COOH (60 °C)

Sample	t/min	C <sub>t</sub> /ppm	C <sub>t</sub> /C <sub>∞</sub>	t <sup>1/2</sup>
1	0	0.00	0.00	0.00
2	10	9573.11	0.98	3.16
3	20	9523.15	0.98	4.47
4	30	9612.36	0.99	5.48
5	40	9655.18	0.99	6.33
6	50	9598.09	0.99	7.07
7	60	9626.64	0.99	7.75
8	70	9730.12	1.00	8.37
9	80	9630.20	0.99	8.94
10	90	9722.99	1.00	9.49
11	100	9744.40	1.00	10.00
12	110	9708.71	1.00	10.49
13	120	9540.99	0.98	10.95

**Table 3.24** The relevant data of 1.5 wt% DOPO-HQ@UIO-66-COOH (60 °C)

Sample	t/min	$C_t$ /ppm	$C_t/C_\infty$	$t^{1/2}$
1	0	0.00	0.00	0.00
2	10	14166.29	0.98	3.16
3	20	14358.99	0.99	4.47
4	30	14144.88	0.98	5.48
5	40	14237.66	0.98	6.33
6	50	14351.86	0.99	7.07
7	60	14348.29	0.99	7.75
8	70	14362.56	0.99	8.37
9	80	14419.66	1.00	8.94
10	90	14469.62	1.00	9.49
11	100	14344.72	0.99	10.00
12	110	14369.70	0.99	10.49
13	120	14334.01	0.99	10.95

According to the calculated data above, the corresponding  $C_t/C_\infty$  with  $t^{1/2}$  curves of DOPO-HQ@UIO-66-COOH in different concentration were achieved as Figure 3.11.

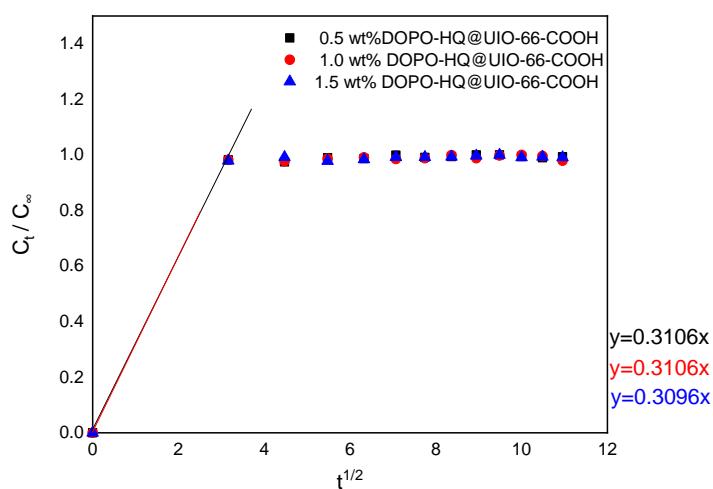


**Figure 3.11** Evolution of DOPO-HQ@UIO-66-COOH in different concentration with  $t^{1/2}$  at 60 °C



At the temperature of 60 °C, DOPO-HQ@UIO-66-COOH composites were absorbed by the cotton tissues very quickly and remained same as previously discussed.

### 90 °C

**Table 3.25** The relevant data of 0.5 wt% DOPO-HQ@UIO-66-COOH (90 °C)

Sample	t/min	C <sub>t</sub> /ppm	C <sub>t</sub> /C <sub>∞</sub>	t <sup>1/2</sup>
1	0	0.00	0.00	0.00
2	10	4430.37	0.92	3.16
3	20	4387.54	0.91	4.47
4	30	4565.97	0.95	5.48
5	40	4694.44	0.98	6.33
6	50	4658.75	0.97	7.07
7	60	4751.54	0.99	7.75
8	70	4751.54	0.99	8.37
9	80	4615.93	0.96	8.94
10	90	4694.44	0.98	9.49
11	100	4758.67	0.99	10.00
12	110	4801.50	1.00	10.49
13	120	4730.12	0.99	10.95

**Table 3.26** The relevant data of 1 wt% DOPO-HQ@UIO-66-COOH (90 °C)

Sample	t/min	C <sub>t</sub> /ppm	C <sub>t</sub> /C <sub>∞</sub>	t <sup>1/2</sup>
1	0	0.00	0.00	0.00
2	10	8984.29	0.91	3.16
3	20	9483.89	0.96	4.47
4	30	9391.11	0.95	5.48
5	40	9733.69	0.98	6.33
6	50	9826.47	0.99	7.07
7	60	9826.47	0.99	7.75
8	70	9808.63	0.99	8.37
9	80	9901.41	1.00	8.94
10	90	9822.91	0.99	9.49
11	100	9797.93	0.99	10.00
12	110	9601.66	0.97	10.49
13	120	9812.20	0.99	10.95

**Table 3.27** The relevant data of 1.5 wt% DOPO-HQ@UIO-66-COOH (90 °C)

Sample	t/min	$C_t$ /ppm	$C_t/C_\infty$	$t^{1/2}$
1	0	0.00	0.00	0.00
2	10	8984.29	0.91	3.16
3	20	9483.89	0.96	4.47
4	30	9391.11	0.95	5.48
5	40	9733.69	0.98	6.33
6	50	9826.47	0.99	7.07
7	60	9826.47	0.99	7.75
8	70	9808.63	0.99	8.37
9	80	9901.41	1.00	8.94
10	90	9822.91	0.99	9.49
11	100	9797.93	0.99	10.00
12	110	9601.66	0.97	10.49
13	120	9812.20	0.99	10.95

According to the calculated data above, the corresponding  $C_t/C_\infty$  with  $t^{1/2}$  curves of DOPO-HQ@UIO-66-COOH in different concentration were achieved as Figure 3.12.

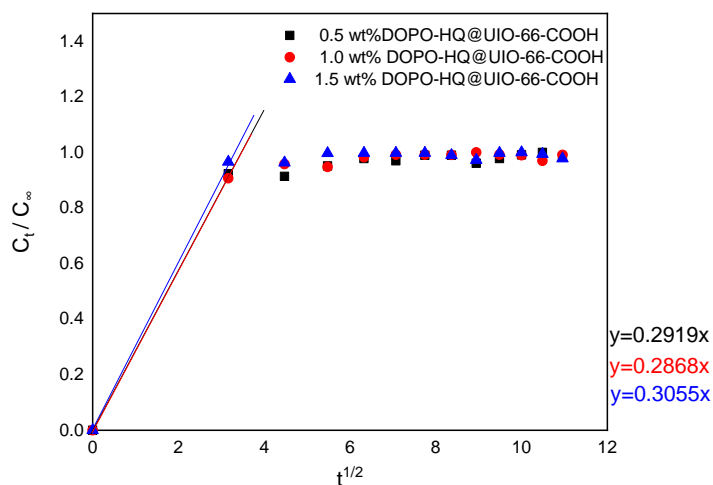


**Figure 3.12** Evolution of DOPO-HQ@UIO-66-COOH in different concentration with  $t^{1/2}$  at 90 °C

With reference to the previous discussion, it was easy to see that the absorption behavior of cotton tissues to DOPO-HQ@UIO-66-COOH at the temperature of 90 °C was similar to that at 30 °C and 60 °C.

### 3.3 Summary

From the evolution study above, it was possible to draw the conclusion that the temperature of water bath didn't cause a substantial effect on the absorption behaviour of cotton tissue to DOPO-HQ@UIO-66-COOH composites in certain concentrations. Also, it was observed that the absorption behavior of cotton tissue to DOPO-HQ@UIO-66-COOH at different temperatures was more similar with that to UIO-66-COOH. Moreover, the value of apparent diffusion coefficient ( $D/r^2$ ) would be presented for further analysis.

Based on the constant A and slope value of each figure displayed above, the corresponding value of  $D/r^2$  could be calculated by KILBY mathematical model for DOPO-HQ, UIO-66-COOH, and DOPO-HQ@UIO-66-COOH, which were respectively summarized in Table 3.28, Table 3.29 and Table 3.30.

**Table 3.28** The relevant data of DOPO-HQ by KILBY mathematical model

Temperature	Sample	A	$D/r^2$
30 °C	0.5 wt% DOPO-HQ	8.73	1.31E-03
	1.0 wt% DOPO-HQ	1.00	8.52E-02
	1.5 wt% DOPO-HQ	11.98	2.73E-04
60 °C	0.5 wt% DOPO-HQ	10428.50	9.20E-10
	1.0 wt% DOPO-HQ	68202.18	2.15E-11
	1.5 wt% DOPO-HQ	16.96	2.00E-04
90 °C	0.5 wt% DOPO-HQ	13.69	5.34E-04
	1.0 wt% DOPO-HQ	67.86	1.26E-06
	1.5 wt% DOPO-HQ	1.00	1.00E-01

**Table 3.29** The relevant data of UIO-66-COOH by KILBY mathematical model

Temperature	Sample	A	D/r <sup>2</sup>
30 °C	0.5 wt% UIO-66-COOH	6149.80	2.64E-09
	1.0 wt% UIO-66-COOH	1.00	1.00E-01
	1.5 wt% UIO-66-COOH	52705.93	3.60E-11
60 °C	0.5 wt% UIO-66-COOH	1.00	1.00E-01
	1.0 wt% UIO-66-COOH	1.00	9.98E-02
	1.5 wt% UIO-66-COOH	1.00	6.87E-03
90 °C	0.5 wt% UIO-66-COOH	6.93	2.08E-03
	1.0 wt% UIO-66-COOH	10.47	2.80E-04
	1.5 wt% UIO-66-COOH	68.49	1.72E-05

**Table 3.30** The relevant data of DOPO-HQ@UIO-66-COOH by KILBY mathematical model

Temperature	Sample	A	D/r <sup>2</sup>
30 °C	0.5 wt% DOPO-HQ@UIO-66-COOH	361.89	7.39E-07
	1.0 wt% DOPO-HQ@UIO-66-COOH	107.36	8.55E-06
	1.5 wt% DOPO-HQ@UIO-66-COOH	168.66	3.44E-06
60 °C	0.5 wt% DOPO-HQ@UIO-66-COOH	88.61	1.23E-05
	1.0 wt% DOPO-HQ@UIO-66-COOH	90.35	1.18E-05
	1.5 wt% DOPO-HQ@UIO-66-COOH	93.30	1.10E-05
90 °C	0.5 wt% DOPO-HQ@UIO-66-COOH	77.31	1.43E-05
	1.0 wt% DOPO-HQ@UIO-66-COOH	216.21	1.76E-06
	1.5 wt% DOPO-HQ@UIO-66-COOH	122.78	6.19E-06

From the adsorption behaviour of cotton fabrics to DOPO-HQ, the value of apparent diffusion coefficient ( $D/r^2$ ) first decreased and then raised slightly under the condition of the same initial concentration with the increasing temperature. This indicated that the adsorption rate of DOPO-HQ to cotton substrates increased as the temperature was elevated. Thus, the cotton fabric became more

hydrophobic with the introduction of higher amounts of DOPO-HQ. And then some DOPO-HQ were resolved from the cotton fabric and transported to the water bath due to the insufficient affinity. From the adsorption behaviour of cotton fabrics to UIO-66-COOH, it was found that in addition to the possible experimental error at 30 °C, as the initial reagent concentration increased, more amount of UIO-66-COOH were able to be absorbed into the cotton fabric with the same temperature conditions. Consequently, the values of  $D/r^2$  were reduced and tended to 0. Also, the good absorption of DOPO-HQ@UIO-66-COOH by cotton fabrics was demonstrated since all the  $D/r^2$  values were kept at a low level close to 0. Comparing all the results of above, it was shown that the behavioural pattern of DOPO-HQ@UIO-66-COOH was more consistent with that of UIO-66-COOH according to the values of apparent diffusion coefficient ( $D/r^2$ ). It may be inferred that the formation of DOPO-HQ@UIO-66-COOH composites with ultrasonic assistance was driven predominantly by UIO-66-COOH.

### 3.4 References

- Crank, J., 1980. *The Mathematics of Diffusion*, 2nd edition. ed. Oxford University Press, Oxford.
- Kilby, W.F., 1960. Relation of Apparent Diffusion Coefficient to the Time of Half-dyeing. *Journal of the Society of Dyers and Colourists* 76, 479–484. <https://doi.org/10.1111/j.1478-4408.1960.tb02390.x>
- Lis Arias, M.J. (Manuel J., 2002. *Comportamiento cinético de fibras Tencel con colorantes directos* (Ph.D. Thesis). TDX (Tesis Doctorals en Xarxa). Universitat Politècnica de Catalunya.

## **Chapter IV. Final conclusions and future perspectives**



## 4.1 Final conclusions

Due to the current demand for fire safety and environmental protection, the structural barriers based on combustion mechanism were developed and assembled onto cotton fabrics in this study. The important conclusions can be summarized as follows:

- Two types of metal-organic frameworks, Zr-based MOFs (UIO-66-COOH) and Zn-based MOFs (ZIF-8), were investigated and analyzed through a variety of testing results, which indicated that the use of UIO-66-COOH was more advantageous for developing barrier effects of cotton fabrics.
- The comparison of two synthetic approaches, layer-by-layer and hydrothermal synthesis, showed that the latter could provide more efficient introduction and production of UIO-66-COOH for the fire barriers assembled onto cotton fabrics. The organic–inorganic composites consisting of UIO-66-COOH, BPEI, and VTES were considered promising to produce barrier effects. In the vertical burning test, the flame-retardancy behavior and carbon-forming properties of sample UIO-66-COOH/BPEI/VTES were positively demonstrated. According to the photos of SEM, the produced carbonized residuals of sample UIO-66-COOH/BPEI/VTES partially retained the original cellulosic fiber structure after burning. During combustion, the maximum weight loss rate ( $R_{\max}$ ) of fabric sample was reduced from 37.6 wt%/min to 17.2 wt%/min and the temperature of the maximum rate of weight loss ( $T_{\max}$ ) was increased from 479 °C to 523.3 °C compared to the untreated cotton sample. At 800 °C, the pristine cotton burned out without residues whereas the residual char content of sample UIO-66-COOH/BPEI/VTES was up to 7.2355 wt%. For the treated cotton samples, the thermal degradation was strongly inhibited and the thermal stability at high temperatures was notably enhanced because of the synergistic effects of UIO-66-COOH, BPEI and VTES.
- DOPO-HQ was adequately incorporated into porous UIO-66-COOH support for applications onto cotton substrates. By UV-vis absorption spectroscopy, it was observed that the absorption behavior of cotton tissue to DOPO-

HQ@UIO-66-COOH at different temperatures was more similar with that to UIO-66-COOH. It may be inferred that the formation of DOPO-HQ@UIO-66-COOH composites with ultrasonic assistance was driven predominantly by UIO-66-COOH.

- After successfully applying the DOPO-HQ@UIO-66-COOH composites dispersion onto cotton fabrics, it helped to promote the formation of carbonaceous insulating layer and thus maintain the original morphology of cotton fabrics in the burning process. Compared to pristine cotton, the treated cotton sample exhibited superior thermal stability and smoke suppression properties from the results of vertical burning test and thermal analysis. Therefore, DOPO-HQ@UIO-66-COOH was anticipated to work as a potential flame-retardant for cotton textiles.
- The structural barriers composed of DOPO-HQ@UIO-66-COOH and TEOS presented broad prospects for fire protection. It could substantially reduce the redundancy of application process and achieve excellent synergistic barrier effects when DOPO-HQ@UIO-66-COOH was utilized in combination with TEOS for cotton substrates. At second stage of cotton degradation, the  $T_{max}$  of sample DOPO-HQ@UIO-66-COOH/TEOS was increased from 479 °C to 494.8 °C and the  $R_{max}$  was decreased from 93.4 wt%/min to 79.3 wt%/min. Meanwhile, the initial decomposition temperature ( $T_{10\%}$ ) was slightly enhanced from 318.5 °C to 321.6 °C, and the final char yield at 800 °C was proved a significant increase from -1.21 wt% to 6.7143 wt%.

## 4.2 Future perspectives

So far, the development of fire barrier properties for cotton fabrics has remained a challenging work. Additionally, the use of a facile and eco-friendly approach to replace complicated and time-consuming processes has greater potential for industrial applications such as food, pharmaceuticals, clothing, wood, and cosmetics. On basis of the obtained results in this thesis, there are several points that need further exploring and researching.

- The gravitational separation time of DOPO-HQ@UIO-66-COOH composites dispersion can be further improved, the enhanced stability of finishing solution will provide more possibilities for industrial application.
- Use and compare more treatment methods. It can be an option to extensively investigate the differences in dipping, padding, and spraying processes for finishing cotton fabrics.
- The proposed structural barriers can be applied to other textile substrates such as silk, polyester and nylon for investigating their fire performances.
- In addition to endowing cotton fabrics with fire protection through the proposed structural barriers, it should be also possible to pursue the prospect of developing more properties such as anti-wrinkle, anti-UV, etc. The multifunctional finishing agents for cotton fabrics will considerably increase the added value.

## **Appendix. List of publications**

## List of publications

1. Wu, Q.; Cassia.; Rita.; José.; Fabricio.; Meng, Xu.; Lis, M.J. Recent progress of DOPO-containing compounds as flame retardants for versatile polymeric materials: review. *World Journal of Textile Engineering and Technology* 2020, vol. 6, p. 89-103. <http://hdl.handle.net/2117/335445>.
2. Wu, Q.; Lis, M.J. Barrier Effects of Cellulosic Fibers with Hybrid Coating Based on Zirconium Metal-Organic Framework. *Polymers* 2022, 14, 3071. <https://doi.org/10.3390/polym14153071>.
3. Da Costa, B.L.; Rosa, I.L.A.A.; Silva, V.H.; Wu, Q.; Samulewski, R.B.; Scacchetti, F.A.P.; Moisés, M.P.; Lis, M.J.; Bezerra, F.M. Direct Synthesis of HKUST-1 onto Cotton Fabrics and Properties. *Polymers* 2022, 14, 4256. <https://doi.org/10.3390/polym14204256>.
4. Wu, Q.; Lis, M.J.; Ko, Y. Fire performances of cotton fabrics with the incorporation of DOPO-HQ@Zr-MOF microcomposites  
(Journal: *Cellulose*, accepted for editorial processing)

## **Appendix. General bibliography**

## General bibliography

### A

- A Brief History of FR, 2015. WorkingPerson.me. URL <https://workingperson.me/a-brief-history-of-fr/> (accessed 1.7.21).
- Agrawal, S., Narula, A.K., 2014. Synthesis and characterization of phosphorus- and silicon-containing flame-retardant curing agents and a study of their effect on thermal properties of epoxy resins. *J Coat Technol Res* 11, 631–637. <https://doi.org/10.1007/s11998-014-9579-6>
- Al-Kutubi, H., Gascon, J., Sudhölter, E.J.R., Rassaei, L., 2015. Electrosynthesis of Metal–Organic Frameworks: Challenges and Opportunities. *ChemElectroChem* 2, 462–474. <https://doi.org/10.1002/celec.201402429>
- Alongi, J., Carletto, R., Bosco, F., Carosio, F., Di Blasio, A., Cuttica, F., Antonucci, V., Giordano, M., Malucelli, G., 2013a. Caseins and hydrophobins as novel green flame retardants for cotton fabrics. *Polymer Degradation and Stability* 99. <https://doi.org/10.1016/j.polymdegradstab.2013.11.016>
- Alongi, J., Carletto, R.A., Di Blasio, A., Cuttica, F., Carosio, F., Bosco, F., Malucelli, G., 2013b. Intrinsic intumescent-like flame retardant properties of DNA-treated cotton fabrics. *Carbohydrate Polymers* 96, 296–304. <https://doi.org/10.1016/j.carbpol.2013.03.066>
- Alongi, J., Ciobanu, M., Malucelli, G., 2011a. Novel flame retardant finishing systems for cotton fabrics based on phosphorus-containing compounds and silica derived from sol–gel processes. *Carbohydrate Polymers* 85, 599–608. <https://doi.org/10.1016/j.carbpol.2011.03.024>
- Alongi, J., Ciobanu, M., Malucelli, G., 2011b. Sol–gel treatments for enhancing flame retardancy and thermal stability of cotton fabrics: optimisation of the process and evaluation of the durability. *Cellulose* 18, 167–177. <https://doi.org/10.1007/s10570-010-9470-2>
- Ameloot, R., Liekens, A., Alaerts, L., Maes, M., Galarneau, A., Coq, B., Desmet, G., Sels, B.F., Denayer, J.F.M., De Vos, D.E., 2010. Silica–MOF Composites as a Stationary Phase in Liquid Chromatography. *European Journal of Inorganic Chemistry* 2010, 3735–3738. <https://doi.org/10.1002/ejic.201000494>
- Andrés, M.A., Sicard, C., Serre, C., Roubeau, O., Gascón, I., 2019. Ultrathin hydrophobic films based on the metal organic framework UiO-66-COOH(Zr). *Beilstein J. Nanotechnol.* 10, 654–665. <https://doi.org/10.3762/bjnano.10.65>
- Ardila-Suárez, C., Rodríguez-Pereira, J., Baldovino-Medrano, V.G., Ramírez-Caballero, G.E., 2019. An analysis of the effect of zirconium precursors of MOF-808 on its thermal stability, and structural and surface properties. *CrystEngComm* 21, 1407–1415. <https://doi.org/10.1039/C8CE01722K>
- Aroke, U.O., Abdulkarim, A., Ogubunka, R.O., 2013. Fourier-transform Infrared Characterization of Kaolin, Granite, Bentonite and Barite. *ATBU Journal of Environmental Technology* 6, 42–53.

### B

- Bakshia, P., Selvakumara, D., Kadirvelub, K., Kumara, N.S., 2019. Chitosan as an environment friendly biomaterial - a review on recent modifications and applications. *International Journal of Biological Macromolecules* 150. <https://doi.org/10.1016/j.ijbiomac.2019.10.113>
- Barton, H.F., Jamir, J.D., Davis, A.K., Peterson, G.W., Parsons, G.N., 2021. Doubly Protective MOF-Photo-Fabrics: Facile Template-Free Synthesis of PCN-222-Textiles Enables Rapid Hydrolysis, Photo-Hydrolysis and Selective Oxidation of Multiple Chemical Warfare Agents and Simulants. *Chemistry – A European Journal* 27, 1465–1472. <https://doi.org/10.1002/chem.202003716>
- Basak, S., Samanta, K.K., Chattopadhyay, S.K., 2015. Fire retardant property of cotton fabric treated with herbal extract. *The Journal of The Textile Institute* 106, 1338–1347. <https://doi.org/10.1080/00405000.2014.995456>
- Beg, M.A.A., Clark, H.C., 1962. CHEMISTRY OF THE TRIFLUOROMETHYL GROUP: PART V. INFRARED SPECTRA OF SOME PHOSPHORUS COMPOUNDS CONTAINING CF<sub>3</sub>. *Can. J. Chem.* 40, 393–398. <https://doi.org/10.1139/v62-063>
- Beulah, P., Jinu, U., Ghorbanpour, M., Venkatachalam, P., 2019. Chapter 14 - Green Engineered Chitosan Nanoparticles and Its Biomedical Applications—An Overview, in: Ghorbanpour, M., Wani, S.H. (Eds.), *Advances in Phytonanotechnology*. Academic Press, pp. 329–341. <https://doi.org/10.1016/B978-0-12-815322-2.00015-8>
- Bojana, B.P., Marica, S., 2016. Microencapsulation technology and applications in added-value functional textiles. *Physical Sciences Reviews* 1. <https://doi.org/10.1515/psr-2015-0003>
- Bourbigot, S., Bras, M.L., Duquesne, S., Rochery, M., 2004. Recent Advances for Intumescent Polymers. *Macromolecular Materials and Engineering* 289, 499–511. <https://doi.org/10.1002/mame.200400007>
- Bugaev, K.O., Zelenina, A.A., Volodin, V.A., 2011. Vibrational Spectroscopy of Chemical Species in Silicon and Silicon-Rich Nitride Thin Films. *International Journal of Spectroscopy* 2012, e281851. <https://doi.org/10.1155/2012/281851>

## C

- Cabrales, Luis, and Noureddine Abidi. 2010. 'On the Thermal Degradation of Cellulose in Cotton Fibers'. *Journal of Thermal Analysis and Calorimetry* 102 (November): 485–91. <https://doi.org/10.1007/s10973-010-0911-9>.
- Carosio, F., Fontaine, G., Alongi, J., Bourbigot, S., 2015. Starch-Based Layer by Layer Assembly: Efficient and Sustainable Approach to Cotton Fire Protection. *ACS Appl. Mater. Interfaces* 7, 12158–12167. <https://doi.org/10.1021/acsami.5b02507>
- Carosio, F., Laufer, G., Alongi, J., Camino, G., Grunlan, J.C., 2011. Layer-by-layer assembly of silica-based flame retardant thin film on PET fabric. *Polymer Degradation and Stability* 96, 745–750. <https://doi.org/10.1016/j.polymdegradstab.2011.02.019>
- Cassidy, T., Goswami, P., 2017. *Textile and Clothing Design Technology*. CRC Press.
- Cazes, J., 2004. *Analytical Instrumentation Handbook*. CRC Press.



- Chang, S., Sachinvala, N., Sawhney, P., Parikh, D., Jarrett, W., Grimm, C., 2007. Epoxy phosphonate crosslinkers for providing flame resistance to cotton textiles. *Polymers for Advanced Technologies* 18, 611–619. <https://doi.org/10.1002/pat.867>
- Cheema, H.A., El-Shafei, A., Hauser, P.J., 2013. Conferring flame retardancy on cotton using novel halogen-free flame retardant bifunctional monomers: synthesis, characterizations and applications. *Carbohydrate Polymers* 92, 885–893. <https://doi.org/10.1016/j.carbpol.2012.09.081>
- Chen, Gu, X., Jin, X., Sun, J., Zhang, S., 2016. The effect of chitosan on the flammability and thermal stability of polylactic acid/ammonium polyphosphate biocomposites. *Carbohydrate Polymers* 157. <https://doi.org/10.1016/j.carbpol.2016.11.035>
- Chen, L., Wang, Y.-Z., 2009. A review on flame retardant technology in China. Part I: development of flame retardants. <https://doi.org/10.1002/PAT.1550>
- Chen, L., Xu, Q., 2019. Metal-Organic Framework Composites for Catalysis. *Matter* 1, 57–89. <https://doi.org/10.1016/j.matt.2019.05.018>
- Chen, T., Hong, J., Peng, C., Chen, G., Yuan, C., Xu, Y., Zeng, B., Dai, L., 2019. Superhydrophobic and flame retardant cotton modified with DOPO and fluorine-silicon-containing crosslinked polymer. *Carbohydrate Polymers* 208, 14–21. <https://doi.org/10.1016/j.carbpol.2018.12.023>
- Chen, T., Hong, J., Peng, C., Chen, G., Yuan, C., Xu, Y., Zeng, B., Dai, L., 2019. Superhydrophobic and flame retardant cotton modified with DOPO and fluorine-silicon-containing crosslinked polymer. *Carbohydrate Polymers* 208, 14–21. <https://doi.org/10.1016/j.carbpol.2018.12.023>
- Chen, Z., Li, X., Yang, C., Cheng, K., Tan, T., Lv, Y., Liu, Y., 2021. Hybrid Porous Crystalline Materials from Metal Organic Frameworks and Covalent Organic Frameworks. *Advanced Science* 8, 2101883. <https://doi.org/10.1002/adv.202101883>
- Chen, Z., Ma, K., Mahle, J.J., Wang, H., Syed, Z.H., Atilgan, A., Chen, Y., Xin, J.H., Islamoglu, T., Peterson, G.W., Farha, O.K., 2019. Integration of Metal–Organic Frameworks on Protective Layers for Destruction of Nerve Agents under Relevant Conditions. *J. Am. Chem. Soc.* 141, 20016–20021. <https://doi.org/10.1021/jacs.9b11172>
- Cheng, B., Pei, B., Wang, Z., Hu, Q., 2017. Advances in chitosan-based superabsorbent hydrogels. *RSC Adv.* 7, 42036–42046. <https://doi.org/10.1039/C7RA07104C>
- Cheng, C., Xu, J., Gao, W., Jiang, S., Guo, R., 2019. Preparation of flexible supercapacitor with RGO/Ni-MOF film on Ni-coated polyester fabric. *Electrochimica Acta* 318, 23–31. <https://doi.org/10.1016/j.electacta.2019.06.055>
- Cheng, Genyin, and Ming Gao. 2016. 'Thermal Stability of Cotton Cellulose Modified with Dysprosium Complexes'. In *Proceedings of the 2016 6th International Conference on Machinery, Materials, Environment, Biotechnology and Computer*. Tianjin, China: Atlantis Press. <https://doi.org/10.2991/mmebc-16.2016.386>
- Chernyy, S., Ulah, S., Sørensen, G., Tordrup, S.W., Pedersen, P.B., Almdal, K., 2015. DOPO-VTS-based coatings in the realm of fire retardants for cotton textile. *J. Appl. Polym. Sci.* 132, n/a-n/a. <https://doi.org/10.1002/app.41955>
- Cheung, Y.H., Ma, K., van Leeuwen, H.C., Wasson, M.C., Wang, X., Idrees, K.B., Gong, W., Cao, R., Mahle, J.J., Islamoglu, T., Peterson, G.W., de Koning,

- M.C., Xin, J.H., Farha, O.K., 2021. Immobilized Regenerable Active Chlorine within a Zirconium-Based MOF Textile Composite to Eliminate Biological and Chemical Threats. *J. Am. Chem. Soc.* 143, 16777–16785. <https://doi.org/10.1021/jacs.1c08576>
- Choi, K., Seo, S., Kwon, H., Kim, D., Park, Y.T., 2018. Fire protection behavior of layer-by-layer assembled starch–clay multilayers on cotton fabric. *J Mater Sci* 53, 11433–11443. <https://doi.org/10.1007/s10853-018-2434-x>
- Chu, P.K., Chen, J.Y., Wang, L.P., Huang, N., 2002. Plasma-surface modification of biomaterials. *Materials Science and Engineering: R: Reports* 36, 143–206. [https://doi.org/10.1016/S0927-796X\(02\)00004-9](https://doi.org/10.1016/S0927-796X(02)00004-9)
- Chung, C., Lee, M., Choe, E., 2004. Characterization of cotton fabric scouring by FT-IR ATR spectroscopy. *Carbohydrate Polymers* 58, 417–420. <https://doi.org/10.1016/j.carbpol.2004.08.005>
- Cireli, A., Onar, N., Ebeoglugil, M.F., Kayatekin, I., Kutlu, B., Culha, O., Celik, E., 2007. Development of flame retardancy properties of new halogen-free phosphorous doped SiO<sub>2</sub> thin films on fabrics. *J. Appl. Polym. Sci.* 105, 3748–3756. <https://doi.org/10.1002/app.26442>
- Colleoni, C., Donelli, I., Freddi, G., Guido, E., Migani, V., Rosace, G., 2013. A novel sol-gel multi-layer approach for cotton fabric finishing by tetraethoxysilane precursor. *Surface and Coatings Technology* 235, 192–203. <https://doi.org/10.1016/j.surfcoat.2013.07.033>
- Cortés, P.H., Macías, S.R., 2021. *Metal-Organic Frameworks in Biomedical and Environmental Field*. Springer Nature.
- Costes, L., Laoutid, F., Brohez, S., Dubois, P., 2017. Bio-based flame retardants: When nature meets fire protection. *Materials Science and Engineering: R: Reports* 117, 1–25. <https://doi.org/10.1016/j.mser.2017.04.001>
- Crake, A., Christoforidis, K.C., Gregg, A., Moss, B., Kafizas, A., Petit, C., 2019. The Effect of Materials Architecture in TiO<sub>2</sub>/MOF Composites on CO<sub>2</sub> Photoreduction and Charge Transfer. *Small* 15, 1805473. <https://doi.org/10.1002/smll.201805473>
- Crank, J., 1980. *The Mathematics of Diffusion*, 2nd edition. ed. Oxford University Press, Oxford.

## D

- D'Amato, R., Bondi, R., Moghdad, I., Marmottini, F., McPherson, M.J., Naïli, H., Taddei, M., Costantino, F., 2021. “Shake 'n Bake” Route to Functionalized Zr-Uio-66 Metal-Organic Frameworks. *Inorg Chem* 60, 14294–14301. <https://doi.org/10.1021/acs.inorgchem.1c01839>
- Donatti, D.A., Ruiz, A.I., Vollet, D.R., 2002. A dissolution and reaction modeling for hydrolysis of TEOS in heterogeneous TEOS–water–HCl mixtures under ultrasound stimulation. *Ultrasonics Sonochemistry* 9, 133–138. [https://doi.org/10.1016/S1350-4177\(01\)00120-1](https://doi.org/10.1016/S1350-4177(01)00120-1)
- Donatti, D.A., Vollet, D.R., 2000. Effects of the Water Quantity on the Solventless TEOS Hydrolysis Under Ultrasound Stimulation. *Journal of Sol-Gel Science and Technology* 17, 19–24. <https://doi.org/10.1023/A:1008748702656>

- Duan, H., Ji, S., Yin, T., Tao, X., Chen, Y., Ma, H., 2019. Phosphorus–nitrogen-type fire-retardant vinyl ester resin with good comprehensive properties. *J Appl Polym Sci* 136, 47997. <https://doi.org/10.1002/app.47997>
- Duan, H., Ji, S., Yin, T., Tao, X., Chen, Y., Ma, H., 2019. Phosphorus–nitrogen-type fire-retardant vinyl ester resin with good comprehensive properties. *J Appl Polym Sci* 136, 47997. <https://doi.org/10.1002/app.47997>

## E

- Ebnesajjad, S., 2014. Chapter 4 – Surface and Material Characterization Techniques. undefined.

## F

- Férey, G., Mellot-Draznieks, C., Serre, C., Millange, F., Dutour, J., Surblé, S., Margiolaki, I., 2005. A Chromium Terephthalate-Based Solid with Unusually Large Pore Volumes and Surface Area. *Science* 309, 2040–2042. <https://doi.org/10.1126/science.1116275>
- Férey, G., Serre, C., Mellot-Draznieks, C., Millange, F., Surblé, S., Dutour, J., Margiolaki, I., 2004. A Hybrid Solid with Giant Pores Prepared by a Combination of Targeted Chemistry, Simulation, and Powder Diffraction. *Angewandte Chemie* 116, 6456–6461. <https://doi.org/10.1002/ange.200460592>

## G

- Gaan, S., Sun, G., Hutches, K., Engelhard, M.H., 2008. Effect of nitrogen additives on flame retardant action of tributyl phosphate: Phosphorus–nitrogen synergism. *Polymer Degradation and Stability* 93, 99–108. <https://doi.org/10.1016/j.polymdegradstab.2007.10.013>
- Gao, M., Zeng, L., Nie, J., Ma, G., 2016. Polymer–metal–organic framework core–shell framework nanofibers via electrospinning and their gas adsorption activities. <https://doi.org/10.1039/C5RA23147G>
- Gaspar, V.M., Moreira, A.F., de Melo-Diogo, D., Costa, E.C., Queiroz, J.A., Sousa, F., Pichon, C., Correia, I.J., 2016. Chapter 6 - Multifunctional nanocarriers for codelivery of nucleic acids and chemotherapeutics to cancer cells, in: Grumezescu, A.M. (Ed.), *Nanobiomaterials in Medical Imaging*. William Andrew Publishing, pp. 163–207. <https://doi.org/10.1016/B978-0-323-41736-5.00006-6>
- Giraud, S., Rault, F., Cayla, A., Salaün, F., 2016. HISTORY AND EVOLUTION OF FIRE RETARDANTS FOR TEXTILES.
- González, C.M.O., Morales, E.M.C., Tellez, A. de M.N., Quezada, T.E.S., Kharissova, O.V., Méndez-Rojas, M.A., 2021. Chapter 18 - CO<sub>2</sub> capture by MOFs, in: Kharisov, B., Kharissova, O. (Eds.), *Handbook of Greener Synthesis of Nanomaterials and Compounds*. Elsevier, pp. 407–448. <https://doi.org/10.1016/B978-0-12-822446-5.00018-6>

- Gordon, S., Hsieh, Y.-L. (Eds.), 2007. Introduction, in: Cotton, Woodhead Publishing Series in Textiles. Woodhead Publishing, pp. xv–xx. <https://doi.org/10.1016/B978-1-84569-026-7.50020-2>
- Griffiths, P.R., Haseth, J.A.D., 2007. Fourier Transform Infrared Spectrometry. John Wiley & Sons.
- Guin, T., Krecker, M., Milhorn, A., Grunlan, J.C., 2014. Maintaining hand and improving fire resistance of cotton fabric through ultrasonication rinsing of multilayer nanocoating. *Cellulose* 21, 3023–3030. <https://doi.org/10.1007/s10570-014-0286-3>
- Guo, D.-M., An, Q.-D., Xiao, Z.-Y., Zhai, S.-R., Shi, Z., 2017. Polyethylenimine-functionalized cellulose aerogel beads for efficient dynamic removal of chromium( vi ) from aqueous solution. *RSC Advances* 7, 54039–54052. <https://doi.org/10.1039/C7RA09940A>

## H

- Halima, N.B., 2016. Poly(vinyl alcohol): review of its promising applications and insights into biodegradation. *RSC Adv.* 6, 39823–39832. <https://doi.org/10.1039/C6RA05742J>
- Hamdani - Devarenes, S., Longuet, C., Perrin, D., Lopez-cuesta, J.-M., Ganachaud, F., 2009. Flame retardancy of silicone-based materials. *Polymer Degradation and Stability* 94, 465–495. <https://doi.org/10.1016/j.polymdegradstab.2008.11.019>
- He, M., Zhang, D., Zhao, W., Qin, S., Yu, J., 2019. Flame retardant and thermal decomposition mechanism of poly(butylene terephthalate)/DOPO-HQ composites. *Polym. Compos.* 40, 974–985. <https://doi.org/10.1002/pc.24772>
- Hergenrother, P.M., Thompson, C.M., Smith, J.G., Connell, J.W., Hinkley, J.A., Lyon, R.E., Moulton, R., 2005. Flame retardant aircraft epoxy resins containing phosphorus. *Polymer* 46, 5012–5024. <https://doi.org/10.1016/j.polymer.2005.04.025>
- Höfer, R., 2012. 10.21 - Processing and Performance Additives for Plastics, in: Matyjaszewski, K., Möller, M. (Eds.), *Polymer Science: A Comprehensive Reference*. Elsevier, Amsterdam, pp. 369–381. <https://doi.org/10.1016/B978-0-444-53349-4.00272-7>
- Horrocks, A.R., 1983. An Introduction to the Burning Behaviour of Cellulosic Fibres. *Journal of the Society of Dyers and Colourists* 99, 191–197. <https://doi.org/10.1111/j.1478-4408.1983.tb03686.x>
- Horrocks, A.R., 2008. Flame-retardant Finishing of Textiles. *Review of Progress in Coloration and Related Topics* 16, 62–101. <https://doi.org/10.1111/j.1478-4408.1986.tb03745.x>
- Hosseini Ravandi, S.A., Valizadeh, M., 2011. 2 - Properties of fibers and fabrics that contribute to human comfort, in: Song, G. (Ed.), *Improving Comfort in Clothing*, Woodhead Publishing Series in Textiles. Woodhead Publishing, pp. 61–78. <https://doi.org/10.1533/9780857090645.1.61>
- Hou, Y., Hu, W., Gui, Z., Hu, Y., 2017. Preparation of Metal-Organic Frameworks and Their Application as Flame Retardants for Polystyrene. *Industrial & Engineering Chemistry Research* 56. <https://doi.org/10.1021/acs.iecr.6b04920>

- Hsieh, Y.L., 2007. Chemical structure and properties of cotton, in: Cotton. Elsevier, pp. 3–34. <https://doi.org/10.1533/9781845692483.1.3>
- Hu, S., Hu, Y., Song, L., Lu, H., 2011. Effect of modified organic–inorganic hybrid materials on thermal properties of cotton fabrics. *J Therm Anal Calorim* 103, 423–427. <https://doi.org/10.1007/s10973-010-1093-1>
- Huang, G., Liang, H., Wang, X., Gao, J., 2012. Poly(acrylic acid)/Clay Thin Films Assembled by Layer-by-Layer Deposition for Improving the Flame Retardancy Properties of Cotton. *Ind. Eng. Chem. Res.* 51, 12299–12309. <https://doi.org/10.1021/ie300820k>
- Huong, N., Vu, K., Ngô, T., Phan, D.-N., 2020. Application of Plasma Activation in Flame-Retardant Treatment for Cotton Fabric. *Polymers* 12. <https://doi.org/10.3390/polym12071575>

## I

- Inan, T.Y., 2017. 2 - Thermoplastic-based nanoblends: Preparation and characterizations, in: Visakh, P.M., Markovic, G., Pasquini, D. (Eds.), *Recent Developments in Polymer Macro, Micro and Nano Blends*. Woodhead Publishing, pp. 17–56. <https://doi.org/10.1016/B978-0-08-100408-1.00002-9>

## J

- J. Katz, M., J. Brown, Z., J. Colón, Y., W. Siu, P., A. Scheidt, K., Q. Snurr, R., T. Hupp, J., K. Farha, O., 2013. A facile synthesis of UiO-66, UiO-67 and their derivatives. *Chemical Communications* 49, 9449–9451. <https://doi.org/10.1039/C3CC46105J>
- Jiang, W., Jin, F.-L., Park, S.-J., 2015. Synthesis of a novel phosphorus-nitrogen-containing intumescent flame retardant and its application to fabrics. *Journal of Industrial and Engineering Chemistry* 27, 40–43. <https://doi.org/10.1016/j.jiec.2015.01.010>
- Jiang, X., Zhao, C., Zhong, C., Li, J., 2017. The Electrochemical Sensors Based on MOF and Their Applications. *Progress in Chemistry* 29, 1206–1214. <https://doi.org/10.7536/PC170619>
- Jiang, Zhiming, Hao Li, Yewei He, Yun Liu, Chaohong Dong, and Ping Zhu. 2019. Flame Retardancy and Thermal Behavior of Cotton Fabrics Based on a Novel Phosphorus-Containing Siloxane. *Applied Surface Science* 479 (June): 765–775. <https://doi.org/10.1016/j.apsusc.2019.02.159>

## K

- Kappes, R.S., Urbainczyk, T., Artz, U., Textor, T., Gutmann, J.S., 2016. Flame retardants based on amino silanes and phenylphosphonic acid. *Polymer Degradation and Stability* 129, 168–179. <https://doi.org/10.1016/j.polymdegradstab.2016.04.012>

- Kashiwagi, T., Gilman, J., Butler, K., Harris, R., Shields, J., Asano, A., 2000. Flame retardant mechanism of silica gel/silica. *Fire and Materials* 24, 277–289. [https://doi.org/10.1002/1099-1018\(200011/12\)24:6<277::AID-FAM746>3.0.CO;2-A](https://doi.org/10.1002/1099-1018(200011/12)24:6<277::AID-FAM746>3.0.CO;2-A)
- Kaya, H., Ngo, D., Gin, S., Kim, S.H., 2020. Spectral changes in Si–O–Si stretching band of porous glass network upon ingress of water. *Journal of Non-Crystalline Solids* 527, 119722. <https://doi.org/10.1016/j.jnoncrysol.2019.119722>
- Kayal, S., Sun, B., Chakraborty, A., 2015. Study of metal-organic framework MIL-101(Cr) for natural gas (methane) storage and compare with other MOFs (metal-organic frameworks). *Energy* 91, 772–781. <https://doi.org/10.1016/j.energy.2015.08.096>
- Khabzina, Y., Dhainaut, J., Ahlhelm, M., Richter, H.-J., Reinsch, H., Stock, N., Farrusseng, D., 2018. Synthesis and Shaping Scale-up Study of Functionalized UiO-66 MOF for Ammonia Air Purification Filters. *Ind. Eng. Chem. Res.* 57, 8200–8208. <https://doi.org/10.1021/acs.iecr.8b00808>
- Khanjani, S., Morsali, A., 2014. Ultrasound-promoted coating of MOF-5 on silk fiber and study of adsorptive removal and recovery of hazardous anionic dye “congo red.” *Ultrasonics Sonochemistry* 21, 1424–1429. <https://doi.org/10.1016/j.ultsonch.2013.12.012>
- Kilby, W.F., 1960. Relation of Apparent Diffusion Coefficient to the Time of Half-dyeing. *Journal of the Society of Dyers and Colourists* 76, 479–484. <https://doi.org/10.1111/j.1478-4408.1960.tb02390.x>
- Kilinc, M., 2014. Silicon Based Flame Retardants. *Non-Halogenated Flame Retardant Handbook* 169–199. <https://doi.org/10.1002/9781118939239.ch5>
- Klinowski, J., Paz, F.A.A., Silva, P., Rocha, J., 2010. Microwave-Assisted Synthesis of Metal–Organic Frameworks. *Dalton Trans.* 40, 321–330. <https://doi.org/10.1039/C0DT00708K>
- Kwon, H.T., Jeong, H.-K., 2013. In situ synthesis of thin zeolitic-imidazolate framework ZIF-8 membranes exhibiting exceptionally high propylene/propane separation. *J Am Chem Soc* 135, 10763–10768. <https://doi.org/10.1021/ja403849c>

## L

- Laufer, G., Kirkland, C., Morgan, A.B., Grunlan, J.C., 2012. Intumescent Multilayer Nanocoating, Made with Renewable Polyelectrolytes, for Flame-Retardant Cotton [WWW Document]. ACS Publications. <https://doi.org/10.1021/bm300873b>
- Lazar, S.T., Kolibaba, T.J., Grunlan, J.C., 2020. Flame-retardant surface treatments. *Nat Rev Mater* 5, 259–275. <https://doi.org/10.1038/s41578-019-0164-6>
- Lee, Y.-R., Kim, J., Ahn, W.-S., 2013. Synthesis of metal-organic frameworks: A mini review. *Korean J. Chem. Eng.* 30, 1667–1680. <https://doi.org/10.1007/s11814-013-0140-6>
- Levchik, S., 2007. Introduction to Flame Retardancy and Polymer Flammability. *Flame Retardant Polymer Nanocomposites* 1–29.

- Levchik, S., 2014. Phosphorus-Based FRs, in: *Non-Halogenated Flame Retardant Handbook*. John Wiley & Sons, Ltd, pp. 17–74. <https://doi.org/10.1002/9781118939239.ch2>
- Levința, N., Vuluga, Z., Teodorescu, M., Corobea, M.C., 2019. Halogen-free flame retardants for application in thermoplastics based on condensation polymers. *SN Appl. Sci.* 1, 422. <https://doi.org/10.1007/s42452-019-0431-6>
- Lewin, M., 2001. Synergism and catalysis in flame retardancy of polymers. *Polymers for Advanced Technologies* 12, 215–222. <https://doi.org/10.1002/pat.132>
- Li, D., Zhou, Q., Hu, X., Mu, L., Zeng, H., Luo, J., 2022. Environmental decomposition and remodeled phytotoxicity of framework-based nanomaterials. *J Hazard Mater* 422, 126846. <https://doi.org/10.1016/j.jhazmat.2021.126846>
- Li, D.-J., Lei, S., Wang, Y.-Y., Chen, S., Kang, Y., Gu, Z.-G., Zhang, J., 2018. Helical carbon tubes derived from epitaxial Cu-MOF coating on textile for enhanced supercapacitor performance. *Dalton Trans.* 47, 5558–5563. <https://doi.org/10.1039/C8DT00761F>
- Li, G., Xia, L., Dong, J., Chen, Y., Li, Y., 2020. 10 - Metal-organic frameworks, in: Poole, C.F. (Ed.), *Solid-Phase Extraction, Handbooks in Separation Science*. Elsevier, pp. 285–309. <https://doi.org/10.1016/B978-0-12-816906-3.00010-8>
- Li, H., Li, L., Lin, R.-B., Zhou, W., Zhang, Z., Xiang, S., Chen, B., 2019. Porous metal-organic frameworks for gas storage and separation: Status and challenges. *EnergyChem* 1, 100006. <https://doi.org/10.1016/j.enchem.2019.100006>
- Li, H., Wang, K., Sun, Y., Lollar, C.T., Li, J., Zhou, H.-C., 2018. Recent advances in gas storage and separation using metal–organic frameworks. *Materials Today* 21, 108–121. <https://doi.org/10.1016/j.mattod.2017.07.006>
- Li, Jinfeng, and Wei Jiang. 2021. 'Synthesis of a Novel P-N Flame Retardant for Preparing Flame Retardant and Durable Cotton Fabric'. *Industrial Crops and Products* 174 (December): 114205. <https://doi.org/10.1016/j.indcrop.2021.114205>.
- Li, N., Ming, J., Yuan, R., Fan, S., Liu, L., Li, F., Wang, X., Yu, J., Wu, D., 2020. Novel Eco-Friendly Flame Retardants Based on Nitrogen–Silicone Schiff Base and Application in Cellulose. *ACS Sustainable Chem. Eng.* 8, 290–301. <https://doi.org/10.1021/acssuschemeng.9b05338>
- Li, P., Wang, B., Liu, Y.-Y., Xu, Y.-J., Jiang, Z.-M., Dong, C.-H., Zhang, L., Liu, Y., Zhu, P., 2020. Fully bio-based coating from chitosan and phytate for fire-safety and antibacterial cotton fabrics. *Carbohydrate Polymers* 237, 116173. <https://doi.org/10.1016/j.carbpol.2020.116173>
- Li, Y., Wang, B., Sui, X., Xie, R., Xu, H., Zhang, L., Zhong, Y., Mao, Z., 2018. Durable flame retardant and antibacterial finishing on cotton fabrics with cyclotriphosphazene/polydopamine/silver nanoparticles hybrid coatings. *Applied Surface Science* 435, 1337–1343. <https://doi.org/10.1016/j.apsusc.2017.11.269>
- Li, Y.-C., Schulz, J., Mannen, S., Delhom, C., Condon, B., Chang, S., Zammarano, M., Grunlan, J.C., 2010. Flame Retardant Behavior of Polyelectrolyte–Clay Thin Film Assemblies on Cotton Fabric. *ACS Nano* 4, 3325–3337. <https://doi.org/10.1021/nn100467e>

- Li, Z.-F., Zhang, C.-J., Cui, L., Zhu, P., Yan, C., Liu, Y., 2017. Fire retardant and thermal degradation properties of cotton fabrics based on APTES and sodium phytate through layer-by-layer assembly. *Journal of Analytical and Applied Pyrolysis* 123, 216–223. <https://doi.org/10.1016/j.jaap.2016.11.026>
- Lian, X., Fang, Y., Joseph, E., Wang, Q., Li, J., Banerjee, S., Lollar, C., Wang, X., Zhou, H.-C., 2017. Enzyme–MOF (metal–organic framework) composites. *Chem. Soc. Rev.* 46, 3386–3401. <https://doi.org/10.1039/C7CS00058H>
- Liang, J., Huang, Y.-B., Cao, R., 2019. Metal–organic frameworks and porous organic polymers for sustainable fixation of carbon dioxide into cyclic carbonates. *Coordination Chemistry Reviews, Special issue on the 8th Chinese Coordination Chemistry Conference* 378, 32–65. <https://doi.org/10.1016/j.ccr.2017.11.013>
- Lin, C.-F., Tseng, W., Feng, M., 2000. Formation and characteristics of silicon nanocrystals in plasma-enhanced chemical-vapor-deposited silicon-rich oxide. *Journal of Applied Physics - J APPL PHYS* 87, 2808–2815. <https://doi.org/10.1063/1.372260>
- Lin, D., Zeng, X., Li, H., Lai, X., Wu, T., 2018. One-pot fabrication of superhydrophobic and flame-retardant coatings on cotton fabrics via sol-gel reaction. *Journal of Colloid and Interface Science* 533. <https://doi.org/10.1016/j.jcis.2018.08.060>
- Lis Arias, M.J. (Manuel J., 2002. Comportamiento cinético de fibras Tencel con colorantes directos (Ph.D. Thesis). TDX (Tesis Doctorals en Xarxa). Universitat Politècnica de Catalunya.
- Liu, G., Han, Y., Zhao, Y., Zheng, H., Zheng, L., 2020. Development of CO<sub>2</sub> utilized flame retardant finishing: Solubility measurements of flame retardants and application of the process to cotton. *Journal of CO<sub>2</sub> Utilization* 37, 222–229. <https://doi.org/10.1016/j.jcou.2019.12.015>
- Liu, M., Yin, H., Chen, X., Yang, J., Liang, Y., Zhang, J., Yang, F., Deng, Y., Lu, S., 2018. Preliminary ecotoxicity hazard evaluation of DOPO-HQ as a potential alternative to halogenated flame retardants. *Chemosphere* 193, 126–133. <https://doi.org/10.1016/j.chemosphere.2017.10.142>
- Liu, Q., Wang, D., Li, Zekun, Li, Zhifa, Peng, X., Liu, C., Zhang, Y., Zheng, P., 2020. Recent Developments in the Flame-Retardant System of Epoxy Resin. *Materials* 13, 2145. <https://doi.org/10.3390/ma13092145>
- Liu, S., Fang, Z., Yan, H., Chevali, V.S., Wang, H., 2016. Synergistic flame retardancy effect of graphene nanosheets and traditional retardants on epoxy resin. *Composites Part A: Applied Science and Manufacturing* 89, 26–32. <https://doi.org/10.1016/j.compositesa.2016.03.012>
- Liu, X., Li, Y., Hu, J., Jiao, J., Li, J., 2014. Smart moisture management and thermoregulation properties of stimuli-responsive cotton modified with polymer brushes. *RSC Adv.* 4, 63691–63695. <https://doi.org/10.1039/C4RA11080C>
- Liu, Y., He, J., Yang, R., 2016. The preparation and properties of flame-retardant polyisocyanurate–polyurethane foams based on two DOPO derivatives. *Journal of Fire Sciences* 34, 431–444. <https://doi.org/10.1177/0734904116662667>
- Livage, J., 2004. Basic Principles of Sol-Gel Chemistry, in: Aegerter, M.A., Mennig, M. (Eds.), *Sol-Gel Technologies for Glass Producers and Users*.



- Springer US, Boston, MA, pp. 3–14. [https://doi.org/10.1007/978-0-387-88953-5\\_1](https://doi.org/10.1007/978-0-387-88953-5_1)
- Lu, A.X., McEntee, M., Browe, M.A., Hall, M.G., DeCoste, J.B., Peterson, G.W., 2017. MOFabric: Electrospun Nanofiber Mats from PVDF/UiO-66-NH<sub>2</sub> for Chemical Protection and Decontamination. *ACS Appl Mater Interfaces* 9, 13632–13636. <https://doi.org/10.1021/acsami.7b01621>
- Luo, D., Duan, W., Liu, Y., Chen, N., Wang, Q., 2019. Melamine cyanurate surface treated by nylon of low molecular weight to prepare flame-retardant polyamide 66 with high flowability. *Fire and Materials* 43, 323–331. <https://doi.org/10.1002/fam.2703>

## M

- Ma, H., Tong, L., Xu, Z., Fang, Z., Jin, Y., Lu, F., 2007. A novel intumescent flame retardant: Synthesis and application in ABS copolymer. *Polymer Degradation and Stability* 92, 720–726. <https://doi.org/10.1016/j.polymdegradstab.2006.12.009>
- Ma, K., Idrees, K.B., Son, F.A., Maldonado, R., Wasson, M.C., Zhang, X., Wang, X., Shehayeb, E., Merhi, A., Kaafarani, B.R., Islamoglu, T., Xin, J.H., Farha, O.K., 2020. Fiber Composites of Metal–Organic Frameworks. *Chem. Mater.* 32, 7120–7140. <https://doi.org/10.1021/acs.chemmater.0c02379>
- Ma, K., Wang, Y., Chen, Z., Islamoglu, T., Lai, C., Wang, X., Fei, B., Farha, O.K., Xin, J.H., 2019. Facile and Scalable Coating of Metal–Organic Frameworks on Fibrous Substrates by a Coordination Replication Method at Room Temperature. *ACS Appl. Mater. Interfaces* 11, 22714–22721. <https://doi.org/10.1021/acsami.9b04780>
- Ma, T., Li, H., Ma, J.-G., Cheng, P., 2020. Application of MOF-based materials in electrochemical sensing. *Dalton Trans.* 49, 17121–17129. <https://doi.org/10.1039/D0DT03388J>
- Ma, Yanan, Xiaolei Luo, Lin Liu, Cong Zhang, Xiaolei Shang, and Juming Yao. 2021. 'Eco-Friendly, Efficient and Durable Fireproof Cotton Fabric Prepared by a Feasible Phytic Acid Grafting Route'. *Cellulose* 28 (6): 3887–99. <https://doi.org/10.1007/s10570-021-03767-0>.
- Mahmoodi, N.M., Abdi, J., Oveisi, M., Alinia Asli, M., Vossoughi, M., 2018. Metal-organic framework (MIL-100 (Fe)): Synthesis, detailed photocatalytic dye degradation ability in colored textile wastewater and recycling. *Materials Research Bulletin* 100, 357 – 366. <https://doi.org/10.1016/j.materresbull.2017.12.033>
- Malucelli, G., 2020. Flame-Retardant Systems Based on Chitosan and Its Derivatives: State of the Art and Perspectives. *Molecules* 25, 4046. <https://doi.org/10.3390/molecules25184046>
- Mark, R.E., Borch, J., Habeger, C., 2002. *Handbook of Physical Testing of Paper*. CRC Press.
- Martínez-Ahumada, E., Díaz-Ramírez, M.L., Velásquez-Hernández, M. de J., Jancik, V., Ibarra, I.A., 2021. Capture of toxic gases in MOFs: SO<sub>2</sub>, H<sub>2</sub>S, NH<sub>3</sub> and NO<sub>x</sub>. *Chem. Sci.* 12, 6772–6799. <https://doi.org/10.1039/D1SC01609A>
- Marturano, V., Cerruti, P., Ambrogi, V., 2017. Polymer additives. *Physical Sciences Reviews* 2. <https://doi.org/10.1515/psr-2016-0130>

- Materials, N.R.C. (U.S.) C. on F.S.A. of P., 1979. Fire Safety Aspects of Polymeric Materials: Report of the Committee on Fire Safety Aspects of Polymeric Materials, National Materials Advisory Board, Commission on Sociotechnical Systems, National Research Council. National Academy of Sciences.
- Mehra, S., Poliseti, V., Damarla, K., Ray, P., Kumar, A., 2021. Ionic Liquid-Based Colloidal Formulations for the Synthesis of Nano-MOFs: Applications in Gas Adsorption and Water Desalination. *ACS Appl. Mater. Interfaces* 13, 41249–41261. <https://doi.org/10.1021/acsami.1c10184>
- Mercado, L.A., Galià, M., Reina, J.A., 2006. Silicon-containing flame retardant epoxy resins: Synthesis, characterization and properties. *Polymer Degradation and Stability* 91, 2588–2594. <https://doi.org/10.1016/j.polymdegradstab.2006.05.007>
- Mohamed, M.A., Jaafar, J., Ismail, A. F., Othman, M.H.D., Rahman, M.A., 2017. Chapter 1 - Fourier Transform Infrared (FTIR) Spectroscopy, in: Hilal, N., Ismail, Ahmad Fauzi, Matsuura, T., Oatley-Radcliffe, D. (Eds.), *Membrane Characterization*. Elsevier, pp. 3–29. <https://doi.org/10.1016/B978-0-444-63776-5.00001-2>
- Moltó, Julia, Rafael Font, Juan A. Conesa, and Ignacio Martín-Gullón. 2006. 'Thermogravimetric Analysis during the Decomposition of Cotton Fabrics in an Inert and Air Environment'. *Journal of Analytical and Applied Pyrolysis* 76 (1): 124–31. <https://doi.org/10.1016/j.jaap.2005.09.001>.
- Mudalige, T., Qu, H., Van Haute, D., Ansar, S.M., Paredes, A., Ingle, T., 2019. Chapter 11 - Characterization of Nanomaterials: Tools and Challenges, in: López Rubio, A., Fabra Rovira, M.J., Martínez Sanz, M., Gómez-Mascaraque, L.G. (Eds.), *Nanomaterials for Food Applications, Micro and Nano Technologies*. Elsevier, pp. 313–353. <https://doi.org/10.1016/B978-0-12-814130-4.00011-7>
- Mukherjee, S., Kumar, A., Zaworotko, M.J., 2019. 2 - Metal-organic framework based carbon capture and purification technologies for clean environment, in: Ghosh, S.K. (Ed.), *Metal-Organic Frameworks (MOFs) for Environmental Applications*. Elsevier, pp. 5–61. <https://doi.org/10.1016/B978-0-12-814633-0.00003-X>

## N

- Nabipour, H., Nie, S., Wang, X., Song, L., Hu, Y., 2020a. Highly flame retardant zeolitic imidazole framework-8@cellulose composite aerogels as absorption materials for organic pollutants. *Cellulose* 27, 2237–2251. <https://doi.org/10.1007/s10570-019-02860-9>
- Nabipour, H., Wang, X., Song, L., Hu, Y., 2020b. Metal-organic frameworks for flame retardant polymers application: A critical review. *Composites Part A: Applied Science and Manufacturing* 139, 106113. <https://doi.org/10.1016/j.compositesa.2020.106113>
- Nabipour, H., Wang, X., Song, L., Hu, Y., 2020c. Graphene oxide/zeolitic imidazolate frameworks-8 coating for cotton fabrics with highly flame retardant, self-cleaning and efficient oil/water separation performances. *Materials Chemistry and Physics* 256, 123656. <https://doi.org/10.1016/j.matchemphys.2020.123656>

**O**

Ozer, D., 2020. Fabrication and Functionalization Strategies of MOFs and Their Derived Materials “MOF Architecture,” in: Applications of Metal–Organic Frameworks and Their Derived Materials. John Wiley & Sons, Ltd, pp. 63–100. <https://doi.org/10.1002/9781119651079.ch3>

**P**

- P.M, V., Arao, Y., 2015. Flame Retardants: Polymer Blends, Composites and Nanocomposites. <https://doi.org/10.1007/978-3-319-03467-6>
- Pan, Y.-T., Zhang, Z., Yang, R., 2020. The rise of MOFs and their derivatives for flame retardant polymeric materials: A critical review. *Composites Part B: Engineering* 199, 108265. <https://doi.org/10.1016/j.compositesb.2020.108265>
- Park, K.S., Ni, Z., Côté, A.P., Choi, J.Y., Huang, R., Uribe-Romo, F.J., Chae, H.K., O’Keeffe, M., Yaghi, O.M., 2006. Exceptional chemical and thermal stability of zeolitic imidazolate frameworks. *Proceedings of the National Academy of Sciences* 103, 10186–10191. <https://doi.org/10.1073/pnas.0602439103>
- Parvez, K., 2019. Chapter 2 - Characterization Techniques of Two-Dimensional Nanomaterials, in: Nurunnabi, M., McCarthy, J.R. (Eds.), *Biomedical Applications of Graphene and 2D Nanomaterials, Micro and Nano Technologies*. Elsevier, pp. 27–41. <https://doi.org/10.1016/B978-0-12-815889-0.00002-7>
- Pascanu, V., González Miera, G., Inge, A.K., Martín-Matute, B., 2019. Metal–Organic Frameworks as Catalysts for Organic Synthesis: A Critical Perspective. *J. Am. Chem. Soc.* 141, 7223–7234. <https://doi.org/10.1021/jacs.9b00733>
- Peng, C., Li, J., Wu, Z., Peng, W., Zhou, D., 2016. Investigating into the liquid oxygen compatibility of a modified epoxy resin containing silicon/phosphorus and its mechanical behavior at cryogenic temperature. *RSC Adv.* 6, 38300–38309. <https://doi.org/10.1039/C6RA06033A>
- Pentassuglia, S., Agostino, V., Tommasi, T., 2018. EAB—Electroactive Biofilm: A Biotechnological Resource, in: Wandelt, K. (Ed.), *Encyclopedia of Interfacial Chemistry*. Elsevier, Oxford, pp. 110–123. <https://doi.org/10.1016/B978-0-12-409547-2.13461-4>
- Pirzadeh, K., Ghoreyshi, A.A., Rahimnejad, M., Mohammadi, M., 2018. Electrochemical synthesis, characterization and application of a microstructure Cu<sub>3</sub>(BTC)<sub>2</sub> metal organic framework for CO<sub>2</sub> and CH<sub>4</sub> separation. *Korean Journal of Chemical Engineering* 35. <https://doi.org/10.1007/s11814-017-0340-6>
- Portella, E.H., Romanzini, D., Angrizani, C.C., Amico, S.C., Zattera, A.J., 2016. Influence of Stacking Sequence on the Mechanical and Dynamic Mechanical Properties of Cotton/Glass Fiber Reinforced Polyester Composites. *Mat. Res.* 19, 542–547. <https://doi.org/10.1590/1980-5373-MR-2016-0058>

**Q**

- Qi, X.-L., Zhou, D.-D., Zhang, J., Hu, S., Haranczyk, M., Wang, D.-Y., 2019. Simultaneous Improvement of Mechanical and Fire-Safety Properties of Polymer Composites with Phosphonate-Loaded MOF Additives. *ACS Appl. Mater. Interfaces* 11, 20325–20332. <https://doi.org/10.1021/acsami.9b02357>

**R**

- Rakotomalala, M., Wagner, S., Döring, M., 2010. Recent Developments in Halogen Free Flame Retardants for Epoxy Resins for Electrical and Electronic Applications. *Materials* 3, 4300–4327. <https://doi.org/10.3390/ma3084300>
- Ratna, D., 2012. 3 - Thermal properties of thermosets, in: Guo, Q. (Ed.), *Thermosets*. Woodhead Publishing, pp. 62–91. <https://doi.org/10.1533/9780857097637.1.62>
- Ren, L., Zhao, X., Liu, B., Huang, H., 2021. Synergistic effect of carboxyl and sulfate groups for effective removal of radioactive strontium ion in a Zr-metal-organic framework. *Water Science and Technology* 83, 2001–2011. <https://doi.org/10.2166/wst.2021.103>
- Rezvani Ghomi, E., Khosravi, F., Mossayebi, Z., Saedi Ardahaei, A., Morshedi Dehaghi, F., Khorasani, M., Neisiany, R.E., Das, O., Marani, A., Mensah, R.A., Jiang, L., Xu, Q., Försth, M., Berto, F., Ramakrishna, S., 2020. The Flame Retardancy of Polyethylene Composites: From Fundamental Concepts to Nanocomposites. *Molecules* 25, 5157. <https://doi.org/10.3390/molecules25215157>
- Rodríguez, H.S., Hinestroza, J.P., Ochoa-Puentes, C., Sierra, C.A., Soto, C.Y., 2014. Antibacterial activity against *Escherichia coli* of Cu-BTC (MOF-199) metal-organic framework immobilized onto cellulosic fibers. *Journal of Applied Polymer Science* 131. <https://doi.org/10.1002/app.40815>
- Rowell, J.L.C., Yaghi, O.M., 2004. Metal–organic frameworks: a new class of porous materials. *Microporous and Mesoporous Materials* 73, 3–14. <https://doi.org/10.1016/j.micromeso.2004.03.034>
- Rubio-Martinez, M., Avci-Camur, C., Thornton, A.W., Imaz, I., Maspoch, D., Hill, M.R., 2017. New synthetic routes towards MOF production at scale. *Chem. Soc. Rev.* 46, 3453–3480. <https://doi.org/10.1039/C7CS00109F>

**S**

- Saini, A., Rauert, C., Simpson, M.J., Harrad, S., Diamond, M.L., 2016. Characterizing the sorption of polybrominated diphenyl ethers (PBDEs) to cotton and polyester fabrics under controlled conditions. *Science of The Total Environment* 563–564, 99–107. <https://doi.org/10.1016/j.scitotenv.2016.04.099>
- Sakho, E.H.M., Allahyari, E., Oluwafemi, O., Thomas, S., Kalarikkal, N., 2017. Dynamic Light Scattering (DLS), in: *Thermal and Rheological*

- Measurement Techniques for Nanomaterials Characterization. pp. 37–49. <https://doi.org/10.1016/B978-0-323-46139-9.00002-5>
- Salmeia, K.A., Jovic, M., Ragaisiene, A., Rukuiziene, Z., Milasius, R., Mikucioniene, D., Gaan, S., 2016. Flammability of Cellulose-Based Fibers and the Effect of Structure of Phosphorus Compounds on Their Flame Retardancy. *Polymers (Basel)* 8, 293. <https://doi.org/10.3390/polym8080293>
- Samuel, M.S., Bhattacharya, J., Parthiban, C., Viswanathan, G., Pradeep Singh, N.D., 2018. Ultrasound-assisted synthesis of metal organic framework for the photocatalytic reduction of 4-nitrophenol under direct sunlight. *Ultrasonics Sonochemistry* 49, 215–221. <https://doi.org/10.1016/j.ultsonch.2018.08.004>
- Schelling, M., Kim, M., Otal, E., Aguirre, M., Hinestroza, J.P., 2020. Synthesis of a zinc–imidazole metal–organic framework (ZIF-8) using ZnO rods grown on cotton fabrics as precursors: arsenate absorption studies. *Cellulose* 27, 6399–6410. <https://doi.org/10.1007/s10570-020-03216-4>
- Schelling, M., Kim, M., Otal, E., Hinestroza, J., 2018. Decoration of Cotton Fibers with a Water-Stable Metal-Organic Framework (UiO-66) for the Decomposition and Enhanced Adsorption of Micropollutants in Water. *Bioengineering (Basel)* 5. <https://doi.org/10.3390/bioengineering5010014>
- Schwarz, I., Kovacevic, S., 2017. Textile Application: From Need to Imagination. <https://doi.org/10.5772/intechopen.68376>
- Shang, M., Zhang, X., Zhang, J., Sun, J., Zhao, X., Yu, S., Liu, X., Liu, B., Yi, X., 2021. Nitrogen-doped carbon composite derived from ZIF-8/polyaniline@cellulose-derived carbon aerogel for high-performance symmetric supercapacitors. *Carbohydrate Polymers* 262, 117966. <https://doi.org/10.1016/j.carbpol.2021.117966>
- Shaw, S., 2010. Halogenated Flame Retardants: Do the Fire Safety Benefits Justify the Risks? *Reviews on Environmental Health* 25. <https://doi.org/10.1515/REVEH.2010.25.4.261>
- Shekhah, O., Fu, L., Sougrat, R., Belmabkhout, Y., Cairns, A.J., Giannelis, E.P., Eddaoudi, M., 2012. Successful implementation of the stepwise layer-by-layer growth of MOF thin films on confined surfaces: mesoporous silica foam as a first case study. *Chem. Commun.* 48, 11434–11436. <https://doi.org/10.1039/C2CC36233C>
- Shekhah, O., Liu, J., Fischer, R.A., Wöll, C., 2011. MOF thin films: existing and future applications. *Chem. Soc. Rev.* 40, 1081–1106. <https://doi.org/10.1039/C0CS00147C>
- Shi, X., Peng, X., Zhu, J., Lin, G., Kuang, T., 2018. Synthesis of DOPO-HQ-functionalized graphene oxide as a novel and efficient flame retardant and its application on polylactic acid: Thermal property, flame retardancy, and mechanical performance. *Journal of Colloid and Interface Science* 524, 267–278. <https://doi.org/10.1016/j.jcis.2018.04.016>
- Singh, R., Gautam, S., Sharma, B., Jain, P., Chauhan, K.D., 2021. Chapter 2 - Biopolymers and their classifications, in: Thomas, S., Gopi, S., Amalraj, A. (Eds.), *Biopolymers and Their Industrial Applications*. Elsevier, pp. 21–44. <https://doi.org/10.1016/B978-0-12-819240-5.00002-X>
- Siriviriyannun, A., O'Rear, E., Yanumet, N., 2008. Self-extinguishing cotton fabric with minimal phosphorus deposition. *Cellulose* 15, 731–737. <https://doi.org/10.1007/s10570-008-9223-7>

- Smith, C.B., Mishra, R.S., 2014. Chapter 2 - Fundamentals of Formability, in: Smith, C.B., Mishra, R.S. (Eds.), *Friction Stir Processing for Enhanced Low Temperature Formability*. Butterworth-Heinemann, Boston, pp. 7–9. <https://doi.org/10.1016/B978-0-12-420113-2.00002-7>
- So, M.C., Beyzavi, M.H., Sawhney, R., Shekhah, O., Eddaoudi, M., Al-Juaid, S.S., Hupp, J.T., Farha, O.K., 2014. Post-assembly transformations of porphyrin-containing metal–organic framework (MOF) films fabricated via automated layer-by-layer coordination. *Chem. Commun.* 51, 85–88. <https://doi.org/10.1039/C4CC05727A>
- Su, Z., Zhang, M., Lu, Z., Song, S., Zhao, Y., Hao, Y., 2018. Functionalization of cellulose fiber by in situ growth of zeolitic imidazolate framework-8 (ZIF-8) nanocrystals for preparing a cellulose-based air filter with gas adsorption ability. *Cellulose* 25, 1997–2008. <https://doi.org/10.1007/s10570-018-1696-4>
- Sun, Y., Zheng, L., Yang, Y., Qian, X., Fu, T., Li, X., Yang, Z., Yan, H., Cui, C., Tan, W., 2020. Metal–Organic Framework Nanocarriers for Drug Delivery in Biomedical Applications. *Nano-Micro Lett.* 12, 103. <https://doi.org/10.1007/s40820-020-00423-3>

## T

- Tanaka, S., 2020. Chapter 10 - Mechanochemical synthesis of MOFs, in: Mozafari, M. (Ed.), *Metal-Organic Frameworks for Biomedical Applications*. Woodhead Publishing, pp. 197–222. <https://doi.org/10.1016/B978-0-12-816984-1.00012-3>
- Tang, H., Zhu, Z., Chen, R., Wang, J., Zhou, H., 2019. Synthesis of DOPO-based pyrazine derivative and its effect on flame retardancy and thermal stability of epoxy resin. *Polym Adv Technol* 30, 2331 – 2339. <https://doi.org/10.1002/pat.4674>
- Toldy, A., Tóth, N., Anna, P., Marosi, G., 2006. Synthesis of phosphorus-based flame retardant systems and their use in an epoxy resin. *Polymer Degradation and Stability* 91, 585–592. <https://doi.org/10.1016/j.polymdegradstab.2005.02.025>

## V

- Varghese, A.M., Mittal, V., 2018. 5 - Surface modification of natural fibers, in: Shimpi, N.G. (Ed.), *Biodegradable and Biocompatible Polymer Composites*, Woodhead Publishing Series in Composites Science and Engineering. Woodhead Publishing, pp. 115–155. <https://doi.org/10.1016/B978-0-08-100970-3.00005-5>
- Vasiljević, J., Jerman, I., Jakša, G., Alongi, J., Malucelli, G., Zorko, M., Tomšič, B., & Simončič, B., 2015. Functionalization of cellulose fibres with DOPO-polysilsesquioxane flame retardant nanocoating. *Cellulose* 22, 1893–1910. <https://doi.org/10.1007/s10570-015-0599-x>
- Velencoso, M.M., Battig, A., Markwart, J.C., Schartel, B., Wurm, F.R., 2018. *Molecular Firefighting—How Modern Phosphorus Chemistry Can Help*

- Solve the Challenge of Flame Retardancy. *Angew Chem Int Ed Engl* 57, 10450–10467. <https://doi.org/10.1002/anie.201711735>
- Venier, M., Salamova, A., Hites, R.A., 2015. Halogenated Flame Retardants in the Great Lakes Environment. *Acc. Chem. Res.* 48, 1853–1861. <https://doi.org/10.1021/acs.accounts.5b00180>

## W

- Wan, Caiyan, Mingsheng Liu, Shidong Liu, Yv Chen, Guangxian Zhang, and Fengxiu Zhang. 2021. 'An Efficient and Durable DOPO/H<sub>3</sub>PO<sub>4</sub>-Based Flame Retardant for Cotton Fabric'. *Cellulose* 28 (11): 7421–34. <https://doi.org/10.1007/s10570-021-03981-w>.
- Wang, D.-Y., 2016. *Novel Fire Retardant Polymers and Composite Materials*. Woodhead Publishing.
- Wang, H., Qiao, H., Guo, J., Sun, J., Li, H., Zhang, S., Gu, X., 2019. Preparation of cobalt-based metal organic framework and its application as synergistic flame retardant in thermoplastic polyurethane (TPU). *Composites Part B: Engineering* 182, 107498. <https://doi.org/10.1016/j.compositesb.2019.107498>
- Wang, L., Zhang, T., Yan, H., Peng, M., Fang, Z., Li, Y., Hao, W., 2014. Flame-retardant coating by alternate assembly of poly(vinylphosphonic acid) and polyethylenimine for ramie fabrics. *Chin J Polym Sci* 32, 305–314. <https://doi.org/10.1007/s10118-014-1408-y>
- Wang, P., Cai, Z., 2017. Highly efficient flame-retardant epoxy resin with a novel DOPO-based triazole compound: Thermal stability, flame retardancy and mechanism. *Polymer Degradation and Stability* 137, 138–150. <https://doi.org/10.1016/j.polymdegradstab.2017.01.014>
- Wang, S., Sui, X., Li, Y., Li, J., Xu, H., Zhong, Y., Zhang, L., Mao, Z., 2016. Durable flame retardant finishing of cotton fabrics with organosilicon functionalized cyclotriphosphazene. *Polymer Degradation and Stability* 128, 22–28. <https://doi.org/10.1016/j.polymdegradstab.2016.02.009>
- Wang, Shihao, Ling Sun, Yuyang Li, Huixin Wang, Jie Liu, Ping Zhu, and Chaohong Dong. 2021. 'Properties of Flame-Retardant Cotton Fabrics: Combustion Behavior, Thermal Stability and Mechanism of Si/P/N Synergistic Effect'. *Industrial Crops and Products* 173 (December): 114157. <https://doi.org/10.1016/j.indcrop.2021.114157>.
- Wang, X., Lu, Y., Zhang, Q., Wang, K., Carmalt, C., Parkin, I., Zhang, Z., Zhang, X., 2020. Durable Fire Retardant, Superhydrophobic, Abrasive Resistant and Air/UV Stable Coatings. *Journal of Colloid and Interface Science* 582. <https://doi.org/10.1016/j.jcis.2020.07.084>
- Wang, Z.-Y., Liu, Y., Wang, Q., 2010. Flame retardant polyoxymethylene with aluminium hydroxide/melamine/novolac resin synergistic system. *Polymer Degradation and Stability - POLYM DEGRAD STABIL* 95, 945–954. <https://doi.org/10.1016/j.polymdegradstab.2010.03.028>
- Wei, Dongdong, Chaohong Dong, Jian Liu, Zheng Zhang, and Zhou Lu. 2019. 'A Novel Cyclic Polysiloxane Linked by Guanidyl Groups Used as Flame Retardant and Antimicrobial Agent on Cotton Fabrics'. *Fibers and Polymers* 20 (7): 1340–46. <https://doi.org/10.1007/s12221-019-9008-7>.

- Wei, Z., Gu, X., Wu, J., Wei, M., Yu, Q., Xiujian, T., Wang, Z., 2019. Performance comparison of epoxy resins modified with diphenylphosphine oxide and DOPO. *Fire and Materials* 43, 892–902. <https://doi.org/10.1002/fam.2749>
- Wilkie, C.A., Morgan, A.B., 2009. *Fire Retardancy of Polymeric Materials*, Second Edition. CRC Press.
- Williams, B.L., Ding, H., Hou, Z., Paul, P.O., Lewis, F.A., Smith, A.T., Sun, L., 2021. Highly efficient polyvinyl alcohol/montmorillonite flame retardant nanocoating for corrugated cardboard. *Adv Compos Hybrid Mater* 4, 662–669. <https://doi.org/10.1007/s42114-021-00299-w>
- Wolff, S., 1996. Chemical Aspects of Rubber Reinforcement by Fillers. *Rubber Chemistry and Technology* 69, 325–346. <https://doi.org/10.5254/1.3538376>
- Wu, M.-X., Yang, Y.-W., 2017. Metal–Organic Framework (MOF)-Based Drug/Cargo Delivery and Cancer Therapy. *Advanced Materials* 29, 1606134. <https://doi.org/10.1002/adma.201606134>

## X

- Xiangze, J., Bin, Z., Bin, Z., Bin, Z., Bin, Z., Chun, C., Chun, C., Chun, C., Xiong, F., Xiong, F., Xiong, F., Qiang, H., Qiang, H., Qiang, H., 2021. Immobilization of chitosan grafted carboxylic Zr-MOF to porous starch for sulfanilamide adsorption. *Carbohydrate Polymers* 253.
- Xie, K., Gao, A., Zhang, Y., 2013. Flame retardant finishing of cotton fabric based on synergistic compounds containing boron and nitrogen. *Carbohydrate polymers* 98, 706–10. <https://doi.org/10.1016/j.carbpol.2013.06.014>
- Xing, W., Jie, G., Song, L., Hu, S., Lv, X., Wang, X., Hu, Y., 2011. Flame retardancy and thermal degradation of cotton textiles based on UV-curable flame retardant coatings. *Thermochimica Acta* 513, 75–82. <https://doi.org/10.1016/j.tca.2010.11.014>
- Xue, Y., Zheng, S., Xue, H., Pang, H., 2019. Metal–organic framework composites and their electrochemical applications. *Journal of Materials Chemistry A* 7, 7301–7327. <https://doi.org/10.1039/C8TA12178H>

## Y

- Yan, H., Yuanhao, W., Hongxing, Y., 2015. TEOS/Silane-Coupling Agent Composed Double Layers Structure: A Novel Super-hydrophilic Surface. *Energy Procedia, Clean, Efficient and Affordable Energy for a Sustainable Future: The 7th International Conference on Applied Energy (ICAE2015)* 75, 349–354. <https://doi.org/10.1016/j.egypro.2015.07.384>
- Yang, D., Odoh, S., Wang, T., Farha, O., Hupp, J., Cramer, C., Prof. Dr, L., Gates, B., 2015. Metal–Organic Framework Nodes as Nearly Ideal Supports for Molecular Catalysts: NU-1000- and UiO-66-Supported Iridium Complexes. *Journal of the American Chemical Society* 137. <https://doi.org/10.1021/jacs.5b02956>
- Yi, S., Su, Y., Wan, Y., 2010. Preparation and characterization of vinyltriethoxysilane (VTES) modified silicalite-1/PDMS hybrid



- pervaporation membrane and its application in ethanol separation from dilute aqueous solution. *Journal of Membrane Science* 11.
- Yu, C., 2015. Chapter 2 - Natural Textile Fibres: Vegetable Fibres, in: Sinclair, R. (Ed.), *Textiles and Fashion*, Woodhead Publishing Series in Textiles. Woodhead Publishing, pp. 29–56. <https://doi.org/10.1016/B978-1-84569-931-4.00002-7>
- Yu, J., Mu, C., Yan, B., Qin, X., Shen, C., Xue, H., Pang, H., 2017. Nanoparticle/MOF composites: preparations and applications. *Mater. Horiz.* 4, 557–569. <https://doi.org/10.1039/C6MH00586A>
- Yu, M., Li, W., Wang, Z., Zhang, B., Ma, H., Li, L., Li, J., 2016. Covalent immobilization of metal–organic frameworks onto the surface of nylon—a new approach to the functionalization and coloration of textiles. *Sci Rep* 6, 22796. <https://doi.org/10.1038/srep22796>
- Yu, Z.-L., Yang, N., Apostolopoulou-Kalkavoura, V., Qin, B., Ma, Z.-Y., Xing, W.-Y., Qiao, C., Bergström, L., Antonietti, M., Yu, S.-H., 2018. Fire-Retardant and Thermally Insulating Phenolic-Silica Aerogels. *Angewandte Chemie International Edition* 57, 4538–4542. <https://doi.org/10.1002/anie.201711717>

## Z

- Zhang, J., Li, Z., Qi, X.-L., Wang, D.-Y., 2020. Recent Progress on Metal–Organic Framework and Its Derivatives as Novel Fire Retardants to Polymeric Materials. *Nano-Micro Lett.* 12, 173. <https://doi.org/10.1007/s40820-020-00497-z>
- Zhang, Y., Chang, C., Tan, B., Xu, D., Wang, Y., Qi, T., 2019. Application of a Sustainable Bioderived Solvent (Biodiesel) for Phenol Extraction. *ACS Omega* 4, 10431–10437. <https://doi.org/10.1021/acsomega.9b00977>
- Zhang, Yingnan, Mingju Jing, Shuya Hou, Yawen Gong, Zhi Wang, Juncheng Jiang, and Bin Zhang. 2022. 'Preparation and Fire-Retardant Mechanism of Self-Hardening Silica Foam for Wood Fire Prevention'. *Silicon*, June. <https://doi.org/10.1007/s12633-022-01975-2>.
- Zhang, Z., Dong, C., Liu, J., Kong, D., Sun, L., Lu, Z., 2020. Preparation of a synergistic reactive flame retardant based on silicon, phosphorus and nitrogen and its application to cotton fabrics. *Cellulose* 27, 1799–1815. <https://doi.org/10.1007/s10570-019-02900-4>
- Zhao, B., Kolibaba, T.J., Lazar, S., Grunlan, J.C., 2021. Environmentally-benign, water-based covalent polymer network for flame retardant cotton. *Cellulose* 28, 5855–5866. <https://doi.org/10.1007/s10570-021-03874-y>
- Zhao, B., Liu, Y.-T., Zhang, C.-Y., Liu, D.-Y., Li, F., Liu, Y.-Q., 2017. A novel phosphoramidate and its application on cotton fabrics: Synthesis, flammability and thermal degradation. *Journal of Analytical and Applied Pyrolysis* 125, 109–116. <https://doi.org/10.1016/j.jaap.2017.04.011>
- Zhou, S., Huangfu, W., You, F., Li, D., Fan, D., 2019. Flame Retardancy and Mechanism of Cotton Fabric Finished by Phosphorus Containing SiO<sub>2</sub> Hybrid Sol, in: 2019 9th International Conference on Fire Science and Fire Protection Engineering (ICFSFPE). Presented at the 2019 9th International Conference on Fire Science and Fire Protection Engineering

- (ICFSFPE), IEEE, Chengdu, China, pp. 1–5.  
<https://doi.org/10.1109/ICFSFPE48751.2019.9055847>
- Zhou, W., Yang, C.Q., Lickfield, G.C., 2004. Mechanical strength of durable press finished cotton fabric part V: Poly(vinyl alcohol) as an additive to improve fabric abrasion resistance. *Journal of Applied Polymer Science* 91, 3940–3946. <https://doi.org/10.1002/app.13606>
- Zhu, P., Sui, S., Wang, B., Sun, K., Sun, G., 2004. A study of pyrolysis and pyrolysis products of flame-retardant cotton fabrics by DSC, TGA, and PY–GC–MS. *Journal of Analytical and Applied Pyrolysis* 71, 645–655. <https://doi.org/10.1016/j.jaap.2003.09.005>
- Zia, K.M., Zuber, M., Rizwan, A., Jamil, T., Tabasum, S., Shahid, M., 2012. Modification of cellulosic fabric using polyvinyl alcohol—Part-I: Physicochemical properties. *Carbohydrate Polymers* 87, 2063–2067. <https://doi.org/10.1016/j.carbpol.2011.10.021>